คุณลักษณะและสมบัติในการเร่งปฏิกิริยาของตัวเร่งปฏิกิริยาทอง-แพลเลเดียมบน
ไทเทเนียมไดออกไซด์ที่เตรียมโดยวิธีเฟลมสเปรย์ไพโรไลซิสในปฏิกิริยาไฮโดรจิเนชันแบบเลือกเกิด

นางสาวบุญธิดา พงษ์ถาวรสกุล

วิทยานิพนธ์นี้เป็นส่วนหนึ่งของการศึกษาตามหลักสูตรปริญญาวิศวกรรมศาสตรดุษฎีบัณฑิต
สาขาวิชาวิศวกรรมเคมี ภาควิชาวิศวกรรมเคมี
คณะวิศวกรรมศาสตร์ จุฬาลงกรณ์มหาวิทยาลัย
ปีการศึกษา 2558

THE CHARACTERISTICS AND CATALYTIC PROPERTIES OF TiO_2 SUPPORTED Au-Pd CATALYSTS PREPARED BY FLAME SPRAY PYROLYSIS IN SELECTIVE HYDROGENATION REACTIONS

Miss Boontida Pongthawornsakun

A Dissertation Submitted in Partial Fulfillment of the Requirements
for the Degree of Doctor of Engineering Program in Chemical Engineering
Department of Chemical Engineering
Faculty of Engineering
Chulalongkorn University
Academic Year 2015

Thesis Title	THE CHARACTERISTICS AND CATALYTIC PROPERTIES OF TiO_2 SUPPORTED Au-Pd CATALYSTS PREPARED BY FLAME SPRAY PYROLYSIS IN SELECTIVE HYDROGENATION REACTIONS
By	Miss Boontida Pongthawornsakun
Field of Study	Chemical Engineering
Thesis Advisor	Associate Professor Joongjai Panpranot, Ph.D.
Thesis Co-Advisor	Professor Sotiris E. Pratsinis, Ph.D.

Accepted by the Faculty of Engineering, Chulalongkorn University in Partial Fulfillment of the Requirements for the Doctoral Degree

.....Dean of the Faculty of Engineering
(Professor Bundhit Eua-arporn, Ph.D.)

THESIS COMMITTEE

.....Chairman
(Associate Professor Tawatchai Charinpanitkul, D.Eng.)

.....Thesis Advisor
(Associate Professor Joongjai Panpranot, Ph.D.)

.....Thesis Co-Advisor
(Professor Sotiris E. Pratsinis, Ph.D.)

.....Examiner
(Akawat Sirisuk, Ph.D.)

.....Examiner
(Chutimon Satirapipathkul, D.Eng.)

.....External Examiner
(Assistant Professor Okorn Mekasuwandumrong, D.Eng.)

บุญธิดา พงษ์ถาวรสกุล : คุณลักษณะและสมบัติในการเร่งปฏิกิริยาของตัวเร่งปฏิกิริยาทอง-แพลเลเดียมบนไทเทเนียมไดออกไซด์ที่เตรียมโดยวิธีเฟลมสเปรย์ไพโรไลซิสในปฏิกิริยาไฮโดรจิเนชันแบบเลือกเกิด (THE CHARACTERISTICS AND CATALYTIC PROPERTIES OF TiO_2 SUPPORTED Au-Pd CATALYSTS PREPARED BY FLAME SPRAY PYROLYSIS IN SELECTIVE HYDROGENATION REACTIONS) อ.ที่ปรึกษาวิทยานิพนธ์หลัก: รศ. ดร. จูงใจ ปั้นประณต, อ.ที่ปรึกษาวิทยานิพนธ์ร่วม: ศ. ดร. โซติริส อี พรัทซินิส, 194 หน้า.

การเตรียมตัวเร่งปฏิกิริยาโลหะสองชนิด ทอง-แพลเลเดียมบนไทเทเนียมไดออกไซด์ด้วยวิธีเฟลมสเปรย์ไพโรไลซิสในขั้นตอนเดียว พบว่ามีการกระจายตัวของอนุภาคโลหะผสมทอง-แพลเลเดียมขนาดเล็ก (เส้นผ่านศูนย์กลางประมาณ 5 นาโนเมตร) บนตัวรองรับไทเทเนียมไดออกไซด์ ในขณะที่การเตรียมตัวเร่งปฏิกิริยาด้วยวิธีทั่วไป เช่น วิธีเคลือบฝังและวิธีพอกพูน-ตกตะกอน ทำให้เกิดอนุภาคหลายขนาดและมีการบดบังรูพรุนของตัวรองรับและเกิดโครงสร้างรูพรุนใหม่ของตัวรองรับไทเทเนียมไดออกไซด์ ตัวเร่งปฏิกิริยาทอง-แพลเลเดียมบนไทเทเนียมไดออกไซด์ที่เตรียมด้วยวิธีเฟลมสเปรย์ไพโรไลซิส ให้ประสิทธิภาพที่ดีในการเกิดปฏิกิริยาไฮโดรจิเนชันแบบเลือกเกิดของ 1-เฮปไทน์ องค์ประกอบของแต่ละอนุภาคทอง-แพลเลเดียมมีลักษณะเป็นเนื้อเดียวกันมากขึ้นเมื่อผ่านการรีดักชันที่อุณหภูมิ 500 องศาเซลเซียส โดยที่ไม่มีการเปลี่ยนแปลงขนาดอนุภาคและองค์ประกอบโดยรวม อย่างไรก็ตามอัตราส่วนอะตอมของแพลเลเดียมต่อไทเทเนียมที่พื้นผิวลดลง เนื่องจากการเคลื่อนที่ของไทเทเนียมไดออกไซด์ที่ถูกรีดิวซ์ขึ้นมาบนโลหะ (ผลของอันตรกิริยาที่แข็งแรงระหว่างโลหะและตัวรองรับ) เป็นผลทำให้ความว่องไวในการเกิดปฏิกิริยาลดลง ดังนั้นกระบวนการรีดักชันที่อุณหภูมิสูงไม่จำเป็นสำหรับตัวเร่งปฏิกิริยาทอง-แพลเลเดียมบนไทเทเนียมไดออกไซด์ที่เตรียมด้วยวิธีเฟลมสเปรย์ไพโรไลซิสในการเร่งปฏิกิริยาไฮโดรจิเนชันแบบเลือกเกิดของ 1-เฮปไทน์ โดยค่าผลได้สูงสุดของ 1-เฮปทีนเท่ากับ 93% เมื่อใช้ตัวเร่งปฏิกิริยาทอง-แพลเลเดียมบนไทเทเนียมไดออกไซด์ที่ผ่านการรีดิวซ์ที่ 40 องศาเซลเซียส ที่เวลาทำปฏิกิริยา 20 นาที คุณลักษณะของตัวเร่งปฏิกิริยาที่เตรียมด้วยวิธีเฟลมสเปรย์ไพโรไลซิสสามารถปรับปรุงเพิ่มเติมได้โดยการเปลี่ยนอัตราส่วนของอัตราการไหลของสารละลายที่เข้าเตาปฏิกรณ์ (PF) และอัตราการไหลของแก๊สออกซิเจนที่ช่วยในการกระจาย (DO) พบว่าความว่องไวในการเกิดปฏิกิริยาของตัวเร่งปฏิกิริยาแพลเลเดียมบนไทเทเนียมไดออกไซด์ที่เตรียมที่ 7PF3DO สามารถกำจัดอะเซทิลีนได้หมดที่ 60 องศาเซลเซียส เทียบเท่ากับตัวเร่งปฏิกิริยาทอง-แพลเลเดียมบนไทเทเนียมไดออกไซด์ นอกจากนี้ได้นำเฟลมสเปรย์ไพโรไลซิสแบบสองหัวฉีดมาใช้ในการเตรียมตัวเร่งปฏิกิริยาทอง-แพลเลเดียมบนไทเทเนียมไดออกไซด์ให้มีลักษณะรูปแบบของอนุภาคที่หลากหลายโดยการควบคุมการผสมของแต่ละองค์ประกอบที่ได้จากเปลวไฟจากคนละหัวฉีด พบว่าประสิทธิภาพของตัวเร่งปฏิกิริยาทอง-แพลเลเดียมบนไทเทเนียมไดออกไซด์ในปฏิกิริยาไฮโดรจิเนชันแบบเลือกเกิดของอะเซทิลีนที่ 40 องศาเซลเซียส มีประสิทธิภาพสูงขึ้นได้โดยการแยกฉีดสารตั้งต้นของไทเทเนียมไดออกไซด์และสารตั้งต้นผสมของโลหะแพลเลเดียมและทองคนละหัวฉีด

ภาควิชา วิศวกรรมเคมี	ลายมือชื่อนิสิต .....
สาขาวิชา วิศวกรรมเคมี	ลายมือชื่อ อ.ที่ปรึกษาหลัก .....
ปีการศึกษา 2558	ลายมือชื่อ อ.ที่ปรึกษาร่วม .....

5371820621 : MAJOR CHEMICAL ENGINEERING

KEYWORDS: AU-PD BIMETALLIC CATALYSTS, FLAME SPRAY PYROLYSIS, SELECTIVE HYDROGENATION, 1-HEPTYNE, ACETYLENE

BOONTIDA PONGTHAWORNSAKUN: THE CHARACTERISTICS AND CATALYTIC PROPERTIES OF TiO_2 SUPPORTED Au-Pd CATALYSTS PREPARED BY FLAME SPRAY PYROLYSIS IN SELECTIVE HYDROGENATION REACTIONS. ADVISOR: ASSOC. PROF. JOONGJAI PANPRANOT, Ph.D., CO-ADVISOR: PROF. SOTIRIS E. PRATSINIS, Ph.D., 194 pp.

The preparation of bimetallic AuPd/TiO_2 catalysts by one-step flame spray pyrolysis (FSP) resulted in narrow particle size distribution of small AuPd alloy particles ($đ_p$ ~5 nm) on the TiO_2 support. The conventional methods such as impregnation and deposition-precipitation methods, on the other hand, resulted in wider particle size distribution with some pore blockages and formation of new pore structure of the TiO_2. The FSP-made AuPd/TiO_2 showed good catalytic performances in the selective hydrogenation of 1-heptyne. More homogeneous composition of the individual AuPd nanoparticles was obtained upon reduction at 500 °C without significant changes of particle size and bulk composition. Nevertheless, the surface atomic Pd/Ti ratio decreased due to the TiO_x migration onto the metals (so-called the strong metal-support interaction effect), resulting in lower activity. Reduction at high temperature was found to be unnecessary for the FSP-made AuPd/TiO_2 catalysts in the selective hydrogenation of 1-heptyne. The highest yield of 1-heptene was 93% over FSP-AuPd/TiO_2 R40 catalyst after 20 min reaction time. The characteristics of FSP-made catalysts were modified by changing the stoichiometric of precursor flow rate (PF) and dispersion O_2 gas flow rate (DO). The activity of Pd/TiO_2 catalyst prepared at 7PF3DO was improved so that it gave full acetylene elimination at 60 °C similar to the AuPd/TiO_2 catalyst. Furthermore, the 2-nozzle FSP was employed for the preparation of AuPd/TiO_2 catalysts with various particle configurations by controlling the mixing of the individual components from different flames. The catalyst performances for the selective hydrogenation of acetylene at 40 °C of the AuPd/TiO_2 catalysts could be enhanced by separation of the TiO_2 precursor from the mixed precursor of Pd and Au metals (TiO_2 + AuPd).

Department:	Chemical Engineering	Student's Signature	.....
Field of Study:	Chemical Engineering	Advisor's Signature	.....
Academic Year:	2015	Co-Advisor's Signature	.....

ACKNOWLEDGEMENTS

The author would like to express my deep sense of gratitude to my advisor, Associate Prof. Dr. Joongjai Panpranot for her invaluable guidance, support and encouragement through my research study. Her timely advice and teaching have helped me to a very great extent to accomplish this research study.

I would grateful to thank to Prof. Dr. Sotiris E. Pratsinis of the Swiss Federal Institute of Technology (ETH Zurich) for all his suggestion and guidance. In addition, I am very much thankful to Dr. Büchel Robert for his support and advice and Prof. Alfons Baiker for his suggestion about my research during my visiting at ETH Zurich. In addition, I am also grateful for Prof. Masahiko Arai of Hokkaido University and Shin-ichiro Fujita as Sensei for their support, suggestion and guidance in both of research and life in Japan during my visiting at Hokkaido University. Moreover, I also thank profusely to Dr. Francisco J. Cadete Santos Aires for his support, suggestion and guidance in both of research, especially TEM-EDX characterization, and life in France during my visiting at IRCELYON.

I also would like to thank Associate Prof. Dr. Tawatchai Charinpanitkul as the chairman, Dr. Akawat Sirisuk, Dr. Chutimon Satirapipathkul, and Assistant Prof. Dr. Okorn Mekasuwandumrong as the members of the thesis committee for their comment and suggestion.

I gratefully thank the financial supports form the Chulalongkorn University Dutsadi Phiphat Scholarship, the National Research Council of Thailand-Japan Society for the Promotion of Science (NRCT-JSPS) Joint Research Program, and research program PHC SIAM N°29626VJ.

Finally, I acknowledge with thanks to my parents, my family, and my friends in Center of Excellence in Catalysis and Catalytic Reaction Engineering for worthy support, encouragement all times, and co-operation throughout my study period.

CONTENTS

Page

Page

Page

Page

Page

Page

LIST OF TABLES

Page

Page

Page

LIST OF FIGURES

Page

Page

Page

Page

Page

CHAPTER I
INTRODUCTION

1.1 Rationale

Recent interest in using bimetallic nanoparticles in many applications including electrochemistry and catalytic processes has greatly increased. Several bimetallic nanoparticles have been demonstrated to be effective catalysts because of their high catalytic activity, selectivity, and stability [1-7]. The bimetallization not only can improve catalytic properties of the primary monometallic catalysts, but also can establish new properties [8]. Modification of catalyst properties by addition of a second metal (bimetallization) is commonly described in two categories consisting of ensemble (or geometric) effect and ligand (or electronic) effect [9, 10]. The ensemble effect was ascribed to the formation of an optimal ensemble of the active metal atoms after the second metal addition. For example, the selectivity was improved by controlling the over-reaction with smaller ensemble sizes and the activity was either decreased by reduction size of active ensemble or increased with active ensemble of the second metal or with mixed ensemble of the two metals. These effects are especially important for the structure-sensitive reactions. On the other hand, the ligand effect was ascribed to the change of local electronic structure by modification of electronic properties after the second metal addition owing to charge transfer, orbital rehybridization or other charges about electronic structure.

Bimetallic Au-Pd supported nanoparticles have attracted much attention as bimetallic catalysts and have been used in many catalytic reactions including CO oxidation [11], H_2O_2 synthesis [12], vinyl chloride synthesis by hydrochlorination of acetylene [13], vinyl acetate synthesis [14], hydrodesulfurization (HDS) [15], trichloroethene hydrodechlorination [16], CH_4 combustion [17], N_2O decomposition [18], total oxidation of volatile organic compounds (VOCs) [19], selective oxidation of alcohols to aldehydes or ketones [20, 21], epoxidation [22], oxidative dehydrogenation [23], and selective hydrogenation [6].

The selective hydrogenation of multiple unsaturation (alkynes to alkenes) is industrially significant reaction in the fundamental process for the petrochemical industry and the fine chemicals manufacture in order to form more stable products or intermediate compounds. The production of final products of high added value or intermediate compounds for the synthesis of fine chemicals is both of industrial and academic importance. Alkenes are much appreciated products used in the food industry (flavours), the pharmaceutical industry (vitamins, anesthetises, sedatives), and the perfumes industry (fragrances). They are also used as raw materials in the production of active compounds, polymers, lubricants, and resins [24]. In the view of industry, the main purpose of the hydrogenation of alkynes to alkenes is the elimination of alkynes from alkenes feedstocks [25].

Noble metals have been widely used as catalysts for hydrogenation such as Pd, Pt, Rh, and Ru. For the group VIII noble metals, Pd metal is known to be the best catalyst with highest selectivity with respect to alkenes in alkyne and (cyclo-) alkadiene hydrogenation [26].

While the monometallic Au catalysts have been used as selective catalysts to control product selectivity because the ability to dissociate H_2 molecules of gold with a completely filled Au d-band is limited [27]. The use of monometallic Au catalyst appears in selective hydrogenation reactions such as selective hydrogenation of unsaturated ketones [28], crotonaldehyde [29], acrolein [30], 1,3-butadiene [31], ethyne (acetylene) [32], propyne [33],and citral [6]. However, the catalytic behaviour of Au catalysts shows poor activity in selective hydrogenation compared to the conventional monometallic Pd catalysts [6, 34, 35]. To improve the catalytic performance in selective hydrogenation, incorporation of Au and Pd as the bimetallic catalysts can potentially enhance the catalytic activity, selectivity, and resistance to catalyst deactivation by the synergistic effect of the combination between Au and Pd. Many studies have shown that bimetallic Au-Pd catalysts were effective catalysts in hydrogenation of different organic compounds such as aromatics [36], acetylene [34], benzaldehyde [37], ethylene [10], cinnamaldehyde [38], 1,3-butadiene [39], and so on.

Additionally, another crucial role on the catalytic efficiency is the use of support for preparation of highly dispersed metal catalysts. The bimetallic Au-Pd nanoparticles have been prepared on different support materials such as carbon [40-42], titania [11, 43, 44], alumina [36, 45, 46], silica [47-49], and iron oxide [50, 51]. Titania is one of the interesting supports because of the phenomenon "the strong metal-support interaction (SMSI)" which has been observed on noble metal supported on reducible metal oxides after reduced at high temperature. This interaction provides great beneficial effect on the catalytic activity and selectivity in hydrogenation reactions [52, 53], compared with the use of un-reducible supports [54].

Generally, catalyst preparation method has been found to strongly and directly affect the final structure and properties of catalysts. Furthermore, the catalytic performance depends significantly on the nature, structural, and properties of catalyst. For the bimetallic Au-Pd nanoparticles, a number of research has reported several catalyst preparation techniques of bimetallic Au-Pd catalysts, including impregnation [55], deposition precipitation [55], sol-immobilisation [56], electroless deposition [57], encapsulation [58], microwave application [59], and redox method [34]. Nevertheless, these methods need various post-treatment steps such as filtration, washing, drying and calcination [60].

Flame aerosol technology is introduced for the production of nanoparticles in nanotechnology industry. The variety of nanoparticle products are carbon black, fumed silica, titania pigments, optical fiber, alumina and other ceramic nanoparticles [61-63]. The flame aerosol synthesis, especially the so-called flame spray pyrolysis (FSP), has been applied as an alternative catalyst preparation in a single-step without post-treatment steps. From the literatures, monometallic Au and Pd supported nanoparticles have been synthesized by FSP such as Au/TiO_2 [64], Pd/SiO_2 [65, 66], and Pd/TiO_2 [67, 68]. Nevertheless, the synthesis of bimetallic Au-Pd via FSP has not well been investigated.

Therefore, in this study, the FSP process was employed for the preparation of TiO_2 supported bimetallic Au-Pd nanoparticles. The characteristics and catalytic

properties of FSP-synthesized bimetallic Au-Pd nanoparticles were investigated by several characterization techniques and compared to those prepared by other commonly used methods such as co-impregnation and co-deposition precipitation. The effect of reduction temperature on the catalytic performances of monometallic Pd/TiO_2 and bimetallic $AuPd/TiO_2$ catalysts synthesized by FSP was also investigated in order to study the SMSI phenomena over the FSP synthesized catalysts.

Furthermore, it is well-known that the FSP process is quite attractive for catalyst preparation because of its great potential for the rapid, flexible and scalable synthesis of nanoparticles. The flexibility of FSP in obtaining the desired characteristics of FSP synthesized nanoparticles was investigated over conventional one nozzle FSP by tuning the operating conditions i.e., stoichiometric of precursor flow rate and dispersion O_2 gas flow rate. Besides tuning the FSP operating conditions, the application of 2-nozzle FSP system was also investigated for the preparation of multi-component nanoparticles by controlling the mixing of the individual components from the different flames. The liquid-phase selective hydrogenation of 1-heptyne and gas-phase selective hydrogenation of acetylene in excess ethylene were used as the reaction models to test the catalytic performances of the prepared catalysts.

1.2 Research objectives

To investigate the characteristics and catalytic properties of TiO_2 supported bimetallic Au-Pd nanoparticles prepared by one-step FSP in the liquid-phase selective hydrogenation of 1-heptyne to 1-heptene in comparison to those prepared by other common preparation techniques such as co-impregnation and co-deposition precipitation.

To study the effect of reduction temperature (40 $^{\circ}C$ or 500 $^{\circ}C$) on the catalytic properties of TiO_2 supported monometallic Pd and bimetallic Au-Pd catalysts synthesized by FSP in the liquid-phase selective hydrogenation of 1-heptyne to 1-heptene.

To investigate the effects of the stoichiometric of precursor flow rate and the dispersion O_2 gas flow rate on the characteristics and catalytic performances of TiO_2 supported monometallic Pd and bimetallic AuPd catalysts prepared by the conventional one-nozzle FSP in the gas-phase selective hydrogenation of acetylene in excess ethylene.

To investigate the application of 2-nozzle FSP system for the preparation of TiO_2 supported bimetallic AuPd catalysts with various catalyst configurations and catalytic performances in the gas-phase selective hydrogenation of acetylene in excess ethylene.

1.3 Scope of research

- Preparation of TiO_2 support, monometallic Au/TiO_2 and Pd/TiO_2, and bimetallic $AuPd/TiO_2$ catalysts by one-step FSP with 1 wt.% Au and 1 wt.% Pd.
- The stoichiometrics of precursor flow rate (PF) and the dispersion O_2 gas flow rate (DO) are as follows:

Conditions		Nomenclature
Precursor flow rate (ml/min)	Dispersion O_2 gas flow rate (l/min)	
1	9	1PF9DO
3	7	3PF7DO
5	5	5PF5DO
7	3	7PF3DO
9	1	9PF1DO

- The 2-nozzle FSP synthesis of bimetallic AuPd/TiO_2 catalysts with 1 wt.% Au and 1 wt.% Pd by different routes are as follows:

Routes		Nomenclature
1st nozzle	2nd nozzle	
TiO_2 precursor	Au and Pd precursors	TiO_2+AuPd
Au and TiO_2 precursors	Pd precursor	Au/TiO_2+Pd
Pd and TiO_2 precursors	Au precursor	Pd/TiO_2+Au
Pd and TiO_2 precursors	Au and TiO_2 precursors	Pd/TiO_2+Au/TiO_2

- Preparation of TiO_2 supported bimetallic AuPd by co-impregnation on FSP-synthesized TiO_2 with 1 wt.% Au and 1 wt.% Pd.
- Preparation of TiO_2 supported bimetallic AuPd by co-deposition precipitation on FSP-synthesized TiO_2 with 1 wt.% Au and 1 wt.% Pd.
- Catalyst pretreatment of FSP synthesized catalysts by reduction with H_2 at 40 and 500 ^{o}C.
- Characterization of the catalysts using X-ray diffraction (XRD), N_2-physisorption, transmission electron micrographs (TEM-EDX), CO-pulse chemisorption, UV-vis spectroscopy (UV-vis), X-ray photoelectron spectroscopy (XPS), inductively-coupled plasma optical emission spectroscopy (ICP-OES), thermo gravimetric analysis (TGA), and H_2-temperature programmed reduction (H_2-TPR).
- Reaction study of the catalysts in the liquid-phase hydrogenation of 1-heptene by using stirring batch reactor at 30 ^{o}C, 2-4 bar, and reaction time of 5-240 min.
- Reaction study of the catalysts in the gas-phase selective hydrogenation of acetylene in excess ethylene at the reaction temperature of 40-120 ℃ and atmospheric pressure.

1.4 Research methodology

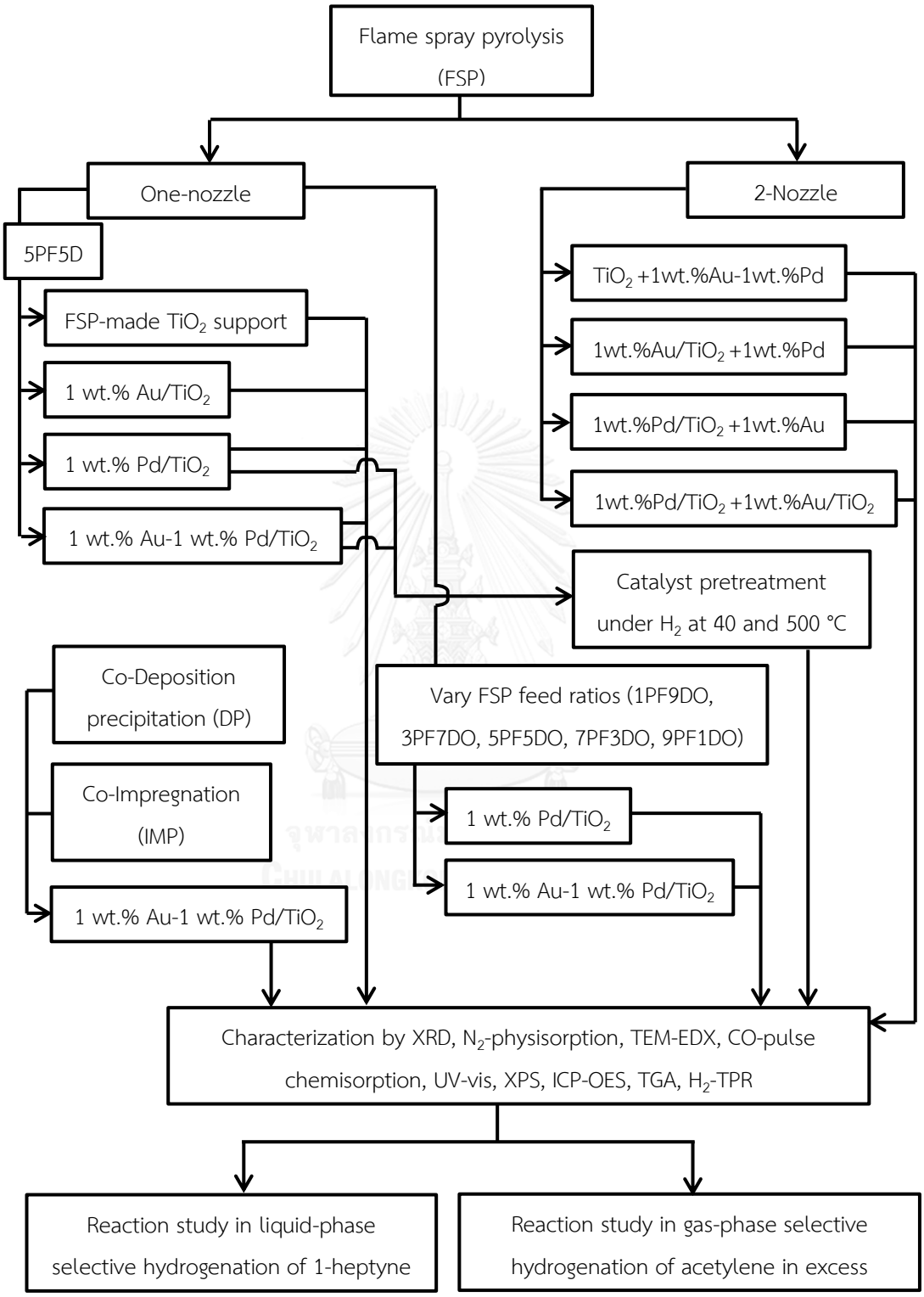

CHAPTER II

THEORY

2.1 Aerosol flame synthesis

The aerosol flame synthesis is the technology for manufacturing of nanoparticles. The flame process occurs from dispersing the metal precursor into the flame and then forming the particles. This technology is the continuous, rapid and scalable process; moreover, they can provide high production rates and relatively low cost [62, 63].

For the catalyst preparation, the main advantage of flame process over the conventional routes is the preparation in one step without several post-treatment steps, such as washing, filtration, drying, and calcinations. In addition, the flame process can be easily synthesized the multicomponent of catalysts.

The process of aerosol flame synthesis can be divided into two main categories based on the state of precursor fed to the flame.

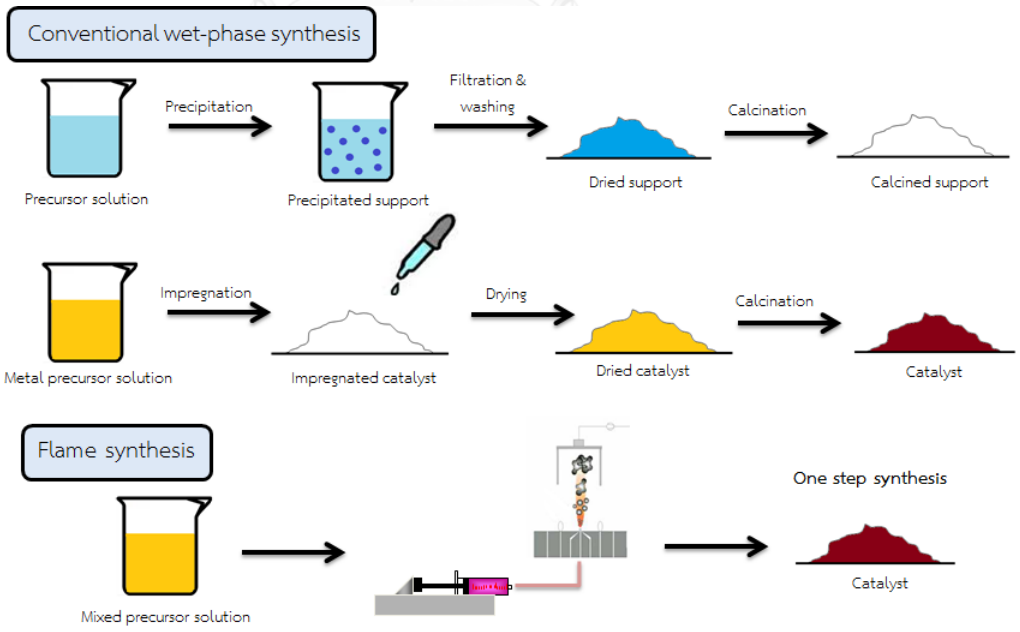

Figure 2.1 Comparing the catalyst preparation between flame synthesis and conventional preparation [63]

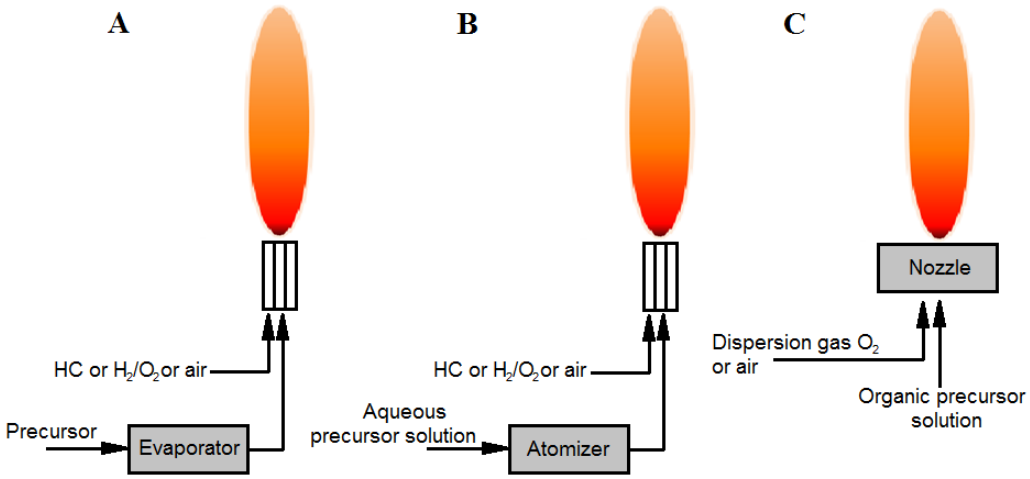

Figure 2.2 Schematic of flame configuration used for the synthesis of heterogeneous catalysts: (A) VAFS, (B) FASP, and (C) FSP [63]

2.1.1 Vapor-fed aerosol flame synthesis (VAFS)

For the vapor-fed aerosol flame synthesis, the state of precursor fed to the flame is in vapor form. Initially, the metal precursors are evaporated to form the vapors, fed to the flame, and then combusted to form the metal oxide vapor. The particle formation occurs by nucleation from the gas phase. The advantages of this process are simple and scalable method; further, the VAFS can produce high purity product because the precursor vapor can be easily purified, but the process for obtaining a high purity volatile precursor is expensive. Nevertheless, the limitation of VAFS is the type of precursor that requires the volatile metal precursors only [62, 63].

2.1.2 Liquid-fed aerosol flame synthesis (LAFS)

The state of precursor fed to the flame in the liquid-fed aerosol flame synthesis is liquid. This class is classified into two classes. One is flame-assisted spray pyrolysis (FASP), and the other is flame spray pyrolysis (FSP).

2.1.2.1 Flame-assisted spray pyrolysis (FASP)

The type of precursor fed to the flame is non-combustible solution or low combustion enthalpy solution (<50% of total combustion energy) which is dispersed

with atomizer forming fine droplet before fed to the flame. The fine droplet precursor is evaporated and pyrolyzed with external flame, resulting in particles. The external flame, such as hydrogen or hydrocarbon flame is used to assist the combustion because of low combustion enthalpy precursor solution.

2.1.2.2 Flame spray pyrolysis (FSP)

The precursor solution fed to the flame uses a combustible liquid metal precursor or high combustion enthalpy (>50% of total combustion energy), which provides the energy to supply the spray flame (more than 50% of the energy). The liquid metal precursor solution is dispersed to the flame and ignited. In the spray flame, the metal precursor droplet is evaporated to the precursor vapor and combusted with the flame. Then the particle formation from the gas phase is started by nucleation.

The FSP can be produced nanoparticle using a high temperature of flame with short residence time (about a few milliseconds). Due to the form of precursor using combustible liquid with high combustion energy, the metal precursors are readily introduced into high temperature zone of flame. Compared to FASP, the FSP synthesized particles feature primarily homogeneous morphologies [63, 69].

2.2 Hydrogenation reaction

Hydrogenation reaction is regard as an important chemical reaction in the synthesis of organic compounds. Many organic compounds containing functional groups can be hydrogenated with hydrogen to produce various useful products. The catalytic hydrogenation is found in many chemical processes, such as petrochemical, pharmaceutical, food and fine chemical industries. In laboratory scale, liquid-phase hydrogenation processes are generally performed in batch reactor. Batch process is suitable for small production due to flexibility in multi-component of products. Moreover, this process is simple and most cost effective because the equipment can be applied to another reaction. The variation of the operating conditions during the cycle (such as temperature and pressure) can be allowed by using the stirred tank reactor (for batch processes).

For a batch hydrogenation system, the reactor is not directly connected to the hydrogen source during reaction. The reactor is filled with hydrogen which replaces the free space within the reactor at the beginning. The hydrogen consumption can be calculated from the pressure decrease within the reactor. Most laboratory liquid-phase hydrogenation in batch system has been carried out over palladium, platinum, or nickel catalysts.

The process characteristics of liquid-phase hydrogenation is exothermic reaction, requiring the temperature and residence time control to achieve full conversion with high selectivity [70].

2.3 Hydrogenation of alkynes

The selective hydrogenation of multiple unsaturation compounds (triple to double bond) especially alkynes is a fundamental process for the production of monomers, intermediate products in pharmaceutical, perfumes, etc. For alkenes production, a carbon-carbon triple bond is added with hydrogen by a chemical process called the selective hydrogenation of alkynes. For the industry, the important aim of hydrogenation of alkynes to alkenes is to eliminate alkynes from alkenes feedstocks [25]. Nevertheless, the careful point of selective hydrogenation of alkynes is the exclusive undertaking of alkynes to alkenes until the alkynes is consumed, which at the same time the product alkenes is very rapidly hydrogenated to alkanes. Due to the high activation energy, the hydrogenation does not take place under normal conditions. Thus the use of catalyst in hydrogenation reaction is applied to remove this restriction for the alkenes synthesis in both laboratory scale and fine chemical industry. The rate of chemical reaction in catalytic hydrogenation will change from non-catalytic hydrogenation owing to the lower activation energy of reaction without becoming a part of reaction.

The mechanism of selective catalytic hydrogenation of alkynes to alkenes can be described as follows:

1. Reaction of hydrogen molecule with the metal atoms on the catalyst surface

Hydrogen molecule (H_2) absorbs on the catalyst surface, dissociates to two hydrogen atoms (H) by broking the strong H-H sigma bond, and replaced with two weak metal-H bonds.

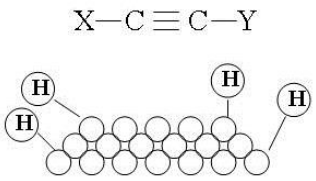

2. Reaction of alkyne with the metal atoms on the catalyst surface

The alkyne reacts with the metal catalyst by interacting of pi component in the triple bond (C≡C) with the metal atoms of catalyst which leads to two weak C-metal sigma bonds.

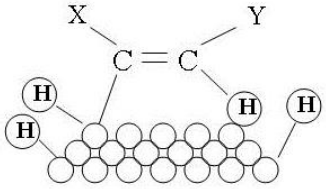

3. Hydrogen transfer

A hydrogen atom (H), which interacts weakly with the metal catalyst, is transferred from the metal catalyst surface to one of the carbons of the triple bond.

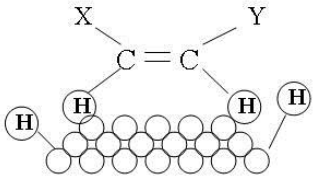

4. Alkene formation

To form the alkene, the second hydrogen atom (H) is transferred to the other carbon of the triple bond and then the alkene is released from the metal

sites. So the metal sites on the catalyst surface are free to get the additional hydrogen and alkyne molecules, occurring the further hydrogenation reaction.

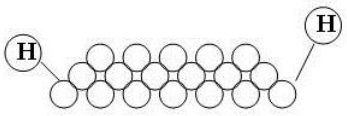

2.4 Nanoparticles

The so called “nanoparticles” are materials with at least one dimension of nanometric less than 100 nm. Nanoparticles, composed of many atoms or molecules, are effective materials. The properties of these materials are different from the properties which are achieved from conventional bulk materials and atoms or molecules [1]. Normally, the properties of conventional bulk material is constant and independent of its size, whereas the chemical, electrical, and optical properties of materials with nanometric size depend significantly on size approaching to nanoscale and percentage of atom at surface. Nanoparticles are widely used in several fields such as pharmaceutical, biomedical, cosmetic, electronic, optoelectronic, magnetic, energy, and catalytic applications.

For the catalytic application, nanoparticles are attractively used as catalysts in order to catalyze the chemical reactions. Nanomaterial based catalysts (called nanocatalysts) exhibit high surface area (large area to contact between the active sites of nanocatalyst and the reactants) resulting in increased catalytic activity due to more catalytic reaction at the same time. Nanocatalysts have been used in several catalytic processes, for examples, hydrogenation, dehalogenation, hydrosilylation, organic redox, and C-C coupling reactions.

2.5 Bimetallic nanoparticles

The use of bimetallic nanoparticles is one of particular interest in the field of catalysis due to superior catalytic properties than monometallic nanoparticles. Bimetallic nanoparticles consist of two metal elements creating the synergistic effect between two metals. The structure of bimetallic nanoparticles is dependent of the

preparation method and the miscibility between two components [71]. The structure of bimetallic nanoparticles can be classified into 3 types, according to the distribution and arrangement of each metal which is not found in the bulks, as follows:

a.) Core-shell structure: One metal forms the inner core and is surrounded by the other metal as shell.

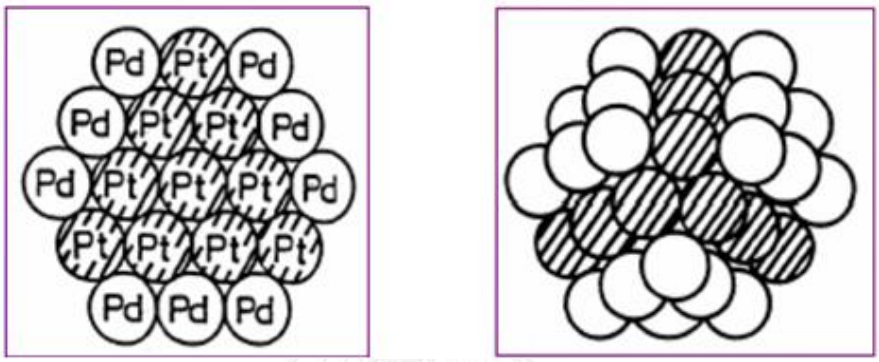

Figure 2.3 Cross-section and three-dimension of PVP stabilized Pt-Pd as core-shell structure [72]

b.) Cluster-in-cluster structure: One metal forms the nanoclusters and is surrounded by the other metal as a binder.

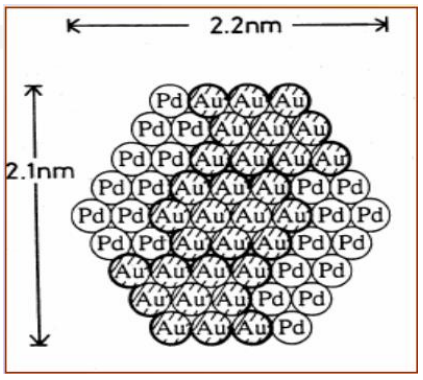

Figure 2.4 Cross-section of PVP stabilized Au-Pd (1:1) as cluster-in-cluster structure [73]

c.) Alloy structure: Two metals may randomly form to alloy if the similarity of atomic sizes between two metals are observed.

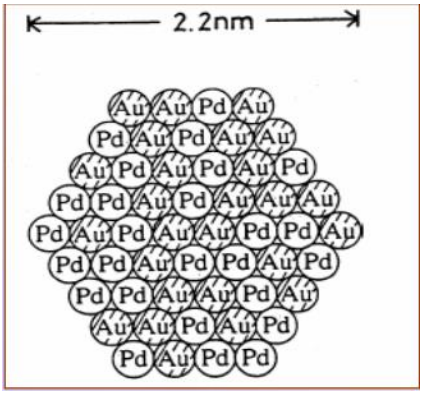

Figure 2.5 Cross-section of PVP stabilized Au-Pd (1:1) as random alloy structure [73]

The effect of second metal addition (bimetallization) relates to the terms of an ensemble and/or a ligand effect [74]. The ensemble effect is ascribed to the particular arrangement of the active sites. In fact, a particular reaction requires certain number of active sites for occurring. The reaction can be restrained by blocking the large ensemble of active sites; hence, the small ensemble of active sites is required for improving the selectivity. The term of ligand effect is interpreted as the effect of charge transfer, orbital rehybridization and lattice strain. This effect is related to the electronic interaction between two metals leading to the modification of catalytic activity and selectivity [75].

2.6 Palladium-based catalysts

Palladium-based catalysts, known as hydrogenation catalysts, are widely used for selective hydrogenation, for examples, in the reduction of C≡C bond to C=C bond, or of C=C bond in the presence of C=O and C≡N bonds [76, 77]. The ability of Pd-based catalysts that is well known to selectively hydrogenate the triple bonds (multiple unsaturated hydrocarbons) is particularly interesting for selective hydrogenation of alkynes [78]. The selectivity series of group 8 metals for the liquid-phase hydrogenation of alkynes (C5 hydrocarbons) have been reported as follows: [79]

Pd > Pt > Ru > Rh > Ir

In the field of applications involving hydrogen, Pd has unique properties such as the high solubility of hydrogen in Pd [80]. Moreover, the Pd-based catalysts can be easily modified for improving the catalytic performance which is strongly influenced by several parameters such as Pd dispersion, nature of the support, the use of promoters and additives, and alloying with other metals [81, 82]. For the partial hydrogenation of alkynes, the activity of Pd-based catalysts is related with the nature and porosity of support [83].

2.7 Gold-based catalysts

For the catalytic selective hydrogenation, the traditional catalysts such as Pt, Pd or Ru-based catalysts have been employed for this reaction but these metals require some modification. In contrast to these metals, Au metal has been regarded as a poor catalyst owing to its super resistance to oxidation reaction. At the end of the 1980s, the Au metal with nano-sized particle dispersed on different supports with proper methodology was found to be an active catalyst [84].

Comparing with the traditional hydrogenation catalysts (Pt, Pd or Ru), gold-based catalysts exhibit remarkable selectivities in several hydrogenation reactions, which contain the multiple functional groups, for example, hydrogenation of alkynes, alkenes, α,β-unsaturated carbonyl compounds and nitro compounds [85, 86]. Thus, supported gold catalysts can act as a potential catalyst to develop the new, clean and sustainable production routes with minimal side product formation.

2.8 Gold-palladium catalysts

The bimetallic Au-Pd catalyst has been widely used for the field of applications involving hydrogen, especially hydrogenation reaction [34-36, 87]. The monometallic palladium catalysts act as active hydrogenation catalysts due to the easily hydrogen molecules (H_2) dissociation on Pd^0 metal surface catalysts relating to the intrinsic hydrogenation activity [36]. On the other hand, the ability to dissociate hydrogen molecules (H_2) of gold is limited due to the completely filled Au d-band, leading to its lower activity than the group VIII metals [27]. Hence, the combination

between gold (high selectivity, poor activity) and palladium (high activity, poor selectivity) metals has been possible to make an appropriated catalyst for selective hydrogenation reaction.

2.9 Liquid-phase hydrogenation of 1-heptyne

The partial hydrogenation of unsaturated organic compounds is essential for the synthesis of fine chemicals in both of industrial and academic importance in order to form more stable organic products or intermediate compounds. Alkenes are organic products of high industrial value used in the industry of food (flavors), pharmaceutical (vitamins, sedatives), cosmetics (perfumes, fragrances), resins, polymer and lubricants. The examples of alkynic compounds used as model reactants for testing the liquid-phase selective catalytic hydrogenation under mild conditions are 1-hexyne [88, 89], 3-hexyne [90], 1-heptyne [65, 66, 91], 4-octyne [92], phenylacetylene [52, 93], and 1-phenyl-1-pentyne [94].

The liquid-phase hydrogenation of 1-heptyne is shown as follows:

2.10 Gas-phase hydrogenation of acetylene

In the polymerization process, the ethylene feed stream obtained from thermal cracking and steam cracking contains a small quantities of acetylene in the range of <2-30% [34, 95-97]. The presence of acetylene trace in ethylene feed results in the poison to the catalysts used for producing polyethylene such as Ziegler and Ziegler-Natta catalysts because acetylene adsorbs at the active sites for ethylene and then suppresses the polymerization process leading to decline in production of polyethylene [98, 99]. In addition, the acetylene can also form the metal acetylides, which are explosive contaminants [99]. Thus, the trace of acetylene in ethylene feed

should be eliminated or reduced to the acceptable level. For the polymer-grade ethylene, the maximum allowable limit of acetylene in ethylene feed should not be higher than 5 ppm [99]. Due to a small quantity of acetylene in the ethylene feed and the high demand for very high purity ethylene, the separation or removal of acetylene trace from ethylene feed stream is a great challenge to ethylene producer and catalyst manufacture.

The acetylene traces are usually removed in ethylene feed stream by using 2 methods: conversion to ethylene [100], or so-called selective hydrogenation of acetylene, and adsorption with zeolite [101]. The former method is more commonly used for acetylene removal [97].

The gas-phase hydrogenation of acetylene is easily shown as follows:

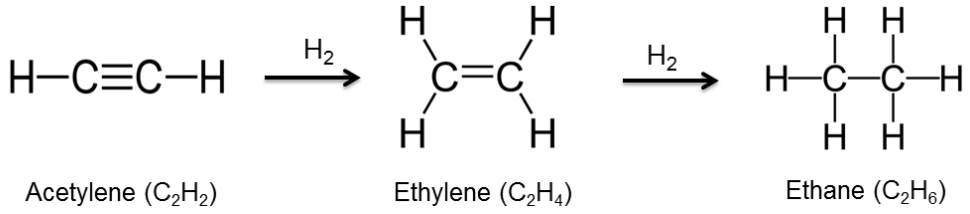

Nevertheless, the selective hydrogenation of acetylene is the sequential reaction. Based on the aim to eliminate the trace of acetylene in ethylene feed, the hydrogenation of acetylene to ethylene is the desired reaction. The desired properties of catalysts for selective acetylene hydrogenation are as follows: high conversion of acetylene with high selectivity to ethylene in order to prevent the over hydrogenation of acetylene (hydrogenation of ethylene to ethane) and long term catalyst stability.

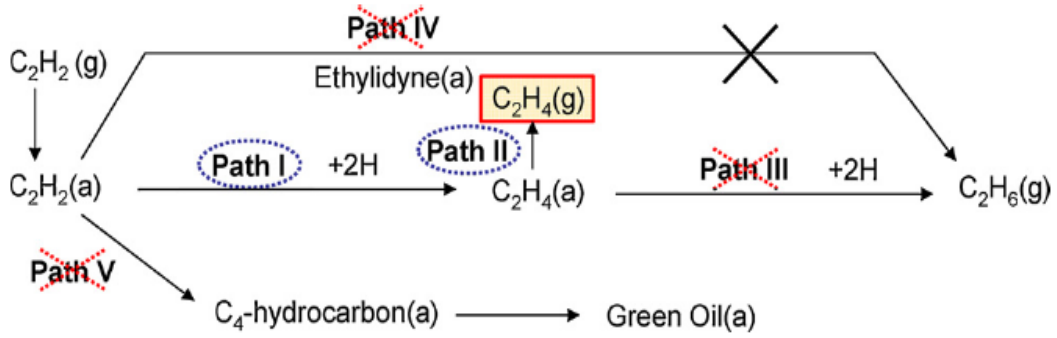

Figure 2.6 Reaction mechanism of selective hydrogenation of acetylene [97]

In order to design or modify the catalyst with improved performance, the reaction mechanism and reaction pathways must be considered. Reaction paths of selective hydrogenation acetylene are shown in **Figure 2.6**. Acetylene is hydrogenated to ethylene in Path I in which this step is called the partial hydrogenation of acetylene to ethylene. However, ethylene formed is either desorbed as ethylene product in gas phase (Path II) or further hydrogenated to ethane (Path III). Based on the aim to eliminate the acetylene, the acetylene conversion can be increased by promoting Path I. In addition, the term of selectivity to ethylene can be improved by increasing Path II and restraining Path III. These two methods are usually used to design the catalyst for acetylene removal in the industrial processes. An alternative way for selectivity improvement by promoting Path II is the addition of a moderator chemical to reaction stream such as CO, which has the ability to adsorb on Pd much stronger than ethylene and then facilitating the desorption of ethylene from the catalyst surface [102]. To suppress the full hydrogenation of ethylene (Path III), a low H_2/C_2H_2 ratio in the feed stream is used to promote the insufficiency in hydrogen concentration at catalyst surface, thus suppressing the further hydrogenation of ethylene [103]. The direct full hydrogenation of acetylene to ethane (Path IV) is insignificant at low partial pressures of hydrogen [104]. In addition, the dimerization of the C_2 species (Path V) can be occurred and produced the green oil accumulation resulting to the catalyst deactivation. According to Path V, the acetylene is consumed upon the dimerization

without producing ethylene indicating to decrease in selectivity to ethylene. Thus, the high performance of acetylene removal could be done by promoting Path I and II and suppressing other paths.

CHAPTER III

LITERATURE REVIEW

3.1 Synthesis of nanoparticles by flame spray pyrolysis

Initially, the flame aerosol technology was started from the well-established vapor-fed flame aerosols reactors which were widely applied in industry for the fabrication of simple materials or commodities such as carbon black, fumed SiO_2, TiO_2, Al_2O_3, and other ceramic nanoparticles [62, 63, 105]. In the last 10 years, the knowledge of FSP process has been developed and is of great potential for the production of nanoparticles, especially metals and mixed metal oxides. Compared to the conventional vapor-fed flame reactors, the FSP process is more attractive because this process can employ a wider array of precursors. It is reported that several types of materials have been successfully synthesized by FSP process. The nano-sized simple oxide materials obtained via flame spray pyrolysis include SiO_2, TiO_2, ZnO, and α-Al_2O_3 [106-109]. The FSP can also produce more complex materials including the multi-component ceramic nanoparticles and multi-component nanophosphor [110]. In the field of catalyst application, the examples of noble metal nanocatalysts prepared by FSP method are Pt/Al_2O_3, Pt/WO_3, $Pt\text{-}Sn/Al_2O_3$, Co/ZrO_2, and V_2O_5/TiO_2 catalysts [111-116].

3.1.1 Synthesis of gold nanoparticles by flame spray pyrolysis

The synthesis of Au nanoparticles supported on TiO_2 and SiO_2 by single-step process in a spray flame reactor (aerosol flame process) was studied by L. Mädler et al., 2002 [64]. The characteristics of flame-made Au/TiO_2 and Au/SiO_2 particles were non-agglomerated, spherical, well-dispersed, and single crystalline. Typically, the nano-sized gold particles show the characteristic of surface plasmon resonance (SPR) in the ultraviolet-visible region. In the case of Au/TiO_2, the position of plasmon absorption band was at 540 nm and red shifted compared to the unsupported gold (522 nm), which indicated to a week interaction between gold and support. Contrary to Au/TiO_2, the red shift of the plasmon absorption for flame-made Au/SiO_2 did not

appear due to the weak interaction between the gold and the amorphous and electronically inert silica support (Silica does not exchange charge with the gold particles.). Moreover, they found that the size of flame-made gold particle did not depend on the metal oxide and surface area of support. Thus, the formation mechanism of gold particles was the homogeneous nucleation of the gold itself before deposition on the metal oxide support, which was formed firstly.

In 2004 [105], the synthesis of Au/TiO_2 catalysts have been employed by using single-step FSP for low-temperature CO-oxidation. The solution of Au and Ti precursors dissolved in n-butanol was atomized with an air-assisted spray nozzle and combusted by hydrogen flame. The quench-cooling was applied to enhance the dispersion of Au particles and the surface area of the support. The flame-made Au/TiO_2 showed the characteristics of mono-dispersed Au particles (2-3 nm) on the aggregated TiO_2 support.

The monometallic Au and bimetallic Au-Ag supported on different supports (TiO_2, SiO_2, Fe_2O_3/Fe_3O_4) prepared by FSP synthesis were investigated by S. Hannemann et al., 2006 [117]. The particle size of monometallic Au catalysts was independent of the metal oxide supports, except for the dispersion. For all the metal oxide supports studied, the Au particle sizes were mainly smaller than 2 nm; furthermore, the average Au particle size was remarkably high when the Au loading increased up to 1 wt.%. For the bimetallization of Au-Ag nanoparticles by flame synthesis, the formation of Au-Ag alloy nanoparticles was achieved. In contrast to the monometallic Au catalysts, the particle size of bimetallic 1 wt.% Au-1 wt.% Ag catalysts depended on the support as follows: iron oxide (2-5 nm), TiO_2 (2-5 nm), and SiO_2 (up to 10 nm). This result implies that the addition of Ag (second metal) resulted in the formation of larger particles (3-10 nm) on SiO_2 or TiO_2.

G. L. Chiarello et al., 2008 [118] investigated the effect of the type of organic solvent/fuel in the synthesis of FSP-photocatalysts (Au/TiO_2). With increasing the combustion heat of the organic solvent, the flame temperature was higher and the rate of particles growth increased, leading to larger particles and lower specific surface area. The FSP-made TiO_2 and Au/TiO_2 photocatalysts consisted of anatase

and rutile phase, while no brookite was detected. The use of carboxylic acids solutions as organic solvents led to a higher rutile content; nevertheless, the use of xylene (an apolar solvent), which has the higher combustion heat than carboxylic acids, revealed a higher anatase content, higher crystallinity, and lower content of crystal defects. It may be postulated that the use of xylene as fuel will produced the higher flame temperature. Furthermore, the gold particle size of the FSP-made Au/TiO_2 was compared to the Au/P25 catalysts prepared by deposition of Au on Degussa P25. It was found that the gold particle size obtained from FSP was smaller than that of deposition. This point indicates to the efficiency of FSP to synthesize the nanoparticles with well metal dispersion on high surface area TiO_2 support.

From a previous research, G. L. Chiarello et al., 2009 [119] synthesized and investigated the 1 wt.% Au/TiO_2 by FSP method with using xylene as organic solvent. The characteristics of Au/TiO_2 obtained from FSP were well dispersed and crystalline micro-aggregated with 1 nm sized Au particles and a few bigger (5-6 nm) Au particles. Moreover, the Au/TiO_2 synthesized from FSP showed more intense of the plasmonic band in visible light adsorption than that of deposition (Au/P25) due to the major role of the fraction of 5-6 nm sized Au particles from FSP while the gold deposited on P25 (Au/P25) with the Au size of 3 nm exhibited the broad plasmonic band.

Besides, the Au-ZnO nanocomposites have been synthesized by FSP for the application of photocatalytic degradation of dyes [120]. The metallic phase of spherical Au particles with averages particle size in the range of 4-7 nm was formed and then deposited on ZnO after the ZnO particles which were already formed during flame synthesis. The addition of Au did not influence the ZnO surface area. For the hydrogen sensor application, W. Chomkitichai et al., 2012 [121] prepared highly crystalline with anatase phase of unloaded TiO_2 and mixed phases between anatase and rutile of Au/TiO_2 nanoparticles by FSP. The spherical unloaded TiO_2 and 0.25-0.75 at% Au/TiO_2 showed the crystallite size of 10-20 nm.

3.1.2 Synthesis of palladium nanoparticles by flame spray pyrolysis

The synthesis of Pd/Al_2O_3 (as hydrogenation catalysts) have been successfully achieved by using FSP process as reported by R. Strobel et al., 2004 [122]. The FSP-derived Pd/Al_2O_3 showed the spherical alumina (10-30 nm) with uniformly dispersed palladium particles (1-5 nm) for 0-7.5 wt.% Pd. The Pd addition did not influence on the specific surface area, morphology or crystallinity of alumina support. The synthesis of FSP-derived Pd/Al_2O_3 (conditions: 3 ml/min of liquid flow rate, 3 L/min of O_2 dispersion gas flow rate) revealed the specific surface area of 120 m^2/g. The FSP-derived Pd/Al_2O_3 catalysts showed high thermal stability; for example, the Pd particle size did not change after pretreatment in flowing H_2 at 500 $^{\circ}C$, and the Pd dispersion was constant up to the pretreatment temperature of 600 $^{\circ}C$; nonetheless, the sintering of Pd would start at temperature higher than 600 $^{\circ}C$. Moreover, the effects of dispersion or sheath gas and liquid flow rate on the specific surface area were also investigated. They found that changing the dispersion or sheath gas (O_2, air, N_2) did not mainly influence the specific surface area, morphology and Pd dispersion due to similar flame heights and particle residence times; however, changing the liquid flow rate (from 6 to 1 ml/min) resulted in different the specific surface area (from 70 to 200 m^2/g). The formation of Pd/Al_2O_3 nanoparticles was considered as follows: the formation of Al_2O_3 particles was occurred earlier owing to much lower vapor pressure of Al_2O_3 than Pd/PdO in the hot flame zone. Further downstream zone of flame with lower temperature, the Pd/PdO was formed to small particles and/or deposited on the Al_2O_3 support.

The bimetallic $Pd\text{-}Pt/Al_2O_3$ nanoparticles was successfully prepared by FSP and the structural properties were investigated by R. Strobel et al., 2005 [123]. After the flame synthesis, the noble metal components (1-5 nm) exhibited as the oxidized state and finely dispersed on the agglomerated alumina support. The alloy formation of bimetallic Pd-Pt supported on Al_2O_3 was occurred after the reduction in hydrogen. Furthermore, the flame-made $Pd/La_2O_3/Al_2O_3$ nanoparticles also have been achieved by FSP synthesis. The small Pd particles (<5 nm) were deposited on the surface of La_2O_3/Al_2O_3 ceramic nanoparticles with the specific surface area of 50-180 m^2/g. The

flame-made catalysts revealed high thermal stability in term of specific surface area up to 1200 ^{o}C and retarded the transformation of **γ** to **α**-Al_2O_3.

S. Somboonthanakij et al., 2007 [65] prepared Pd nanoparticles with average sizes of 0.5-3 nm on SiO_2 supports. The spherical Pd clusters with narrow size distribution were finely dispersed on the surface of SiO_2. The flame-made catalyst presented mostly meso- and macro-pores which facilitate diffusion of the reactants and products. For the flame-made catalysts with low Pd loading (0.5-2 wt.%), the surface of metal may be covered with Si-O groups because of the simultaneous crystallization in gas phase of Pd and SiO_2 during FSP. It indicates that some of the Pd metal surfaces were partially oxidized, whilst the kernel of the Pd particle showed the state of metallic. The formation of Pd/SiO_2 nanoparticles by FSP was as follows: the precursor solution was dispersed forming sprayed droplets, evaporated and combusted at very high temperature of flame. The metal atoms were released and started to form particles by nucleation, coagulation and condensation along the axial direction of flame. The formation of SiO_2 particle started earlier because the vapor pressure of Pd/PdO was higher than SiO_2 in the hot flame zone. Further downstream of the flame (at lower temperature), the small particles of Pd/PdO were formed and deposited on the SiO_2.

Different Al_2O_3-supported noble metal catalysts (Ru, Pd, Pt, Rh) with the metal loadings in the range of 0.1-10 wt.% were prepared as reported by S. Hannemann et al., 2007 [124]. For the catalyst preparation, this study used the precursor solutions based on $Al(acac)_3$ and methanol-acetic acid instead of xylene because they were advantageous in case of volatile metal oxides owing to the lower flame temperature; moreover, they showed the better stability and also were less sensitive to air/moisture than xylene. This indicates to the effect of precursor solutions on the stability and combustibility. The yield of catalysts from FSP process was about 0.5 g during the preparation time of 30 min. The noble metal loadings were fully recovered without losing (absolute deviation about ±0.03% to ±0.24%) indicating to the advantages of FSP method to efficiently control the composition of multi-component catalysts. The particle sizes of well-dispersed noble metals (Rh, Ru,

Pd and Pt) supported on Al_2O_3 and Al_2O_3 support were about 2 nm and 10 nm, respectively. Furthermore, the obtained catalysts showed relatively high surface area because of the rapid quenching of the combustion temperature; however, the high temperature has a limitation which can lead to the undesired structural transformations that can be added by secondary quenching. After reduction, the formation of alloyed noble metal particles was occurred. Consequently; the FSP method is the feasible approach and attractive alternative for the preparation of multi-metallic catalysts within single step.

G. L. Chiarello et al., 2007 [125] presented that the synthesis of perovskite supported noble metal ($Pd/LaCoO_3$) was successful by using the FSP method. The FSP-made materials exhibited high specific surface area (106 m^2/g), structure of perovskite and the aggregation of single nano-crystal spheres (5-10 nm). For the catalytic reaction test ($NO/H_2/O_2$ reaction), the FSP-made $Pd/LaCoO_3$ catalysts showed the higher catalytic activity and durability than corresponding catalysts prepared by the traditional method (impregnation). This may be because of the higher Pd dispersion of FSP-made $Pd/LaCoO_3$ catalysts. In fact, from the FT-EXAFS analysis, the FSP-made $Pd/LaCoO_3$ presented more surface atoms and smaller particle size than that of impregnated catalysts.

C. Siriwong et al., 2008 [126] prepared Pd-doped ZnO nanoparticles (0.25-1.0 mol% Pd) from FSP process by using zinc naphthenate and palladium(II) acetylacetonate as Zn and Pd precursor solutions, respectively. The FSP-made pure ZnO and Pd-doped ZnO were highly crystalline and exhibited the similarity of intensity and sharpness in diffraction patterns, indicating that the doping with Pd did not affect the structure of ZnO crystallinity. Furthermore, it was found that low amount of Pd loading did not affect the ZnO particle size which was about 23 nm for all samples. The structure of FSP-made Pd-doped ZnO was found to have the spherodical, hexagonal and rod-like morphologies. For the crystallite size of each of ZnO morphology, the spheroidal and hexagonal ZnO particles revealed the crystallite size in the range of 5-25 nm, but the rod-like ZnO particles revealed the ranging from 10-20 nm in width, 20-40 nm in length. C. Liewhiran et al., 2008 [127]

was successful in the production of the FSP-made 0-5 mol% Pd/ZnO nanoparticles used as the ethanol gas sensors by FSP process. The characteristic of FSP-made Pd/ZnO was similar to that of C. Siriwong et al., 2008 [126].

The characteristics and catalytic properties of the FSP-made Pd/SiO_2 (single step synthesis) were investigated and compared to the conventional impregnation of Pd on FSP-made SiO_2 (two step synthesis) as published by O. Mekasuwandumrong et al., 2009 [66]. The FSP-made Pd/SiO_2 with prepared in single step exhibited the better Pd metal cluster dispersion on the SiO_2 support. The FSP-made Pd/SiO_2 catalysts revealed polyhedral SiO_2 primary particles in size of 10-20 nm and Pd^0 metal with average diameter of 0.5-3 nm for Pd loadings of 0.5-10 wt.%. Whereas, for the impregnated catalysts, the average crystallite sizes of PdO were larger in the range of 5-12 nm for Pd loadings of 0.5-10 wt.%. As the Pd loadings increased from 0 to 5 wt.%, the BET surface areas of FSP-made catalysts increased from 195 to 305 m^2/g and remained constant although Pd loading increased up to 10 wt.%. The pore volumes were not significantly altered (ca. 0.5 cm^3/g) as the Pd loading increased and the typical for mesopore structure was observed. For the impregnated catalysts, a decrease in the BET surface areas (from 196 to 128 m^2/g) with increasing Pd loading was found probably because of sintering during the calcination process and pore blockage of Pd/PdO clusters. Nevertheless, increase in the BET surface areas with increasing Pd loading is possible for the catalysts with prepared by single step FSP. With the Pd addition, the surface area of the SiO_2 support increased as the particle size decreased, indicating to the inhibition of the growth of the SiO_2 support. For the FSP-made catalysts, the Pd particles were in partially oxidized state of PdO and may be surrounded by a support matrix with in the form of Si-O group which the interaction between the Pd and the SiO_2 support was stronger than that of impregnated catalysts. The better catalytic performances and high turnover frequency (TOF) values for selective hydrogenation of 1-heptyne of FSP-made Pd/SiO_2 compared to the impregnated catalysts were due to the formation of active ensembles of Pd in the SiO_2 matrix during FSP.

N. V. Vegten et al., 2009 [128] investigated the characteristic structural features of the FSP-derived Pd catalysts based on different metal oxide supports (Al_2O_3, SiO_2, ZrO_2, TiO_2, $MgAl_2O_4$, and CeO_2). The characteristics of the FSP-made Pd/MO_x catalysts have been elucidated as follows: (i) the non-porous structure; (ii) the embedding of some Pd in the bulk of the metal oxide support; (iii) amount of PdO in the range of 13-60% for as-prepared FSP-made catalysts, (iv) higher resistance sintering for FSP-made 9.1 wt.% Pd/Al_2O_3 compared to the commercial catalysts. The superior stability of the FSP-made catalyst was advantageous for catalytic methane combustion, resulting in the higher catalytic activity after one cycle. Besides, this study illustrates to the formation of noble metal deposited on the support during FSP. The noble metal will occur the nucleation after the support has been formed, and then interacts with the metal oxide support in the colder downstream flame in a stage where the formation of particle is not yet complete.

The synthesis of Pd/TiO_2 nanoparticles (Pd loadings 0.5-10 wt.%) by one step FSP has been reported by O. Mekasuwandumrong et al., 2010 [67]. The FSP-made catalysts consisted of aggregated spherical primary particles with average size of 10-45 nm and small Pd/PdO particles which were confined in the TiO_2 matrix. The typical phases of TiO_2 obtained from FSP were anatase phase with small amount of rutile phase. The interparticle voids in the FSP-made catalysts resulted in the macropore structure with large pore size. With increasing Pd loading, the increase in BET surface area was occurred in the FSP synthesis unlike the conventional impregnation method. During the FSP process, the simultaneous crystallization of Pd and TiO_2 in gas phase led to the covering of TiO_2 support on the Pd particles forming the Ti-O groups. Some of the Pd metals on catalyst surface were partially oxidized, while the kernel of the Pd particles was metallic. Compared to the impregnation of Pd on the FSP-made TiO_2, the FSP-made Pd/TiO_2 exhibited the better catalytic performances (higher selectivities to 1-heptene at complete 1-heptyne conversion) for the liquid-phase selective hydrogenation of 1-heptyne. These results were attributed to the stronger interaction between the Pd particles and the TiO_2 support obtained by FSP process.

From the previous study, O. Mekasuwandumrong et al., 2011 [68] studied the influence of flame conditions on the 5 wt.% Pd/TiO_2 synthesized by FSP method. The nanocrystalline Pd/TiO_2 catalysts with crystallite sizes of 9.7, 15.7, and 24.6 nm were synthesized under different flame conditions (precursor concentration, feed flow rate, and O_2 dispersing gas). With increasing the precursor concentration and the feed flow rate as well as decreasing in O_2 dispersion gas resulted in increasing the particle size. The formation of single crystal during FSP process was observed, especially TiO_2 with average size of 10 to 26 nm. As the crystal size of catalyst increased, the decrease in BET surface area, pore volume, and anatase phase content was found because the longer residence times in the flame at high temperature resulted in sintering and phase transformation. The amount of Pd active sites depended significantly on the FSP conditions though all catalysts were prepared with the same Pd loading. Furthermore, this work found that the shorter residence time in flame and/or the lower combustion energy led to not only the smaller crystallite size of TiO_2 but also the smaller Pd/PdO particles which could be easily covered by the Ti-O groups, resulting in the lower amount of active Pd surface.

J. Huang et al., 2011 [129] applied the single-step FSP synthesis to prepare the Pd nanoparticles supported on SiO_2-Al_2O_3. The acidity of the SiO_2-Al_2O_3 support could be easily tuned by adjusting the Si/Al ratio in the precursor solutions fed to the flame. For the Pd nanoparticles on the pure SiO_2 support, the non-acidic silanol groups were observed while the Pd nanoparticles were located in the vicinity of SiOH groups and blocked interactions between the silanol groups. The aluminum addition led to Brønsted acid sites due to aluminum atoms in the vicinity of SiOH groups. The concentration of Brønsted acid sites increased with the aluminum content up to 70 at%. The tuning of the support acidity resulted in the changing of the electronic properties of the supported Pd nanoparticles.

For the application of ultra-sensitive H_2 gas sensors, C. Liewhiran et al., 2013 [130] synthesized the Pd-loaded SnO_2 nanoparticles by one-step FSP process. The FSP-made Pd-loaded SnO_2 crystalline nanoparticles with high specific surface area and well-controlled size were successfully achieved. The addition of Pd loading up

to 2 wt.% had little effect on the phase (cassiterite-tetragonal phase), crystal structure as well as crystallinity of the FSP-made SnO_2 nanoparticles, but the size of the FSP-made SnO_2 did not depend on the amount of Pd loading. However, the amount of Pd loading significantly affected the BET specific surface area. At low Pd loading (0.2 wt.%), the fine Pd particles were uniformly dispersed and attached on the surface of SnO_2 nanoparticles, leading to high specific surface area. Whereas, at high Pd loading, the agglomeration of small deposited Pd particles was occurred and resulted in poor Pd dispersion on the SnO_2 support, leading to decrease in specific surface area.

3.2 Preparation of bimetallic AuPd nanoparticles supported on TiO_2

The characteristics and properties of catalyst are very sensitive to the preparation method. For the bimetallic AuPd catalyst, many studies attempted to synthesize the bimetallic catalysts from various methods such as impregnation, precipitation, sol-immobilization, and so on.

3.2.1 Impregnation

The basic catalyst preparation with impregnation is widely used to synthesize the bimetallic Au-Pd catalysts. From the literature reviews, the bimetallic Au-Pd catalysts were prepared by impregnation preparation method including wet impregnation and incipient wetness impregnation.

3.2.1.1 Incipient wetness impregnation

All of the AuPd/TiO_2 nanoparticles prepared by incipient wetness impregnation method were alloy nanoparticles with the gold rich core and palladium rich shell morphology [20, 23, 131]. The AuPd/TiO_2 catalysts prepared via incipient wetness impregnation revealed the bimodal metal particle size distribution. The particle size distribution of 2.5 wt.% Au-2.5 wt.% Pd/TiO_2 has been reported by J. K. Edwards et al., 2005 [12]. For the uncalcined 2.5 wt.% Au-2.5 wt.% Pd/TiO_2, the bimodal particle size distribution consisted of most of the smaller particle size with 1-8 nm in size and a few larger particles with 40-70 nm in size. The larger particles all consisted of Au-Pd alloys; in contrast, the smaller particles consisted mainly of pure

Au and a very small fraction of pure Pd. Meanwhile, the bimodal particle size distribution of calcined 2.5 wt.% Au-2.5 wt.% Pd/TiO_2 was similar to the uncalcined catalysts. Most of particles were in the smaller particle size distribution with 2-10 nm, and most of the larger particle size ranged in 35-80 nm. Moreover, a few particles greater than 120 nm were found. All of the large particles contained alloy of Au-Pd, but pure Pd particles were observed in all of the smaller particles. Similar to N. F. Dummer et al., 2010 [23], the 2.5 wt.% Au-2.5 wt.% Pd/TiO_2 catalysts exhibited the dispersions of nanoparticles in the size range of 2-50 nm with most particles in the 8-10 nm particle diameter.

For the H_2O_2 synthesis, J. K. Edwards et al., 2007 [132] found that the AuPd/TiO_2 catalysts prepared by using incipient wetness impregnation method and calcined at 400°C are much more active for the H_2O_2 synthesis than precipitation method. Moreover, The heat treatment (calcination at 400°C) will improve the stability of catalyst by preventing the leaching of Pd and Au and inhibiting the catalyst deactivation with reuse [12]. While the uncalcined catalysts and catalysts calcined at 400°C were unstable and exhibited the loss of Pd and Au and a decrease in activity in subsequent reuse tests.

3.2.1.2 Wet impregnation

The catalysts obtained from impregnation method showed the structure of Au core-Pd shell because of the calcinations step [20, 40, 55, 133, 134]. It has been reported [20] that the calcinations at 400 $^{\circ}$C can generate stable re-useable catalysts inhibiting Au and Pd leaching. The Au-Pd/TiO_2 catalysts prepared by wet impregnation had a broader particle size distribution (mainly in 2-5 nm range with >20 nm larger particles) and greater particle size than sol-immobilisation method [40, 56]. As reported from other studies [55], the obtained catalyst appeared the bimodal particle size distribution consisting of Au with larger particles in size range of 20-80 nm and Pd with smaller particles in size range of 2-8 nm; in addition, no strong alloying of Au or Pd were shown in nanoparticles. D. I. Enache et al., 2006 [20] reported that the catalysts with calcined at 673 K were stable than the uncalcined catalysts, indicating that the catalyst stability could be improved by the heat

treatment. During the calcination, the Pd surface segregation occurred to produce the alloy nanoparticles when the oxide was used as the support.

However, the effect of acidic pretreatment of TiO_2 over Au-Pd/TiO_2 prepared by using wet impregnation has been studied [133]. The results demonstrated that the acidic pretreatment of TiO_2 support prior to loading the metals did not affect the Au rich core- Pd rich shell morphology of Au-Pd alloy nanoparticles, but this effect could efficiently increase the gold dispersion resulting in the enhanced proportion of smaller Au-Pd nanoparticles.

3.2.2 Deposition-precipitation

The precipitating agents used in the deposition-precipitation method were sodium carbonate [55, 56], ammonia [22], sodium hydroxide [135], and urea [136]. A. Zwijnenburg et al., 2002 [22] chose the deposition-precipitation method by using ammonia as precipitating agent to prepare the bimetallic Pd-Au and Pt-Au catalysts for propene epoxidation. Both catalysts exhibited homogeneous distribution of metal particles in the size up to 5 nm. While Z. Gu et al., 2007 [135] reported about the crystallite size of Au in AuPd/Al_2O_3 and Au-Pd/TiO_2-Al_2O_3 catalysts which used sodium hydroxide in the deposition precipitation method was about 3.3 and 2.4 nm, respectively.

J. A. Lopez-Sanchez et al., 2011 [136] used the urea as precipitating agent instead of sodium hydroxide. The use of urea afforded the deposition of the total nominal metal loading on the support with retaining small particle size about 2-5 nm. Nonetheless, when urea was used, the pre-treatment heating step following synthesis was necessary to remove the organic precursor residues deposited on the support, the ligands on the metal nanoparticles, and residual urea residues. The pre-treatment heating step in the temperature range of 120-400°C did not affect the catalytic performance of TiO_2-supported catalysts for benzyl alcohol oxidation. These reasons could be attributed to the strong metal-support interaction of TiO_2-supported catalyst, which inhibits the sintering of nanoparticles. Additionally, the alternative way to obviate the need for pre-treatment heating step was the

treatment with $NaBH_4$ of the Au-Pd/TiO_2 synthesised by deposition-precipitation, which can lead to increase the formation of small Au-Pd nanoparticles having a narrow particle distribution.

Form P. J. Miedziak et al., 2011 [55, 56], the bimetallic Au-Pd/TiO_2 catalysts were synthesized by the deposition precipitation method using sodium carbonate. The conditions of deposition-precipitation method between setting the pH constant at 8 all over the preparation and raising the pH to 8 during precipitation were also investigated. No bimodal particle size distribution and no large particle, especially Au, were observed in both conditions; in addition, all nanoparticles were found to have high degree of AuPd alloys (2-10 nm) with Au core-Pd shell morphology formed during calcinations step and more Au dispersion compared with catalysts prepared by impregnation. However, these different conditions led to significant difference in metals concentrations at surface. The catalyst prepared with raising the pH exhibited a higher metals surface concentration before calcinations. On the calcinations step, the decreasing in metals surface concentration was found possibly on account of sintering, particularly the catalyst prepared with raising the pH.

3.2.3 Impregnation/deposition-precipitation

The bimetallic catalyst can be prepared by using more than one preparation method. For example, Au-Pd/TiO_2 catalysts were prepared by using impregnation and deposition-precipitation preparation methods [19]. Gold supported catalysts were deposited by deposition-precipitation method, while palladium supported catalysts were prepared by impregnation method. Either gold or palladium can be firstly loaded onto support and then followed by loading another metal. The different sequential metal loadings affected the structure of obtained catalysts. The bimetallic catalysts with prepared by Au loading prior Pd (Pd-Au/TiO_2) exhibited a core-shell morphology with Au-rich core and Pd-rich shell. In contrast, the structure of Pd-rich core and Au-rich shell was found in the bimetallic catalysts with prepared by Pd loading prior Au (Au-Pd/TiO_2). The bimetallic catalysts preparation with Au loading prior Pd gave the smaller nanoparticles (10-12 nm) than Pd loading prior Au (12-16 nm). Additionally, it has been found that the reduction process in the bimetallic

catalyst prepared by loading Pd onto Au/TiO_2 resulted the formation of larger Pd-Au alloy particles with Au-rich on surface; however, the core-shell structure was not observed in this study [35]. Furthermore, the impregnation of Pd onto Au deposited on TiO_2 showed the individual Pd and Au particles on TiO_2 suggesting to no interaction between Pd and Au [34].

3.2.4 Sol-immobilization

The sol-immobilization preparation method can control the particle size distributions and composition of the catalyst [137]. The main advantage of sol-immobilization preparation method is to minimize the large particles formation (> 10 nm) which is usually obtained from impregnation method. L. Kesavan et al., 2011 [137] found that the sol-immobilized nanoparticles showed the characteristic of homogeneous Au-Pd alloys and particle size of 2.9 nm. The Au-Pd particles through the low-temperature drying step showed an increase of particle size (3.9 nm). Corresponding to other studies [56, 136, 138, 139], the Au-Pd nanoparticles were typical homogeneous alloys, and the particle size of Au-Pd alloy was around 3.8 nm on TiO_2 support. Moreover, the sol-immobilization method resulted in a narrower particle size distribution compared to the deposition-precipitation and impregnation method [56]. Nevertheless, the pre-treatment step is necessary to remove the stabilizing ligands for the sol-immobilized materials, preventing the bock of the active sites. E. Cao et al., 2011 [140] proved the efficiency of this method that all metals were immobilized onto support, confirming no metal ions in filtrate solution.

A. Beck et al., 2007 [141] synthesized the bimetallic AuPd nanoparticles on TiO_2 by deposition of bimetallic aqueous sols formed in different 3 ways: (i) co-reduction of the precursor Au and Pd ions by Na-citrate/tannic acid mixture, (ii) reduction of Au(III) ions onto performed Pd sol, and (iii) reduction of Pd(II) ions onto performed Au sol. It was found that the Au/Pd ratio in sol-derived AuPd/TiO_2 catalysts differed significantly in the different 3 preparation ways. The calcination/reduction treatment for removal of organic residues caused the effect on the crystallite and the metal particle size, resulting in increased the metal particle size and broadened particle size distribution; moreover, the calcination step led to

some Pd migration to the surface, but this treatment did not affect the composition of the bimetallic crystalline phase.

3.2.5 Others

The bimetallic AuPd supported on TiO_2 nanoparticles synthesized by the other preparation methods such as redox reaction [34, 142], encapsulation [58], and microwave-assisted method [59] were also reported.

3.3 Gold-palladium catalysts for the liquid-phase hydrogenation of alkynes

The bimetallic Au-Pd nanoparticles have much attraction in many fields of catalytic processes. The typical applications for the use of bimetallic Au-Pd nanoparticles include oxidation of CO [136], hydrodesulfurization [15], synthesis of vinyl chloride [13], selective oxidation of alcohols to aldehydes or ketones [21], selective oxidation of alkenes to epoxides [143], synthesis of H_2O_2 [43], and selective hydrogenation [6].

For the selective hydrogenation of alkyne over bimetallic Au-Pd nanoparticles, the previous researches mainly focused on the gas-phase selective hydrogenation, especially acetylene. Conversely, the study about the liquid-phase hydrogenation of alkynes over bimetallic Au-Pd catalysts is rarely reported.

Table 3.1 Examples of bimetallic Au-Pd nanoparticles for liquid-phase hydrogenation

Substrate	Catalysts	Comments	Ref.
1-Heptyne	$Au/Pd/TiO_2$ (IM of Pd followed by DP of Au)	- Formation of small Au-Pd alloy particles - Changing the Pd electronic properties - The 2nd step 1-heptene hydrogenation was promoted - The heptene hydrogenation was more sensitive to electronic effect than 1-heptyne	[144]
	$Pd/Au/TiO_2$ (DP of Au followed by IM of Pd)	- Unclearly alloy formation - Large Au aggregates (30-50 nm) - Similar to Pd/TiO_2	
1-Octyne	$Pd\text{-}Au/SiO_2$ (simultaneous impregnation)	- Alloying Au-Pd - Air-treatment of catalysts resulted in increased activity for 1-octene hydrogenation, attributing to surface carbon removal - The rate of 1-octyne hydrogenation was unaffected by treatment	[145]
Citral	$Au\text{-}Pd/TiO_2$ (Co-impregnation) $Au/TiO_2+Pd/TiO_2$ (Physical mixing)	- The catalytic activity and selectivity to citronellal was enhanced due to synergistic effect between Au and Pd for physically and chemically mixed Au and Pd bimetallic catalysts	[6]
Cyclohexene	Au@Pd bimetallic catalyst (Seeding growth technique)	- Au Core- Pd shell structure - High catalytic activity due to synergy effect of Au and Pd - Better reusability (4 times) than commercial Pd/C	[146]

Substrate	Catalysts	Comments	Ref.
3-Hexyn-1-ol	Pd-Au alloy colloids embedded in SiO2 sol-gel matrix	- Alloying Pd with Au in bimetallic colloids - The increased catalytic activity and improved selectivity was obtained - Very stable against poisoning	[147]
Allyl alcohol 1,3-Cycloocta-diene Cinnamaldehyde 3-Hexyn-1-ol	PdAu nanoparticles solubilized in 1-butyl-3-methyl-imidazolium hexafluorophos-phate ionic liquid with poly (vinyl-pyrrolidone) as stabilizer	- Varying the Au-Pd composition, both the activity and selectivity of hydrogenation reactions could be tuned. - Good activities for the hydrogenation of these substrates - With high Pd loadings, the highest catalytic activities were obtained.	[148]

3.4 Catalysts used for liquid-phase selective hydrogenation of 1-Heptyne

A few studies dealing with the liquid-phase selective hydrogenation of 1-heptyne has been studied under mild reaction conditions. The reaction results of the liquid phase 1-heptyne hydrogenation in the literature are summarized in **Table 3.2**.

Table 3.2 Comparison of the catalytic activity of catalysts in the liquid-phase hydrogenation of 1-heptyne under mild conditions

Catalysts	Preparation	Reaction condition	Time (min)	Conv (%)	Selec (%)	Yield (%)	Ref.
0.4%Pd-2.4%W/γ-Al_2O_3reduced 120 ^{o}C	IMP	303 K,150 kPa	30	18	98	18	[149]
			180	100	98	98	
0.4%Pd/Al_2O_3	IMP	303 K, 150 kPa	30	10	95	9.5	[150]
			150	18	98	18	
0.4%Pd-1%Ni/Al_2O_3			30	13	96	12	
			150	30	98	29	
Lindlar	Commercial		30	5	88	4	
			150	45	81	36	
[$PdCl_2(NH_2(CH_2)_{12}CH_3)_2$]/ γ-Al_2O_3	IMP	303 K, 150 kPa	n/a	90	63	57	[151]
0.5%Pd-1%Au/TiO_2	IMP/DP	303 K, 1 bar	10	73	96	70	[152]
			30	100	55	55	
1%Pd/TiO_2	FSP	303 K, 1 bar	5	80	94	75	[67]
			40	100	90	90	
1%Pd/SiO_2	FSP	303 K, 105 kPa	5	43	92	40	[153]
			40	100	62	62	
1.61% WO_x/Al_2O_3	IMP	293-323 K, 1.4 bar	150	100	-	-	[154]
4%Ni/Al_2O_3	IMP	323 K, 1.4 bar	150	100	-	-	[24]
0.4%Pd/Al_2O_3			90	100	-	-	
1.62%Pd/AC	IMP	303 K, 150 kPa	150	100	58	58	[155]
1.71%Pt/AC			240	97	64	62	
1.28%Ru/AC			240	71	77	55	
5%Pd/Al_2O_3	IMP	303 K, 150 kPa	240	92	87	80	[91]
5%Pd/C			240	62	93	58	
Lindlar catalyst (5%Pd on calcium carbonate poisoned with lead)	Commercial		240	74	-	-	

Conv: Conversion, Selec: Selectivity, FSP: Flame spray pyrolysis, IMP: Impregnation, DP: Deposition

For the commercial catalyst, the catalytic performance of classic Lindlar catalyst has been reported to be very low (5-45 %conversion with reaction time up to 150 min) [150]. Moreover, the Lindlar catalyst has the limitations and difficulty in operating because it cannot be pelletized and must be performed under slurry conditions; thus, the reactant solution must be purified after reaction by the expensive procedure to recover the catalyst [91]. Typically, Pd catalyst has been well-known and mainly considered as a metal catalyst used for hydrogenation of 1-heptyne. However, several works studied and tried to investigate the catalytic performance of Pd-based catalyst for hydrogenation of 1-heptyne in comparison with other metals as follows:

M. J. Maccarrone et al., (2012) [24] investigated the comparison between Pd and Ni catalysts. It could be clearly seen that Ni was less active than Pd due to its more electron deficient, resulting in weak adsorption of alkyne. In addition, C. R. Lederhos et al., (2013) [155] suggested that the different activities between Pd, Pt, and Ru supported on activated carbon were attributed to a different electronic density in the external d orbital of metal. The cleavage of hydrogen bond was more easily occurred on the metal with highest amount of d electron (i.e, Pd), leading to higher hydrogenation activity, and more difficultly on the metal with lower amount of d electron (Pt and Ru).

Not only the conventional form of Pd or Pd oxide catalysts, a palladium complex with chloride and tridecylamine as ligands supported on γ-Al_2O_3 prepared as a heterogeneous catalyst was found to be more active and selective than the classic Lindlar catalyst due to electronic and geometric effects [151]. Thus, it can be seen that the Pd-based catalyst has been proved as the suitable hydrogenation catalyst for 1-heptyne hydrogenation; however, the other catalysts such as tungsten oxide were investigated for selective hydrogenation of 1-heptyne as reported by M. Maccarrone et al., (2012) [154]. The cheaper catalyst based on low W loading (1.61% WO_x/Al_2O_3) was active and selective for hydrogenation of 1-heptyne, but the reaction time for requiring 100% conversion was longer more than 120 min.

Regarding the effect of support for Pd-based catalysts, C. R. Lederhos et al., (2005) [91] compared the monometallic Pd/Al_2O_3, Pd/C, and the classic Lindlar catalysts. In addition, Pd as an electron-deficient species for Pd/Al_2O_3 and Pd/C did not promote the over hydrogenation of 1-heptene to heptane because the interaction between Pd^0 and 1-heptene was inhibited by an electronic effect, decreasing its electron-donor character. The electron-deficient Pd species was positive view for selectivity, although they were less active for hydrogenation of 1-heptyne. In term of support, the different catalytic behaviors of Pd/Al_2O_3 and Pd/C were attributed to the different porosities of support. Due to the planar end characteristic of 1-heptene, the using C as a support resulted in the location of active Pd species in narrow pores; hence, the heptane formation will be hindered leading to increase in selectivity. However, at the same time, the narrower porosity of activated carbon could suppress the 1-heptyne conversion because fewer 1-heptyne molecules could reach the Pd active sites deposited in the supermicropores.

Accordingly, the catalyst performances of Pd-based catalysts have been improved for the liquid-phase hydrogenation of 1-heptyne under mild conditions. The second metal addition such as W, Ni, and Au was an alternative way to modify the Pd-based catalysts [149, 150, 152] as follows:

C. R. Lederhos et al., (2010) [150] modified the catalytic performance of low-loaded Pd catalysts for selective hydrogenation of 1-heptyne by adding Ni as a second metal. The Ni addition as promoter for the Pd monometallic catalyst would modify the conversion without changing the high selectivity of Pd. The activity improvement was due to the modification of electronic state of Pd to more electron-deficient with increasing Ni loading. While the high selectivities of Pd monometallic and PdNi bimetallic catalysts were attributed to the disappearance of the β-PdH phase.

After that, the addition of a second metal in order to improve both of activity and selectivity was successful such as the W addition as reported by C. R. Lederhos et al., (2011) [149]. For each monometallic catalyst, low loaded Pd monometallic catalyst exhibited high selectivity but low activity, while W monometallic catalyst

was active but less selective. The addition of a second metal to form PdW or WPd catalysts could greatly improve the activity compared to Lindlar catalyst. Especially the addition of Pd to W/γ-Al_2O_3 catalyst improved not only the activity but also selectivity. This was because the interaction between d and f electron orbitals of Pd and W would favor the formation of Pd-WO_x/Al_2O_3 highly active interface with highly exposed Pd atoms.

P. Kittisakmontree et al., (2013) [152] investigated the Au addition as a second metal to form the bimetallic Au-Pd/TiO_2 catalysts by using the combination of impregnation and deposition methods. The hydrogenation rate was dependent on the number of exposed Pd atoms in the bimetallic Au-Pd/TiO_2 catalysts without the electronic modification. However, in the case of the bimetallic Au-Pd/TiO_2 catalysts with the presence of AuPd alloy, the Au would act as an electronic promoter for Pd which favored the hydrogenation of 1-heptene to heptane. Furthermore, the hydrogenation of 1-heptene was found to be more sensitive to the electronic effect that that of 1-heptyne.

Comparison the second metal addition in **Table 3.2**, the presence of Au and W over Pd-based catalysts demonstrated markedly high conversion and high selectivity, especially Au addition that took shorter reaction time [152].

For the FSP synthesized Pd-based catalysts, the monometallic Pd supported on SiO_2 and TiO_2 catalysts prepared by FSP synthesis were tested in the selective hydrogenation of 1-heptyne [67, 153]. The preparation by FSP synthesis resulted in the large pores, thus facilitating the diffusion of reactants and products. According to S. Somboonthanakij et al., (2007) [153], the as-synthesized FSP catalysts showed higher catalytic activity compared to conventional prepared Pd/SiO_2 so that the further pre-treatment was not necessary. The TOF of FSP synthesized Pd/SiO_2 decreased with increasing Pd particle, indicating that the 1-heptyne hydrogenation activity was dependent on Pd dispersion. In addition, O. Mekasuwandumrong et al., (2010) [67] found that the better catalytic performances of FSP synthesized Pd/TiO_2 catalysts were suggested to be due to the strong interaction between very fine Pd particles and TiO_2 support upon FSP synthesis.

3.5 Gold and palladium catalysts for the gas-phase hydrogenation of acetylene

3.5.1 Au-based catalysts

Gold (Au) is typically considered as a chemically inert metal. Interestingly, the Au nanoparticles less than 5 nm have been found to be very effective catalysts for several chemical reactions such as CO oxidation, ethylene hydrochlorination, selective partial oxidation, water gas shift reaction, and hydrogenation [156-158]. This suggests that the particle size of Au metal is dramatically responsible for the catalytic properties of Au [159]. Although many works dealing with Au catalysis have been published, the origin of the active sites of supported Au nanoparticles is still highly under debate because of their complex nature.

For the acetylene hydrogenation, Au nanoparticle catalysts need to be in a highly dispersed form to be active for the acetylene hydrogenation reaction. Well-dispersed Au catalysts exhibited high selectivity to ethylene but the acetylene conversion (activity) and catalyst stability were inferior to the Pd-based catalysts [32, 34]. The Au catalysts would be active for acetylene hydrogenation but the conditions have been performed under higher temperature, higher H_2/C_2H_2 ratio and higher contact time [34]. According to T.V. Choudhary et al.[34], the 0.95 wt.% Au/TiO_2 catalysts could be active for acetylene hydrogenation at 180 °C and H_2/C_2H_2 ratio of 4; however, Au catalysts were still not stable and occurred the continuous deactivation with time. This deactivation of Au catalysts in the acetylene hydrogenation might be attributed to sintering of the Au particles or poisoning by carbon.

Jia et al. [32] reported that Au/Al_2O_3 with the particle size 3 nm of Au exhibited extremely high selectivity to ethylene under the reaction temperature range of 323-523 K. Moreover, 100% selectivity to ethylene was found to occur over 1.95 wt.% Au/CeO_2 (Au particle size 2 nm) at the temperature below 573 K [160]. As reported by Sárkány et al. [161], the hydrogenation activity for Au catalysts essentially followed the Au particle size: smaller Au particle size was more active than that of larger ones. The selectivity to ethylene for Au catalysts depended on the reaction temperature. High selectivity was obtained at $T<473$ K, while selectivity was

decreased upon ethane formation at T>500 K. Comparing between TiO_2 and SiO_2 supports, the Au/SiO_2 showed higher selectivity to ethylene.

3.5.2 Pd-based catalysts

Pd-based catalysts have been well-known as the best catalyst for the partial hydrogenation of highly unsaturated compounds. Industrially, Pd-based catalysts are typically applied for selective hydrogenation of acetylene to remove or reduced them to acceptable levels (ppm) [162, 163]. They exhibited much higher catalytic performance for selective hydrogenation of acetylene—higher activity for acetylene removal—than that of other catalysts such as Pt/Al_2O_3 [164]. Despite their superior activity, Pd-based catalysts have limitations; they showed low selectivity to ethylene at high acetylene conversion [34, 165]; moreover, Pd catalysts have been reported to be deactivated largely because they tended to form oligomers leading to the green oil accumulation on the Pd active sites [97]. Low selectivity to ethylene at high acetylene conversion suggests that not only acetylene is hydrogenated, but also a large amount of ethylene is also hydrogenated at the same time resulting in the waste of feed gas (ethylene). The low selectivity to ethylene has been attributed to a very strong adsorption of both the reactants and the products on Pd active sites [162].

In order to improve the selectivity to ethylene of Pd catalysts, the contact of Pd with the reactants and products should be reduced by diluting Pd with a second metal [162]. In addition, Au metal is a good candidate as the second metal added to the supported Pd catalyst. The interaction between Au and Pd is expected to be beneficial to catalytic performances for selective hydrogenation of acetylene.

3.6 Catalysts used for selective hydrogenation of acetylene in excess ethylene

Several works dealing with catalytic selective hydrogenation of acetylene have been investigated under the condition of feed gases without ethylene feed such as the feed gases mixed with only acetylene and hydrogen. However, based on industrial process, the acetylene trace is mixed in the excess ethylene feed stream obtained from thermal cracking and steam cracking. Consequently, the study should

be performed under the reaction condition in which the feed gases are similar to the industrial condition—selective hydrogenation of acetylene in the excess ethylene.

Table 3.3 Comparison of the catalytic activity of catalysts in the gas-phase hydrogenation of acetylene in excess ethylene

Catalysts	Condition	Performances	Ref.
Pd/TiO_2 reduced at 300	T= 40 ℃, H_2/C_2H_2=2 Space velocity=1000/h 0.91%C_2H_2 in C_2H_4	conversion 54 % selectivity -10 %	[166]
Pd/TiO_2 reduced at 500		conversion 28 % selectivity 90 %	
Pd/TiO_2 with 44%rutile reduced at 500 ℃	T=40 ℃ H_2/C_2H_2=1.71/1.46 1.46%C_2H_2,1.71%H_2, 15.47%C_2H_6, balanced C_2H_4 GHSV=5400/h	conversion 95 % selectivity 50 %	[167]
Bulk Pd_2Ga	T=200 ℃ 0.15 g cat 0.5%C_2H_2, 5%H_2, 50%C_2H_4 in He Total flow rate=30 ml/min	after 20h, conversion 94 % selectivity 74 %	[168]
$Pd_2Ga/MgO/MgGa_2O_4$		after 24h, conversion 98 % selectivity 70 %	
5%Pd/Al_2O_3		after 20h, conversion 44 % selectivity 20 %	
Pd-Nb/SiO_2 reduced at 300 ℃	T= 60 ℃, H_2/C_2H_2=2 Total flow rate= 60 ml/min, 0.03 g cat GSHV=120,000 ml/h/g	conversion 78 % selectivity 36 %	[169]
Pd/TiO_2 treated with H_2	T= 80 ℃, H_2/C_2H_2=1.7/1.5 Total flow rate = 100 ml/min, 0.15 g cat GSHV = 40,000 ml/h/g	conversion 100 % selectivity 85 %	[170]

Catalysts	Condition	Performances	Ref.
3% cubic Pd/Al_2O_3	T=60 ℃ 0.03 g cat 1.2%H_2, 0.6%C_2H_2, 49.3%C_2H_4, balanced N_2	at GHSV=10000/h, conversion 90 % selectivity 5 % at GHSV=46000/h, conversion 67 % selectivity 45 %	[171]
3% sphere Pd/Al_2O_3		at GHSV=10000/h, conversion 75 % selectivity -5 % at GHSV=46000/h, conversion 44 % selectivity 43 %	
Pd/MgAl-LDH/Al_2O_3 by in situ precipitation-reduction	T=50 ℃ GHSV=10056/h H_2/C_2H_2=2 0.91%C_2H_2 in C_2H_4	conversion 47 % selectivity 97 %	[172]
Pd/MgO-Al_2O_3 by in situ precipitation-reduction		conversion 95 % selectivity 85 %	
$AuPd_{0.01}/SiO_2$	T=160 ℃ Space velocity=60000 ml/h/g 1%C_2H_2, 20%H_2, 20%C_2H_4, balanced He	conversion 85 % selectivity 60 %	[162]
$AuPd_{0.025}/SiO_2$		conversion 95 % selectivity 25 %	
PdAg0.55/SiO_2	T=65 ℃ GHSV=600000 1%C_2H_2, 5%H_2, 20%C_2H_4, balanced He	conversion 70 % selectivity 45 %	[173]
PdAu0.45/SiO_2		conversion 50 % selectivity 55 %	
O_2 treated Au/SiO_2 reduced at 250 ℃	T=175 ℃ Space velocity=92000 ml/h/g 0.8%C_2H_2, 16%H_2, balanced C_2H_4	conversion 95 % selectivity 45 %	[174]
Pd-Ti/SiO_2 reduced at 500 ℃	T=40 ℃ SV=3000/min H_2/C_2H_2=2 0.91%C_2H_2 in C_2H_4	conversion 75 % selectivity 80 %	[175]

Catalysts	Condition	Performances	Ref.
Pd/anatase TiO_2	T=40 ℃ GSHV=5400/h	conversion 59 % selectivity 57 %	[176]
Pd/rutile TiO_2	1.46%C_2H_2, 1.71%H_2, 15.47%C_2H_6, balanced C_2H_4	conversion 40 % selectivity -3 %	

Typically, Pd-based catalyst is considered as a main catalyst used for selective hydrogenation in excess ethylene. However, several works have tried to investigate and modify the Pd-based catalyst. The acetylene conversion of Pd-based catalyst such as Pd/TiO_2 appeared to depend on the Pd dispersion [167, 170, 176]. In addition, the selectivity to ethylene was modified by several ways. For example, the reduction at high temperature (500 ℃) over TiO_2-modified Pd catalysts, including TiO_2 either as an additive (Pd-Ti/SiO_2) or as a support (Pd/TiO_2), was an alternative way to modify the catalytic performance [166]. The reduction at high temperature caused the strong metal-support interaction (SMSI) leading to electronic modification of Pd by TiO_2 and thus weakening in the adsorption of ethylene on Pd surface. Moreover, the Ti^{3+} presence in TiO_2 support was reported to be responsible for the selectivity to ethylene [167, 170, 176]. As reported by J. Panpranot et al., 2006 [167], increasing the ethylene selectivity was attributed to much lower adsorption strength of ethylene on Pd due to the existence of Ti^{3+} in contact with Pd. It has been reported that the Ti^{3+} amount was dependent of TiO_2 phase, so the ethylene selectivity also depended on TiO_2 phase. The pure anatase TiO_2 which contained Ti^{3+} showed high ethylene selectivity, while the pure rutile TiO_2 promoted the over-hydrogenation due to Ti^{3+} absence [176]. Moreover, J. Panpranot et al., 2006 [167] also found that the Pd/TiO_2 catalysts with 0-44% rutile which composed of significant Ti^{3+} amounts showed higher ethylene selectivity up to 58-93% than that of 85%-100% rutile. The optimum rutile composition was found to be 44% rutile (95% conversion and 50% selectivity). The formation of Ti^{3+} sites due to the pretreatment with H_2 has been reported [170]. The pretreatment of Pd/TiO_2 catalysts under H_2 atmosphere was

found to result in higher Pd dispersion and more surface Ti^{3+} sites which led to the formation of more isolated Pd adsorption sites.

From the previous paragraph, it could be summarized that the Pd dispersion and Ti^{3+} presence were mainly responsible for acetylene conversion and ethylene selectivity, respectively. However, most of previous works on the modification of Pd-based catalyst were also investigated about the effect of structure and shape of Pd catalyst, intermetallic compound form, and the promoter addition.

Some studies reported about the importance of the Pd (100) structure in catalyst design for selective hydrogenation such as Pd nanocubes which showed higher selectivity to ethylene than that of Pd nanoparticles prepared by impregnation [171]. X. Y. Ma et al., (2011) [172] synthesized the Pd/MgAl-layered double hydroxide synthesized on the spherical Al_2O_3 surface (Pd/MgAl-LDH/Al_2O_3) by using in situ precipitation-reduction method. This catalyst preparation method favored the uniform size and specific shape of Pd particles for Pd/MgAl-LDH/Al_2O_3 and Pd/MgO-Al_2O_3 that promoted the amount of active sites resulting in higher activity than that of Pd/Al_2O_3. While their lower surface acidity and strong metal-support interaction would decrease the deposition of hydrocarbon residues and increase the ethylene desorption.

In addition, A. Ota et al., 2011 [168] applied the intermetallic Pd_2Ga compound as a selective catalyst for hydrogenation of acetylene in excess ethylene. The Pd_2Ga/MgO/$MgGa_2O_4$ catalyst was found to exhibit the superior activity (28,600.4 activity/mol C_2H_2/mol Pd) than bulk Pd_2Ga (4.9 activity/mol C_2H_2/mol Pd) due to high dispersion and structural integrity of intermetallic compound; moreover, its performances in terms of selectivity and stability were higher than commercial Pd catalysts.

For the case of the promoter addition, several works studied the addition of promoter in order to modify the catalytic performance of Pd-based catalysts for selective hydrogenation of acetylene in excess ethylene. As reported by J.H. Kang et al., 2000 [175], the addition of transition-metal oxides, such as Nb, Ce, and especially

Ti oxides, to Pd/SiO_2 catalysts played the roles in the modification both of geometric and electronic terms of Pd after reduced at 500 °C. The transition-metal oxide on the Pd/SiO_2 catalyst suppressed the sintering of dispersed Pd particles, so the ethylene adsorption as multiply-bound was retarded resulting in more ethylene desorption.

The addition of La_2O_3 and Nb_2O_5 as promoter over Pd/SiO_2 catalysts was also studied by I.Y. Ahn et al., 2006 [169]. The La_2O_3-promoted catalyst exhibited lower acetylene conversion but higher selectivity to ethylene and slower deactivation rate compared to Pd/SiO_2 catalyst. On the other hand, the use of Nb_2O_5 as promoter was found to improve conversion, selectivity, and catalysts lifetime compared to Pd/SiO_2 catalyst. The addition of oxides as promoter resulted in a strong interaction between Pd and promoted oxides that suppressed H_2 chemisorption on Pd and then promoted the ethylene desorption from Pd, thus leading to the improved catalytic performance (selectivity and lifetime). For the Nb_2O_5 promoter, the improved conversion was due to the additional hydrogenation activity of reduced Nb oxides.

However, the study dealing with the bimetallic AuPd catalysts has not been investigated too much for the selective hydrogenation of acetylene in excess ethylene as follows:

Y. Zhang et al., 2014 [173] found that both of bimetallic Ag- and $Au-Pd/SiO_2$ catalysts prepared by electroless deposition exhibited improved selectivity to ethylene at high surface coverage of Ag and Au on the Pd surface. At high surface coverage of Ag and Au on the Pd, the formation of small ensemble of Pd sites was found and promoted the adsorption of acetylene as **π**-bonded species (weakly adsorption) leading to hydrogenation to ethylene. On the other hand, the larger ensemble size of contiguous Pd surface sites was found at low surface coverage and resulted in the ethane formation, and then lowering the ethylene selectivity due to the strong adsorption of acetylene as multi **σ**-bonded species.

Not only the amount of Au surface coverage, but also the feature of bimetallic AuPd alloy catalyst was reported to play a crucial role for the selectivity improvement. As reported by the study dealing with the preparation of Pd single-

atom alloy (SSA) structure supported on SiO_2 by decreasing the Pd amount to ppm-level upon alloying Pd with Au nanoparticles (3 nm) [162], it was found that the Pd single-atom alloy (SSA) structure was formed at Pd/Au ratio less than 0.025. The Pd addition promoted much higher acetylene conversion at lower the reaction temperature compared to monometallic Au. In addition, the Au addition was responsible for isolating the Pd atoms and suppressing the hydrogenation of ethylene to ethane (selectivity improvement). Especially, the $AuPd/SiO_2$ catalysts at Pd/Au ratio less than 0.025 (Pd SSA structure) improved more ethylene selectivity compared to the $AuPd/SiO_2$ catalysts at Pd/Au ratio more than 0.025. The higher selectivity to ethylene for Pd SSA structure in $AuPd/SiO_2$ catalysts compared to the monometallic Pd could be ascribed to weaker ethylene adsorption than that of monometallic Pd/SiO_2.

Although most reports dealing with selective hydrogenation in excess ethylene have mainly studied over Pd-based catalyst, a few of studies on the Au-based catalyst used in the selective hydrogenation of acetylene in excess ethylene appeared. The Au/SiO_2 catalysts treated with O_2 plasma at room temperature could be catalytically active with conversion up to 95% [174]. The role of O_2 plasma treatment in the improvement of catalytic performance of Au/SiO_2 catalysts was attributed to 2 effects: 1) small size of Au nanoparticles (c.a. 3 nm) and 2) nearly neutral surface charge on the Au nanoparticles leading to favor the H_2 activation. Nevertheless, it still could be noted that the high temperature and H_2/C_2H_2 ratio were still required for Au-based catalyst.

CHAPTER IV
EXPERIMENTAL

4.1 Catalyst Preparation

4.1.1 FSP Synthesis

4.1.1.1 Conventional one-nozzle FSP synthesis of TiO_2 supports, monometallic Au/TiO_2 and Pd/TiO_2, and bimetallic AuPd/TiO_2 catalysts

The chemicals used in the synthesis of FSP-derived catalysts in part 5.1 and 5.2 are listed in **Table 4.1**.

Table 4.1 Chemicals used in the synthesis of flame spray pyrolysis derived catalysts in part 5.1 and 5.2

Chemical	Supplier
Palladium (II) acetylacetonate, $(C_5H_7O_2)_2Pd$	Aldrich
Tetrachloroauric acid trihydrate, $HAuCl_4\ 3H_2O$	Sigma-Aldrich
Titanium (IV) butoxide, $Ti(OCH_2CH_2CH_2CH_3)_4$	Aldrich
Xylene (99.8 vol%)	Panreac
Acetonitrile	Fisher Scientific

The synthesis of bimetallic 1 wt.% Au-1 wt.% Pd/TiO_2 nanoparticle catalysts was carried out by flame spray pyrolysis reactor. The raw materials used in the preparation of liquid phase precursor were palladium (II) acetylacetonate, tetrachloroauric acid trihydrate and titanium (IV) butoxide. The liquid phase precursor solution was prepared by dissolving all precursors in xylene/acetonitrile mixtures (70/30 vol%) at total concentration of 0.5 M. The liquid precursor solution was fed at 5 ml/min into the flame reactor by syringe pump and dispersed by 5 l/min of oxygen to form a fine spray. The orifice gap area at nozzle was adjusted to keep a maintain pressure drop at capillary tip of 1.5 bar. The ring around the nozzle outlet provided 3 l/min oxygen and 1.5 l/min methane as the supporting flame fed gases to ignite the

spray. The additional 25 l/min sheath oxygen was supplied through a sintered metal plate ring to support the flame. The glass fiber filter with the aid of vacuum pump was used for product particle collection.

The monometallic 1 wt.% Au/TiO_2, 1 wt.% Pd/TiO_2, and titania supports were prepared by flame spray pyrolysis method in the similar procedures as those for the preparation of bimetallic 1 wt.% Au-1 wt.% Pd/TiO_2 catalyst. The flame spray pyrolysis derived TiO_2 supports were used as support for impregnated catalysts and deposition-precipitation derived catalysts.

For part 5.3, the conventional one-nozzle FSP synthesis of monometallic 1 wt.% Pd/TiO_2 and bimetallic 1 wt.% Au-1 wt.% Pd/TiO_2 catalysts with different stoichiometric of precursor flow rate and the dispersion O_2 gas flow rate was performed as follows: The chemicals used in the synthesis of FSP synthesized catalysts, consisted of monometallic 1 wt.% Pd/TiO_2 and bimetallic 1 wt.% Au-1 wt.% Pd/TiO_2 catalysts, are listed in **Table 4.2**.

Table 4.2 Chemicals used in the synthesis of flame spray pyrolysis derived catalysts in part 5.3

Chemical	Supplier
Palladium (II) acetylacetonate, $(C_5H_7O_2)_2Pd$	Aldrich
Tetrachloroauric acid hydrate, $HAuCl_4$ H_2O	Sigma-Aldrich
Titanium (IV) isopropoxide, $Ti(OCH(CH_3)_2)_4$	Sigma-Aldrich
Xylene	Sigma Aldrich
Acetonitrile	Aldrich

For the conventional one-nozzle FSP in part 5.3, all precursors were dissolved in the xylene/acetonitrile mixture solution (70/30 vol%) at total concentration of 0.5 M. The liquid precursor was fed into the flame reactor by using a syringe pump and dispersed with oxygen to form a fine droplet. The precursor flow rate and O_2 dispersion flow rate were varied between 1 and 9 ml/min and between 9 and 1 l/min, respectively. The supporting premixed flame feed gases consisted of oxygen (2

l/min) and methane (1 l/min) were provided through a ring around the nozzle outlet to ignite the spray flame resulting in a self-sustaining spray flame. The produced particles were collected by a glass fiber filter with the aid of vacuum pump.

4.1.1.2 Two-nozzle FSP synthesis of bimetallic AuPd/TiO_2 catalysts

For 2-nozzle FSP in part 5.4, the chemicals used in the 2-nozzle FSP synthesis of bimetallic 1 wt.% Au-1 wt.% Pd/TiO_2 catalysts were similar in part 5.3 as listed in **Table 4.2.** The liquid precursor solutions were prepared in pairs as 4 types: a TiO_2 solution and Pd+Au solution, a Pd solution and Au+TiO_2 solution, a Au solution and Pd+TiO_2 solution, or a Pd+TiO_2 solution and Au+TiO_2 solution which are denoted as TiO_2 + AuPd, Au/TiO_2 + Pd, Pd/TiO_2 + Au, and Pd/TiO_2 + Au/TiO_2; respectively. The procedure for catalyst preparation by using 2-nozzle FSP was similar to the conventional one-nozzle FSP in part 5.3 except the precursor flow rate and O_2 dispersion flow rate. For each nozzle, the liquid precursor solutions were fed into the flame reactor by using a syringe pump at 5 ml/min and then dispersed with oxygen at 5 l/min forming a fine droplet.

4.1.2 Incipient wetness impregnation method

The bimetallic AuPd/TiO_2 catalysts were prepared by incipient wetness impregnation method for loading of palladium and gold. Palladium nitrate and tetrachloroauric acid trihydrate were used as palladium and gold precursors; respectively, as shown in **Table 4.3**. Both precursors were dissolved together in deionized water which its volume equals to pore volume of support. TiO_2 support was impregnated with the mixture precursor solution, then dried at 80 ℃ for 16 h and calcined in static air at 400 ℃ for 3 h.

Table 4.3 Chemicals used in the synthesis of impregnated catalysts

Chemical	Supplier
Palladium (II) nitrate hydrate, $Pd(NO_3)_2$ xH_2O	Aldrich
Tetrachloroauric acid trihydrate, $HAuCl_4$ $3H_2O$	Sigma-Aldrich

4.1.3 Deposition-precipitation method

The chemicals used in the synthesis of deposition precipitation derived bimetallic AuPd/TiO_2 catalysts are listed in **Table 4.4**. The slurry of titania support in deionized water (300 ml) was stirred, heated to 60 ^{o}C, and then adjusted to pH 8 with 1 M sodium carbonate solution. Palladium nitrate and tetrachloroauric acid trihydrate were dissolved together in deionized water. This mixture precursor solution was added dropwise to slurry of titania with the simultaneous addition of 1 M sodium carbonate solution to keep the maintain overall pH at 8. After the mixture precursor solution had been completely added to slurry, the resulting slurry with vigorous stirring was maintained at pH 8 for 1.5 h. The resulting slurry was centrifuged and washed with deionized water around 5 times. Finally, the solid material was dried at 80 ℃ for 16 h and calcined in static air at 400 ℃ for 3 h.

Table 4.4 Chemicals used in the synthesis of deposition-precipitation derived catalysts

Chemical	Supplier
Palladium (II) nitrate hydrate, $Pd(NO_3)_2$ xH_2O	Aldrich
Tetrachloroauric acid trihydrate, $HAuCl_4$ $3H_2O$	Sigma-Aldrich
Sodium carbonate, Na_2CO_3	Riedel-de Haen

4.2 Catalyst pretreatment

For part 5.2, the catalyst samples were reduced before to the reaction tests and characterized by using various techniques. Glass wool was placed into the bottom of glass tube. Then approximately 0.15 g of catalyst was filled on the glass wool. After the glass tube was set up already, the catalyst was reduced with 50 ml/min of hydrogen gas at 40 ℃ for 2 h. Comparison the reduction temperature at 500 ℃, the procedure of catalyst pretreatment was still unchanged but the temperature was set at 500 ℃ instead of 40 ℃.

4.3 Reaction study in hydrogenation reactions

4.3.1 Reaction study in the liquid-phase selective hydrogenation of 1-heptyne

The liquid-phase selective hydrogenation of 1-heptyne was used to study the catalytic performances of the synthesized catalysts. Toluene was chosen as the reaction medium between 1-heptyne and hydrogen. The chemicals and reagents used in liquid-phase hydrogenation reaction are presented as follows in **Table 4.5**.

Table 4.5 Chemicals and reagents used in liquid phase hydrogenation reaction

Chemicals and reagents	Supplier
High purity grade Hydrogen	Thai Industrial Gases Limited
1-heptyne	Aldrich
1-heptene	Aldrich
n-heptane	Aldrich
Toluene	Wako (for part 5.1)
	Merck (for part 5.2)

4.3.1.1 Instruments and apparatus

The instruments and apparatus for studying liquid-phase hydrogenation reaction consisted of:

4.3.1.1.1 Autoclave reactor

A 100 ml stainless steel autoclave (JASCO, Tokyo, Japan) was used as reactor. The combined hot plate and magnetic stirrer device was used for heating the liquid and for mixing between reactant and catalyst.

4.3.1.1.2 Gas chromatography

The gas chromatography was used as the instrument to analyze, separate and identify the chemical compounds. The type of gas detector was a flame ionization detector (FID). Operating conditions for gas chromatography in part 5.1 and 5.2 were given in **Table 4.6** and **4.7**, respectively.

Table 4.6 Operating conditions for gas chromatography for part 5.1

Gas Chromatograph	Shimadzu GC-2014
Detector	FID
Packed column	TC-WAX (df = 0.25 μm, i.d.= 0.25 mm, length = 30 m)
Carrier gas	Helium
Make-up gas	Helium
Column Temperature (°C)	37
Injector Temperature (°C)	230
Detector Temperature (°C)	230

Table 4.7 Operating conditions for gas chromatography for part 5.2

Gas Chromatograph	Shimadzu GC-14B
Detector	FID
Packed column	GS-Alumina capillary
Carrier gas	Helium
Make-up gas	Nitrogen
Column Temperature (°C)	200
Injector Temperature (°C)	250
Detector Temperature (°C)	280

4.3.1.2 Procedure for the liquid-phase hydrogenation of 1-heptyne

The procedure for the liquid-phase hydrogenation reaction of 1-heptyne can be divided into 2 main parts as follows: Firstly, for the reduction step, glass wool was placed into the bottom of glass tube. Then approximately 0.15 g of catalyst was filled on the glass wool. After the glass tube was set up already, the catalyst was reduced with 50 ml/min of H_2 gas at 40 °C for 2 h. For the reaction step, the catalytic reaction tests were conducted under the absence of mass transfer/diffusion resistance. The highest stirring speed (1000 rpm) was used to eliminate the external mass transfer resistance and the effect due to pore diffusion was minimized by using

small particle size catalysts. The catalysts were thoroughly grinded into powder form prior to the reaction tests. Approximately 10 mg of catalyst, 9.8 ml of toluene and 0.2 ml of 1-heptyne were added into the autoclave reactor and then set up. After the autoclave reactor was purged with H_2 about 3 times, the 1-heptyne hydrogenation reaction was carried out with 2 bar of H_2 at 30 ℃ for 10-240 min.

For part 5.2, the procedure for testing the catalyst in the liquid-phase hydrogenation of 1-heptyne under mild reaction conditions is similar to part 5.1, except the absence of the reduction step. Since the catalysts were reduced earlier in the catalyst pretreatment step, the reduced catalysts could be used to test in the reaction without the reduction step. Approximately 5 mg of reduced catalyst was dispersed in 10 cm^3 reactant mixture of 1-heptyne (Aldrich) in toluene (2 %v/v). The reaction was performed in a 100 cm^3 stainless steel autoclave reactor at a pressure of 4 bar H_2 and at temperature of 30 ℃ for 5-120 min.

The resulting product was filtered to separate the liquid product from catalyst. After that, the resulting liquid product was collected and analyzed by using gas chromatography equipped with flame ionization detector (FID).

For the liquid-phase hydrogenation reaction of 1-heptene in part 5.1, the procedure of liquid-phase hydrogenation reaction of 1-heptene (as a hydrogenated product) was also performed with similar procedure as used in the liquid-phase hydrogenation of 1-heptyne in part 5.1.

4.3.2 Reaction study in the gas-phase selective hydrogenation of acetylene

The gas-phase selective hydrogenation of acetylene in excess ethylene was used to study the catalytic performances of the synthesized catalysts. The gases used in gas-phase hydrogenation reaction are presented in **Table 4.8.**

Table 4.8 Gases used in gas-phase hydrogenation reaction

Gases	Supplier
Helium	PanGas
Hydrogen	PanGas
Acetylene	PanGas
Ethylene	PanGas

4.3.2.1 Instruments and apparatus

The instruments and apparatus for studying gas-phase hydrogenation reaction consist of:

4.3.2.1.1 Quartz reactor

The quartz glass fixed-bed reactor consisted of an inner diameter of 4 mm which was contracted to 2 mm after the catalyst bed.

4.3.2.1.2 Gas chromatography

The online gas chromatography (Agilent Technologies) was used as the instrument to analyze, separate and identify the gas mixture compounds. The type of gas detector was a flame ionization detector (FID). The HP-PLOT Q column was chosen as the separation column. The detail of column was given as follows: 30 m long, 0.32 mm in diameter and 0.2 μm film thickness fitted with TCD and FID.

4.3.2.2 Procedure for the gas-phase hydrogenation of acetylene in excess ethylene

The procedure for the gas-phase selective hydrogenation reaction can be divided into 2 main parts consisted of reduction and reaction steps. Firstly, the reduction step, a little bit of quartz wool was placed into the quartz reactor before packing the catalyst. Then approximately 50 mg of catalyst was filled on the quartz wool. After that, a little bit of quartz wool was placed again on the catalyst filled in the quartz reactor. After setting the reactor already, the catalyst was reduced with 50 ml/min of H_2 gas at 150 °C for 2 h, and then cooled down to the temperature at 40 °C under 30 ml/min of He.

For the reaction step, a gaseous mixture containing 1.5% C_2H_2, 2% H_2 and balanced C_2H_4 was introduced into the quartz reactor at a total flow rate of 100 ml/min. The selective hydrogenation of acetylene in excess ethylene was performed in the quartz reactor from the temperature of 40, 60, 80, 100, and 120 °C. Each reaction temperature was kept constant for 1 h before increasing to the next point. The gas mixture product at the outlet of reactor was analyzed by an on-line gas chromatograph equipped with a flame ionization detector (FID).

The selective hydrogenation of acetylene has been investigated in the large amount of ethylene and small quantity of acetylene in the feed, so the ethylene selectivity is calculated based on the ethane formation from hydrogenation reaction [177]. The calculation of ethylene selectivity based on the difference of ethylene may lead to error of selectivity calculation. The ethylene and ethane are assumed as the only products for selective hydrogenation of acetylene. The oligomerization during the hydrogenation reaction was negligible due to the short contact time. The definitions of acetylene conversion and ethylene selectivity are shown as follows [103, 162, 174, 177]:

$$\text{Acetylene conversion} = \frac{C_2H_2(\text{feed}) - C_2H_2}{C_2H_2(\text{feed})} \times 100\%$$

$$\text{Ethylene selectivity} = \left(1 - \frac{C_2H_6 - C_2H_6(\text{feed})}{C_2H_2(\text{feed}) - C_2H_2}\right) \times 100\%$$

4.4 Catalyst characterizations

The catalysts were characterized to study properties by several techniques as follows:

4.4.1 X-ray diffraction (XRD)

The X-ray diffraction analysis (for part 5.1) was performed on SIEMENS D5000 X-ray diffractometer and CuK_α radiation with Ni-filter. The X-ray diffraction pattern of sample was detected from 20° to 80° 2θ. This technique was used to identify and quantify the crystalline phases in sample. The crystallite size was determined from

the Scherrer's equation with using the full width of the diffraction peak at half maximum (FWHM).

For part 5.2, the X-ray diffraction analysis was conducted on XRD D8 Advance of Bruker AXS with Ni-filter CuK_{α} (λ = 1.54056 A°) radiation from 20° to 80° 2θ and step size of 0.020563 (step time = 88.5 s).

For part 5.3 and 5.4, the x-ray diffraction pattern was recorded from 20° to 70° by using a Bruker AXS D8 Advance diffractrometer instrument (40 kV, 40 mA, λ = 0.154 nm) with CuK_{α} radiation. The crystallite sizes were calculated by using Topas 3 software with the Rietveld refinement.

4.4.2 N_2 physisorption

The N_2 physisorption analysis (for part 5.1 and 5.2) was conducted using a Micromeritics ASAP 2020 automated system (surface area and porosity analyzer) for determining the BET specific surface areas, pore volumes, and pore size diameters. The sample was degassed at 200 ℃ for 2 h (heating rate of 2.0 ℃ /min) under vacuum prior to N_2 adsorption analysis, which was carried out at liquid nitrogen temperature (-196 ℃). The characteristics of pore structure were estimated from the adsorption-desorption isotherm based on IUPAC classification.

For part 5.3 and 5.4, the BET measurement was performed by nitrogen adsorption at 77 K with using a MicromeriticsTristar instrument. The BET specific surface area (SSA) of samples was measured by 5 points nitrogen adsorption isotherm after degassed with N_2 at 200 ℃ for at least 1 h.

4.4.3 Transmission electron microscopy (TEM)

The transmission electron microscope (for part 5.1) of JEOL JEM-2010 equipped with LaB_6 thermoionic electron gun operating at voltage range of 80-200 kV and optical point resolution of 0.23 nm was employed for TEM analysis. This TEM technique provided morphology images (TEM images) and crystallite size. This technique was analyzed at National Metal and Materials Technology Center.

For part 5.2 and 5.3, the TEM observations were performed in a JEOL JEM 2010 transmission electron microscope equipped with a LaB_6 electron beam source, a UHR polepiece (point resolution : 0.196 nm) and a Pentafet-Link Energy-Dispersive X-ray (EDX) spectrometer (and INCA software) from Oxford Instruments.

For part 5.4, the scanning transmission electron microscopy (STEM) was performed by using an aberration-corrected STEM microscope [HD-2700CS (Hitachi)]; in addition, the EDX analysis of selected spots was performed with an energy-dispersive X-ray spectrometer [EDXS, Genesis Spectrum version 6.2 (EDAX)].

4.4.4 Ultraviolet-visible absorption spectroscopy (UV-Vis)

The UV-vis spectroscopy was performed using a Perkin Elmer Lambda 650 spectrophotometer. The absorbance spectra were recorded in the wavelength range of 200-800 nm (ultraviolet-visible spectral region). This technique was used to study the characteristics of the optical properties of sample.

4.4.5 CO-pulse chemisorption

The CO-pulse chemisorption technique (for part 5.1) was carried out on Micromeritics ChemiSorb 2750 (chemisorption system analyzer) with ChemiSoft TPx software for measuring the amounts of CO chemisorbed on the catalyst.

The quartz wool was put into the bottom of quartz tube. Approximately 0.2 g of sample was placed in the quartz tube, and then the sample cell was set up to TPx. He was introduced through the sample cell with a flow rate 30 ml/min to take out air. Before to chemisorp, the sample was heated from room temperature to 40 °C and reduced with 50 ml/min H_2 at this temperature for 2 h. After sample was cooled down to 35°C in He flow, CO was injected into the sample cell to adsorb on the active sites while unabsorbed CO was detected by the thermal conductivity detector. Pulse injection was performed until peak areas of TCD reading were not much different, indicating the active sites were fully adsorbed with CO.

For part 5.3 and 5.4, the amounts of CO chemisorbed on the samples were measured by CO-pulse chemisorption technique. CO-chemisorption was analyzed by using a MicromeriticsAutochem II 2920 instrument equipped with a thermal

conductivity detector (TCD) and mass spectrometer (MS). Before to chemisorption, the sample was reduced with 5% H_2/Ar at 150 °C for 2 h. The CO was injected to chemisorb on the reduced catalysts with 10 pulses at 40 °C or until the MS signal of effluent CO gas was constant.

4.4.6 X-ray photoelectron spectroscopy (XPS)

The X-ray photoelectron spectroscopy (for part 5.1) was performed on Kratos AMICUS X-ray photoelectron spectrometer using MgK_α X-ray radiation as X-ray source at voltage of 20 kV and current of 10 mA. The Kratos VISION2 software was conducted in computer controlled system. XPS spectra were recorded with energy step size of 0.1 eV and analyzer pass energy of 75 eV. The XPS spectra of C 1s line at binding energy of 285.0 eV was chosen as internal standard. XPS was used to analyze the surface properties of catalyst such as elemental composition, chemical state and electronic state.

For part 5.2, XPS was performed using a Kratos Ultra DLD X-ray photoelectron spectrometer. The *in situ* high-energy XPS analysis was performed under reducing condition to ensure that the catalysts are in the active form. The C1s peak was used as reference at binding energy of 285.0 eV to calibrate for all XPS spectra.

For part 5.4, XPS was performed on a Kratos AMICUS X-ray photoelectron spectrometer using MgK_α as X-ray radiation. The C 1s line (binding energy at 285.0 eV) was specified as internal standard.

4.4.7 Inductively-coupled plasma optical emission spectroscopy (ICP-OES)

The inductively-coupled plasma optical emission spectroscopy (for part 5.1 and 5.2) using the Optima 2100 DV spectrometer was employed for measuring the metal content in catalyst.

For bimetallic AuPd/TiO_2 catalysts, approximately 0.03 g of catalyst was dissolved in aqua regia solution (HCl : HNO_3, volume ratio of 3 : 1 ml) and stirred for 1 h to digest gold metal. Then 6 ml HF was added into this solution and stirred for 1 h at 75 °C to digest palladium metal and titania support. After the solution was held completely at 75 °C for 1 h, the solution was continued to stir until the clear solution

was observed. The resulting clear solution was diluted to 100 ml and analyzed with ICP-OES technique.

For monometallic Au/TiO_2 catalyst, approximately 0.03 g of catalyst was dissolved in aqua regia solution (HCl : HNO_3, volume ratio of 3 : 1 ml) and stirred for 3 h to digest gold metal. Then 6 ml HF was added into this solution, stirred for 3 h to digest titania support, and then diluted to 100 ml.

For monometallic Pd/TiO_2 catalyst, approximately 0.03 g of catalyst was dissolved in 6 ml HF and stirred for 1 h at 75 °C to digest palladium metal and titania support. After that, the solution was continued to stir at room temperature until the clear solution was observed, and then the resulting clear solution was diluted to 100 ml.

Both of gold and palladium standards were prepared at concentrations of 2 ppm, 4 ppm, 6 ppm, 8 ppm, and 10 ppm. For the blank preparation, each blank was prepared similar to the digestion of each sample.

For part 5.3 and 5.4, the inductively-coupled plasma optical emission spectroscopy using the ICP-OES ACTIVA from Horiba Jobin-Yvon (Palaiseau, France) equipped with a CCD detector was employed for determination of the metallic element content in catalyst sample.

4.4.8 H_2-temperature programmed reduction (H_2-TPR)

The reducibility of catalyst as a function of temperature (TPR profile) was investigated by temperature programmed reduction technique using a MicromeriticsChemiSorb 2750 with ChemiSoftTPx software. Approximately 0.1 g of catalyst was pretreated under N_2 (25 mL/min) at 400 °C for 1 h before the TPR analysis in order to remove possible impurities contained in the samples. After cooling down to room temperature under N_2, the sample was exposed to mixture of 10% H_2 in Ar flowing at 25 ml/min with the temperature ramped of 10 °C/min from 35 °C to 700 °C. The temperature was held at 700 °C for 1 h and then cooled to room temperature.

4.4.9 Thermo gravimetric analysis (TGA)

Thermo gravimetric analysis was performed by using a TA Instruments SDT Q600 analyzer. 10-30 mg of samples was heated form 25 to 1000 °C under air. The weight loss of samples was recorded as a function of temperature.

CHAPTER V
RESULTS AND DISCUSSION

The results and discussion of the FSP synthesized monometallic Pd/TiO_2 and bimetallic $AuPd/TiO_2$ catalysts are divided into four parts. In the first part, the effect of Au addition forming the bimetallic AuPd catalysts was mainly studied. The characteristics and catalytic properties of bimetallic AuPd catalysts obtained from different preparation methods including FSP, conventional co-impregnation (IMP), and deposition-precipitation (DP) were investigated and evaluated in the liquid phase selective hydrogenation of 1-heptyne under mild conditions. The effect of reduction temperature over the monometallic Pd and bimetallic AuPd catalysts synthesized by FSP was investigated in the second part. The catalysts were pretreated under hydrogen at reduction temperature of 40 or 500 °C. The catalytic performance of catalysts with different reduction temperatures was tested in the liquid phase selective hydrogenation of 1-heptyne under mild conditions. In the third part, the flexibility of FSP process for catalyst preparation was investigated over the conventional one-nozzle FSP by tuning the operating conditions such as the stoichiometric of precursor flow rate and dispersion gas O_2 flow rate. The catalytic characteristics of monometallic Pd and bimetallic AuPd catalysts synthesized by FSP were investigated by several characterizations. The catalytic performance of FSP synthesized catalyst was evaluated in the gas phase selective hydrogenation of acetylene in the excess ethylene. Moreover, the catalytic performance of the monometallic Au catalyst was also evaluated. Due to the limitation of the conventional one-nozzle FSP in obtaining the desired configuration, the application of 2-nozzle FSP system was also investigated in part 5.4 in order to increase the process flexibility. The catalyst characteristics and configuration form different routes were investigated. The catalytic performances of bimetallic AuPd nanoparticles synthesized from different routes of the 2-nozzle FSP system was tested in the gas phase selective hydrogenation of acetylene in the excess ethylene and then compared to the conventional one-nozzle FSP process.

5.1 Mono- and bi-metallic AuPd/TiO_2 catalysts synthesized by one-step flame spray pyrolysis for liquid-phase hydrogenation of 1-heptyne

In this part, the monometallic Au and Pd and bimetallic AuPd supported on TiO_2 catalysts were synthesized by one-step FSP. The effect of Au addition forming the bimetallic AuPd catalysts supported on TiO_2 was the main purpose of the study. The characteristics and catalytic properties of the FSP synthesized catalysts were also investigated by various techniques such as XRD, ICP-OES, TEM, XPS, N_2 physisorption, and CO pulse chemisorption. Moreover, a comparative study of characteristics and catalytic behaviors of bimetallic AuPd/TiO_2 catalysts prepared by different methods including FSP, co-impregnation (IMP), and co-deposition precipitation (DP) was performed in the liquid phase selective hydrogenation of 1-heptyne under mild conditions.

5.1.1 Characteristics of catalysts

5.1.1.1 X-ray diffraction (XRD)

The crystal structure, phase composition, and crystallite size of TiO_2 support and FSP synthesized catalysts were analyzed by X-ray diffraction technique. The XRD patterns of the bimetallic AuPd/TiO_2 catalysts (prepared by IMP, DP, and FSP), monometallic Au/TiO_2 and Pd/TiO_2 catalysts (prepared by FSP), and TiO_2 supports (prepared by FSP) are illustrated in **Figure 5.1**. The XRD characteristic peaks of the crystalline phases of TiO_2, consisting of anatase at 25.2° (major), 36.9°, 37.7°, 48.0°, 53.9°, 55.0°, 62.7°, 68.9°, 70.3°, 75.1° 2θ and rutile at 27.4° (major), 36.0°, 41.3°, 54.3°, 56.6° 2θ phases without formation of brookite, were observed for all samples [68, 178].

No diffraction peaks for Pd or PdO were detected for all catalysts. This is probably because of well-dispersed of Pd nanoparticles on the TiO_2 support and/or low content of Pd loading [35, 68, 179, 180]. The additional diffraction peaks at 38.5° and 44.4° for the monometallic FSP-Au/TiO_2 was attributed to the position of Au metal at (111) and (200) planes [71, 181]. In addition, in the case of bimetallic AuPd catalysts, most apparent of Au metallic peaks in XRD patterns was observed for the

IMP-AuPd/TiO_2. It is suggested that the impregnation preparation resulted in some fairly larger Au particles deposited on TiO_2 support compared to bimetallic AuPd catalysts prepared by FSP and DP.

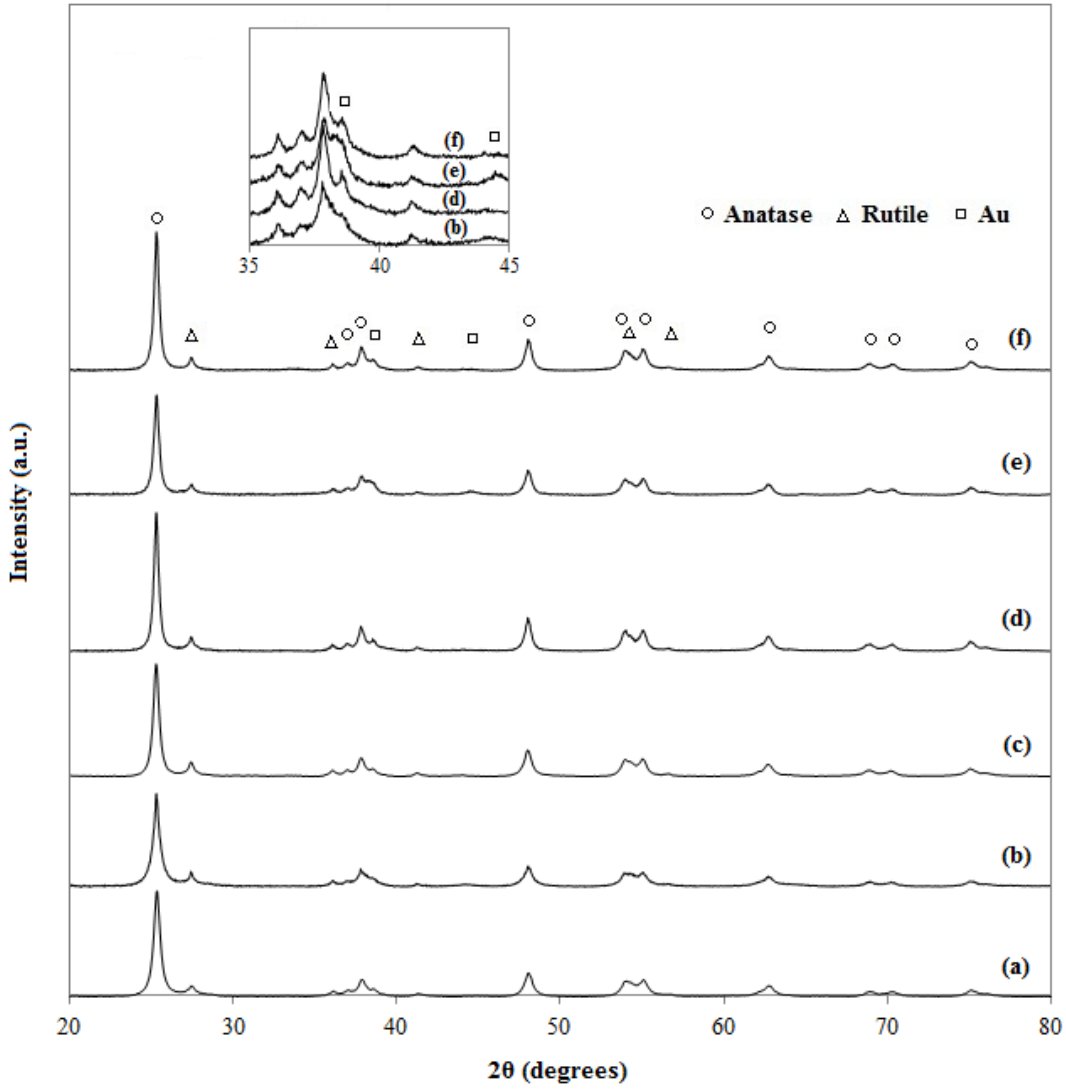

Figure 5.1 XRD patterns of (a) FSP-TiO_2, (b) FSP-Au/TiO_2, (c) FSP-Pd/TiO_2, (d) FSP-AuPd/TiO_2, (e) IMP-AuPd/TiO_2, (f) DP-AuPd/TiO_2

The crystallite size of anatase phase TiO_2 and the ratio phase of anatase to rutile are shown in **Table 5.1**. The crystallite size of anatase phase TiO_2 based on the Scherrer equation is performed by measuring the broadening of a particular XRD

diffraction peak. For the pure FSP-TiO_2 support and monometallic FSP-Au/TiO_2 and FSP-Pd/TiO_2 catalysts, the crystallite sizes of anatase phase TiO_2 were calculated to be in the range of 20-22 nm. The crystallite sizes of anatase phase TiO_2 for the bimetallic catalysts were found to be increased to 25-29 nm. Upon the addition of metal species, the ratio phase of anatase to rutile decreased compared to the pure FSP-TiO_2 support. It may be postulated that Au and/or Pd addition during FSP promoted phase transformation to rutile in the TiO_2 support.

Table 5.1 XRD analysis results of the TiO_2 support, monometallic Au and Pd, and bimetallic AuPd catalysts

Catalyst	Crystallite size of anatase TiO_2 (nm)	Ratio phase anatase to rutile
FSP-TiO_2	20	6.9
FSP-Au/TiO_2	20	6.0
FSP-Pd/TiO_2	22	5.2
FSP-AuPd/TiO_2	29	5.3
IMP-AuPd/TiO_2	25	4.4
DP-AuPd/TiO_2	28	4.8

5.1.1.2 Inductively-coupled plasma optical emission spectroscopy (ICP-OES)

The actual bulk composition of Au and Pd metal contents in the catalyst samples was determined by using ICP-OES technique as shown in **Table 5.2**. The actual loadings of Au and Pd metals for FSP and IMP synthesized catalysts were close to the expected amount (1 wt.% for each metal), except for the DP-AuPd/TiO_2 catalyst. The relatively low amount of actual Au loading for DP-AuPd/TiO_2 catalyst was observed at 0.61 wt.% because some Au metal probably loss during washing and centrifuging processes. The decrease in fraction of Au deposition for Au catalysts prepared by precipitation method was in agreement with Wolf et al. [182]. The fraction of Au deposited on the support has been reported to depend on the pH

during precipitation. Especially at pH of 8, the fraction of Au deposition over support was found to be decreased by about 35-70%.

Table 5.2 Actual metal loading of the TiO_2 support, monometallic Au and Pd, and bimetallic Au-Pd catalysts

Catalyst	Metal loadings	
	Au (wt.%)	Pd (wt.%)
FSP-TiO_2	-	-
FSP-Au/TiO_2	0.9	-
FSP-Pd/TiO_2	-	0.8
FSP-AuPd/TiO_2	0.9	0.9
IMP-AuPd/TiO_2	1.1	1.0
DP-AuPd/TiO_2	0.6	1.0

*Expected metal loading: Au 1 wt.%, Pd 1 wt.%

5.1.1.3 N_2 physisorption

The N_2 adsorption-desorption isotherms of FSP-TiO_2 support and bimetallic FSP-AuPd/TiO_2, IMP-AuPd/TiO_2, and DP-AuPd/TiO_2 catalysts are given in **Figure 5.2**. According to the Brunauer-Deming-Deming-Teller (BDDT) classification of sorption isotherms, the FSP-TiO_2, FSP-AuPd/TiO_2, and DP-AuPd/TiO_2 showed type-IV physisorption isotherm with a well-defined hysteresis loop at high relative pressure (P/P_0) in the range of 0.8 to 1.0, corresponding the characteristic of mesoporous materials (pore diameters between 2 and 50 nm). However, the shape characteristic of hysteresis loop for FSP synthesized catalysts (FSP-TiO_2 and FSP-AuPd/TiO_2) and DP synthesized catalyst (DP-AuPd/TiO_2) was different. The characteristic of hysteresis loop for both of FSP-TiO_2 and FSP-AuPd/TiO_2 was type H3 which described to the slit shaped pores. Meanwhile, DP-AuPd/TiO_2 showed the hysteresis loop of type H1 indicating to the narrow distribution of relatively uniform pores. The characteristic of isotherm and hysteresis loop for IMP-AuPd/TiO_2 was remarkably different from other bimetallic catalysts. The isotherm for IMP-AuPd/TiO_2 was found to be type-IV

isotherm with 2 types of hysteresis loops. The hysteresis loops of IMP-AuPd/TiO_2 were consisted of type H2 hysteresis loop at relative pressures (P/P_0) between 0.7 and 0.95 presenting the characteristics of narrow necks and wider bodies of pores and type H3 hysteresis loop at relative pressures (P/P_0) between 0.95 and 1.0 presenting the narrow slit shaped pores.

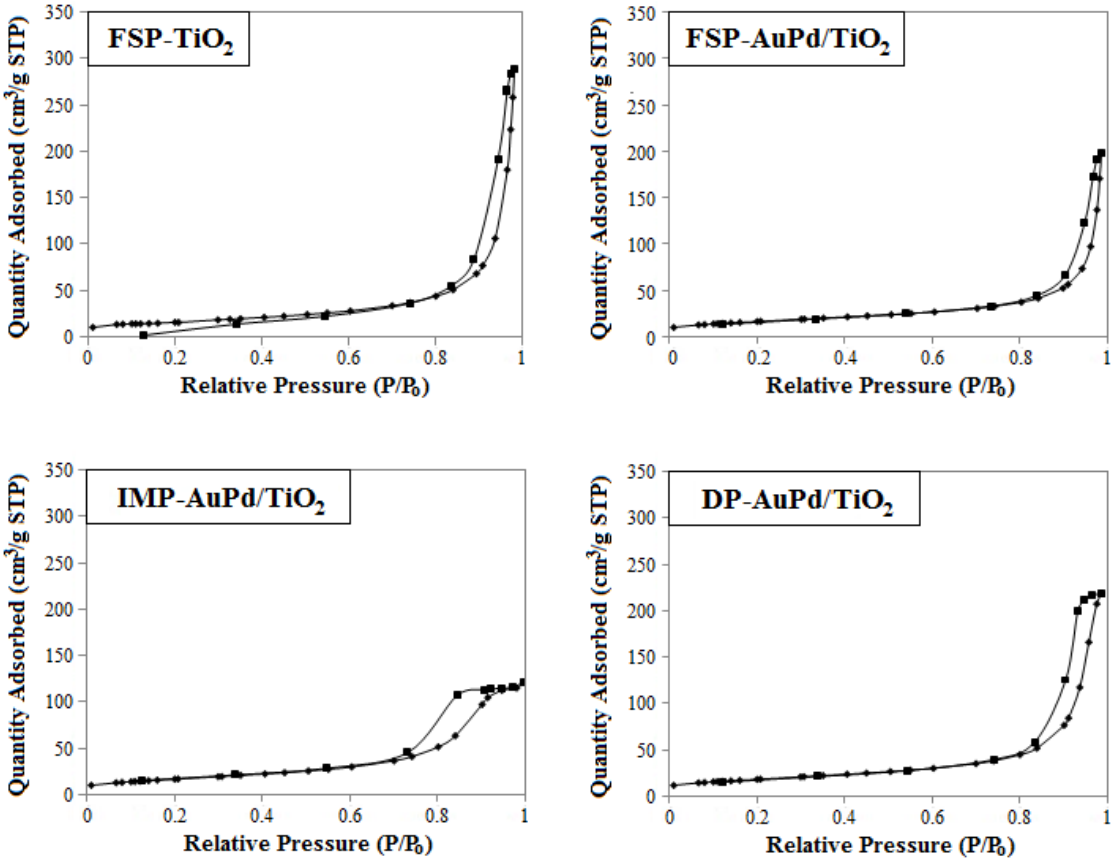

Figure 5.2 N_2 physisorption isotherms of FSP-TiO_2, FSP-AuPd/TiO_2, IMP-AuPd/TiO_2, DP-AuPd/TiO_2

The BET specific surface area, pore volume, and average pore diameter of the catalysts were determined by using N_2 physisorption technique as shown in **Table 5.3**. The BET specific surface areas of monometallic FSP-Au/TiO_2 and FSP-Pd/TiO_2 catalysts were determined to be 91.8 and 79.8 m^2/g, respectively. Compared to the bare FSP-TiO_2 support (56.7 m^2/g), the BET surface areas of the FSP synthesized

monometallic catalysts were larger because of the inhibition of TiO_2 particle's growth by metal doping (Au or Pd), corresponding to the other previous reports of FSP synthesized supported catalysts [65, 117]. Furthermore, it was found that the simultaneous addition of Au and Pd during FSP synthesis (FSP-AuPd/TiO_2) resulted in lower BET surface area compared to the monometallic ones. The BET surface areas of the bimetallic AuPd/TiO_2 catalysts prepared by FSP, IMP, and DP method were found to be in the range of 60.1-65.1 m^2/g.

Regarding the changes in pore volume and average pore diameter and N_2 physisoption isotherms upon metal loading, the catalyst preparation (both of monometallic and bimetallic catalysts) by FSP synthesis did not result in the formation of any new pore stucture which was absent in the bare FSP-TiO_2 support (metal unloading); moreover, the metal particles were mostly deposited on the support. In contrat to the FSP synthesis, the pore blockages and new pore structure were formed upon the catalyst preparation by IMP and DP methods. Some of the metals were located in the pores of the TiO_2.

Table 5.3 N_2 physisorption properties of the TiO_2 support, monometallic Au and Pd, and bimetallic AuPd catalysts

Catalyst	N_2 physisorption results		
	BET surface area (m^2/g)	Pore volume (cm^3/g)	Average pore diameter (nm)
FSP-TiO_2	56.7	0.44	31
FSP-Au/TiO_2	91.8	0.45	20
FSP-Pd/TiO_2	79.8	0.36	18
FSP-AuPd/TiO_2	60.1	0.30	20
IMP-AuPd/TiO_2	60.4	0.18	12
DP-AuPd/TiO_2	65.1	0.34	21

5.1.1.4 CO chemisorption

The amounts of active surface Pd sites on the catalysts, Pd dispersion, and average Pd^0 particle size were determined by CO chemisorption as presented in **Table 5.4**. The CO chemisorption was based on the assumption that there was no CO adsorbed on Au particles [11, 141]. The amounts of CO adsorbed on the bimetallic FSP-AuPd/TiO_2, IMP-AuPd/TiO_2 and DP-AuPd/TiO_2 catalysts were found to be in the range of 9.1-19.4 $\times 10^{18}$ molecules CO/g cat., that were larger than that on the monometallic FSP-Pd/TiO_2 catalyst (3.9 $\times 10^{18}$ molecules CO/g cat.). It could be postulated that an increase in CO adsorbed amounts of bimetallic catalysts compared to the monometallic Pd catalyst was probably because the adsorption stoichiometry of CO on active surface Pd sites might be changed and/or the interaction between Au and Pd might activate Au to adsorb the additional CO. In consonance with Beck et al. [141], the adsorption stoichiometry of Pd/CO was reported to be 1.5 and 1.0 for the monometallic FSP-Pd/TiO_2 and bimetallic AuPd/TiO_2 catalysts, respectively

Table 5.4 CO chemisorption results of the TiO_2 support, monometallic Au and Pd, and bimetallic AuPd catalysts

Catalyst	CO chemisorption results		
	CO uptake ($\times 10^{18}$ molecules CO/g catalyst)	% Dispersion	D_p (nm)
FSP-TiO_2	-	-	-
FSP-Au/TiO_2	0.17	-	-
FSP-Pd/TiO_2	3.91	14.18	7.92
FSP-AuPd/TiO_2	9.12	19.63	5.72
IMP-AuPd/TiO_2	19.36	38.43	2.92
DP-AuPd/TiO_2	17.22	34.91	3.22

*%Dispersion: Percentage of Pd dispersion, D_p: Average diameter of Pd particles

According to the adsorption stoichiometry of Pd/CO reported by Beck et al. [141], the Pd dispersion based on the actual amount of Pd metal from ICP-OES results was determined to be 19.6, 34.9, and 38.4% for the FSP-AuPd/TiO_2, DP-AuPd/TiO_2, and IMP-AuPd/TiO_2 catalysts, respectively. The corresponding calculated Pd^0 particle sizes were 5.7, 3.2, and 2.9 nm.

5.1.1.5 X-ray photoelectron spectroscopy (XPS)

The surface chemistries of materials such as electronic states and elemental compositions at surface were characterized by XPS analysis. The XPS results including binding energies of Pd $3d_{5/2}$ and Au $4f_{7/2}$ and the surface elemental composition of monometallic Pd/TiO_2, Au/TiO_2 and bimetallic AuPd/TiO_2 catalysts are presented in **Figure 5.3** and **5.4** and summarized in **Table 5.5**.

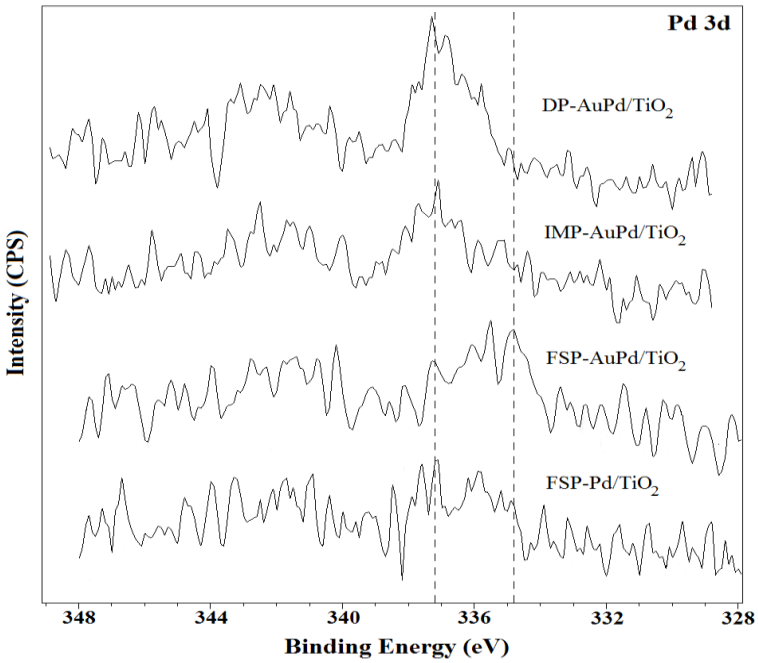

Figure 5.3 XPS Pd 3d core level spectra of FSP-Pd/TiO_2, FSP-AuPd/TiO_2, IMP-AuPd/TiO_2, DP-AuPd/TiO_2

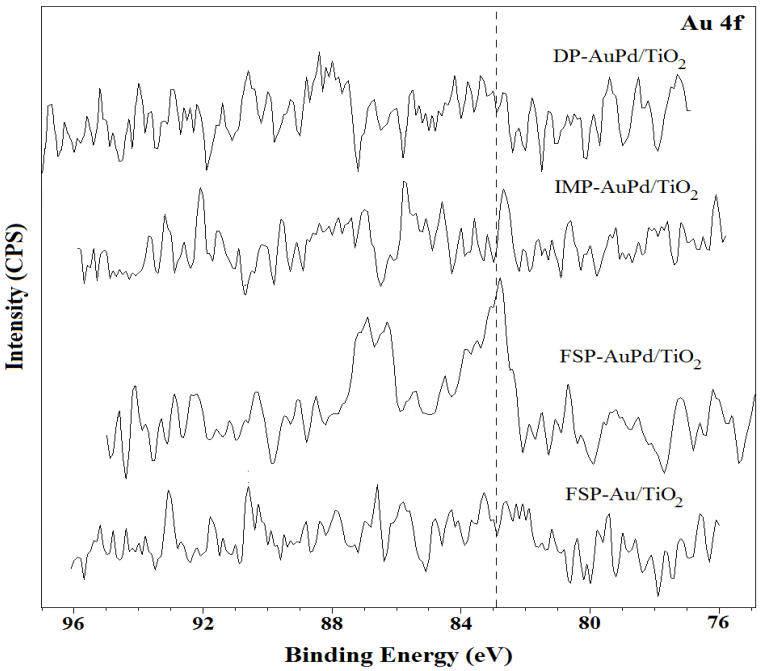

Figure 5.4 XPS Au 4f core level spectra of FSP-Au/TiO_2, FSP-AuPd/TiO_2, IMP-AuPd/TiO_2, DP-AuPd/TiO_2

Table 5.5 XPS analysis results of the monometallic Au and Pd, and bimetallic AuPd catalysts

Catalyst	Pd $3d_{5/2}$		Au $4f_{7/2}$		Atomic concentration		Atomic ratio
	B.E. (eV)	FWHM	B.E. (eV)	FWHM	Pd (%)	Au (%)	Au/Pd
FSP-AuPd/TiO_2	334.8	1.928	82.9	0.935	0.14	0.08	0.57
IMP-AuPd/TiO_2	337.2	1.586	n.d	n.d	0.16	n.d	n.d.
DP-AuPd/TiO_2	337.2	1.532	n.d.	n.d.	0.28	n.d.	n.d.

B.E.: Binding energy, FWHM: Full width at half maximum

n.d.: Not determined

For the FSP synthesized monometallic catalysts (Pd/TiO_2 and Au/TiO_2), the XPS peaks for Pd $3d_{5/2}$ and Au $4f_{7/2}$ were not apparently observed. Nevertheless, the XPS peaks for Pd $3d_{5/2}$ and Au $4f_{7/2}$ of the bimetallic FSP-AuPd/TiO_2 catalyst were

detected at 334.8 eV and 82.9 eV, respectively. Typically, the binding energy of Pd and Au metals has been reported in the range of 335.0-335.4 eV [183] and 83.8-84.0 eV [141], respectively. Shifting in both of $Pd3d_{5/2}$ and $Au4f_{7/2}$ peaks for the FSP-AuPd/TiO_2 to lower binding energies was attributed to Au–Pd alloy formation and/or charge transfer from TiO_2 support to metal [184, 185]. On the other hand, the XPS peaks for Pd $3d_{5/2}$ of the bimetallic IMP-AuPd/TiO_2 and DP-AuPd/TiO_2 catalysts were observed at 337.2 eV, attributing to PdO (335.4-337.5 eV) [186], while the XPS peaks of Au $4f_{7/2}$ were not apparently seen. Based on undetected Au particles at surface, it could be suggested that most of the surface of Au nanoparticles were covered with PdO in the bimetallic catalysts prepared by IMP and DP methods. The surface atomic ratio of Au/Pd for the FSP-AuPd/TiO_2 catalyst was found to equal to 0.57. While the surface atomic ratios of Au/Pd for IMP-AuPd/TiO_2 and DP-AuPd/TiO_2 catalysts could not determine due to undetected Au $4f_{7/2}$ peak.

5.1.1.6 UV-visible spectroscopy

UV-Vis absorption spectra of the TiO_2 supports and the TiO_2 supported monometallic and bimetallic catalysts are illustrated in **Figure 5.5**. The FSP-Au/TiO_2 (b) catalyst exhibited absorption spectrum peak at 561 nm, which can be referred to the characteristic of surface plasmon resonance (SPR) [51]. No SPR absorption was detected in the FSP-Pd/TiO_2 (d) catalyst [187]. The SPR of Au was not observed for all the bimetallic catalysts because the presence of Pd suppressed the SPR band of Au. It was reported that the surface plasmon energies of group 11 metal ($d^{10}s^1$) are suppressed by the group 10 metal (d^8s^2) in various bimetallic nanoparticles [181, 188-190]. Additionally, the background of the absorption spectra in the bimetallic nanoparticles (c, e, f) was increased compared to the monometallic FSP-Au/TiO_2 catalyst (b), owing to the existence of Pd nanoparticles in the bimetallic system [190].

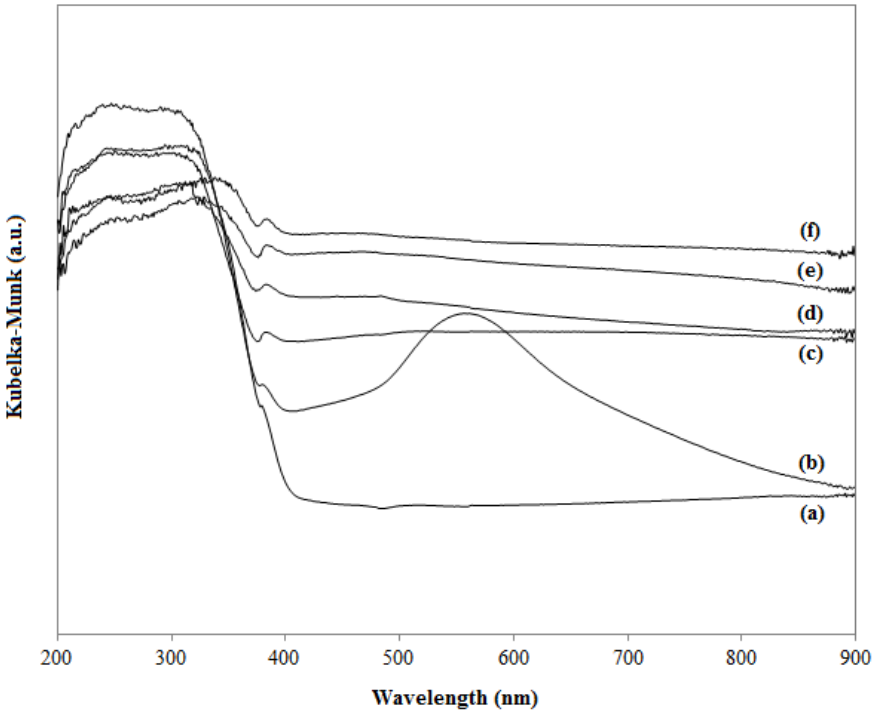

Figure 5.5 UV-vis spectra of (a) FSP-TiO_2, (b) FSP-Au/TiO_2 (c) FSP-AuPd/TiO_2, (d) FSP-Pd/TiO_2, (e) DP-AuPd/TiO_2, (f) IMP-AuPd/TiO_2

5.1.1.7 Transmission electron microscope (TEM) and structural features

The morphology and particle size of the particles were determined by TEM technique. The metal dispersion state of the particles can also be seen from the TEM micrographs. The TEM micrographs of the bimetallic catalysts with different catalyst preparations, consisted of FSP-AuPd/TiO_2, DP-AuPd/TiO_2, and IMP-AuPd/TiO_2 catalysts, are illustrated in **Figure 5.6**. The morphology of TiO_2 support was a spherical primary structure with an average particle size about 17 nm, showing good agreement with the TiO_2 size from the XRD results calculated by using the Scherrer equation. The uniform distribution of metal particles was observed on the FSP-AuPd/TiO_2 and the average metal particle size was about 5 nm (presented as darker spots), attributing to the particles of AuPd alloy. Compared to the FSP-AuPd/TiO_2, the less uniform distribution of metal particle size was found for DP-AuPd/TiO_2 and IMP-AuPd/TiO_2, in which the metal particle size was consisted of small particles (2-4 nm) and some large particles (15-26 nm).

In accordance with the XPS, XRD, and TEM results, the IMP-AuPd/TiO_2 consisted of larger Au particles which may be covered by PdO on their surface. The TEM-EDX analysis was used to confirm the existence of both Au and Pd metals in these larger particles; in addition, the small metal particles on these catalysts may be attributed to the monometallic Pd/PdO particles. The morphology of metal particles on the DP-AuPd/TiO_2 was rather similar to that of IMP-AuPd/TiO_2; however, the Au particle size for DP-AuPd/TiO_2 appeared to be smaller. These results are in good agreement with the literature that the Au catalyst preparation by DP method resulted in smaller Au particle size compared to that prepared by IMP [55]. Much higher CO chemisorption ability of DP-AuPd/TiO_2 and IMP-AuPd/TiO_2 in comparison with FSP-AuPd/TiO_2 was probably because of the existence of smaller monometallic Pd/PdO particles. As shown in TEM micrographs of IMP-AuPd/TiO_2 (**Figure 5.6 e** and **f**), not only some of small Pd/PdO particles seem to agglomerate, but also are occluded within the interparticles pores of the FSP synthesized TiO_2 particles.

Thus, such results (from XPS, XRD, and especially TEM characterizations) strongly support our previous discussion in N_2 physisorption results that the catalyst preparation by IMP method led to the formation of new pore structure and pore blockages as presented by changes of hysteresis loop [65, 66].

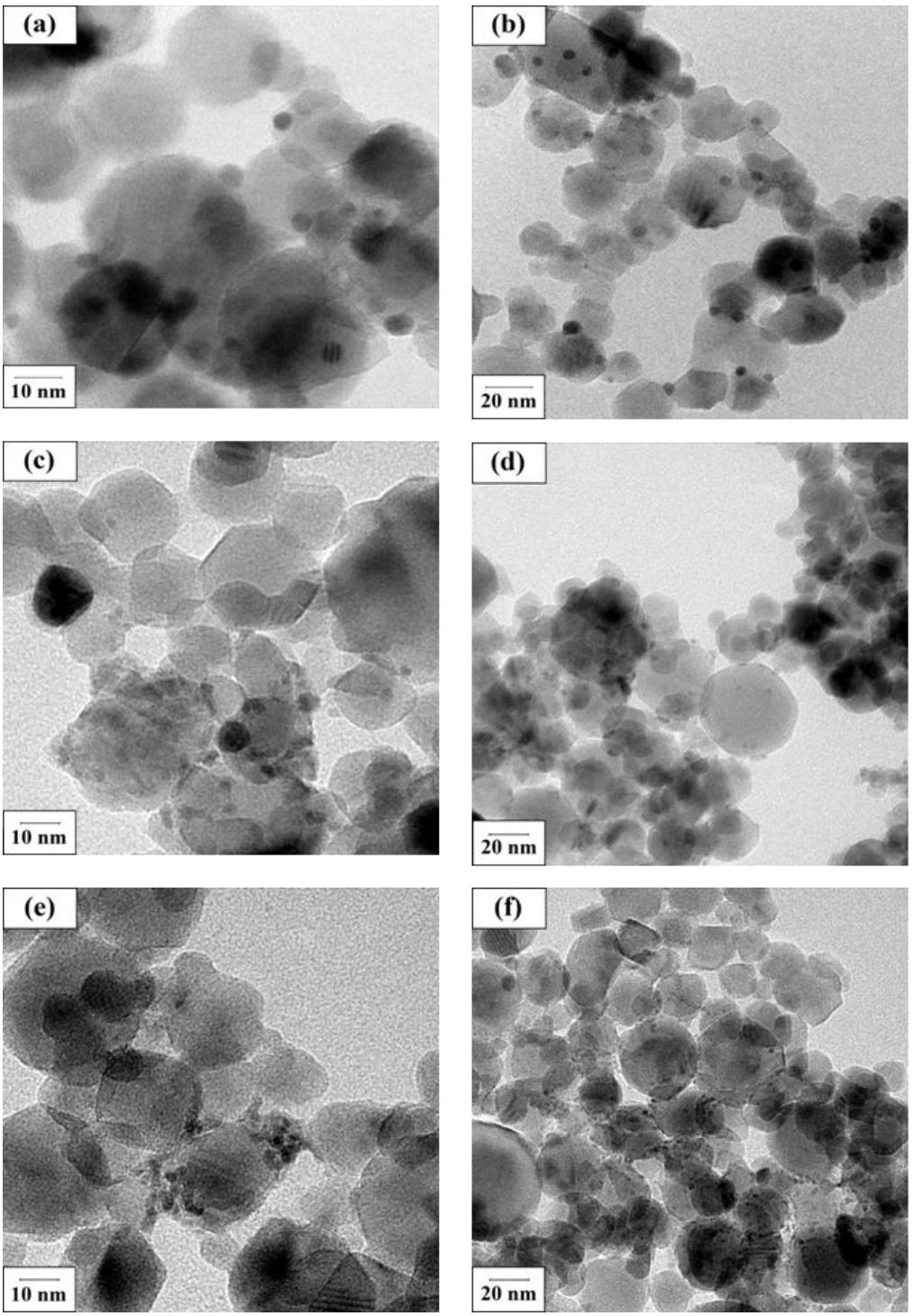

Figure 5.6 TEM images of the bimetallic FSP-AuPd/TiO_2 (a,b), DP-AuPd/TiO_2 (c,d), IMP-AuPd/TiO_2 (e, f)

According to several characterization techniques consisted of XRD, N_2 physisorption, XPS, CO chemisorption, UV-visible spectroscopy, and TEM, the structural features of catalysts prepared by FSP, DP, and IMP methods are given in **Figure 5.7**. It is clearly demonstrated that the bimetallic AuPd/TiO_2 preparation by FSP synthesis resulted in more uniform AuPd alloy particles; moreover, the size of AuPd alloy particles was smaller than those bimetallic catalysts prepared by DP or IMP method.

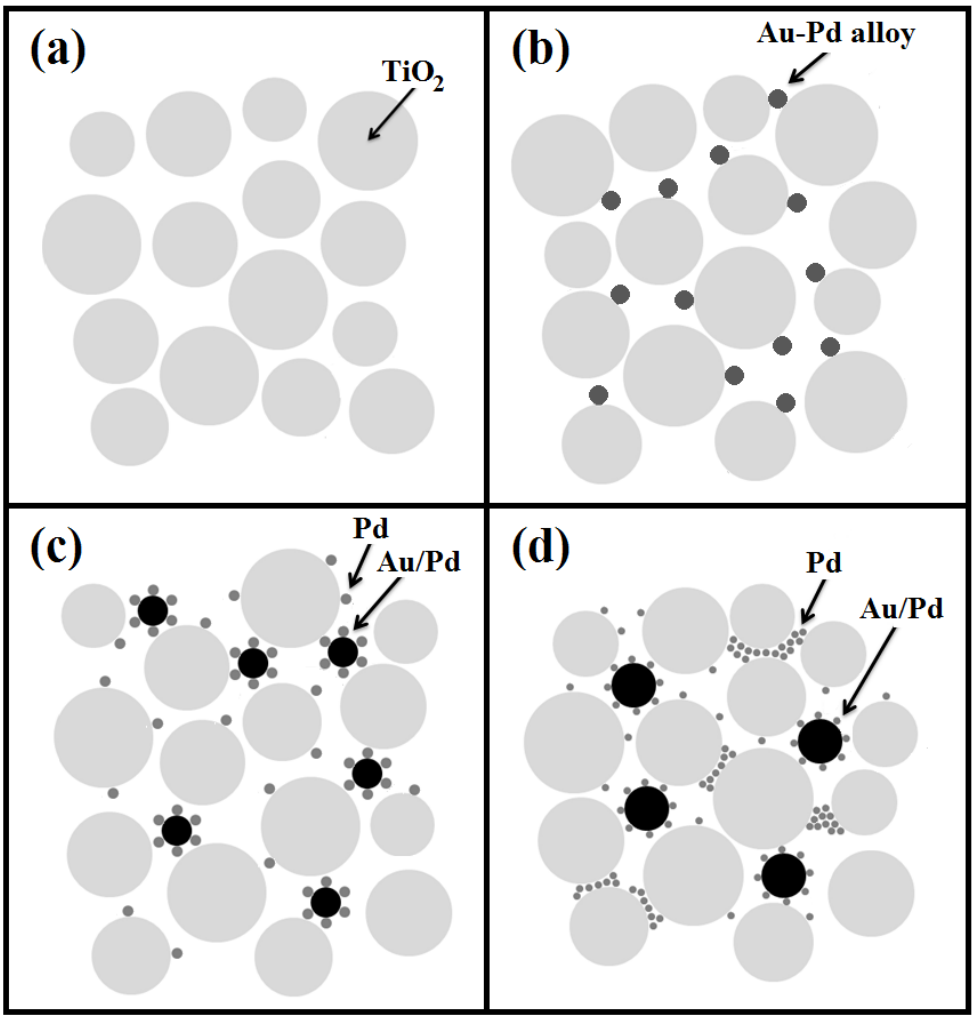

Figure 5.7 Structural features of (a) FSP-TiO_2, (b) FSP-AuPd/TiO_2, (c) DP-AuPd/TiO_2, and (d) IMP-AuPd/TiO_2

5.1.2 Catalytic study in liquid-phase selective hydrogenation of 1-heptyne

The liquid-phase selective hydrogenation of 1-heptyne under mild reaction conditions was used to evaluate the catalytic performance of all catalysts synthesized. According to H_2-TPR results (as described in part 5.2), the PdO could be fully reduced by H_2 at ambient temperature. Thus, the catalysts were reduced in H_2 atmosphere at 40 °C for 2 h prior to the reaction study. The conversion of 1-heptyne and the selectivity to 1-heptene as a function of time are demonstrated in **Figure 5.8** and **5.9**.

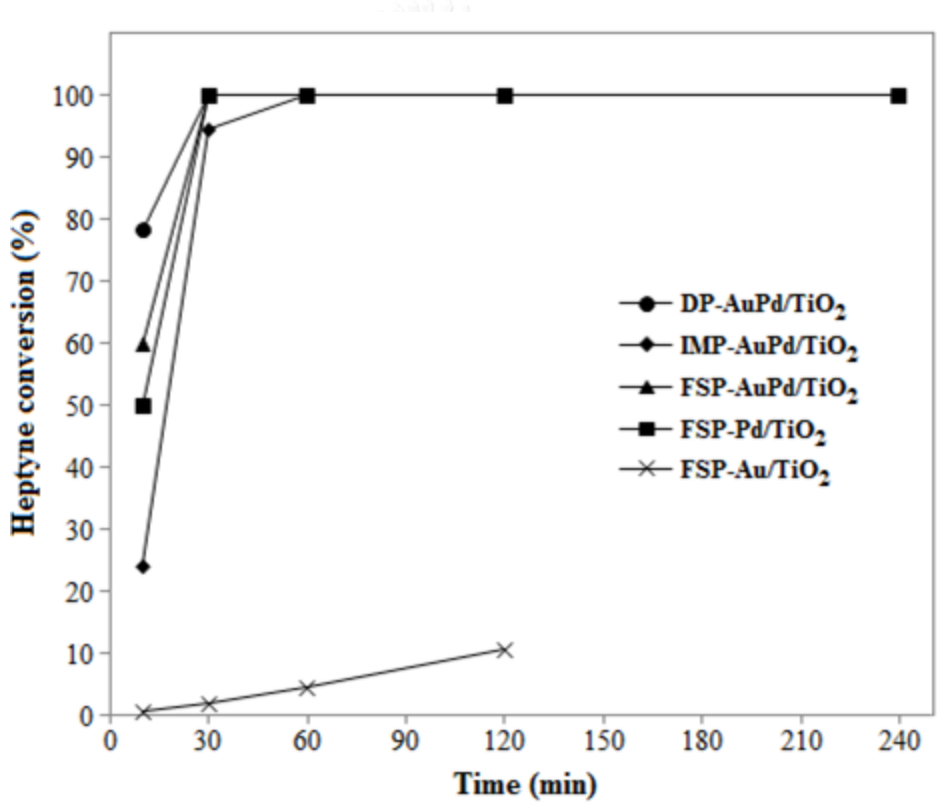

Figure 5.8 Heptyne conversion (%) of FSP-Au/TiO_2, FSP-Pd/TiO_2, FSP-AuPd/TiO_2, IMP-AuPd/TiO_2, DP-AuPd/TiO_2 catalysts in liquid-phase selective hydrogenation of 1-heptyne

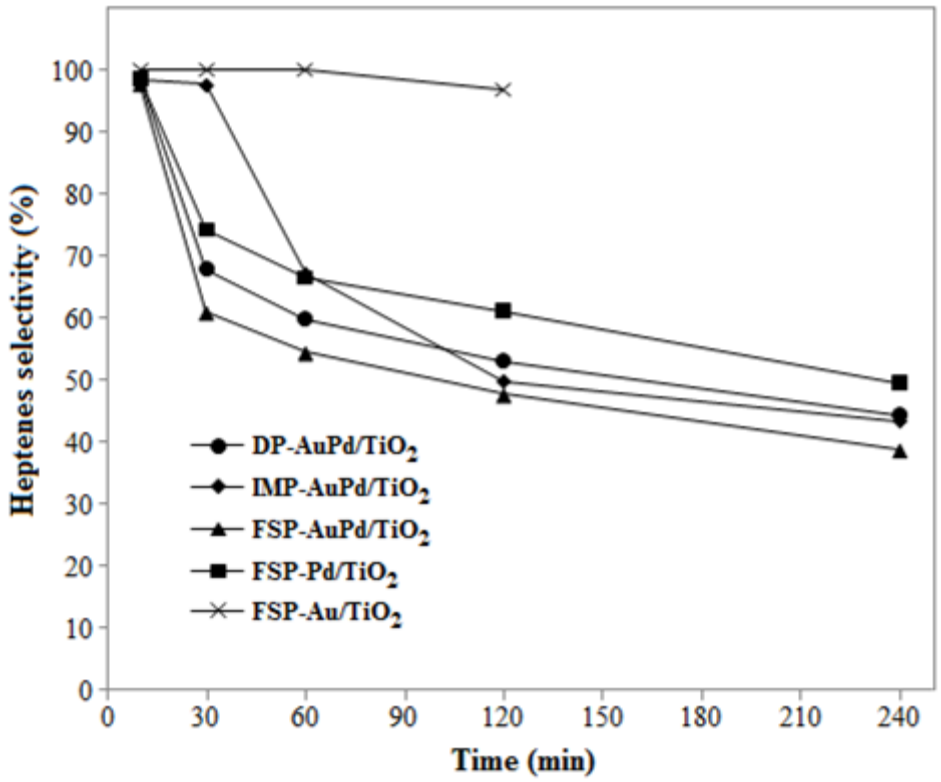

Figure 5.9 Heptenes selectivity (%) of FSP-Au/TiO_2, FSP-Pd/TiO_2, FSP-AuPd/TiO_2, IMP-AuPd/TiO_2, DP-AuPd/TiO_2 catalysts in liquid-phase selective hydrogenation of 1-heptyne

The order of the activity for selective hydrogenation of 1-heptyne was ranged as follows: DP-AuPd/TiO_2 > FSP-AuPd/TiO_2 > FSP-Pd/TiO_2 > IMP-AuPd/TiO_2 >> FSP-Au/TiO_2. Within 30 min of reaction time, all the Pd-based catalysts exhibited the full conversion of 1-heptyne (100% conversion), except for the IMP-AuPd/TiO_2. The catalytic activity of the FSP-Au/TiO_2 was found to be very low due to the relatively large Au particles being formed during FSP synthesis. However, it has been reported that Au nanoparticles in the range of 2-4 nm in size are catalytically active in hydrogenation reactions [191].

In comparison with the monometallic FSP-Au/TiO_2 or FSP-Pd/TiO_2 nanoparticles, the superior activity of FSP-AuPd/TiO_2 catalysts has been attributed to the synergistic effects of the AuPd alloy [192]. In spite of higher CO chemisorption

ability, the catalytic activity of the IMP-AuPd/TiO_2 was lower than other bimetallic catalysts prepared by DP or FSP. Based on N_2 physisorption results, the IMP-AuPd/TiO_2 exhibited the smallest pore volume and pore diameter; moreover, the change of hysteresis loop indicated to the modification of pore structure of FSP synthesized TiO_2 through impregnation and calcination of Pd and Au precursors. Furthermore, some agglomeration of small Pd/PdO particles, which are occluded within the TiO_2 pore was also observed on the IMP-AuPd/TiO_2 according to the structural features. The characteristic of large pore in FSP synthesized catalysts has been reported to facilitate the diffusion of both the reactants and products in liquid-phase hydrogenation reactions [65, 193]. Except the IMP-AuPd/TiO_2, their catalytic activity results of 1-heptyne hydrogenation are also correlated well with the dispersion of Pd.

The desired product for the liquid-phase selective hydrogenation of 1-heptyne is 1-heptene, while the other product formed is heptane (hydrogenation of 1-heptene to heptane). The selectivity to 1-heptene after 30 min of reaction time (full conversion of 1-heptyne) for FSP-Pd/TiO_2, DP-AuPd/TiO_2, and FSP-AuPd/TiO_2 was found to be 74.3, 67.9, and 60.9%, respectively. However, at the same reaction time (after 30 min), the selectivity to 1-heptene of the IMP-AuPd/TiO_2 catalyst was exhibited at 97.6% because of uncompleted conversion of 1-heptyne. It has been reported previously that the 1-heptyne presence could prevent the re-adsorption of 1-heptene on active sites and restrain the further hydrogenation of 1-heptene to heptane [194, 195]. Prolonging the reaction time to 240 min, the selectivity to 1-heptene for monometallic FSP-Pd/TiO_2 was maintained at ca. 50 %; meanwhile, the selectivity to 1-heptene for other bimetallic catalysts, including DP-AuPd/TiO_2, FSP-AuPd/TiO_2, and IMP-AuPd/TiO_2, decreased further to 44, 39, and 44 %, respectively. It is obvious that after complete 1-heptyne conversion, the 1-heptene selectivity for all of bimetallic AuPd/TiO_2 catalysts was lower compared to the monometallic FSP-Pd/TiO_2.

The selectivity to alkene formation has been typically reported to be irrespective of Pd particle size for most reactants in the selective alkyne

hydrogenation [55, 196, 197]. It is rather affected by electronic modification of the Pd metal. From our recent study [144], the electron-rich Pd species in the AuPd alloy particles prepared by sequential loading of Pd by IMP and Au by DP exceedingly promoted the hydrogenation of 1-heptene to heptane in the second step. Especially when the AuPd alloy particles less than 10 nm in size, such effect was more pronounced. According to the present study, the structure feature of AuPd alloy particles was found to affect the catalytic behavior in the hydrogenation of 1-heptene to heptane in the second step. Based on the XPS analysis which is the surface technique, both of Au and Pd were detected and found on the surface of Au–Pd alloy particles for the FSP-AuPd/TiO_2 indicating to the more exertion in electronic modification compared to the DP-AuPd/TiO_2 and IMP-AuPd/TiO_2, in which most of the Au particle surface was covered with smaller Pd/PdO particles.

5.1.3 Catalytic study in liquid-phase hydrogenation of 1-heptene

The liquid-phase hydrogenation of 1-heptene was also performed under similar mild reaction conditions in order to investigate the catalytic performance (ability to convert 1-heptene to heptane) of all catalysts synthesized. The 1-heptene conversion as compared to that of 1-heptyne hydrogenation after 10 min of reaction time is illustrated in **Figure 5.10**. For the FSP-AuPd/TiO_2 catalyst, the highest conversion of 1-heptene in the hydrogenation of 1-heptene corresponded to the lowest 1-heptene selectivity in the hydrogenation of 1-heptyne. Whereas the DP-AuPd/TiO_2 catalyst exhibited lower activity in the hydrogenation of 1-heptene despites its highest hydrogenation rate of 1-heptyne. However, it can maintain moderately high selectivity to 1-heptene after full conversion of 1-heptyne.

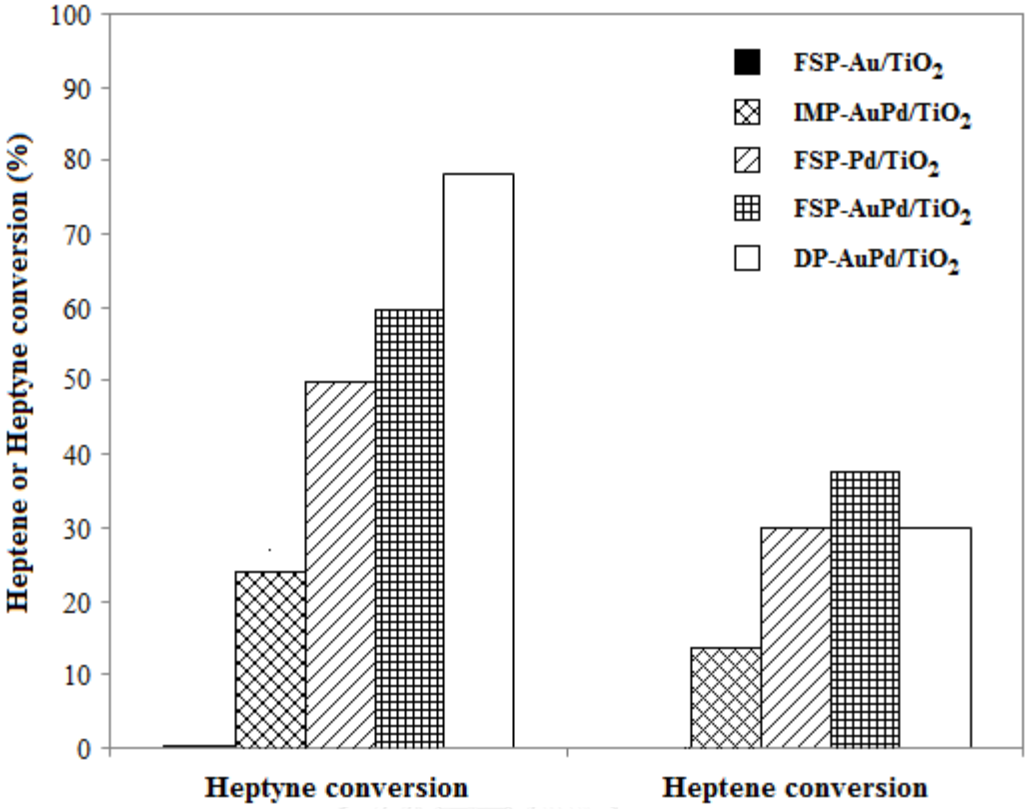

Figure 5.10 Catalytic performance of FSP-Au/TiO_2, FSP-Pd/TiO_2, FSP-AuPd/TiO_2, IMP-AuPd/TiO_2, DP-AuPd/TiO_2 catalysts in liquid phase hydrogenation of 1-heptene and 1-heptyne at a reaction time of 10 min

5.1.4 Mechanism for Au–Pd alloy formation and activity-structure relation

Based on various characterization techniques including XRD, N_2 physisorption, XPS, CO chemisorption, UV-visible spectroscopy, and TEM, the structural features of the bimetallic Au-Pd/TiO_2 prepared by FSP, IMP, and DP methods can be obtained (as depicted in **Figur 5.7**). For the DP-AuPd/TiO_2 and IMP-AuPd/TiO_2 catalysts, the bimetallic Au/Pd and monometallic Pd/PdO particles existed together on these bimetallic catalysts. The larger particles in 15-26 nm range was represented to the AuPd particles while the smaller particles in 2-4 nm range was attributed to the monometallic Pd/PdO particles. Much higher Pd dispersion based on CO chemisorption ability of DP-AuPd/TiO_2 and IMP-AuPd/TiO_2 in comparison with FSP-AuPd/TiO_2 was probably because of the existence of smaller monometallic Pd/PdO

particles. Nevertheless, the bimetallic catalyst preparation by IMP and DP (IMP-AuPd/TiO_2 and DP-AuPd/TiO_2) resulted in the significant change of the FSP-TiO_2 pore structure unlike the FSP-AuPd/TiO_2. The characteristic of FSP-TiO_2 pores was mostly interparticle-particle pores, so they had little trouble in adsorbing the Pd precursor solution during IMP and DP and in accommodating the Pd/PdO particles formed after calcination step (400 $^{\circ}C$ for 3 h) with a resulting loss of pore volume. Higher Pd dispersion on the DP-AuPd/TiO_2 led to higher catalytic activity for liquid-phase selective hydrogention of 1-heptyne. Interestingly, the lower activity of IMP-AuPd/TiO_2 inspite of highest CO chemisorption ability was found. This result suggests to the limitation in access of the reactants (including 1-heptyne and 1-heptene) to the Pd active sites deposited insides the TiO_2 pore.

Not only the dependence of 1-heptyne hydrogenation activity on the dispersion of Pd (i.e., DP-AuPd/TiO_2) and/or location of Pd particles (i.e., IMP-AuPd/TiO_2) was found in this study, but also the AuPd alloy formation was found to be reponsible for high catalytic activity of 1-heptene hydrogenation in the second step. According to this study, the AuPd particle size on the bimetallic catalysts prepared by IMP and DP (IMP-AuPd/TiO_2 and DP-AuPd/TiO_2) was reported to be larger than that prepared by FSP (FSP-AuPd/TiO_2); furthermore, based on XPS analysis Au could not be detected on the catalyst surface. The electronic effect due to the bimetallic AuPd particles on the IMP-AuPd/TiO_2 and DP-AuPd/TiO_2 was less pronounced than that on the FSP-AuPd/TiO_2 where the AuPd alloy particle size was smaller (less than 10 nm) and both of Au and Pd species could be detected on the catalyst surface.

The formation of bimetallic AuPd alloy supported on TiO_2 nanoparticles during FSP synthesis can be explained as follows: firstly, all of precursor solutions were sprayed forming the droplets and then evaporated and combusted as soon as they met the flame, thus releasing the metal atoms. The nucleation and growth of particles by coagulation and condensation occurred along the axial direction of the flame. The TiO_2 particle formation began earlier because of lower vapor pressure of TiO_2 compared to those of the metals. While the small AuPd alloy particle began to

form at further downstream of the flame (at lower temperature) and then deposited directly on the TiO_2 particles.

Based on our present study, the bimetallic catalyst preparation by using FSP synthesis favored the formation of mixed AuPd alloy particles and not separated monometallic Au and Pd particles. The direct formation of bimetallic alloy particles during FSP synthesis has been previously reported on other supported catalysts such as Au–Ag/TiO_2 [117] and Pt–Pd/Al_2O_3 [123].

5.2 Effect of reduction temperature on the characteristics and catalytic properties of TiO_2 supported AuPd alloy particles prepared by one-step flame spray pyrolysis in the selective hydrogenation of 1-heptyne

This part aims to investigate the effect of low and high reduction temperatures on the monometallic Pd/TiO_2 and bimetallic $AuPd/TiO_2$ catalysts synthesized by FSP in terms of characteristic, such as geometric state, electronic state, and alloy formation, and their catalytic performances in the selective hydrogenation. The high reduction temperature was chosen at 500 °C because TiO_2 support is well-known as the partially reducible oxide after high temperature reduction which has been reported to occur at temperature about 500 °C [52, 198, 199] resulting in the decoration of metal surface (strong metal-support interaction or called SMSI effect). While the low reduction temperature was chosen at 40 °C because PdO can be fully reduced by H_2 at ambient temperature [199] and SMSI effect did not occur at this low reduction temperature. When compared to the high temperature reduction (500 °C), the effect of SMSI on the monometallic Pd/TiO_2 and bimetallic $AuPd/TiO_2$ synthesized by FSP could be seen. The characteristics and catalytic properties of the FSP synthesized catalysts were investigated by various techniques such as XRD, ICP-OES, N_2 physisorption, H_2-TPR, XPS, TEM-EDX. Moreover, the catalytic performance of catalysts was evaluated in liquid-phase selective hydrogenation of 1-heptyne under mild conditions.

5.2.1 Characteristics of catalysts

5.2.1.1 X-ray diffraction (XRD)

The effect of reduction temperature on the crystal structure, phase composition, crystallite size of TiO_2 was investigated by using X-ray diffraction (XRD) technique. XRD patterns of the monometallic Pd/TiO_2 and bimetallic $AuPd/TiO_2$ catalysts reduced at 40 °C and 500 °C are illustrated in **Figure 5.11**. It can be seen that the characteristic XRD peaks for all the catalysts showed the presence of anatase TiO_2 phase at 2θ = 25.3°, 36.9°, 37.8°, 48.0°, 53.9°, 55.0°, 62.2°, 62.7°, 68.9°, 70.3°, 75.0°, 76° and rutile TiO_2 phase at 2θ = 27.4°, 36.0°, 41.2°, 54.3°, 56.6°, 69.8°,

corresponding to the standard #JCPDS 84-1286 and #JCPDS 88-1175, respectively. No XRD diffraction peaks for Pd metal or PdO were detected for both catalysts, probably because of low content of Pd loading and/or well-dispersed of Pd nanoparticles on the TiO_2 supports.

Interestingly, the additional XRD diffraction peak corresponding to the AuPd alloy nanoparticles at (111) plane can be detected for the FSP synthesized bimetallic AuPd/TiO_2 catalysts reduced at 500 ℃ (AuPd/TiO_2 R500) as presented in **Figure 5.11**. As reported previously by literature [200], the XRD diffraction peak for (111) plane of AuPd alloy was observed at 38.7°, whereas the XRD diffraction peak for mixture of separate Pd and Au showed two separated XRD diffraction peaks consisted of Pd (111) plane at 39.8° and Au (111) plane at 38.2°. The intermediate lattice parameter between that of Pd and Au metals in the former was attributed to the AuPd alloy formation, whilst the latter suggested to the presence of two different phases. It has been reported that the adding Au was considered to be helpful to protect Pd^0 from being oxidized into PdO [152].

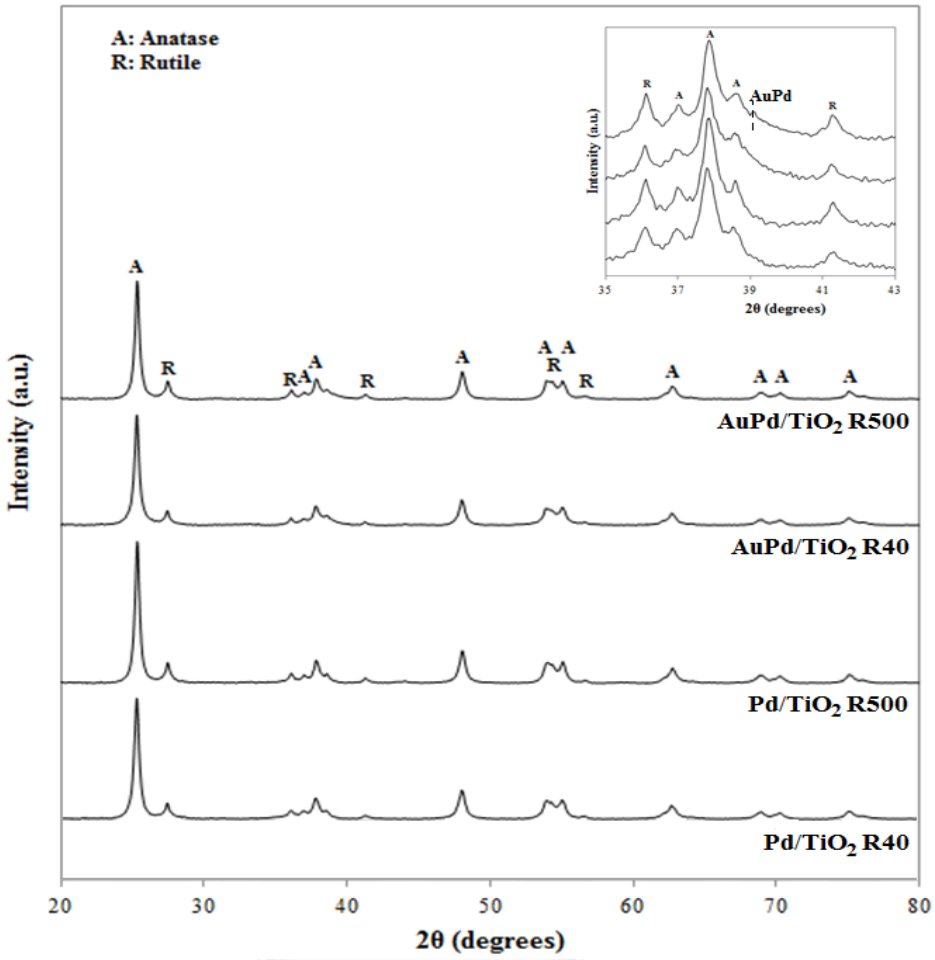

Figure 5.11 XRD patterns over a scan range from 20° to 80° 2θ of (a) Pd/TiO_2 R40 (b) Pd/TiO_2 R500 (c) $AuPd/TiO_2$ R40 (d) $AuPd/TiO_2$ R500 catalysts (in-set: XRD patterns over a scan range from 35° to 45° 2θ of (a) Pd/TiO_2 R40 (b) Pd/TiO_2 R500 (c) $AuPd/TiO_2$ R40 (d) $AuPd/TiO_2$ R500 catalysts)

The TiO_2 crystallite size and the ratio of anatase to rutile phase are shown in **Table 5.6**. The crystallite size of anatase phase TiO_2 was calculated by measuring the broadening of a particular XRD diffraction peak at 25°. With increasing reduction temperature from 40 to 500 °C, both of monometallic Pd/TiO_2 and bimetallic $AuPd/TiO_2$ catalysts did not exhibit the significant change of the crystallite sizes of anatase phase TiO_2 (24-26 nm). Meanwhile, slight decrease in ratio of anatase to rutile phase was observed when reduction temperature increased, indicating to the phase transformation of anatase to rutile TiO_2 upon high reduction temperature. The

reduction at high temperature was reported to weaken the Ti-O-Ti network and to promote the breaking of Ti-O bond, leading to the structural rearrangement to the thermally stable rutile phase [201]. For the bare TiO_2 support, the phase transformation of anatase to rutile at high temperature was also observed. The ratio of anatase to rutile for FSP-TiO_2 after reduction at high temperature decreased from 4.9 to 4.3 indicating to the promotion of rutile formation. However, the ratio of anatase to rutile for TiO_2 support (4.9) was slightly higher than the ones with Pd or AuPd addition during FSP synthesis (4.7). Compared to the monometallic ones, the phase transformation of anatase to rutile upon reduction at high temperature on the bimetallic AuPd/TiO_2 catalysts was suppressed. The decrease in the ratio of anatase to rutile after reduction at high temperature for the bimetallic AuPd/TiO_2 was less than that of monometallic Pd/TiO_2 catalyst.

It is well known that the most importance factor affecting the phase transformation is the presence and amount of defects on the oxygen sublattice (i.e., TiO_{2-x}). Ease of rearrangement and transformation are increased by relaxation of the large oxygen sublattice through the increased presence of oxygen vacancies [202]. One of the kinetics of the anatase to rutile phase transformation typically is considered in term of temperature. The pure bulk anatase is considered widely to begin to transform irreversibly to rutile in air at 600 °C [203-205]; however, the reported transition temperature vary in the range 400-1200 °C [204, 206-211] due to the use of different methods of determining the transition temperatures, raw materials, and processing methods. Moreover, the promotion of the phase transformation through the use of a reducing atmosphere is considered to be due largely to the increased levels of oxygen vacancies during heating in such atmosphere [202].

The role of doping with the metal on the phase transformation of TiO_2 has been reported to be based on the importance of differentiating between the assumption of substitutional and interstitial solid solubility [202]. The dopant with metal in substitutional form may result in increasing the oxygen vacancy level and promoting the phase transformation upon increase in lattice relaxation; on the other

hand, the interstitial form may result in enhancing the lattice constraint and inhibiting the phase transformation [202, 212]. During FSP synthesis, in which the precursors containing Ti, Au, and Pd were fed together into the reactor simultaneously, the role of doping with Au and Pd was considered to be based on the assumption of Ti^{4+} substitution, thus increasing in oxygen vacancy and promoting rutile formation. This results are in good agreement with those reported previously by Paulauskas et al. [213] that the rutile phase was promoted in the metal-doped TiO_2 synthesized by FSP due probably to the formation of the dopant metal oxide through the substitution of Ti^{4+} ion.

Table 5.6 TiO_2 crystallite size and ratio anatase to rutile phase based on the XRD results

Catalysts		Crystallite size of anatase TiO_2 (nm)	Ratio[a] of anatase to rutile phase TiO_2
Pd/TiO_2	R40	24	4.7 (82.3:17.7)
	R500	26	3.8 (79.4:20.6)
$AuPd/TiO_2$	R40	25	4.7 (82.4:17.6)
	R500	27	4.1 (80.3:19.7)

[a]Percentages of anatase and rutile TiO_2 phase compositions were determined according the method described in Ref. [214].

Comparing between monometallic Pd and bimetallic AuPd catalysts, change of anatase to rutile phase ratio upon reduction at high temperature was more pronounced on the monometallic Pd/TiO_2 catalysts. Probably, the reduction of PdO on the monometallic Pd/TiO_2 may result in an increase in the number of oxygen vacancies and increase in lattice relaxation, thus leading to the promotion of phase transformation to rutile at high temperature. Whilst most of Pd in the bimetallic $AuPd/TiO_2$ was in the form of Pd alloying with Au. The decrease in the ratio of anatase to rutile after reduction at high temperature for the bimetallic $AuPd/TiO_2$ was less than that of monometallic Pd/TiO_2 catalyst, probably due to the less

increased levels of oxygen vacancies and/or less lattice relaxation during reduction compared to monometallic Pd/TiO_2 catalyst.

5.2.1.2 N_2 physisorption

The N_2 adsorption-desorption isotherms of FSP synthesized monometallic Pd/TiO_2 and bimetallic $AuPd/TiO_2$ catalysts are given in **Figure 5.12**. According to the Brunauer-Deming-Deming-Teller (BDDT) classification of sorption isotherms, the FSP-TiO_2, FSP-$AuPd/TiO_2$, and DP-$AuPd/TiO_2$ showed type-IV physisorption isotherm with a well-defined hysteresis loop at high relative pressure (P/P_0) in the range of 0.8 to 1.0, corresponding the characteristic of mesoporous materials (pore diameters between 2 and 50 nm).

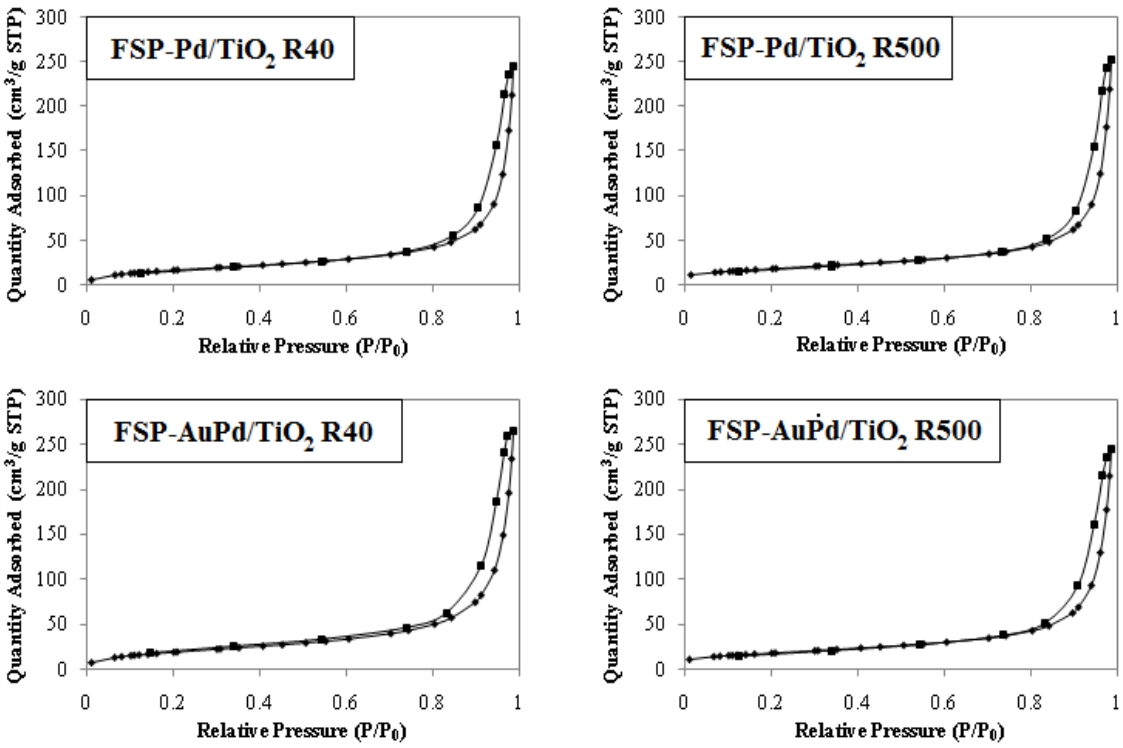

Figure 5.12 N_2 physisorption isotherms of the monometallic Pd/TiO_2 and bimetallic $AuPd/TiO_2$ catalysts reduced at 40 and 500 °C

The BET specific surface area, pore volume, and average pore diameter of the catalysts were determined by using N_2 physisorption technique as shown in **Table**

5.7. The N_2 adsorption-desorption isotherms, BET specific surface area, pore volume, and average pore diameter of both catalysts did not change significantly with increasing reduction temperature. There were not much differences in terms of the physical properties of catalysts reduced at 40 and 500 °C. Preparation under high flame temperature up to 2600-2800 K [62] yielded high thermal stability FSP-made catalysts. Characterization results from XPS and TEM-EDX also suggest no changes in composition and morphology of the AuPd alloy upon high temperature reduction.

Table 5.7 N_2 physisorption properties of the monometallic Pd/TiO_2 and bimetallic $AuPd/TiO_2$ catalysts reduced at 40 and 500 °C

Catalysts		N_2 Physisorption results		
		BET surface area (m^2/g)	Pore volume (cm^3/g)	Average pore diameter (nm)
Pd/TiO_2	R40	66	0.37	22
	R500	67	0.38	23
$AuPd/TiO_2$	R40	74	0.40	22
	R500	65	0.37	23

5.2.1.3 H_2-temperature programmed reduction (H_2-TPR)

The reducibilities of FSP synthesized monometallic Pd/TiO_2 and bimetallic $AuPd/TiO_2$ catalysts were investigated by H_2-TPR and the results are given in **Figure 5.13**. The sample was pretreated at 400 °C for 1 h before the TPR analysis in order to remove possible impurities contained in the samples.

According to the H_2-TPR results, the negative peaks were observed for both of Pd/TiO_2 and $AuPd/TiO_2$ catalysts except the FSP synthesized pure TiO_2 support. These negative TPR peaks at low temperature (~65 °C) has been attributed to H_2 release (H_2 production) due to the decomposition of Pd hydride (PdH_x) formed earlier with H_2 [215, 216]. It is well-known that the Pd metal particles are able to absorb hydrogen within their structure at room temperature resulting in the Pd hydride formation [217]. According to the literature [218-221], there have reported that Pd

hydride decomposition over supported Pd catalysts occurred in the range of 323-373 K. The absence of any detectable H_2 consumption signal (positive TPR peak) in advance of H_2 release signal (negative TPR peak) attributes to a reduction at room temperature [215]. There is a general agreement in the literature that H_2 uptake at room temperature corresponds to the reduction of supported and unsupported PdO occurs at room temperature [199, 222, 223].

At room temperature:

PdO ➔ Pd metal ; Reduction of PdO

Pd metal ➔ Pd hydride ; Absorption of H_2

For this experiment, before to heat the sample from 35 °C to 700 °C, the sample was kept under flowing of 10% H_2/Ar at 35 °C in order to waiting for baseline stable. During this time the PdO can be reduced to from the Pd and then adsorb H_2 forming the Pd hydride, prior to TPR analysis. Thus, amount of Pd hydride could be referred to amount of Pd metal which is reduced from PdO at room temperature and then adsorb H_2 forming the Pd hydride.

For the addition of Au to form the bimetallic AuPd catalysts (AuPd/TiO_2), the H_2-TPR peak area (or H_2 consumption as shown in **Table 5.8**) corresponding the decomposition of Pd hydride (negative TPR peaks at low temperature ~65 °C) was lower in comparison with the monometallic ones (Pd/TiO_2), indicating a low amount of Pd hydride species being formed and/or less amount of Pd metal because most of Pd species in the AuPd/TiO_2 were formed as the state of AuPd alloy nanoparticles. Consequently, it suggested that the presence of AuPd alloy nanoparticles could suppress the Pd hydride formation. Such result is consistent with other previously studies by Krawczyk et al. [224] and Lingaiah et al. [218] such as the addition of second metal (In and Fe) into supported Pd catalysts. The effect of hydride formation over supported Pd catalysts has been reported to be less pronounced than that effect of alloying between Pd and Ag [225, 226]. According to Tew et al. [227], the role of hydride species over oxide-supported Pd nanoparticles for alkyne hydrogenation was reported that hydride species were not necessary for complete

hydrogenation [227]. However, in this study the Pd hydride could be decomposed already upon reduction at high temperature before to test the catalytic study. Considering the reduction of AuPd alloy particles in this study, the small broad peak in the range 90-120 °C which can be observed in FSP synthesized AuPd/TiO_2 could be attributed to the reduction of Au_xPd_yO to Au_xPd_y alloy particles. The reduction of Au_xPd_yO to Au_xPd_y alloy has been reported in the literature to be low temperature reduction peak at 90-100 °C [228, 229].

According to the H_2-TPR profile of the FSP synthesized bare TiO_2 supports, the partial reduction of the bare TiO_2 support itself was observed at higher temperature. The partial reduction of the bare TiO_2 support consisted of the reduction of Ti^{4+} to Ti^{3+} at 485 °C and Ti^{3+} to $Ti^{<3+}$ at > 520 °C. According to the literature [198, 199, 230], the partial reduction of TiO_2 has been found to occur at $T \geq 500$ °C and depend on the TiO_2 structure. Comparing to the FSP synthesized bare TiO_2 supports, slight shifting in partial reduction peak of the TiO_2 towards lower temperature was found on both of monometallic Pd/TiO_2 and bimetallic AuPd/TiO_2 (from 485 °C to 445 °C and 430 °C for Pd/TiO_2 and AuPd/TiO_2, respectively). The existence of noble metals (i.e., Pd or AuPd) has been reported to facilitate the partial reduction of TiO_2 because of hydrogen spillover from group VIII transition metals to the TiO_2 support [231]. The hydrogen molecules on the noble metal particles (i.e., reduced Pd^0) were dissociated into hydrogen atoms and then spilled over onto the TiO_2 support, thus leading to partial reduction of TiO_2 to $TiO_{(2-x)}$ [232-234].

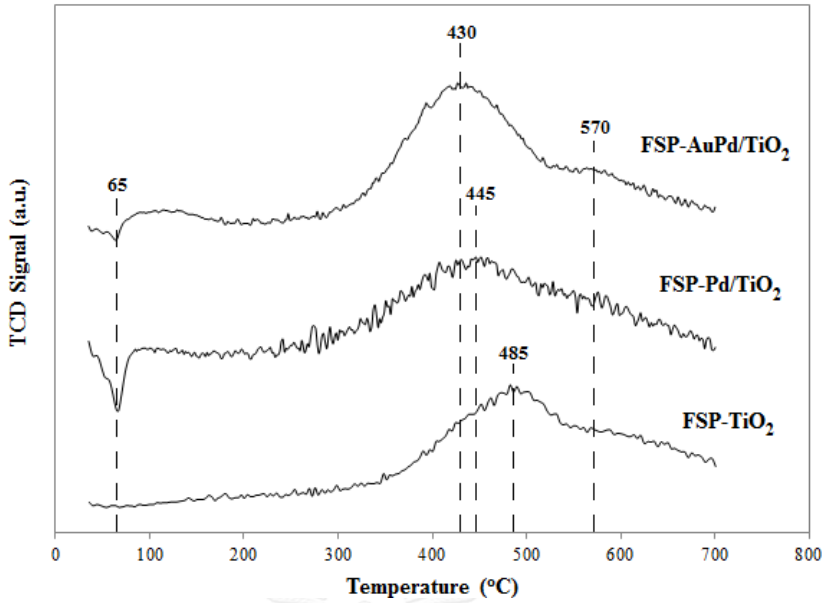

Figure 5.13 H_2 Temperature-programmed reduction profiles of TiO_2 support, Pd/TiO_2, and $AuPd/TiO_2$ catalysts

Table 5.8 H_2 consumption determined from H_2-TPR of TiO_2 support, Pd/TiO_2, and $AuPd/TiO_2$ catalysts

Catalysts	H_2 consumption (mmol/g cat)		
	PdH_x	AuPdO	TiO_2
TiO_2	n/a	n/a	5.156538
Pd/TiO_2	0.44158	n/a	7.121513
$AuPd/TiO_2$	0.16087	0.303995	7.236523

5.2.1.4 X-ray photoelectron spectroscopy (XPS)

The X-ray photoelectron spectrometer (XPS) can be used to characterize the core-level binding energy change indicating to electron transfer and chemical elemental compositions at surface of the catalyst samples. The XPS results including binding energies of Pd $3d_{5/2}$ and Au $4f_{7/2}$ and the surface elemental composition of monometallic Pd/TiO_2 and bimetallic $AuPd/TiO_2$ catalysts are summarized in **Table 5.9**.

Typically, the binding energy of Pd and Au metals has been reported to be in the range of 335.0-335.4 eV [183] and 83.8-84.0 eV [141], respectively. For the monometallic Pd/TiO_2 catalysts, the shift of XPS binding energy for Pd $3d_{5/2}$ from 337.3 eV to 334.6 eV was observed upon reduction at high temperature. Shift in both of $Pd3d_{5/2}$ and $Au4f_{7/2}$ binding energies for the bimetallic $AuPd/TiO_2$ to lower binding energies, as compared to Pd and Au metals, was attributed to AuPd alloy formation. The XPS peaks for Pd $3d_{5/2}$ and Au $4f_{7/2}$ of the $AuPd/TiO_2$ R40 were detected at 334.8 eV and 82.7 eV, respectively. After reduction at high temperature, the binding energy of Pd $3d_{5/2}$ decreased further to 334.5 eV, due probably to more AuPd alloy formation. Typically a shift in core-level binding energy of Pd3d and Au4f towards lower binding energy, as compared to pure metals, has been used to indicate the charge transfer between Pd and Au, and thus proving the AuPd alloy formation [235]. Upon alloying AuPd system, Au gains s, p electron and loses d electron whereas Pd loses s, p electrons but gains d electrons [236, 237]. Charge transfer between Pd and Au also helps to explain why Au is able to fully isolate Pd: there exists some Coulomb Pd-Pd repulsion in bulk Pd whereas Pd-Au attraction is realized as a result of net charge transfer from Pd to Au [237]. Furthermore, Au is one of the most electronegative metallic element, so upon alloying with Pd, a result of net charge transfer from Pd site to Au site is expected [237, 238]. Regarding to XPS results, the negative shift of the Au 4f binding energy for the bimetallic catalysts with respect to monometallic Au catalyst is attributed to a net charge transfer from Pd to Au, possibly increasing the Au s-state occupancy in the AuPd alloy. While the negative shift of Pd 3d binding energy compared to the monometallic Pd is attributed that Pd gains d electrons in AuPd alloy system. The negative shift of Pd 3d binding energy upon AuPd alloying has been reported in literature such as unsupported Pd-Au alloys [235], Au_xPd_y/SiO_2 [15], and $AuPd/CeO_2$ [239].

Regarding the electronic state of Pd 3d for Pd/TiO_2 R40, the XPS binding energy for Pd $3d_{5/2}$ was observed at 337.3 eV indicating to the formation of PdO at surface. As reported in the H_2-TPR results, the PdO reduction occurred after reduction in H_2 at 40° for 2 h, especially at room temperature. However, the re-

oxidation of the Pd metal at the surface for the Pd/TiO_2 catalyst upon contacting with air was likely (i.e., Pd/TiO_2 R40). In this study, after reduced the Pd/TiO_2 catalyst at 40 °C the catalyst was weighted and put into the autoclave reactor. During this time, the surface Pd metal for Pd/TiO_2 R40 is easily re-oxidized to surface PdO. The easily re-oxidation of Pd to PdO has been reported previously by Datye et al. [240] that the small domains of Pd metal at the surface are easy to re-oxidize upon cooling to room temperature in air, resulting in the formation of surface oxide phase which can be observed by XPS analysis (surface technique) while no bulk oxide was found by XRD or TEM. Moreover, such result about the ease of re-oxidation of Pd is also in good agreement with Melendez et al. [241] which reported that the smaller Pd particles are easier to oxidize and to form PdO layer than the larger Pd particles. On the other hand, the XPS binding energy corresponding to PdO was not observed on the Pd/TiO_2 reduced at high temperature (500 °C) and the bimetallic $AuPd/TiO_2$. Such results suggested that the Pd particles were found to be more resistant the re-oxidation at the surface upon reduction at 500 °C or alloying with Au.

Table 5.9 XPS results of the monometallic Pd/TiO_2 and bimetallic $AuPd/TiO_2$ catalysts reduced at 40 and 500 °C

Catalysts		Binding energy (eV)		Atomic concentration		Atomic ratio		
		Pd 3d	Au 4f	Pd(%)	Au(%)	Pd/Ti	Au/Ti	(Pd+Au)/Ti
Pd/TiO_2	R40	337.3	n/a	0.37	n/a	0.013	n/a	n/a
	R500	334.6	n/a	0.32	n/a	0.010	n/a	n/a
$AuPd/TiO_2$	R40	334.8	82.7	0.67	0.40	0.022	0.013	0.035
	R500	334.5	82.7	0.54	0.32	0.017	0.010	0.028

n/a: Not available

The surface elemental compositions of each chemical species are presented in **Table 5.9**. After reduction at high temperature (500 °C), decrease in the Pd/Ti and (Au+Pd)/Ti atomic ratios was probably attributed to the migration of TiO_x species

onto the metals during high temperature reduction, or so-called the SMSI effect [234, 242, 243]. The decrease level in the Pd/Ti atomic ratio at the catalyst surface was found to be ca. 23% for both of monometallic Pd/TiO_2 and bimetallic $AuPd/TiO_2$, suggesting to a similar degree of SMSI effect occurred. However, it should be noticed that the reduction temperature did not affect the bulk metal composition i.e., Au and Pd (as measured by ICP).

Recently, the change of AuPd alloy morphology through heat treatment has been studied in some works; however, there are fewer studies dealing with the effect of H_2 reduction temperature on the surface composition of AuPd alloy. For examples, Herzing et al. [244] reported that the calcination under air atmosphere resulted in a change of bimetallic structure from homogeneous alloy of the as-prepared 2.5 wt.% Au- 2.5 wt.% Pd/Al_2O_3 catalysts to Pd-rich shell/Au-rich core structure. Furthermore, with increasing the heat treatment temperature (from 200 to 400 °C), the ratio of Pd/Au at the catalyst surface increased, suggesting the migration of Pd to surface and the depletion of Au from surface. Nevertheless, the subsequent reduction under H_2 atmosphere (at 500 °C for 5 h) resulted in the reversal of core-shell structure (from Pd-rich shell/Au-rich core to Pd-rich core/Au-rich shell). Edwards et al. [245], however, revealed that the ratio of Pd/Au at the catalyst surface was found to increase slightly from 1.0-1.4 with increasing temperature to 400 °C. Meanwhile, the treatment under different atmospheres such as O_2 and CO/O_2 led to the segregation of Pd at the catalyst surface over $AuPd/TiO_2$ nanoparticles (Au/Pd atomic ratio = 8) [246].

According to the prediction of simple surface energetics, the surface free energies of Pd and Au are reported to be 2.043 J/m^2 and 1.626 J/m^2, respectively. In order to minimize the surface free energy, Au would preferentially decorate on the surface [247]. Nevertheless, as exemplified from the literature, the nature and structure morphology of AuPd particles is also dependent upon both heat treatment temperature and atmosphere. From this study, it could appear that the preparation of TiO_2 supported AuPd alloy nanoparticles by one step FSP synthesis resulted in

uniform AuPd particles with high thermal stability so that the composition of AuPd did not change upon high temperature reduction (500 ℃).

5.2.1.5 Transmission electron microscope (TEM)

The morphology, metal dispersion and particle size of the particles can be determined by using TEM technique. The TEM micrographs of the monometallic Pd/TiO_2 and bimetallic $AuPd/TiO_2$ catalysts reduced at 40 and 500 ℃ are shown in **Figure 5.14** along with the particle size distribution as given in **Figure 5.15**. The average metal particle size was measured from TEM micrographs based on approximately 500 particles.

The uniform distribution of AuPd alloy nanoparticles was observed on the $AuPd/TiO_2$ R40 catalysts with average particle size in the range of 2-5 nm. A slight increase in the average particle size after reduction at high temperature is found from 3.8 nm to 4.5 nm. The geometric standard deviation of the size distribution for $AuPd/TiO_2$ R40 and the $AuPd/TiO_2$ R500 were calculated to be 1.27 and 1.50, respectively. For the TEM micrographs of the monometallic Pd/TiO_2 R40 and Pd/TiO_2 R500 catalysts, the Pd nanoparticles were quite difficult to visualize; however, their particle size was determined to be in the range 2-3 nm whatever the reduction temperature.

The detection of Pd nanoparticles is difficult, probably due to the fact that Pd is lighter than Au (and of course bimetallic AuPd) and so the arising contrasts from very small particles are weaker; also the nature of the support must be taken into account because TiO_2 support could render the detection of very small nanoparticle contrasts rather difficult due to electron absorption which is not found for other oxide supports such as SiO_2 and Al_2O_3 [248-250] or non-oxide supports such as nitrides [250-252] or carbonaceous materials [253-256]. As mentioned in the experimental section that the TEM-EDX analysis with a LaB_6 thermoionic gun was used to perform imaging, the use of such an electron source results in the difficulty in detecting with probes below 5-10 nm in diameter because the amount of current is rather low and, as a result, spectra acquisition in EDX is rather long and

inconsistent with particle evolution under the electron beam (diffusion, damage, and so on), especially on small bimetallic nanoparticles (< 5 nm).

Taking into account previous studies on supported bimetallic nanoparticles [249, 257, 258] and in order to limit damage or any other evolution under the electron beam to negligible levels, three different electron probes is used to analyze different regions over catalyst samples, including a 10 nm electron probe to analyze small individual particles, a slightly decondensed 25 nm electron probe to analyze small groups of particles (2-5), and a (largely) decondensed electron probe to analyze large regions (several μm^2).

The amount of Au (%at) in the bimetallic nanoparticles measured by EDX analysis for the bimetallic AuPd/TiO_2 R40 and AuPd/TiO_2 R500 catalysts is presented in **Figure 5.16**. The EDX measurements were performed both on individual nanoparticles or small groups of nanoparticles (2-5) and on large regions. EDX results clearly suggested that the nanoparticles for both AuPd/TiO_2 R40 and AuPd/TiO_2 R500 catalysts were bimetallic. According to EDX measurement over large regions, the composition for both AuPd/TiO_2 R40 and AuPd/TiO_2 R500 catalysts consisted of (35 ± 3) %at Au and (65 ± 3) %at Pd. The composition determined by EDX was in very good agreement with value expected from ICP (35%at Au) and was very close to the XPS measurement (37 %at Au for both bimetallic catalysts), which were also performed over the large regions. This result reveals indeed that the entirety of the bimetallic nanoparticles were analyzed by both EDX (the electron beam probes all the particles) and XPS (this technique is sensitive to a thickness of around 5-10 nm and the nanoparticles are below 5 nm for a very large majority of them) techniques.

Meanwhile, the EDX measurements on individual nanoparticles as seen in **Figure 5.16** suggested that the composition of nanoparticles for AuPd/TiO_2 R40 was less homogeneous than those for AuPd/TiO_2 R500. The Au composition and a standard deviation based on EDX analysis for AuPd/TiO_2 R40 and AuPd/TiO_2 R500 was determined to be 37.7 %at with a standard deviation ±9.6 and 36.3 %at with a standard deviation ±3.6, respectively. Considering the standard deviation in composition, the composition of the individual nanoparticles tends to homogenize

upon reduction at high temperature. Regarding the Au/Pd ratio based on EDX analysis, the Pd/Au ratio did not change significantly with increasing reduction temperature from 40 to 500 °C, corresponding to the Pd/Au atomic ratio at the catalyst surface based on XPS analysis.

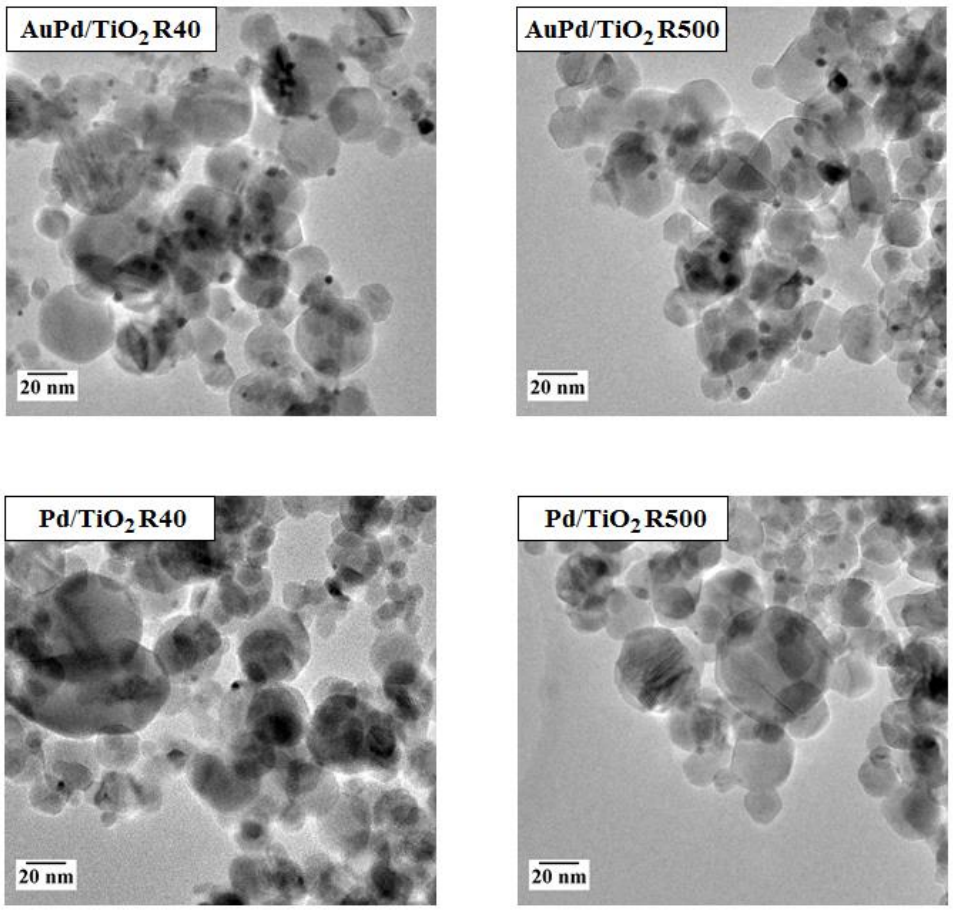

Figure 5.14 TEM images of (a) AuPd/TiO_2 R40 (b) AuPd/TiO_2 R500 (c) Pd/TiO_2 R40 (d) Pd/TiO_2 R500

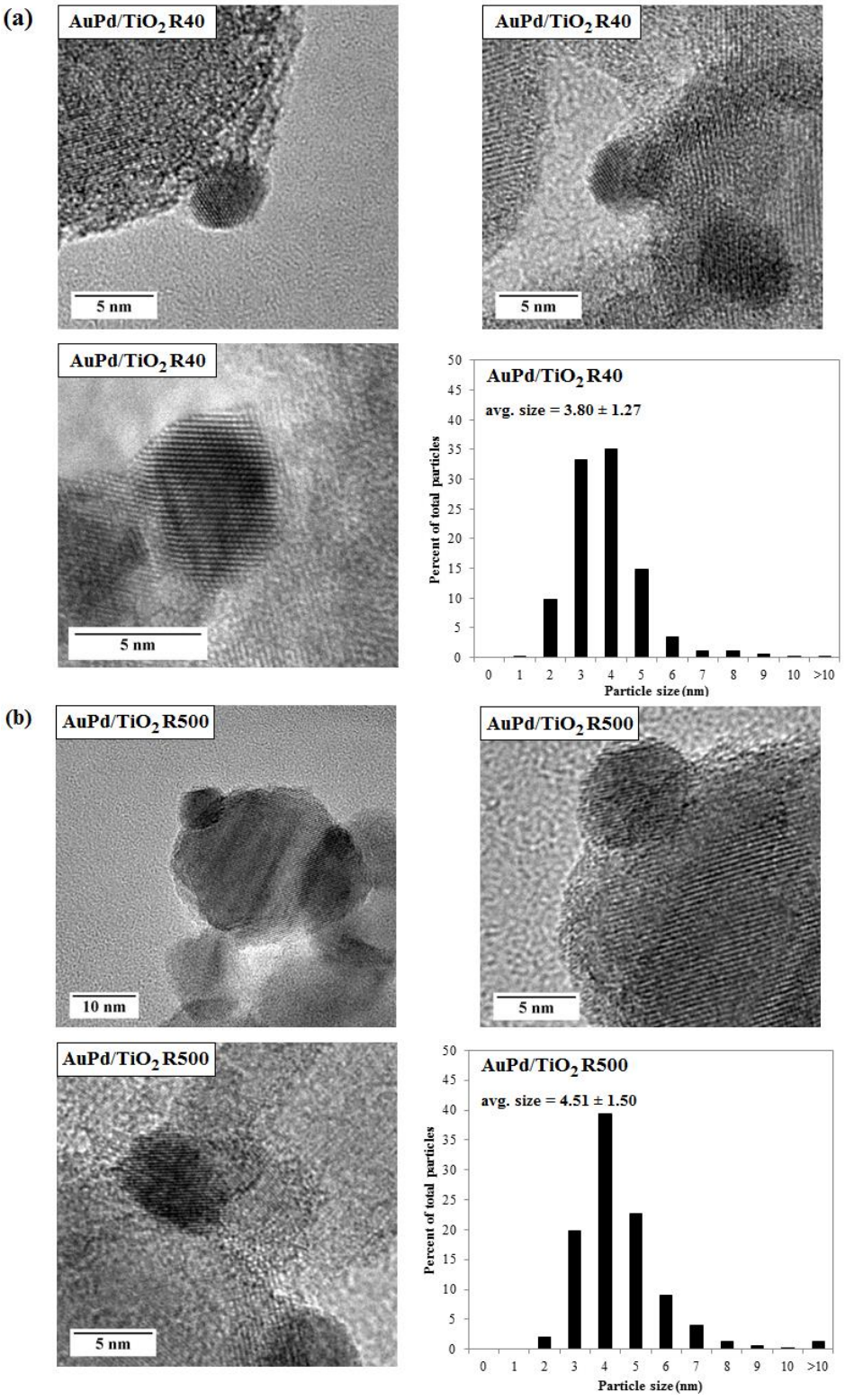

Figure 5.15 HR-TEM images and particle size distribution of the bimetallic AuPd/TiO_2 catalysts reduced at 40 (a) and 500 °C (b)

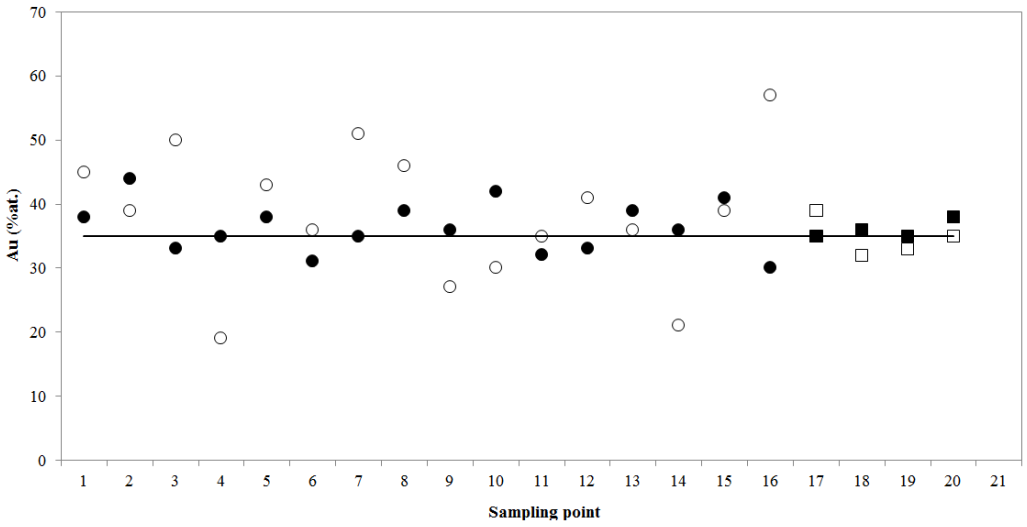

Figure 5.16 Amount of Au (%at) in the bimetallic nanoparticles measured by EDX for AuPd/TiO_2 R40 (open circles and squares) and AuPd/TiO_2 R500 (black circles and squares). Measurements were made on individual nanoparticles or small groups (3-5) nanoparticles (circles) and on large regions (squares). The straight grey line indicates the nominal composition determined by ICP.

5.2.2 Catalytic study in liquid-phase selective hydrogenation of 1-heptyne

The catalytic performances of the FSP synthesized monometallic Pd/TiO_2 and bimetallic Au-Pd/TiO_2 catalysts were evaluated in the liquid-phase selective hydrogenation of 1-heptyne under mild conditions. Prior to reaction study, the catalyst sample was reduced in H_2 atmosphere at 40 °C (or 500 °C) for 2 h. The products from for the liquid-phase selective hydrogenation of 1-heptyne are 1-heptene (desired product) and heptane and no other by-products are detected. The conversion of 1-heptyne, the selectivity to 1-heptene, and the yield of 1-heptene as a function of time for the monometallic and bimetallic catalysts reduced at 40 and 500 °C are demonstrated in **Figure 5.17, 5.18,** and **5.19**, respectively.

The initial hydrogenation rates for all catalysts were calculated at 10 min of reaction time as given in **Table 5.10**. The order of the activity for selective hydrogenation of 1-heptyne was ranged as follows: AuPd/TiO_2 R40 > AuPd/TiO_2 R500 > Pd/TiO_2 R500 > Pd/TiO_2 R40. All FSP synthesized catalysts exhibited complete

conversion of 1-heptyne within 60 min of the reaction time. Regardless of the reduction temperature, the superior catalytic activity for the bimetallic AuPd/TiO_2 catalysts than the monometallic Pd/TiO_2 catalysts was observed. Such results are consistent with those previous studies on the Au addition to form bimetallic AuPd alloy nanoparticles which is helpful to improve the catalytic activity of monometallic Pd/TiO_2 in the selective hydrogenation of 1-heptyne [152, 259, 260]. A small charge transfer from Pd to Au has been reported in the literature to activate Au resulting in the ability of Au to adsorb hydrogen [261-263]. According to Schimpf et al. [263], the electron transfer to Au resulted in the Au being enriched in valence electron density or activated Au. Then a partial transfer of electron density to the π^* orbital of the unsaturated bond is facilitated and the interaction of the active sites with the functional group is altered.

Table 5.10 The reaction rates obtained at 10 min reaction time of the different catalysts

Catalysts	Reaction rate (μmol /s /g cat.)
Pd/TiO_2 R40	169.8
Pd/TiO_2 R500	211.4
AuPd/TiO_2 R40	244.9
AuPd/TiO_2 R500	222.5

Interestingly, although both of monometallic Pd/TiO_2 and bimetallic AuPd/TiO_2 catalysts exhibited a similar degree of SMSI effect, the effect of reduction temperature on the catalyst performances was different between the monometallic Pd/TiO_2 and bimetallic AuPd/TiO_2 catalysts. After reduction at high temperature (500 °C), the increase in catalytic activity of Pd/TiO_2 was attributed to complete reduction of PdO to Pd metal as presented in XPS results, despite lower Pd/Ti atomic ratio at surface on the Pd/TiO_2 R500 catalyst. On the other hand, the catalytic activity of the bimetallic AuPd/TiO_2 R500 was found to be lower than the ones reduced at 40 °C (AuPd/TiO_2 R40). Due to no significant changes in the particle size, morphology, and alloy composition, the lower catalytic activity of bimetallic AuPd/TiO_2 after reduction

at high temperature was considerably attributed to lower amount of the metals on the surface as presented in the result of (Au+Pd)/Ti upon high temperature reduction (decreased from 0.035 to 0.028 as shown in **Table 5.9**). The decrease of catalytic activity for alloying bimetallic particles upon reduction at high temperature has been reported to occur over the other bimetallic catalysts such as Pt-Ge/Al_2O_3 and Pt-Sn/Al_2O_3 in hydrogenation/dehydrogenation reactions [264]. Compared to monometallic Pt/Al_2O_3 and bimetallic Pt-Sn/Al_2O_3 and Pt-Ge/Al_2O_3 catalysts reduced at low temperature (300 °C), the activity of bimetallic Pt-Sn/Al_2O_3 and Pt-Ge/Al_2O_3 catalysts after reduction at high temperature (500 °C) decreased drastically. Consequently, it suggested that the temperature of reduction treatment (i.e., under H_2 atmosphere) plays as one of important factors affecting the hydrogenation activity not only for the bimetallic AuPd alloy nanoparticles (as shown in this study), but also for the bimetallic Au core-Pd shell nanoparticles [163].

Within 30 min of reaction time, the selectivity to 1-heptene for all FSP synthesized catalysts was close to 100%, except for AuPd/TiO_2 R40 (the selectivity to 1-heptene at 87%). Considering at the same level of 1-heptyne conversion (∼99%), the selectivity to 1-heptene for all FSP synthesized catalysts was ranged in the following order: AuPd/TiO_2 R40 > Pd/TiO_2 R40 > AuPd/TiO_2 R500 > Pd/TiO_2 R500 catalysts. Prolonging the reaction time to 120 min, the selectivity to 1-heptene decreased further to 85, 66, and 54% for the Pd/TiO_2 R40, Pd/TiO_2 R500, and AuPd/TiO_2 R40 catalysts, respectively. In addition, the reduction at high temperature (i.e., at 500 °C) resulted in a significant increase in selectivity to 1-heptene after 120 min reaction time for the AuPd/TiO_2 R500 (at ca. 64%) compared to the ones reduced at 40 °C.

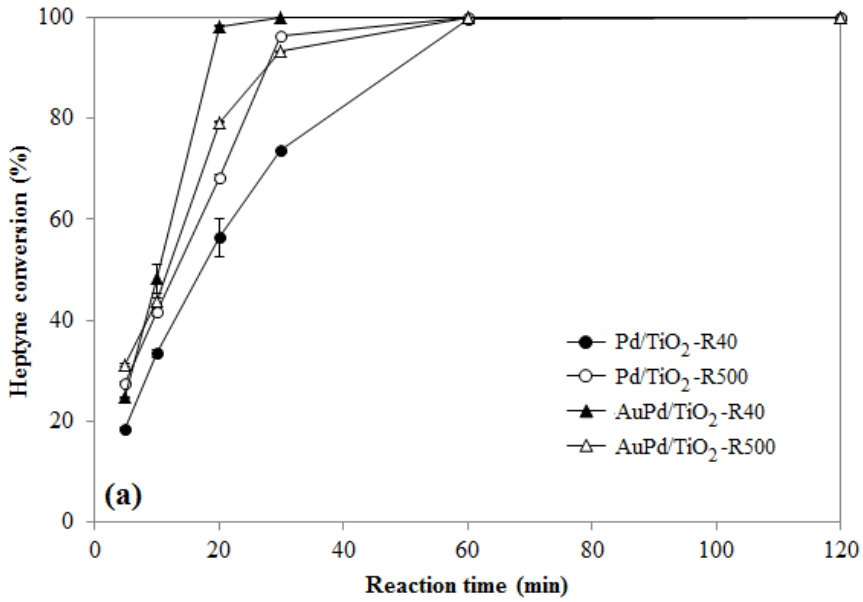

Figure 5.17 Heptyne conversion of the monometallic Pd/TiO_2 and bimetallic $AuPd/TiO_2$ catalysts reduced at 40 and 500 °C

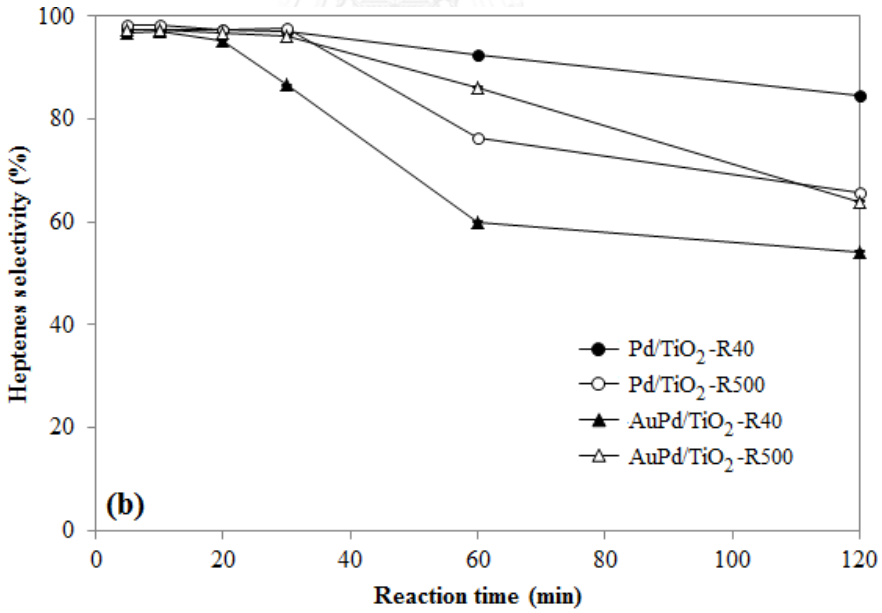

Figure 5.18 Selectivity to 1-heptene of the monometallic Pd/TiO_2 and bimetallic $AuPd/TiO_2$ catalysts reduced at 40 and 500 °C

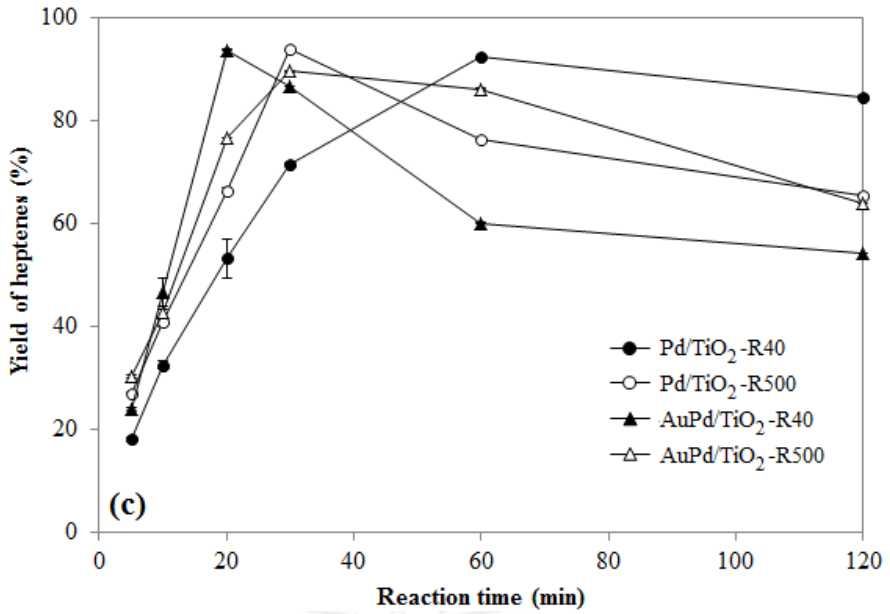

Figure 5.19 1-Heptene yield of the monometallic Pd/TiO_2 and bimetallic $AuPd/TiO_2$ catalysts reduced at 40 and 500 °C

Typically, TiO_2 manifests the SMSI effect with group VIII transition metals after reduction at high temperature, thus resulting in the formation of $Pd\text{-}TiO_x$ species which promotes the selectivity to alkene in several alkyne hydrogenation reactions [52, 166, 265]. Nevertheless, it should be noted that most of the catalysts reported to have such effects were prepared by conventional methods such as impregnation or deposition-precipitation of metal precursors on the TiO_2 supports. Such effects on the FSP synthesized catalyst have not been reported yet. The effect of reduction temperature on the catalytic behaviors of FSP synthesized catalysts are summarized as shown in **Figure 5.20**. According to this study, it suggested that SMSI effect on the monometallic Pd/TiO_2 catalysts may be less pronounced than the bimetallic $AuPd/TiO_2$ catalysts. Although some migration of TiO_x species on the Pd surface might occur for the Pd/TiO_2 R500, the changes of Pd surface species from PdO to metallic Pd^0 (complete reduction of PdO) exhibited greater effect on the catalyst performances in selective hydrogenation of 1-heptyne, thus the Pd/TiO_2 R500 catalyst showed higher hydrogenation activity with lower selectivity to 1-heptene compared to the one reduced at 40 °C. On the other hand, for the bimetallic

$AuPd/TiO_2$ catalysts in which the metal particles were already in the form of AuPd alloy in the as-prepared catalysts, the reduction at high temperature (i.e., 500 °C) can improve the selectivity to 1-heptene from 54 to 64% after complete 1-heptyne conversion (prolonging reaction time to 120 min). According to the H_2-TPR results, the partial reduction of TiO_2 was also easier on the bimetallic $AuPd/TiO_2$ than on the monometallic Pd/TiO_2.

Comparing the yield of 1-heptene as a function of reaction time for the all FSP synthesized catalysts, the highest yield of 1-heptene (~93%) was obtained over the $AuPd/TiO_2$ R40 in the shortest reaction time (within 20 min) while high temperature reduction was required for the monometallic Pd/TiO_2 to exhibit similar level of 1-heptene yield at longer reaction time.

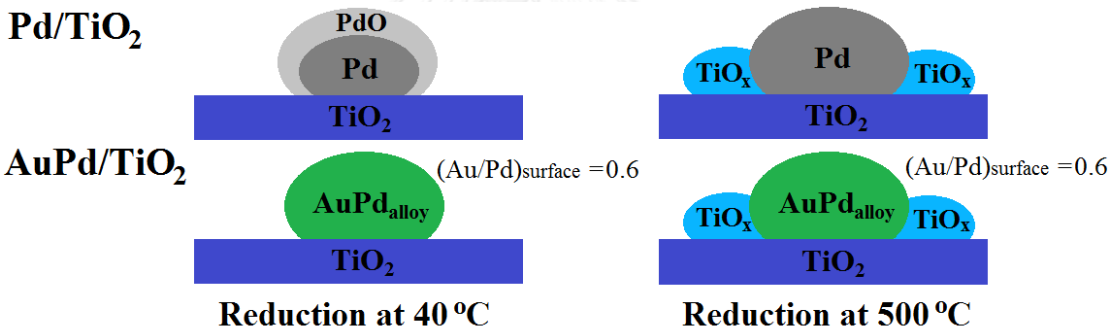

Figure 5.20 Catalytic behavior of FSP synthesized catalysts with different reduction temperatures

The reaction results of the liquid-phase selective hydrogenation of 1-heptyne over supported Pd-based catalysts in this study are also compared to those reported in the literature as summarized in **Table 5.11**. The catalytic activity of the commercial Lindlar catalyst has been reported to be very low (conversion 5-45 % for reaction time up to 150 min) [150]. Accordingly, the catalyst performances of Pd-based catalysts have been improved for the selective hydrogenation of 1-heptyne to 1-heptene under mild conditions. One of alternative ways to modify the Pd-based catalysts was the addition of a second metal such as W, Ni, and Au [149, 150, 152].

Interestingly, the presence of Au and W on the Pd-based catalysts demonstrated remarkedly high conversion and high selectivity, especially Au addition that took shorter reaction time [149, 152]. Furthermore, TiO_2 supported monometallic Pd and bimetallic AuPd catalysts were synthesized in one-step by the FSP method and compared to those obtained by the conventional impregnation technique [67, 153, 259]. The positive effect of Au addition on the hydrogenation activity was still concerned over FSP synthesized Pd catalysts. The catalytic performances of the FSP synthesized AuPd/TiO_2 catalysts in terms of 1-heptene yield are at state-of-the art (1-heptene yield ~93% at reduction temperature of 40 °C, 20 min reaction time). The yield of 1-heptene that has been reported over the non-FSP made Pd-based catalysts was typically lower in the range of 4-75%. There was only one exceptional case of the 0.4%Pd-2.4%W/γ-Al_2O_3 reduced at 120 °C that 98% yield of 1-heptene was obtained at 303 K and 150 kPa after 3 h reaction time [149].

Table 5.11 Comparison of the catalytic activity of supported Pd catalysts in the liquid-phase hydrogenation of 1-heptyne under mild conditions

Catalysts	Preparation	Reaction conditions	Time (min)	Conv (%)	Selec (%)	Yield (%)	Ref.
Pd/TiO_2 R40	FSP	303 K, 4 bar	10	33	97	32	This study
			60	100	93	93	
Pd/TiO_2 R500			10	42	98	41	
			30	96	98	94	
			60	100	76	76	
$AuPd/TiO_2$ R40			10	48	97	47	
			20	98	95	93	
$AuPd/TiO_2$ R500			10	44	97	43	
			30	93	96	89	
			60	100	86	86	
0.4%Pd-2.4%W/γ-Al_2O_3 reduced120 ^{o}C	IMP	303 K,150 kPa	30	18	98	18	[149]
			180	100	98	98	
0.4%Pd/Al_2O_3	IMP	303 K,150 kPa	30	10	95	9.5	[150]
			150	18	98	18	
0.4%Pd-1%Ni/Al_2O_3			30	13	96	12	
			150	30	98	29	
Lindlar	Commercial		30	5	88	4	
			150	45	81	36	
$[PdCl_2(NH_2(CH_2)_{12}CH_3)_2]$/ γ-Al_2O_3	IMP	303 K,150 kPa	n/a	90	63	57	[151]
0.5%Pd-1%Au/TiO_2	IMP/DP	303 K, 1 bar	10	73	96	70	[152]
			30	100	55	55	
1%Pd/TiO_2	FSP	303 K, 1 bar	5	80	94	75	[67]
			40	100	90	90	
1%Pd/SiO_2	FSP	303 K,105 kPa	5	43	92	40	[153]
			40	100	62	62	

Conv: Conversion, Selec: Selectivity, FSP: Flame spray pyrolysis, IMP: Impregnation, DP: Deposition

5.3 Effect of flame conditions on the properties of Pd/TiO_2 and $AuPd/TiO_2$ in the selective hydrogenation of acetylene in excess ethylene

In this part, the $AuPd/TiO_2$ catalysts were synthesized by FSP under various flame conditions and tested in the gas-phase acetylene hydrogenation. Typically, Pd-based catalysts have been attracting much attention for hydrogenation reaction as shown in the previous parts in which the liquid-phase selective hydrogenation of 1-heptyne was used as reaction model. This part reveals the catalytic performances of the FSP synthesized Pd-based catalysts (both monometallic Pd/TiO_2 and bimetallic $AuPd/TiO_2$ catalysts) for the gas-phase hydrogenation. The selective hydrogenation of acetylene in excess ethylene was used as the catalytic study reaction model. Moreover, the catalytic performances of supported monometallic Pd and bimetallic Au-Pd catalysts have rarely been investigated under a large amount of ethylene condition (high C_2H_4 concentration) which is closely similar to the industrial condition. So the selective hydrogenation of acetylene in the excess ethylene was chosen to study in this part.

The FSP technology is quite attractive since this process has the great potential for the rapid, flexible and scalable synthesis of nanoparticles. Especially, the FSP allows synthesis of multi-component nanoparticles by using inexpensive precursors and solvents. The characteristics and performance of flame-made nanoparticles can be tuned by the operating condition of FSP such as type of precursor [61, 266], precursor concentration [106, 107, 267], precursor flow rate [106, 267, 268], type of solvent [269, 270], type of dispersion gas [106], dispersion flow rate [106, 267], and other process conditions [107, 267].

In order to investigate the flexibility of the FSP process for synthesis of the monometallic Pd and bimetallic AuPd nanoparticles, the flexibility of the conventional FSP with single nozzle was studied based on the effect of the stoichiometric proportion of precursor flow rate and dispersion O_2 gas flow rate on the characteristics of catalysts.

5.3.1 Characteristics of flame

The conventional one-nozzle FSP was used for the synthesis of monometallic Pd and bimetallic AuPd supported on TiO_2 under different process conditions. From this study, the characteristics of catalysts could be tuned by controlling the stoichiometric proportion of precursor flow rate and dispersion gas flow rate.

The conditions of the FSP synthesis and the nomenclature of catalysts are presented in **Table 5.12**. The precursor flow rate and O_2 dispersion flow rate was varied between 1 and 9 ml/min and between 9 and 1 l/min, respectively.

Table 5.12 Different conditions of FSP feed ratio and nomenclature of catalysts

Precursor flow rate (ml/min)	O_2 dispersion flow rate (l/min)	Nomenclature of catalysts
1	9	1PF9DO
3	7	3PF7DO
5	5	5PF5DO
7	3	7PF3DO
9	1	9PF1DO

Changing the FSP feed ratio of precursor flow rate to O_2 dispersion flow rate prolongs the variation of flame height and residence time of the particles as illustrated in **Figure 5.21**. Increasing the precursor flow rate results in higher flame enthalpy content and prolongs the particle residence time at high temperature because the added fuel required more oxygen for combustion leading to the longer flame [106, 271]. In addition, increase in O_2 dispersion flow rate intensifies the mixing and then accelerates the combustion of fuel, thus decreasing the flame height.

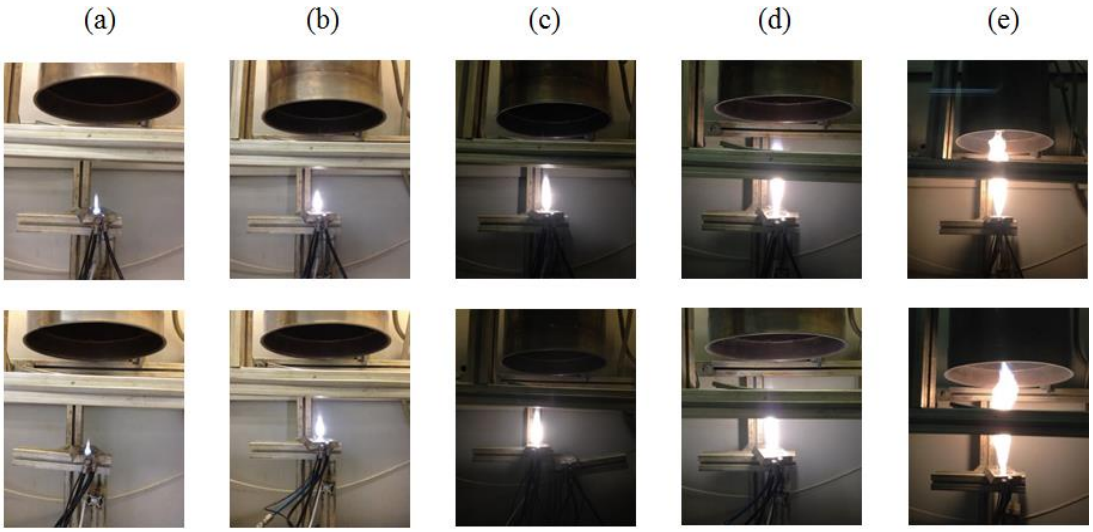

Figure 5.21 Characteristics of flame during the preparation of Pd/TiO_2 (first row) and $AuPd/TiO_2$ (second row) catalysts at different conditions (a) 1PF9DO, (b) 3PF7DO, (c) 5PF5DO, (d) 7PF3DO, and (e) 9PF1DO

5.3.2 Characteristics of catalysts

5.3.2.1 N_2 physisorption

The BET surface area of the monometallic Pd/TiO_2 and bimetallic $AuPd/TiO_2$ catalysts prepared under different conditions is given in **Table 5.13**. For the different conditions FSP feed ratios, the BET specific surface areas of the monometallic Pd/TiO_2 and the bimetallic $AuPd/TiO_2$ catalysts were varied in the range of 30-300 m^2/g. The decrease in FSP feed ratio (precursor flow rate to O_2 dispersion flow rate) resulted in a shorter flame height. The particles had less time to agglomerate into larger particles, leading to higher BET surface area of catalysts.

Table 5.13 BET surface area of the monometallic Pd/TiO_2 and bimetallic $AuPd/TiO_2$ catalysts at different conditions

Catalysts	BET surface area (m^2/g)	
	Pd/TiO_2	$AuPd/TiO_2$
1PF9DO	280.87	297.33
3PF7DO	192.76	201.55
5PF5DO	109.18	105.74
7PF3DO	63.96	63.25
9PF1DO	31.09	31

5.3.2.2 X-ray diffraction (XRD)

The XRD patterns of monometallic Pd/TiO_2 and bimetallic $AuPd/TiO_2$ catalysts are presented in **Figure 5.22** and **5.23**. The XRD pattern shows the characteristics of TiO_2 consisting of anatase and rutile phases. For the brookite phase, the absence of a diffraction peak at 2θ = 31° confirmed that the formation of brookite phase did not occur during FSP synthesis. The broadening of the major XRD peak was ranged in the order: 1PF9DO > 3PF7DO > 5PF5DO > 7PF3DO > 9PF1DO for both monometallic Pd/TiO_2 and bimetallic $AuPd/TiO_2$ catalysts. It is well known that the width of the XRD peak is associated to the crystallite size. At higher FSP feed ratio, the XRD peaks were stronger and sharper than those of lower FSP feed ratio indicating higher crystallinity and larger crystal size being formed. The longer particle residence time resulted in enhanced coagulation and sintering [272, 273]. Less crystallinity was obtained due to insufficient residence time of the particles in flame. Similar results were obtained on the Ag/TiO_2 prepared by FSP at different FSP feed ratio as reported by Fujiwara et al. [273].

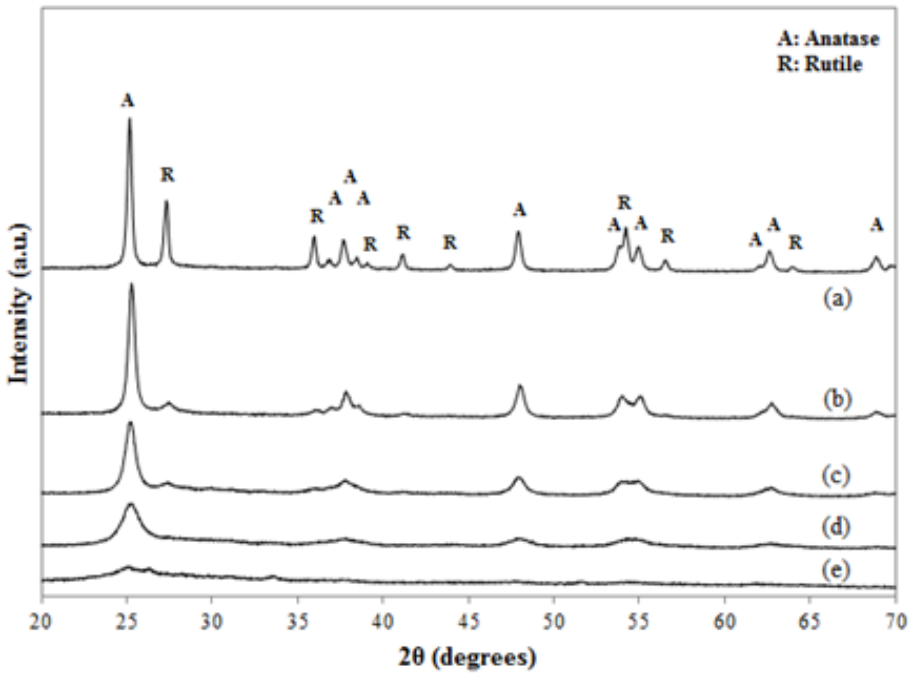

Figure 5.22 XRD patterns of monometallic Pd/TiO_2 catalysts at condition (a) 9PF1DO, (b) 7PF3DO, (c) 5PF5DO, (d) 3PF7DO, and (e) 1PF9DO

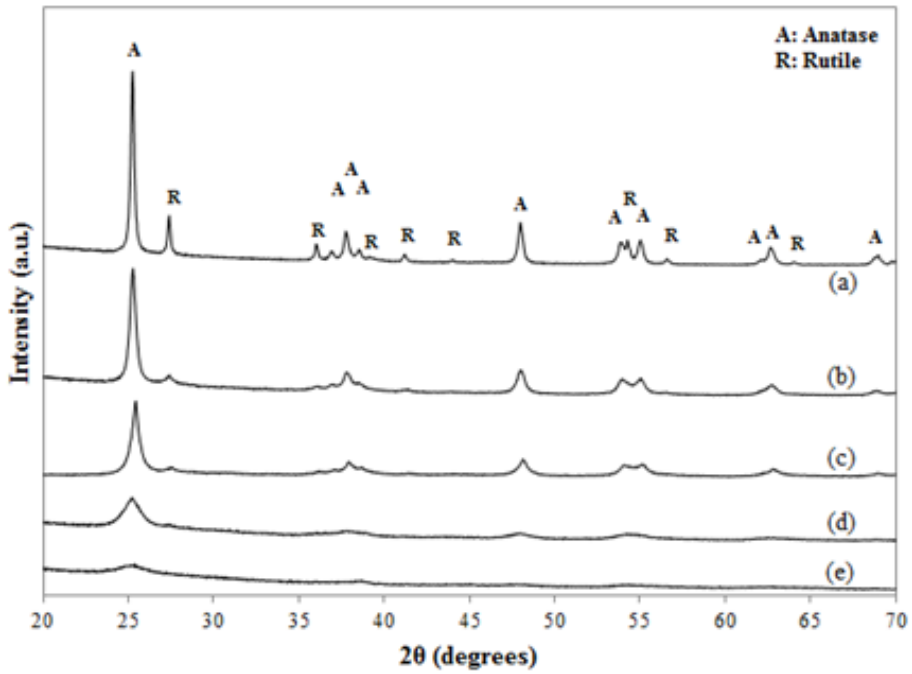

Figure 5.23 XRD patterns of bimetallic $AuPd/TiO_2$ catalysts at condition (a) 9PF1DO, (b) 7PF3DO, (c) 5PF5DO, (d) 3PF7DO, and (e) 1PF9DO

The FSP conditions affected the characteristics of TiO_2 such as phase composition and TiO_2 size as shown in **Figure 5.24**. The BET specific surface areas of catalyst were related with the TiO_2 particle sizes. Increasing the particle residence time at high temperature allowed the TiO_2 particles to grow to larger sizes (up to 45 nm) which were associated with a decrease in surface area for both of Pd/TiO_2 and $AuPd/TiO_2$ catalysts.

Furthermore, when the O_2 dispersion flow rate increases, the droplet concentration of the spray and the flame enthalpy content are decreased [106, 274]. Hence, the particle residence time at high temperature is decreases leading to faster quenching rate. This results in the formation of smaller particles.

Moreover, percentage of anatase was associated with the residence time. Increasing the residence time decreased the anatase phase composition in TiO_2. The formation of rutile phase was favored by increasing the particle residence time at high temperature. These results are in agreement with Bettini et al. [275] who have been reported that the anatase content in TiO_2 decreased with increasing the dispersion flow rate due to additional oxygen and the higher flame temperature promoted the rutile formation. However, the composition of anatase phase in TiO_2 for bimetallic $AuPd/TiO_2$ catalyst was slightly higher than monometallic Pd/TiO_2 catalysts. These results suggested that Au addition could help to retard the rutile formation.

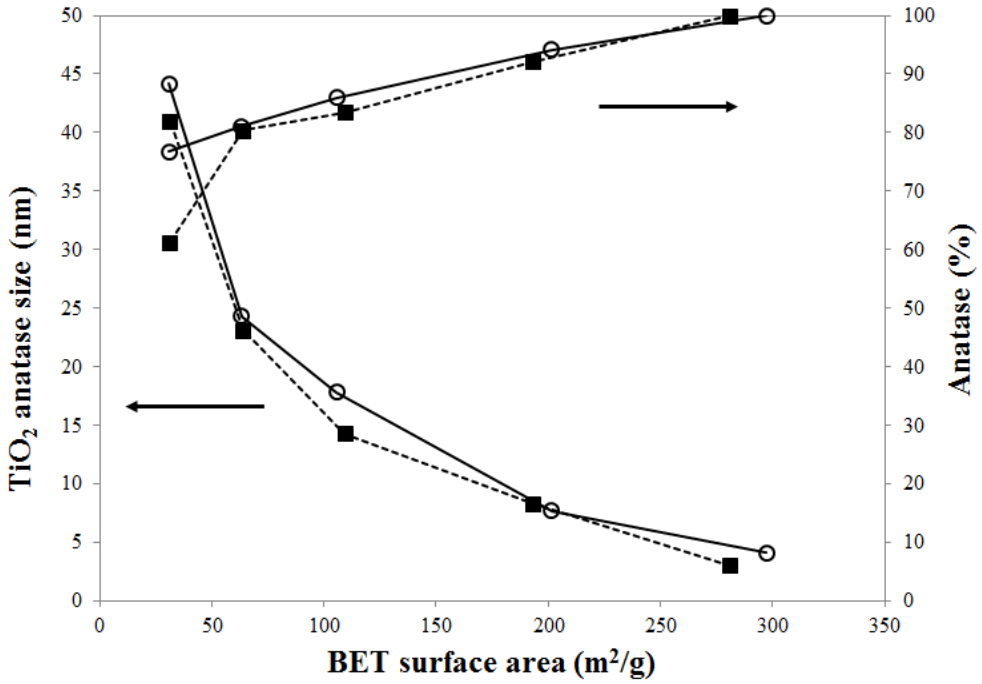

Figure 5.24 TiO_2 anatase size and percentage of anatase phase of monometallic Pd/TiO_2 (dash line) and bimetallic $AuPd/TiO_2$ (solid line) catalysts at different BET surface area (or at different conditions)

5.3.2.3 CO-chemisorption

The amounts of active sites (Pd sites) on the catalysts were measured by using CO-chemisorption technique. The amounts of CO adsorbed on the monometallic Pd/TiO_2 and bimetallic $AuPd/TiO_2$ catalysts are reported in the **Table 5.14** and the Pd dispersions as a function of BET surface area are shown in **Figure 5.25**. Actually, the Pd active sites should be well dispersed on the high surface area support. The Pd dispersion linearly increased with BET surface area up to some conditions: 9PF1DO-5PF5DO for monometallic Pd/TiO_2 and 9PF1DO-7PF3DO for bimetallic $AuPd/TiO_2$ catalysts. Despite their highest BET surface areas obtained from the 1PF9DO conditions, they exhibited the lowest CO uptake. This was due to (1) uncombustible hydrocarbons formed during these conditions which had insufficient residence time and/or (2) soot formation during incomplete combustion from precursor molecules.

Table 5.14 CO chemisorption results of monometallic Pd/TiO_2 and bimetallic $AuPd/TiO_2$ catalysts at different conditions

Catalysts	CO uptake (μmol CO/g cat)	
	Pd/TiO_2	$AuPd/TiO_2$
1PF9DO	0.10	0.68
3PF7DO	13.73	5.09
5PF5DO	18.99	7.92
7PF3DO	7.01	29.03
9PF1DO	1.57	3.55

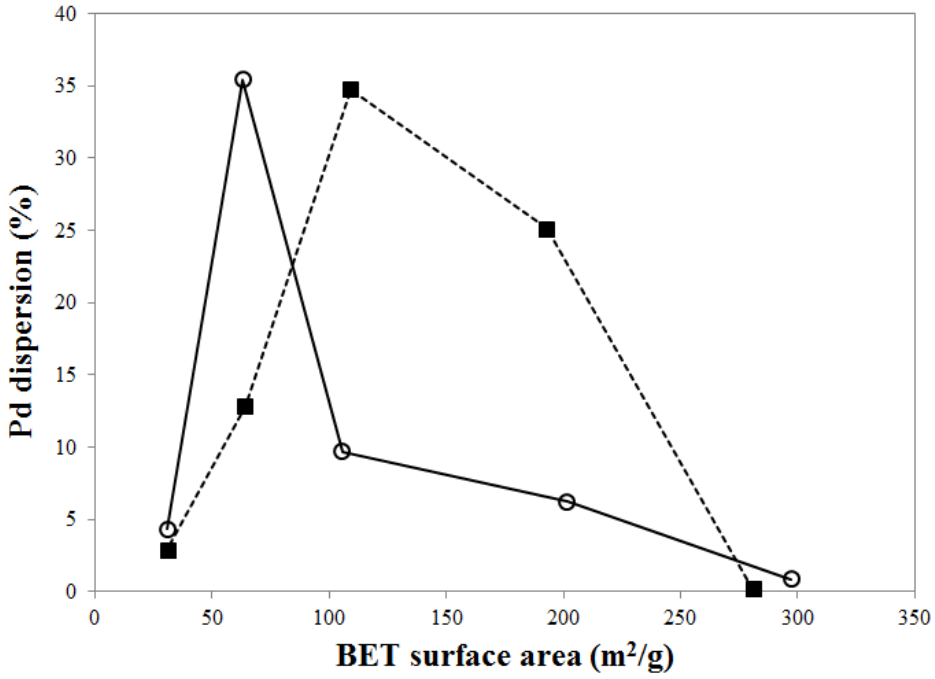

Figure 5.25 Pd dispersions of monometallic Pd/TiO_2 (dash line) and bimetallic $AuPd/TiO_2$ (solid line) catalysts at different BET surface areas (or at different conditions)

5.3.2.4 Thermo gravimetric analysis (TGA)

In order to prove the assumption of the low Pd dispersion for the high BET surface area catalysts, TGA was performed on samples prepared under different FSP

feed conditions and the results are shown in **Figure 5.26** and **5.27**. The weight loss observed from 100 to 200 ℃ can be attributed to the removal of moisture content in the samples (desorption of physically adsorbed water on the catalyst surface). While the mass loss on catalyst samples between 200 and 400 ℃ was attributed to carbon deposited over the active phase [276]. The amount of carbon deposited on the samples depends on the FSP feed ratio condition. It has been reported that decreasing the precursor flow rate induces less added fuel which requires less O_2 for combustion resulting in shorter flame with low temperature [271]. In addition, increasing O_2 dispersion flow rate increases the spray flame velocity and decreases the flame temperature because the entrainment of the surrounding cold air is enhanced. Moreover, the fuel consumption is accelerated by the obtaining increased O_2 mass fraction in the spray leading to shorter flame. So, it could be concluded that the resulting shorter flame and low flame temperature at low FSP feed ratio caused more carbon deposited on the samples. As a result, the adsorption of CO molecules on the active sites might be suppressed due to more carbon deposited leading to lowest CO uptake and lowest Pd dispersion.

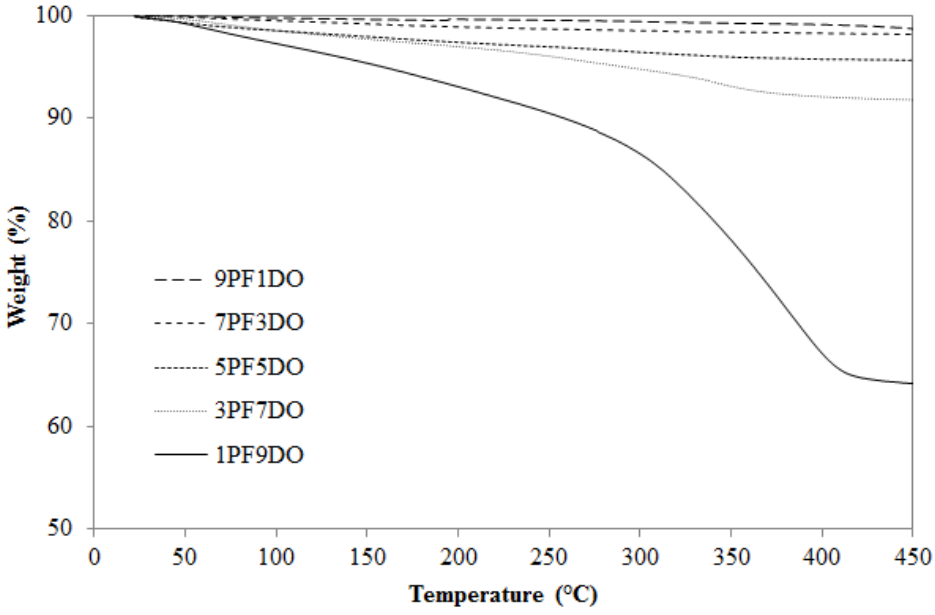

Figure 5.26 TGA results of monometallic Pd/TiO_2 catalysts at different conditions

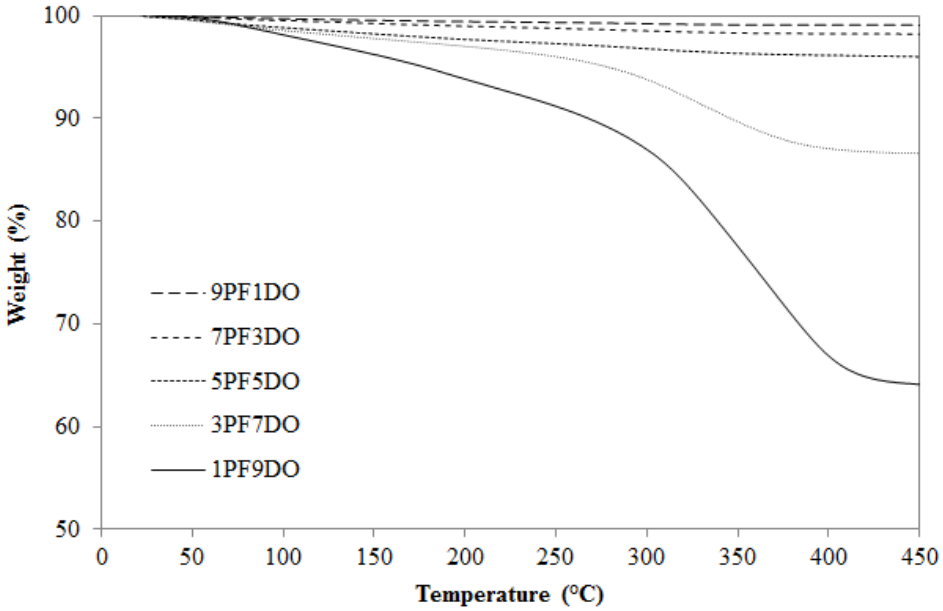

Figure 5.27 TGA results of bimetallic AuPd/TiO_2 catalysts at different conditions

5.3.2.5 Transmission electron microscope (TEM)

TEM images of the bimetallic AuPd/TiO_2 catalysts prepared under different FSP feed ratio conditions are shown in **Figure 5.28**. The TiO_2 support had a spherical shape and the particle size of TiO_2 was varied with the high-temperature particle residence time which was in good agreement with the XRD results. Nevertheless, from my previous work, the synthesis of AuPd/TiO_2 by FSP has shown to result in the formation of Au-Pd alloy particles [259]. The bimetallic AuPd/TiO_2 prepared at 1PF9DO and 3PF7DO exhibited the ambiguous TEM images. Moreover, some hard aggregated metal particles could be observed especially for the AuPd/TiO_2 prepared at 1PF9DO. The appearance of spherical AuPd alloy particles deposited on TiO_2 support was seen for the AuPd/TiO_2 prepared at 5PF5DO, 7PF3DO, and 9PF1DO. The AuPd alloy particle size seems to increase with increasing the particle residence time in the high temperature region as can be seen in Fig 6c, 6d, and 6e. With decreasing the FSP feed ratio, the high temperature region is decreased drastically, thus shortening the high-temperature particle residence time and increasing the cooling rate [277]. Therefore, smaller spherical primary particles were obtained because the high temperature region was not sufficient for complete coagulation-coalescence.

These results are consistent with the FSP preparation of SiO_2 at different O_2 flow rates [277]. Few agglomerated SiO_2 particles were obtained at low O_2 flow rates, while smaller particles with hard agglomerates were found at higher O_2 flow rate.

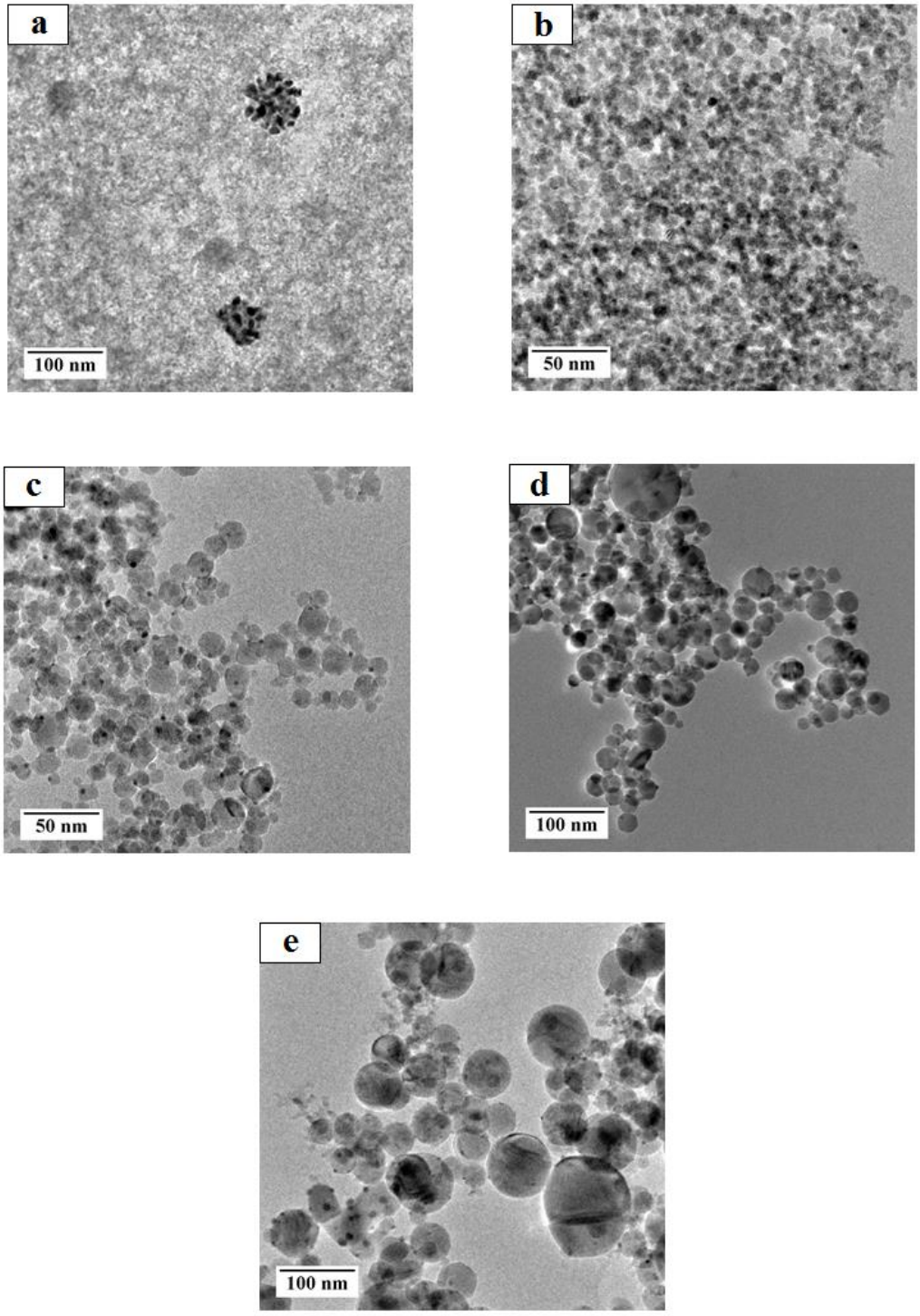

Figure 5.28 TEM images of bimetallic AuPd/TiO_2 catalysts at different conditions (a) 1PF9DO, (b) 3PF7DO, (c) 5PF5DO, (d) 7PF3DO, and (e) 9PF1DO

5.3.3 Catalytic study in the selective hydrogenation of acetylene

The selective hydrogenation of acetylene in excess ethylene was performed. In the industrial process for polyethylene production, a small quantity of acetylene was found in the ethylene feed stream. The first goal of the selective hydrogenation of acetylene is to eliminate acetylene from ethylene feed. However, during hydrogenation further hydrogenation of ethylene to ethane can occur. If the reaction goes too far (such as much more H_2), the ethylene in feed could be hydrogenated to ethane indicating the loss of ethylene feed. Thus, as shown in the calculation of selectivity, the losing of ethylene feed would be defined in term of negative selectivity. Besides high conversion of acetylene, the positive selectivity of ethylene is also the second goal of this catalytic study in point of economics of the industrial process.

5.3.3.1 Catalytic study of monometallic Pd/TiO_2 catalysts

The conversion of acetylene and ethylene selectivity in the selective acetylene hydrogenation from 40-120 °C over the monometallic Pd/TiO_2 catalysts prepared by flame spray pyrolysis at different FSP feed ratios are shown in **Figure 5.29**. It is well known that operating reaction temperature has a crucial role in the catalytic hydrogenation activity of the Pd-based catalyst [170, 278]. As the reaction temperature was increased from 40 to 120 °C, the acetylene conversion increased until fully hydrogenation (100% conversion).

For the monometallic Pd/TiO_2 catalysts, the optimal catalytic activity for hydrogenation of acetylene was observed at condition of 7PF3DO for the synthesis of the monometallic Pd/TiO_2 catalyst. The Pd/TiO_2 prepared at 9PF1DO condition showed lower catalytic activity which was attributed to low BET surface area and low Pd dispersion. Despite its high BET surface area, the lower catalytic activities for the Pd/TiO_2 prepared at 1PF9DO and 3PF7DO were pronounced because of larger carbon deposited over the active phase formed during FSP synthesis as shown by the TGA results.

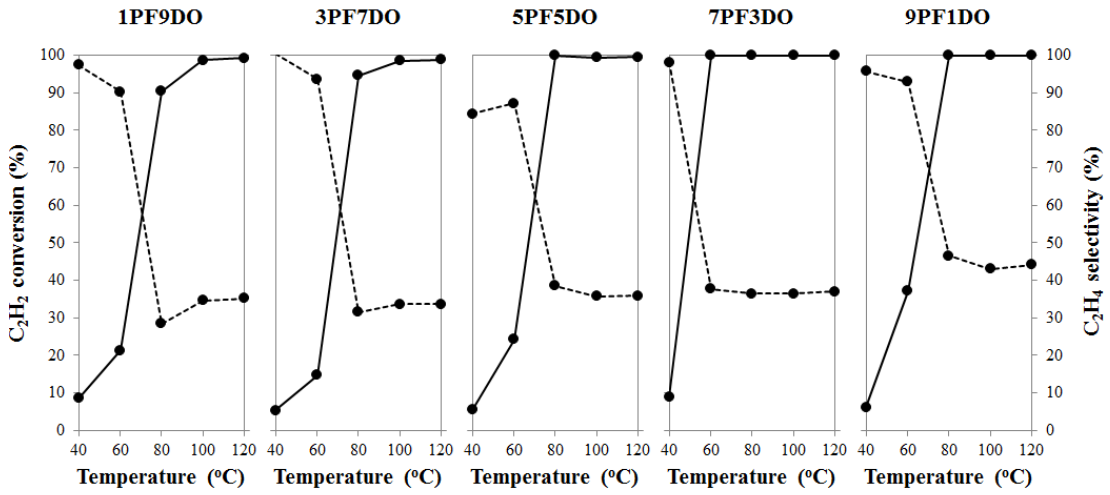

Figure 5.29 Acetylene conversion (solid line) and ethylene selectivity (dash line) of monometallic Pd/TiO_2 catalysts at different conditions

Concerning the degree of Pd dispersion, it is well known that the size of the catalyst particles is related to the degree of dispersion. When the degree of Pd dispersion decreases, the size of the Pd catalyst particles increases because the ratio of the number of surface metal atoms to the total number of atoms decreases. The degree of Pd dispersion or particle size affects the geometric configuration (e.g. surface metal atoms with different coordination numbers) and/or electronic effect (i.e., energy state of the catalyst active sites). It has been noted that the dynamic of catalytic activity variation as a function of the degree of Pd dispersion in the hydrogenation depends slightly on the nature of substrate [279-283]. For acetylene hydrogenation, the dependence of the catalytic activity of Pd/Al_2O_3 catalyst for acetylene hydrogenation on the degree of Pd dispersion has been reported by Gigola et al. [282]. The catalytic activity was found to increase with a decrease in the Pd dispersion from 80% to 10%. This negative size effect of Pd catalyst in alkyne hydrogenation could be attributed to the blocking of the work catalyst surface by chemisorbed acetylene molecules [284]. Moreover, in term of electronic effect, the decrease in the metal nanoparticle size is accompanied by increase in their electron deficiency [285, 286]. So, the strength of acetylene adsorption on the electron-deficient active sites would be increased with increasing the Pd dispersion, then

forming the stable surface complexes. Thus, the hydrogen concentration on the catalyst surface is decreased. The competition between the adsorption of acetylene and hydrogen on small Pd sizes might be one of the main reasons why the activity for acetylene hydrogenation decreased with increasing of Pd dispersion [284].

5.3.3.2 Catalytic study of bimetallic AuPd/TiO_2 catalysts

Compared to the monometallic Pd/TiO_2 catalysts, the bimetallic AuPd/TiO_2 catalysts could improve catalytic activity to eliminate acetylene trace in excess ethylene at lower temperature (60 °C); in addition, the ethylene selectivity was remain positive at 35-40% as shown in **Figure 5.30**. Such results suggest that the Au addition could promote the hydrogenation of acetylene to ethylene.

For the bimetallic AuPd/TiO_2 catalysts, the catalytic activity was not much different, except the AuPd/TiO_2 at 1PF9DO conditions. The lower catalytic activity of the AuPd/TiO_2 prepared at 1PF9DO condition was attributed to larger amount of uncombustible hydrocarbon covered on the active sites. Although the characteristics of bimetallic AuPd/TiO_2 prepared at different FSP feed ratios were different, the catalytic performances were quite similar for the other FSP feed ratio conditions. Such results indicate that the effect of BET surface area, TiO_2 size, phase composition of TiO_2, Pd dispersion, and AuPd alloy size was less pronounced when alloy Au-Pd particles were formed. In other words, the catalytic performance was rather affected by the AuPd alloy formation.

Furthermore, the presence of carbon deposits over the bimetallic AuPd/TiO_2 nanoparticles did not affect the catalytic activity during selective hydrogenation of acetylene, except AuPd/TiO_2 at 1PF9DO condition. It may be postulated that low amount of deposits (much lower than 15 wt% observed from TGA) was a marginal effect on catalytic performance compared to the AuPd alloy property.

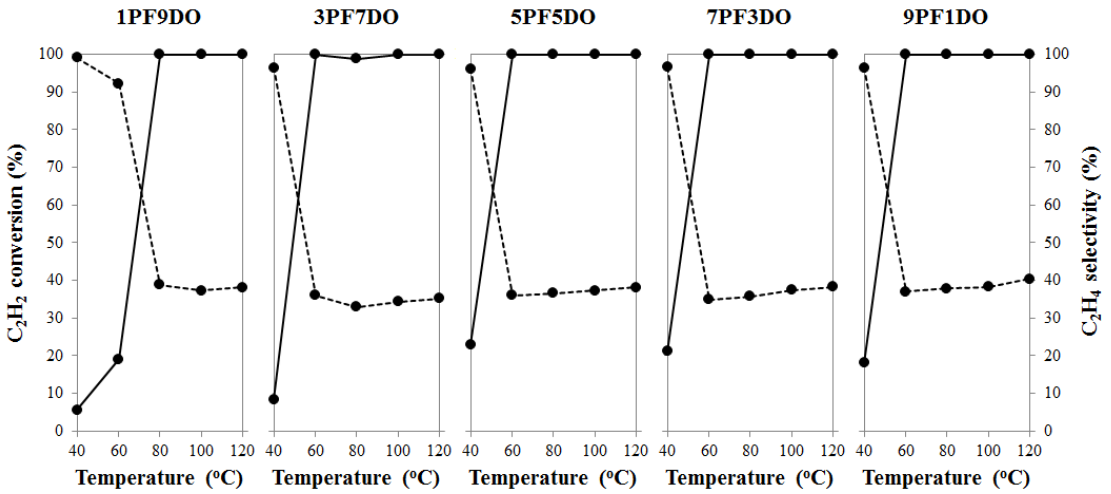

Figure 5.30 Acetylene conversion (solid line) and ethylene selectivity (dash line) of bimetallic AuPd/TiO_2 catalysts at different conditions

5.3.3.3 Catalytic study of monometallic Au/TiO_2 catalysts

The catalytic performance of the monometallic Au/TiO_2 catalysts prepared by flame spray pyrolysis was also synthesized at condition 5 ml/min of precursor flow rate and 5 l/min of dispersion O_2 gas flow rate (5PF5DO) to test the catalytic study for selective hydrogenation of acetylene in excess ethylene. As seen in **Figure 5.31**, the monometallic Au/TiO_2 catalyst was an ineffective catalyst for selective hydrogenation of acetylene. The conversion of acetylene was found to be extremely low (<10%) with superior ethylene selectivity (100%) from the temperature of 40-120 °C. The monometallic Au nanoparticles has the unique properties to desorb olefins (ethylene) at a much lower temperature than alkynes (acetylene) leading to high ethylene selectivity in selective hydrogenation of acetylene [287]. It has been reported that the monometallic Au/TiO_2 catalyst requires higher temperature, higher H_2/C_2H_2 ratio, and higher contact time to obtain high acetylene hydrogenation activity [34, 161, 287].

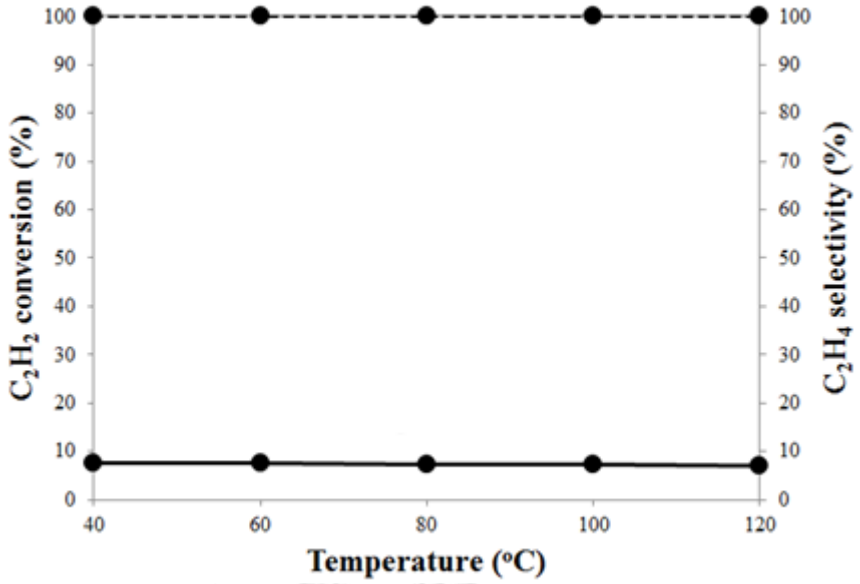

Figure 5.31 Acetylene conversion (solid line) and ethylene selectivity (dash line) of monometallic Au/TiO_2 catalyst at condition 5PF5DO

5.4 Selective hydrogenation of acetylene in excess ethylene over AuPd/TiO_2 prepared by 2-nozzle flame spray pyrolysis

From the previous part, the Au addition to from AuPd alloy nanoparticles could improve the catalytic activity of selective acetylene hydrogenation. Thus, the bimetallic AuPd nanoparticles have a great attention for further investigation and development of catalytic properties and catalytic performances. It is well-known that the characteristics and performance of flame-made nanoparticles can be tuned by the operating condition of FSP as shown in Part 5.3. Nevertheless, the conventional FSP with a single nozzle limits the flexibility in obtaining a specific designs and desirable particle configuration of multi-component nanoparticles [288, 289]. Besides tuning of the FSP conditions, 2-nozzle FSP system can increase the process flexibility by controlling the mixing of the individual components from the different flames [290].

In this part, the application of 2-nozzle FSP in order to increase the FSP process flexibility has been investigated on the catalyst configuration and catalytic performances of bimetallic AuPd nanoparticles supported on TiO_2 supports for selective hydrogenation of acetylene in excess ethylene, and compared to the conventional one-nozzle FSP process. The delivery systems of support and metal precursors were managed and controlled through two independent nozzles. The 2-nozzle FSP is able to adjust and control the mixing of the individual components [290], the interaction between metal and support [291], and the location of deposition of metal on the support [292, 293] during multi-components FSP synthesis. The schematic of the 2-nozzle FSP for the preparation of bimetallic AuPd supported on TiO_2 is illustrated in Fig 10 compared to the conventional one-nozzle FSP in Fig 9. The separation of multi-component precursors on individual stream was prepared in 4 types:

Type 1: separation of TiO_2 support precursor and mixed precursor of Pd and Au metals (TiO_2+AuPd)

Type 2: separation of Pd metal precursor and mixed precursor of Au metal and TiO_2 support (Au/TiO_2+Pd)

Type 3: separation of Au metal precursor and mixed precursor of Pd metal and TiO_2 support (Pd/TiO_2+Au)

Type 4: separation of mixed precursor of Pd metal and TiO_2 support and mixed precursor of Au metal and TiO_2 support (Pd/TiO_2+Au/TiO_2).

5.4.1 Characteristics of catalysts

5.4.1.1 X-ray diffraction (XRD) and N_2 physisorption

The XRD patterns of bimetallic AuPd supported on TiO_2 support prepared by different types of 2-nozzle FSP were not much different compared to the conventional one-nozzle FSP as shown in **Figure 5.32**. The XRD characteristic peaks of TiO_2 phases for all samples consisted of anatase (major) and rutile phases. The catalytic characteristics of bimetallic AuPd supported on TiO_2 support are shown in **Table 5.15**. The crystallite size of TiO_2 anatase phase for bimetallic AuPd supported on TiO_2 support was similar for all types of 2-nozzle FSP and conventional one-nozzle FSP, except the last type (Pd/TiO_2+Au/TiO_2) of 2-nozzle FSP. The last type (Pd/TiO_2+Au/TiO_2) of 2-nozzle FSP had the smallest crystallite size of anatase TiO_2. For this type, the amount of TiO_2 precursor was divided into 2 nozzles, so the precursor concentration of individual nozzle was less than the others. The precursor concentration which is related to the amount of precursor fed into the flame defines the collision frequency of the particles [107]. Decreasing in precursor concentration, the particle size decreases due to the reduction of the collision and sintering rates at high flame temperature. Thus, the 2-nozzle FSP synthesis of bimetallic AuPd supported on TiO_2 support by separating TiO_2 support into individual nozzle (Pd/TiO_2+Au/TiO_2) which has lower precursor concentration on individual nozzle can lead to smaller TiO_2 anatase size. Moreover, the decrease in crystallite size of TiO_2 anatase (12 nm) corresponded to the enhanced BET specific surface area (151.76 m^2/g). For the other synthesis routes, the BET specific surface area was in the range of 99-106 m^2/g.

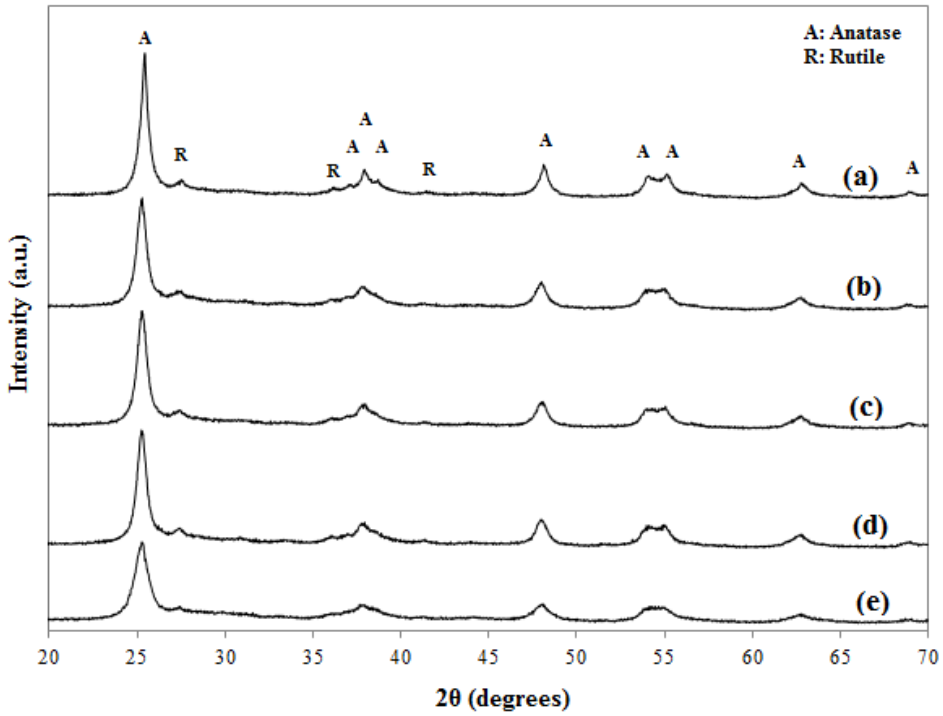

Figure 5.32 XRD patterns of bimetallic AuPd/TiO_2 catalysts prepared by different routes (a) AuPd/TiO_2, (b) Pd/TiO_2+Au, (c) Au/TiO_2+Pd, (d) TiO_2+AuPd (e) Pd/TiO_2+Au/TiO_2

Table 5.15 Catalytic characteristics of bimetallic AuPd/TiO_2 catalysts prepared by 2-nozzle FSP

Catalysts	TiO_2 anatase size (nm)	BET surface area (m^2/g)
TiO_2+AuPd	16.8	104.21
Au/TiO_2+Pd	16.1	104.29
Pd/TiO_2+Au	16.2	99.29
Pd/TiO_2+Au/TiO_2	12	151.76
AuPd/TiO_2	17.8	105.74

5.4.1.2 CO-chemisorption

The amount of CO adsorbed on the bimetallic AuPd supported on TiO_2 support, called CO uptake, and Pd dispersion are reported in the **Table 5.16**. The 2nd

type (Au/TiO_2+Pd) of 2-nozzle FSP showed the best Pd dispersion because the separation of Pd precursor into the 2nd nozzle FSP can prevent the coverage of Pd particle by TiO_2 support. In other words, most of the Pd particles were deposited on the Au/TiO_2 leading to well dispersion of Pd particles. The bimetallic AuPd supported on TiO_2 prepared by conventional one nozzle FSP ($AuPd/TiO_2$ one nozzle FSP) and the 1st type (TiO_2+AuPd) of 2-nozzle FSP exhibited lower Pd dispersion due to AuPd alloy formation. Furthermore, the synthesis of bimetallic AuPd alloy by using one nozzle FSP can lead to the formation of Ti-O groups from TiO_2 support covering the AuPd alloy particles. As a result, the adsorption of CO molecules might be suppressed leading to lowest CO uptake and lowest Pd dispersion. Similar to Mekasuwandumrong et al. [67], during flame synthesis of Pd/TiO_2 catalyst Pd metal particles were covered by Ti-O groups because of the simultaneous crystallization of Pd and TiO_2 in gas-phase reaction. However, from the previous part, it should be noted that at 5PF5DO condition the bimetallic $AuPd/TiO_2$ one nozzle FSP showed lower Pd dispersion compared to the monometallic Pd/TiO_2 one nozzle FSP. The Pd dispersions of the 3rd (Pd/TiO_2+Au) and last (Pd/TiO_2+Au/TiO_2) types of 2-nozzle FSP were 16.77 and 19.88%, respectively.

Table 5.16 CO chemisorption results of bimetallic $AuPd/TiO_2$ catalysts prepared by 2-nozzle FSP

Catalysts	CO uptake (μmol CO/g cat)	Pd dispersion (%)
TiO_2+AuPd	9.34	11.40
Au/TiO_2+Pd	19.12	23.33
Pd/TiO_2 +Au	13.75	16.77
Pd/TiO_2+Au/TiO_2	16.29	19.88
$AuPd/TiO_2$	7.92	9.66

5.4.1.3 X-ray photoelectron spectroscopy (XPS)

The XPS spectra of Pd 3d and Au 4f structure and surface atomic composition of chemical species on the catalyst samples were investigated by using XPS analysis. The results are shown in **Figure 5.33, Table 5.17** and **5.18**.

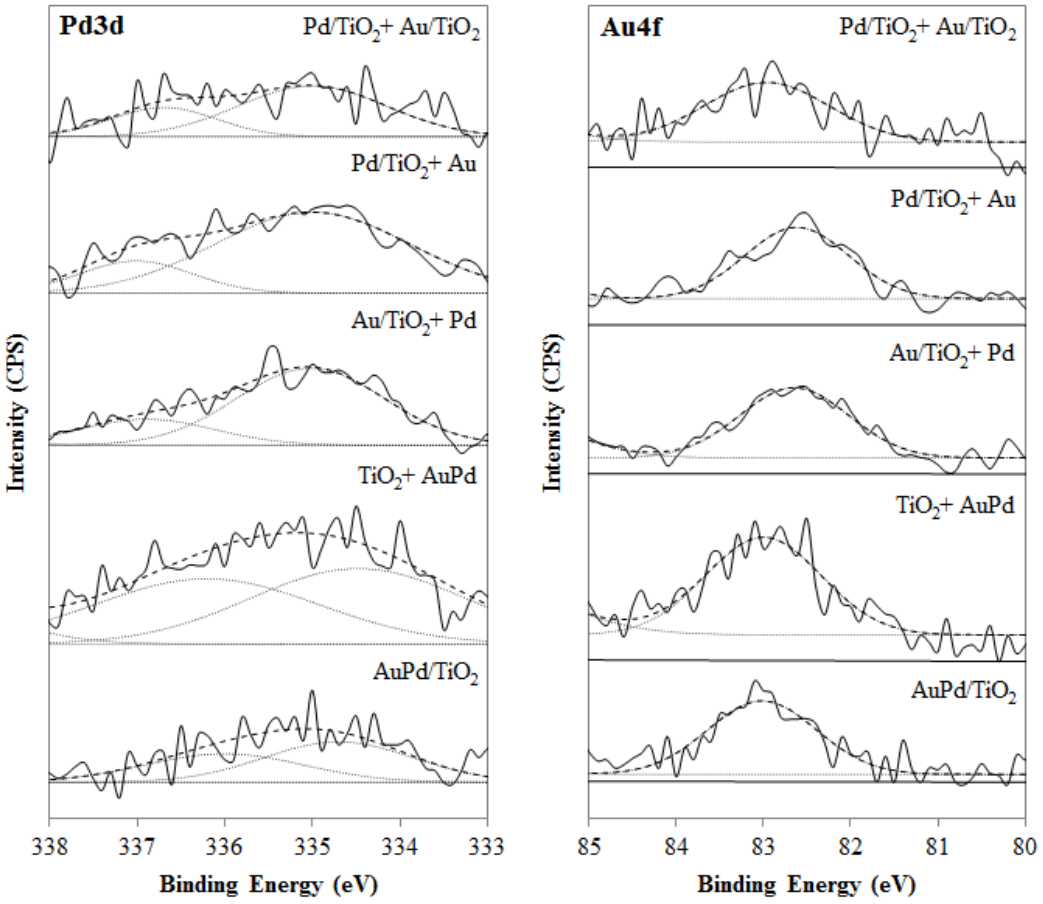

Figure 5.33 XPS Pd 3d and Au 4f core level spectra of bimetallic AuPd/TiO_2 catalysts prepared by different routes

The typical binding energy of Pd 3d for Pd metal was reported to be in the range of 335.0-335.4 eV [183]. The XPS peaks for Pd 3d shift to lower binding energy upon AuPd alloy formation [294, 295]. On the other hand, the shifting toward higher binding energy can be assigned to electron-deficient Pd such as Pd oxide. The XPS Pd 3d spectra for 1st type (TiO_2+AuPd) of 2-nozzle FSP and AuPd/TiO_2 one nozzle FSP were fitted to two pairs of components for Pd species, consisting of Pd in AuPd alloy

and Pd oxide. The binding energy Pd 3d peak of AuPd alloy for the 1st type (TiO_2+AuPd) of 2-nozzle FSP was lower than that of AuPd/TiO_2 one nozzle FSP. It is clearly demonstrated that the separation of the TiO_2 support and the mixed precursor of Au/Pd metals into independent nozzle lead to better mixing of Au and Pd promoting alloy formation. For other routes of 2-nozzle FSP, the XPS Pd 3d spectra consisted of two pairs of Pd species which might be Pd metal and Pd oxide. From the binding energy of Pd in the range of 335.0-335.4 eV, it might be postulated that the separation of individual metal precursor (the separation between Au and Pd precursors) into independent nozzle did not promote the AuPd alloy formation and/or probably caused very weak interaction between Au and Pd in the AuPd alloy nanoparticles. However, the formation of AuPd alloy was still required the confirmation by using other characterization techniques such as TEM-EDX. While the XPS Au 4f spectra for all samples were fitted to one pair of component for Au specie (FWHM < 2).

Table 5.17 Binding energies of Pd 3d and Au 4f of bimetallic AuPd/TiO_2 catalysts prepared by 2-nozzle FSP

Catalysts	Pd 3d5/2		Au 4f7/2	
	B.E. (eV)	FWHM	B.E. (eV)	FWHM
TiO_2+AuPd	334.48	2.88	83.00	1.56
	336.21	3.00		
Au/TiO_2+Pd	335.02	1.98	82.65	1.47
	336.89	1.82		
Pd/TiO_2+Au	335.00	2.61	82.62	1.40
	337.01	1.50		
Pd/TiO_2+Au/TiO_2	335.00	1.99	82.96	1.69
	336.69	1.42		
AuPd/TiO_2	334.70	2.01	83.02	1.46
	336.00	2.13		

For the surface atomic compositions and atomic ratios of Au, Pd, and Ti, the FSP synthesis by using conventional one nozzle FSP resulted in lowest surface atomic composition both of Au and Pd due to TiO_2 blockage. While the 1st type (TiO_2+AuPd) of 2-nozzle FSP showed highest Au and Pd atomic percentages at catalyst surface indicating more AuPd alloy particles deposited on catalyst surface. For other types, the separation of Au or Pd metal precursor from TiO_2 support into independent nozzle resulted in less possibility of TiO_2 blockage on Au or Pd particles, respectively.

Table 5.18 Surface atomic composition of bimetallic AuPd/TiO_2 catalysts prepared by 2-nozzle FSP

Catalysts	Atomic concentration		Atomic ratio		
	Pd (%)	Au (%)	Pd/Ti	Au/Ti	(Pd+Au)/Ti
TiO_2+AuPd	0.501	0.165	0.023	0.008	0.031
Au/TiO_2+Pd	0.280	0.106	0.015	0.006	0.021
Pd/TiO_2+Au	0.249	0.139	0.013	0.008	0.021
Pd/TiO_2+Au/TiO_2	0.259	0.127	0.012	0.006	0.019
AuPd/TiO_2	0.225	0.085	0.012	0.004	0.016

5.4.1.4 Transmission electron microscope (TEM-EDX)

The TEM-EDX images of the bimetallic AuPd/TiO_2 catalysts prepared by 2-nozzle FSP are shown in **Figure 5.34-5.38**. The TEM-EDX analysis confirmed the presence of both Au and Pd metals in the light spots which can be attributed to the AuPd alloy particles. All of the catalysts showed the presence of both Au and Pd metals in the light spots; however, the fraction of Au and Pd in the light spots was different in each type. The TiO_2+AuPd catalyst showed more fraction of Pd in AuPd alloy particles (in the light spots) than other types suggesting the better mixing of Au and Pd forming the AuPd alloy particles (as light spots) dispersed on the TiO_2 support. From the TEM images for other types, the light spots were also found, suggesting that the AuPd alloy particles were also partially formed over other types;

nevertheless, the fractions of Pd in the AuPd alloy (on the light spot) were less than the TiO_2+AuPd catalyst. Less fraction of Pd in the AuPd alloy may be postulated to lower degree mixing of Pd and Au in AuPd alloy. According to XPS results, the interaction between Au and Pd in the AuPd alloy for the Au/TiO_2+Pd, Pd/TiO_2+Au, and Pd/TiO_2+Au/TiO_2 catalysts was weaker compared to the TiO_2+AuPd catalyst. Moreover, these results indicated that not only some of Pd was formed the AuPd alloy in these types (Au/TiO_2+Pd, Pd/TiO_2+Au, and Pd/TiO_2+Au/TiO_2), but also more Pd/PdO particles were formed compared to the TiO_2+AuPd catalyst. It was clearly seen the very small Pd particles dispersed on the TiO_2 support over the Au/TiO_2+Pd catalyst. While Pd/PdO particles over the Pd/TiO_2+Au and Pd/TiO_2+Au/TiO_2 catalysts were quite difficult to obvious, probably due to the coverage of Pd/PdO by TiO_2 support.

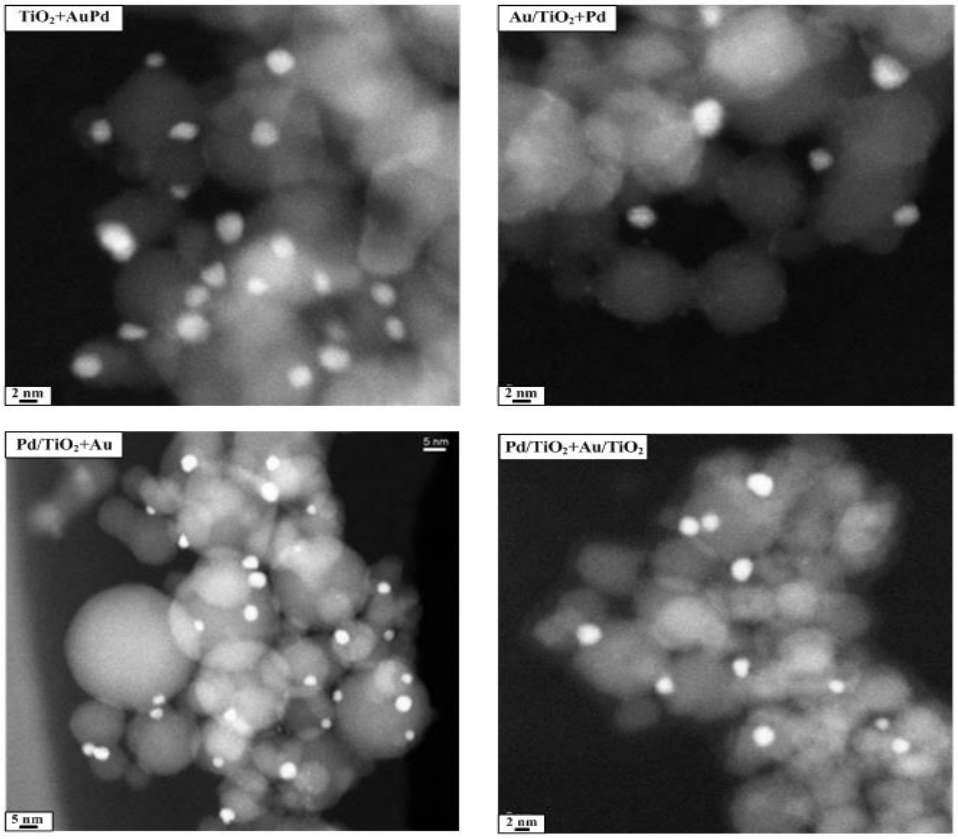

Figure 5.34 TEM images for the bimetallic AuPd/TiO_2 catalysts prepared by 2-nozzles FSP with different routes

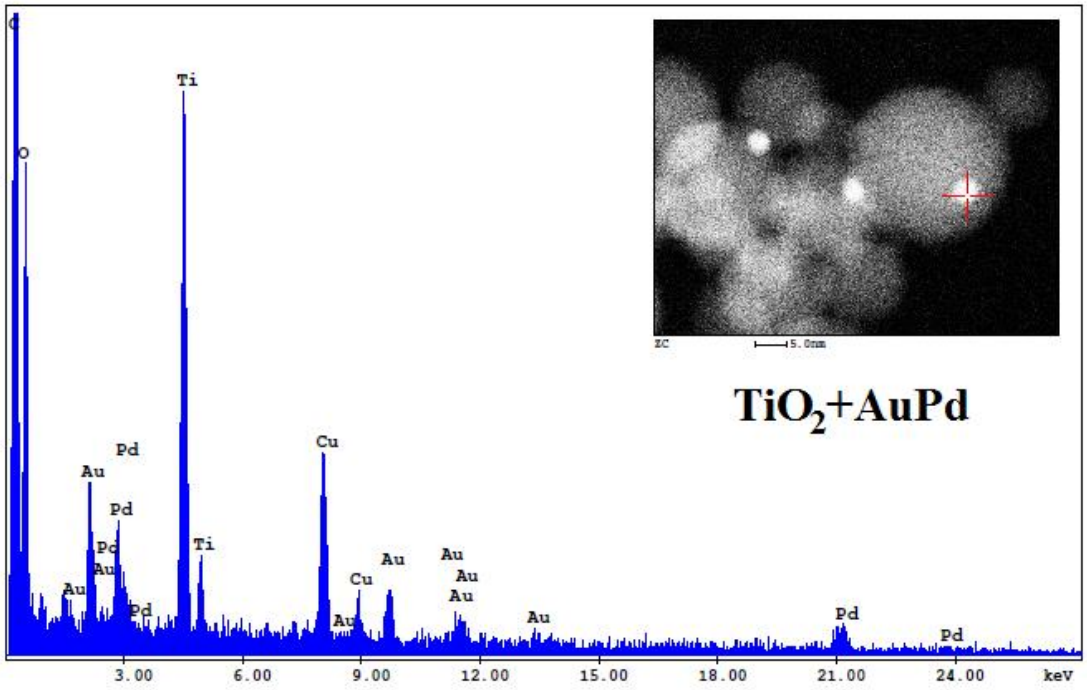

Figure 5.35 EDX analysis for the bimetallic TiO_2+AuPd catalyst

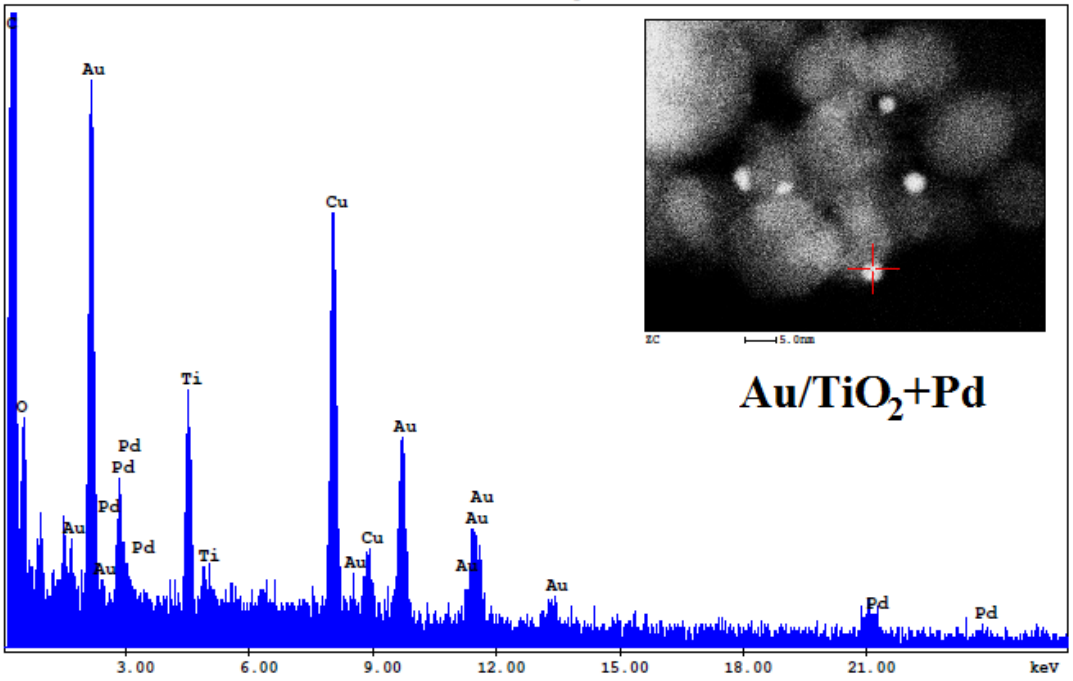

Figure 5.36 EDX analysis for the bimetallic Au/TiO_2+Pd catalyst

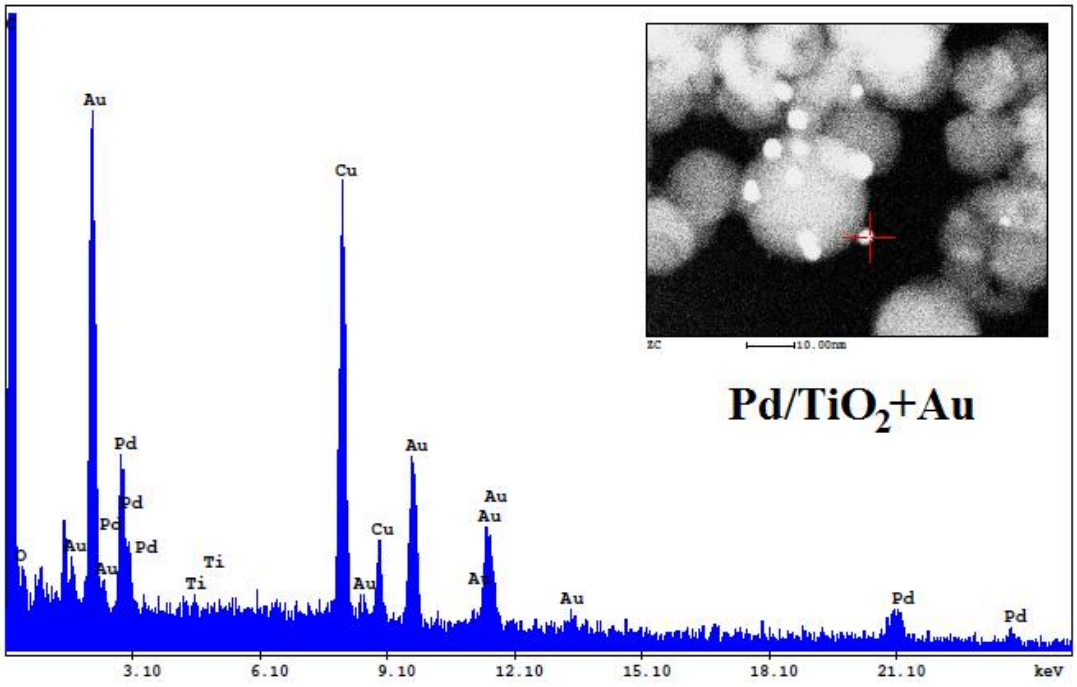

Figure 5.37 EDX analysis for the bimetallic Pd/TiO_2+Au catalyst

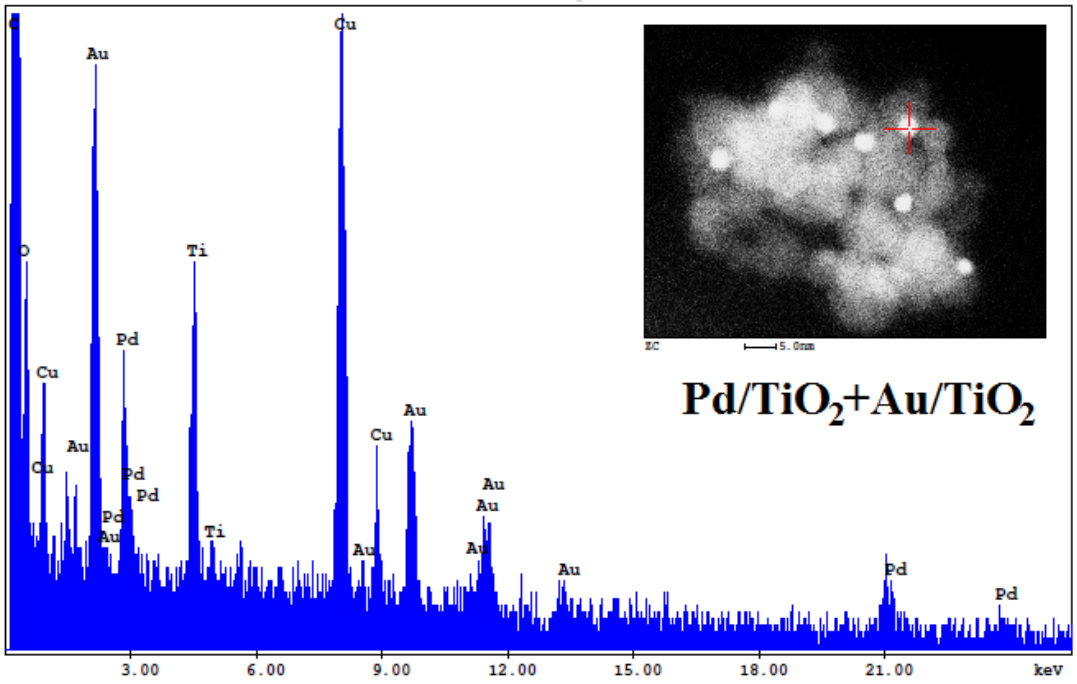

Figure 5.38 EDX analysis for the bimetallic Pd/TiO_2+Au/TiO_2 catalyst

5.4.1.5 Structural features of bimetallic AuPd supported on TiO_2

The structural features of the bimetallic AuPd supported on TiO_2 prepared by different synthetic routes are shown in **Figure 5.39**. The synthesis of bimetallic AuPd supported on TiO_2 by using one nozzle FSP resulted in the AuPd alloy formation which was partially covered by TiO_2 support as indicated by the XPS results. For the 1^{st} type (TiO_2+AuPd) of 2-nozzle FSP, the separation of TiO_2 support and Au/Pd metal precursor into independent nozzle led to better mixing of Au and Pd, forming the AuPd alloy, which was in good agreement with XPS Pd 3d for AuPd alloy and TEM-EDX analysis. Moreover, the possibility of coverage of AuPd alloy by TiO_2 support was decreased. So as a consequence, most of AuPd alloy particles were deposited on the surface of TiO_2 support. It is confirmed by the higher CO chemisorption ability that more CO can be adsorbed on the TiO_2+AuPd than those of the AuPd/TiO_2 one nozzle FSP and by the surface atomic composition calculated from the XPS results.

The separation of individual metal precursor into independent nozzle resulted in the AuPd alloy with less Pd fraction (as shown in TEM-EDX) and promoted the formation of individual Pd metal particle as can be seen in other types of 2-nozzle FSP, especially the Au/TiO_2+Pd catalyst. According to the CO chemisorption and the XPS results, the separation of Pd metal precursor from TiO_2 support precursor as shown in the Au/TiO_2+Pd catalyst resulted in more Pd particles deposited on the surface of TiO_2 support which corresponded to larger amount of CO adsorbed and higher Pd dispersion. On the other hand, the feed of mixed precursor solution between Pd and TiO_2 together led to the formation of TiO_2 support covering Pd particles, which was responsible for the low Pd dispersion in the Pd/TiO_2+Au and Pd/TiO_2+Au/TiO_2 catalysts.

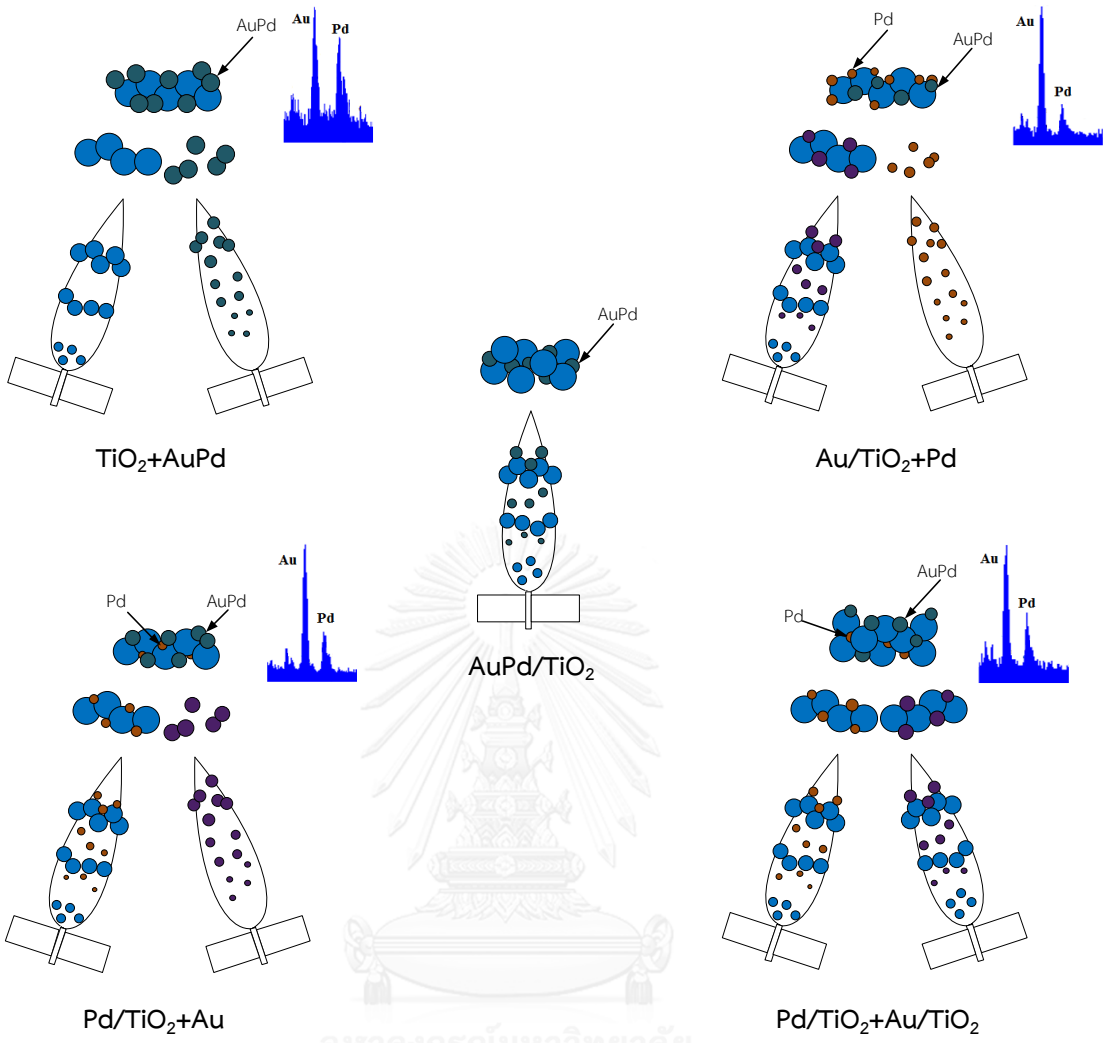

Figure 5.39 Schematic of conventional one-nozzle FSP and 2-nozzle FSP for the preparation of bimetallic AuPd supported on TiO_2 catalysts

5.4.2 Catalytic study of bimetallic AuPd/TiO_2 catalysts prepared by 2-nozzle FSP

The catalytic performances of the bimetallic AuPd supported on TiO_2 prepared by different synthetic routes of 2-nozzle FSP system were investigated in the selective hydrogenation of acetylene from temperature of 40 to 120 °C. For the temperature in the range of 60 to 120 °C, the catalytic performances were similar in which acetylene was fully hydrogenated and the selectivity to ethylene was not much different (35-40%). Nevertheless, at the reaction temperature of 40 °C the

catalytic performance of the bimetallic AuPd supported on TiO_2 catalysts was varied depending on the synthesis conditions.

The catalytic activity in the selective acetylene hydrogenation was ranged in the order of: 1st type (TiO_2+AuPd) > 2nd type (Au/TiO_2+Pd) > AuPd/TiO_2 one nozzle FSP > 3rd type (Pd/TiO_2+Au) ≈ 4th type (Pd/TiO_2+Au/TiO_2), as illustrated in **Figure 5.40**. The highest acetylene conversion of the 1st type (TiO_2+AuPd) of 2-nozzle FSP was attributed to the better mixing between Pd and Au forming the AuPd alloy. Furthermore, the probability of the TiO_2 support covering the AuPd alloy was less than those of AuPd/TiO_2 one nozzle FSP facilitating the adsorption of reactant on the active sites. Meanwhile the 2nd type (Au/TiO_2+Pd) showed higher conversion due to high Pd dispersion and location of Pd, which was deposited on the surface of TiO_2 support, similarly to the 1st type (TiO_2+AuPd). For the 3rd type (Pd/TiO_2+Au) and 4th type (Pd/TiO_2+Au/TiO_2), the separation of Pd and Au precursors into individual nozzle might result in weaker interaction between Pd and Au; in addition, the mixing of Pd and TiO_2 precursor could conduce to the coverage of Pd particles by TiO_2 support during nanoparticle growth leading to low acetylene conversion.

From the catalytic study, the formation of AuPd alloy promoted the catalytic activity at 40 °C; nevertheless, the location of AuPd alloy and/or Pd particles deposited on TiO_2 support plays significant role in developing the catalytic activity in addition to the alloy formation. Consequently, the 2-nozzle FSP system could improve the catalytic activity for selective hydrogenation of acetylene by modifying the interaction between metals and the location of metal deposition on support.

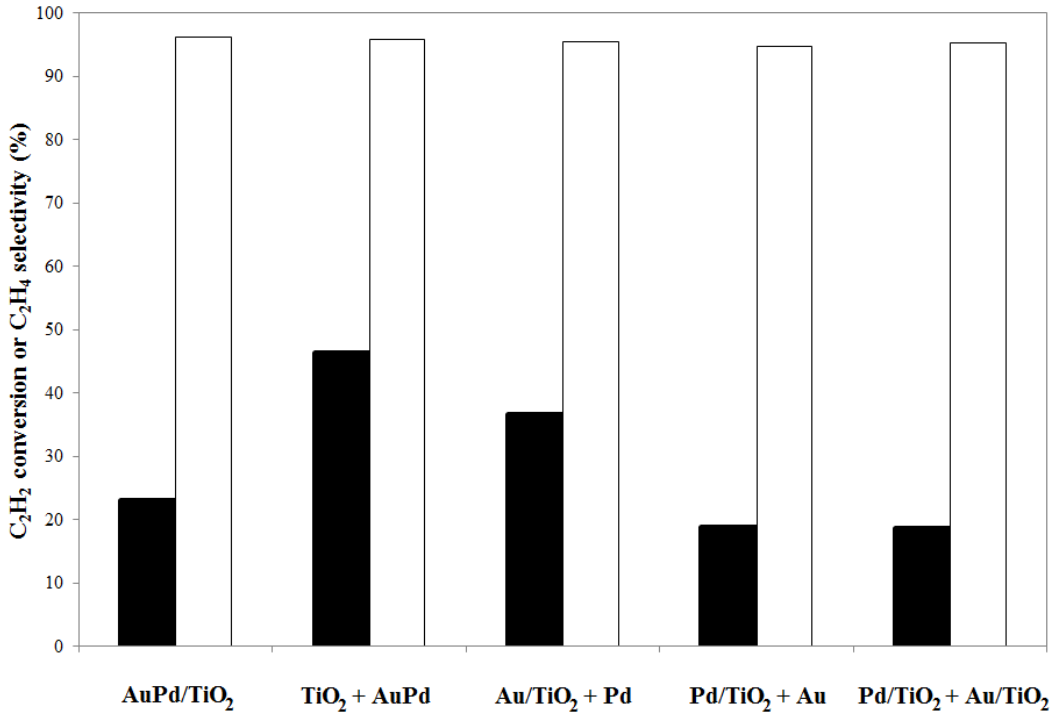

Figure 5.40 Acetylene conversion (black) and ethylene selectivity (white) of bimetallic AuPd/TiO_2 catalysts prepared by different routes

CHAPTER VI
CONCLUSIONS AND RECOMMENDATIONS

6.1 Conclusions

The bimetallic AuPd nanoparticles supported TiO_2 catalysts have been found to exhibit the superior activity for liquid-phase hydrogenation of 1-heptyne compared to both of monometallic Pd/TiO_2 and Au/TiO_2 catalysts due to synergistic effect of AuPd alloy. In the present work, the application of FSP method on the characteristics and catalytic properties of $AuPd/TiO_2$ catalysts was investigated and the results can be concluded as follows:

1) The TiO_2 supported bimetallic AuPd catalysts synthesized by FSP exhibited unique characteristics in which more uniform and smaller AuPd alloy particles were highly dispersed on the TiO_2 compared to those obtained by IMP and DP methods. In addition, the preparation of bimetallic $AuPd/TiO_2$ by IMP and DP methods resulted in some pore blockages and formation of new pore structure. The 1-heptyne hydrogenation rate depended on the Pd dispersion and the location of Pd particles.

2) The bimetallic $AuPd/TiO_2$ exhibited a similar degree of the SMSI effect as the monometallic one upon reduction at 500 $^{\circ}C$ in which the migration of TiO_x species onto the metals were observed for both catalysts. The reduction at higher temperature tended to homogenize the composition of the individual AuPd nanoparticles without significant changes of their average particle size and bulk composition.

3) For the monometallic Pd/TiO_2, reduction at 500 ℃ resulted in a complete reduction of PdO on the catalyst surface, leading to an improvement in hydrogenation activity and 1-heptene yield. On the other hand, the $AuPd/TiO_2$ reduced at 40 $^{\circ}C$ exhibited higher reaction rate and higher yield of 1-heptene (∼93% at reaction time 20 min) than the $AuPd/TiO_2$ reduced at 500 $^{\circ}C$ under similar reaction conditions used. Due to no significant changes in the alloy particle size and the composition of Au:Pd alloy, the lower catalytic activity of the $AuPd/TiO_2$ reduced at

500 ^{o}C was correlated to the lower active metal (Pd+Au)/Ti on the catalyst surface. This result suggested that the high temperature reduction is unnecessary for the improvement of catalyst performances when using supported bimetallic AuPd catalysts.

4) The addition of Au also improved the catalytic performance of Pd/TiO_2 catalysts in the selective hydrogenation of acetylene. The bimetallic AuPd/TiO_2 catalysts could eliminate acetylene trace in excess ethylene at lower temperature (60 °C) compared to the monometallic Pd/TiO_2 which exhibited the acetylene conversion only 24%. In addition, the ethylene selectivities were still positive (35-40% ethylene selectivity). Such results indicated that the Au addition promoted the hydrogenation of acetylene to ethylene but did not promote the hydrogenation of ethylene to ethane.

5) The FSP feed ratios affected the TiO_2 size, phase composition, BET surface area, and Pd dispersion. For selective hydrogenation of acetylene, the effect of FSP feed conditions on catalytic activity was more pronounced on the monometallic Pd/TiO_2 catalysts than those of bimetallic AuPd/TiO_2 catalysts. The catalytic activities of monometallic Pd/TiO_2 catalysts (prepared at 7PF3DO) could be enhanced in order to eliminate acetylene at 60 °C (100% C_2H_2 conversion) similar to the AuPd/TiO_2 catalysts.

6) The one-nozzle FSP synthesis at low FSP feed ratio condition, especially 1PF9DO condition, caused more uncombustible hydrocarbons formed due to insufficient residence time and/or more soot formation due to incomplete combustion of precursor molecules.

7) The AuPd alloy formation, interaction between metals, and the location of metal deposition on support could be further modified by the application of 2-nozzle FSP. The catalytic activity for selective hydrogenation of acetylene at 40 °C of the bimetallic AuPd/TiO_2 catalysts could be improved by separation of the TiO_2 support precursor from the mixed precursor of Pd and Au metals (TiO_2+AuPd) or separation of the Pd metal precursor from the mixed precursor of Au and TiO_2

(Au/TiO_2+Pd). The location of AuPd alloy and/or Pd particles deposited on TiO_2 support played important role in developing the catalytic activity for selective hydrogenation of acetylene in addition to the alloy formation.

6.2 Recommendations

1) The effect of amount of Au loading on the characteristics and properties of bimetallic AuPd nanoparticles should be further studied in the future work. The characteristics of bimetallic AuPd alloy nanoparticles should be investigated by high resolution analytical microscopy such as scanning transmission electron microscopy - X-ray energy dispersive spectrometry (STEM-XEDS) in order to define the morphology structure and the position of Au and Pd metals on individual metal nanoparticles from maping images for each metal.

2) The effect of nozzle geometry and processing parameters on the alloy formation should be studied in the future work.

3) The catalytic performance of bimetallic $AuPd/TiO_2$ catalyst should be investigated in the selective hydrogenation of acetylene in excess ethylene at temperature of 30 °C in comparison to the catalytic performance in the selective hydrogenation of 1-heptyne at same temperature.

REFERENCES

[1] Toshima, N., and Yonezawa, T. Bimetallic nanoparticles-novel materials for chemical and physical applications. New Journal of Chemistry 22 (1998): 1179-1201.

[2] de Ménorval, L.-C., Chaqroune, A., Coq, B., and Figueras, F. Characterization of mono- and bi-metallic platinum catalysts using CO FTIR spectroscopy Size effects and topological segregation. Journal of the Chemical Society, Faraday Transactions 93 (1997): 3715-3720.

[3] Rajashekharam, M.V., and Chaudhari, R.V. Improved stability of a bimetallic Ni-Pt catalyst for hydrogenation of acetophenone and substituted derivatives. Catalysis Letters 41 (1996): 171-176.

[4] Huang, W. Selective hydrogenation of acetylene on zeolite-supported bimetallic catalysts. Doctoral dissertation, University of Delaware, 2007.

[5] Chandra Shekar, S., Krishna Murthy, J., Kanta Rao, P., Rama Rao, K.S., and Kemnitz, E. Selective hydrogenolysis of dichlorodifluoromethane (CCl_2F_2) over CCA supported palladium bimetallic catalysts. Applied Catalysis A: General 244 (2003): 39-48.

[6] Liu, R., and Zhao, F. Selective hydrogenation of citral over Au-based bimetallic catalysts in supercritical carbon dioxide. Science China Chemistry 53 (2010): 1571-1577.

[7] Shan, B., Hyun, J., Kapur, N., and Cho, K. First-principles Study of PdAu Segregation with CO Coverage. MRS Online Proceedings Library 1177 (2009): null-null.

[8] Sinfelt, J.H. Structure of bimetallic clusters. Accounts of Chemical Research 20 (1987): 134-139.

[9] Savargaonkar, N.R. Fundamental Studies of Supported Bimetallic Catalysts by NMR Spectroscopy. Iowa State University, 1996.

[10] Neurock, M., and Mei, D. Effects of Alloying Pd and Au on the Hydrogenation of Ethylene: An *ab initio*-Based Dynamic Monte Carlo Study. Topics in Catalysis 20 (2002): 5-23.

[11] Guczi, L., et al. AuPd bimetallic nanoparticles on TiO_2: XRD, TEM, in situ EXAFS studies and catalytic activity in CO oxidation. Journal of Molecular Catalysis A: Chemical 204–205 (2003): 545-552.

[12] Edwards, J.K., et al. Direct synthesis of hydrogen peroxide from H_2 and O_2 using TiO_2-supported Au–Pd catalysts. Journal of Catalysis 236 (2005): 69-79.

[13] Conte, M., et al. Hydrochlorination of acetylene using supported bimetallic Au-based catalysts. Journal of Catalysis 257 (2008): 190-198.

[14] Chen, M., and Goodman, D.W. Promotional Effects of Au in Pd-Au Catalysts for Vinyl Acetate Synthesis. Chinese Journal of Catalysis 29 (2008): 1178-1186.

[15] Venezia, A.M., La Parola, V., Deganello, G., Pawelec, B., and Fierro, J.L.G. Synergetic effect of gold in Au/Pd catalysts during hydrodesulfurization reactions of model compounds. Journal of Catalysis 215 (2003): 317-325.

[16] Nutt, M.O., Heck, K.N., Alvarez, P., and Wong, M.S. Improved Pd-on-Au bimetallic nanoparticle catalysts for aqueous-phase trichloroethene hydrodechlorination. Applied Catalysis B: Environmental 69 (2006): 115-125.

[17] Guo, X., et al. Synergistic Combination of Plasma Sputtered Pd–Au Bimetallic Nanoparticles for Catalytic Methane Combustion. The Journal of Physical Chemistry C 115 (2011): 11240-11246.

[18] Wei, X., et al. Bimetallic Au–Pd Alloy Catalysts for N_2O Decomposition: Effects of Surface Structures on Catalytic Activity. The Journal of Physical Chemistry C 116 (2012): 6222-6232.

[19] Hosseini, M., et al. Promotional effect of gold added to palladium supported on a new mesoporous TiO_2 for total oxidation of volatile organic compounds. Catalysis Today 122 (2007): 391-396.

[20] Enache, D.I., et al. Solvent-Free Oxidation of Primary Alcohols to Aldehydes Using Au-Pd/TiO_2 Catalysts. Science 311 (2006): 362-365.

[21] Mertens, P.G.N., et al. Selective alcohol oxidation to aldehydes and ketones over base-promoted gold–palladium clusters as recyclable quasihomogeneous and heterogeneous metal catalysts. Journal of Molecular Catalysis A: Chemical 313 (2009): 14-21.

[22] Zwijnenburg, A., Saleh, M., Makkee, M., and Moulijn, J.A. Direct gas-phase epoxidation of propene over bimetallic Au catalysts. Catalysis Today 72 (2002): 59-62.

[23] Dummer, N.F., Bawaked, S., Hayward, J., Jenkins, R., and Hutchings, G.J. Oxidative dehydrogenation of cyclohexane and cyclohexene over supported gold, palladium and gold–palladium catalysts. Catalysis Today 154 (2010): 2-6.

[24] Maccarrone, M.J., et al. Kinetic Study of the Partial Hydrogenation of 1-Heptyne over Ni and Pd Supported on Alumina. 2012.

[25] Molnár, Á., Sárkány, A., and Varga, M. Hydrogenation of carbon–carbon multiple bonds: chemo-, regio- and stereo-selectivity. Journal of Molecular Catalysis A: Chemical 173 (2001): 185-221.

[26] Schimpf, S., Gaube, J., and Claus, P. Selective Hydrogenation of Multiple Unsaturated Compounds. In M. Baerns (ed.), Basic Principles in Applied Catalysis, vol. 75. pp. 85-123. Springer Berlin Heidelberg, 2004.

[27] Bond, G.C., and Thompson, D.T. Catalysis by Gold. Catalysis Reviews 41 (1999): 319-388.

[28] Milone, C., et al. Selective hydrogenation of α,β-unsaturated ketones to α,β-unsaturated alcohols on gold-supported catalysts. Journal of Catalysis 222 (2004): 348-356.

[29] Campo, B., Volpe, M., Ivanova, S., and Touroude, R. Selective hydrogenation of crotonaldehyde on Au/HSA-CeO_2 catalysts. Journal of Catalysis 242 (2006): 162-171.

[30] Mohr, C., Hofmeister, H., Radnik, J., and Claus, P. Identification of Active Sites in Gold-Catalyzed Hydrogenation of Acrolein. Journal of the American Chemical Society 125 (2003): 1905-1911.

[31] Okumura, M., Akita, T., and Haruta, M. Hydrogenation of 1,3-butadiene and of crotonaldehyde over highly dispersed Au catalysts. Catalysis Today 74 (2002): 265-269.

[32] Jia, J., Haraki, K., Kondo, J.N., Domen, K., and Tamaru, K. Selective Hydrogenation of Acetylene over Au/Al_2O_3 Catalyst. The Journal of Physical Chemistry B 104 (2000): 11153-11156.

[33] Lopez-Sanchez, J.A., and Lennon, D. The use of titania- and iron oxide-supported gold catalysts for the hydrogenation of propyne. Applied Catalysis A: General 291 (2005): 230-237.

[34] Choudhary, T.V., Sivadinarayana, C., Datye, A.K., Kumar, D., and Goodman, D.W. Acetylene Hydrogenation on Au-Based Catalysts. Catalysis Letters 86 (2003): 1-8.

[35] Liu, R., et al. Physically and chemically mixed TiO_2-supported Pd and Au catalysts: unexpected synergistic effects on selective hydrogenation of citral in supercritical CO_2. Journal of Catalysis 269 (2010): 191-200.

[36] Pawelec, B., et al. AuPd alloy formation in Au-Pd/Al_2O_3 catalysts and its role on aromatics hydrogenation. Applied Surface Science 242 (2005): 380-391.

[37] Menegazzo, F., Canton, P., Pinna, F., and Pernicone, N. Bimetallic Pd–Au catalysts for benzaldehyde hydrogenation: Effects of preparation and of sulfur poisoning. Catalysis Communications 9 (2008): 2353-2356.

[38] Yang, X., et al. High-performance Pd–Au bimetallic catalyst with mesoporous silica nanoparticles as support and its catalysis of cinnamaldehyde hydrogenation. Journal of Catalysis 291 (2012): 36-43.

[39] Krauth, A.C., Bernstein, G.H., and Wolf, E.E. Novel microfabricated Pd-Au/SiO_2 bimetallic model catalysts for the hydrogenation of 1,3-butadiene. Catalysis Letters 45 (1997): 177-186.

[40] Edwards, J.K., et al. Switching Off Hydrogen Peroxide Hydrogenation in the Direct Synthesis Process. Science 323 (2009): 1037-1041.

[41] Hermans, S., Deffernez, A., and Devillers, M. Preparation of Au–Pd/C catalysts by adsorption of metallic species in aqueous phase for selective oxidation. Catalysis Today 157 (2010): 77-82.

[42] Dimitratos, N., et al. Effect of Particle Size on Monometallic and Bimetallic (Au,Pd)/C on the Liquid Phase Oxidation of Glycerol. Catalysis Letters 108 (2006): 147-153.

[43] Piccinini, M., et al. Effect of the reaction conditions on the performance of Au-Pd/TiO_2 catalyst for the direct synthesis of hydrogen peroxide. Physical Chemistry Chemical Physics 12 (2010): 2488-2492.

[44] Mimura, N., Daté, M., Dumeignil, F., and Fujitani, T. Liquid-Phase Oxidation of Glycerol over Au-Pd/TiO_2 Catalysts Using Molecular Oxygen as an Oxidant. In J. Humphrey (ed.), EuropaCat, Glasgow, Scotland, 2011.

[45] Suo, Z., Ma, C., Jin, M., He, T., and An, L. The active phase of Au–Pd/Al_2O_3 for CO oxidation. Catalysis Communications 9 (2008): 2187-2190.

[46] Xiang, Y., Meng, Q., Li, X., and Wang, J. In situ hydrogen from aqueous-methanol for nitroarene reduction and imine formation over an Au-Pd/Al_2O_3 catalyst. Chemical Communications 46 (2010): 5918-5920.

[47] Suo, Z., Ma, C., Liao, W., Jin, M., and Lv, H. Structure and activity of Au–Pd/SiO_2 bimetallic catalyst for thiophene hydrodesulfurization. Fuel Processing Technology 92 (2011): 1549-1553.

[48] Beck, A., et al. Genesis of Au-Pd Nanoparticles Supported on SiO_2: Structure and Catalytic Activity in CO Oxidation. In, North American Catalysis Society 18, pp. 1-2. Cancun Mexico, 2003.

[49] Rebelli, J., Abbaspour, S., Rodriguez, A., Williams, C., and Monnier, J. Synthesis and Evaluation of Au-Pd/SiO_2 Bimetallic Catalysts Prepared Using Electroless Deposition Method. In, AIChE, 2010.

[50] Edwards, J.K., et al. Direct synthesis of hydrogen peroxide from H_2 and O_2 using Au-Pd/Fe_2O_3 catalysts. Journal of Materials Chemistry 15 (2005): 4595-4600.

[51] Nitani, H., et al. Sonochemically synthesized core-shell structured Au–Pd nanoparticles supported on γ-Fe_2O_3 particles. Journal of Nanoparticle Research 8 (2006): 951-958.

[52] Weerachawanasak, P., et al. Effect of strong metal–support interaction on the catalytic performance of Pd/TiO_2 in the liquid-phase semihydrogenation of phenylacetylene. Journal of Catalysis 262 (2009): 199-205.

[53] Reyes, P., Aguirre, M.C., Melián-Cabrera, I., López Granados, M., and Fierro, J.L.G. Interfacial Properties of an Ir/TiO_2 System and Their Relevance in Crotonaldehyde Hydrogenation. Journal of Catalysis 208 (2002): 229-237.

[54] Englisch, M., Jentys, A., and Lercher, J.A. Structure Sensitivity of the Hydrogenation of Crotonaldehyde over Pt/SiO_2 and Pt/TiO_2. Journal of Catalysis 166 (1997): 25-35.

[55] Miedziak, P.J., et al. Oxidation of benzyl alcohol using supported gold–palladium nanoparticles. Catalysis Today 163 (2011): 47-54.

[56] Miedziak, P., et al. Oxidation of benzyl alcohol using supported gold–palladium nanoparticles. Catalysis Today 164 (2011): 315-319.

[57] Rebelli, J., Detwiler, M., Ma, S., Williams, C.T., and Monnier, J.R. Synthesis and characterization of Au–Pd/SiO_2 bimetallic catalysts prepared by electroless deposition. Journal of Catalysis 270 (2010): 224-233.

[58] Scott, R.W.J., et al. Titania-Supported PdAu Bimetallic Catalysts Prepared from Dendrimer-Encapsulated Nanoparticle Precursors. Journal of the American Chemical Society 127 (2005): 1380-1381.

[59] Shironita, S., Takasaki, T., Kamegawa, T., Mori, K., and Yamashita, H. Application of microwave to the synthesis of nanosized metal and alloy catalysts on titanium dioxide supports. Journal of Physics: Conference Series 165 (2009): 1-4.

[60] Strobel, R., and Pratsinis, S.E. Flame Synthesis of Supported Platinum Group Metals for Catalysis and Sensors. Platinum Metals Review 53 (2009): 11-20.

[61] Kammler, H.K., Mädler, L., and Pratsinis, S.E. Flame Synthesis of Nanoparticles. Chemical Engineering & Technology 24 (2001): 583-596.

[62] Teoh, W.Y., Amal, R., and Mädler, L. Flame spray pyrolysis: An enabling technology for nanoparticles design and fabrication. Nanoscale 2 (2010): 1324-1347.

[63] Strobel, R., Alfons, A., and Pratsinis, S.E. Aerosol flame synthesis of catalysts. Advanced Powder Technology 17 (2006): 457-480.

[64] Mädler, L., Stark, W.J., and Pratsinis, S.E. Simultaneous deposition of Au nanoparticles during flame synthesis of TiO_2 and SiO_2. Journal of Materials Research 18 (2003): 115-120.

[65] Somboonthanakij, S., et al. Characteristics and Catalytic Properties of Pd/SiO_2 Synthesized by One-step Flame Spray Pyrolysis in Liquid-phase Hydrogenation of 1-Heptyne. Catalysis Letters 119 (2007): 346-352.

[66] Mekasuwandumrong, O., Somboonthanakij, S., Praserthdam, P., and Panpranot, J. Preparation of Nano-Pd/SiO_2 by One-Step Flame Spray Pyrolysis and Its Hydrogenation Activities: Comparison to the Conventional Impregnation Method. Industrial & Engineering Chemistry Research 48 (2009): 2819-2825.

[67] Mekasuwandumrong, O., Phothakwanpracha, S., Jongsomjit, B., Shotipruk, A., and Panpranot, J. Liquid-Phase Selective Hydrogenation of 1-Heptyne over Pd/TiO_2 Catalyst Synthesized by One-Step Flame Spray Pyrolysis. Catalysis Letters 136 (2010): 164-170.

[68] Mekasuwandumrong, O., Phothakwanpracha, S., Jongsomjit, B., Shotipruk, A., and Panpranot, J. Influence of flame conditions on the dispersion of Pd on the flame spray-derived Pd/TiO_2 nanoparticles. Powder Technology 210 (2011): 328-331.

[69] Stark, W.J., Mädler, L., Maciejewski, M., Pratsinis, S.E., and Baiker, A. Flame synthesis of nanocrystalline ceria-zirconia: effect of carrier liquid. Chemical Communications (2003): 588-589.

[70] Weissermel, K., and Arpe, H.J. Industrial Organic Chemistry. 4 ed. Darmstadt, Germany: John Wiley & Sons, 2003.

[71] Devarajan, S., Bera, P., and Sampath, S. Bimetallic nanoparticles: A single step synthesis, stabilization, and characterization of Au–Ag, Au–Pd, and Au–Pt in sol–gel derived silicates. Journal of Colloid and Interface Science 290 (2005): 117-129.

[72] Toshima, N., Harada, M., Yonezawa, T., Kushihashi, K., and Asakura, K. Structural analysis of polymer-protected palladium/platinum bimetallic clusters as dispersed catalysts by using extended x-ray absorption fine structure spectroscopy. The Journal of Physical Chemistry 95 (1991): 7448-7453.

[73] Toshima, N., Harada, M., Yamazaki, Y., and Asakura, K. Catalytic activity and structural analysis of polymer-protected gold-palladium bimetallic clusters prepared by the simultaneous reduction of hydrogen tetrachloroaurate and palladium dichloride. The Journal of Physical Chemistry 96 (1992): 9927.

[74] Yuan, D., Gong, X., and Wu, R. The ensemble effects on adsorption and dehydrogenation of ethylene on PdAu (001) bimetallic surfaces. Retrieved from http://arxiv.org/ftp/cond-mat/papers/0701/0701770.pdf

[75] Groß, A. Reactivity of Bimetallic Systems Studied from First Principles. Topics in Catalysis 37 (2006): 29-39.

[76] Tungler, A., and Fogassy, G. Catalysis with supported palladium metal, selectivity in the hydrogenation of C=C, C=O and C=N bonds, from chemo- to enantioselectivity. Journal of Molecular Catalysis A: Chemical 173 (2001): 231-247.

[77] Blaser, H.-U., Indolese, A., Schnyder, A., Steiner, H., and Studer, M. Supported palladium catalysts for fine chemicals synthesis. Journal of Molecular Catalysis A: Chemical 173 (2001): 3-18.

[78] Teschner, D., et al. Understanding Palladium Hydrogenation Catalysts: When the Nature of the Reactive Molecule Controls the Nature of the Catalyst Active Phase. Angewandte Chemie International Edition 47 (2008): 9274-9278.

[79] Bond, G.C., and Rank, J.S. In W. H. M. Sachtler; G. C. A. Schuit; P. Zwietering (eds.), Proceedings of the Third International Congress on Catalysis, p 1225. North-Holland Publishing Company, 1965.

[80] Teschner, D., et al. Role of Hydrogen Species in Palladium-Catalyzed Alkyne Hydrogenation. The Journal of Physical Chemistry C 114 (2010): 2293-2299.

[81] Varga, M., et al. Selective hydrogenation of pentynes over PdZr and PdCuZr prepared from amorphous precursors. Applied Catalysis A: General 234 (2002): 167-178.

[82] Teschner, D., et al. Increased selectivity of Pd based catalysts in alkyne hydrogenation reactions by the modification of their electronic structure. In, Max-Planck-Gesellschaft, Russia, 2009.

[83] Marín-Astorga, N., Pecchi, G., Fierro, J.L.G., and Reyes, P. Alkynes Hydrogenation over Pd-Supported Catalysts. Catalysis Letters 91 (2003): 115-121.

[84] Zhang, Y., Cui, X., Shi, F., and Deng, Y. Nano-Gold Catalysis in Fine Chemical Synthesis. Chemical Reviews 112 (2011): 2467-2505.

[85] Kartusch, C., and Bokhoven, J.A.v. Hydrogenation over gold catalysts: The interaction of gold with hydrogen. Gold Bulletin 42 (2009): 343-348.

[86] Julius, M., Roberts, S., and Fletcher, J.C.Q. A review of the use of gold catalysts in selective hydrogenation reactions Lynsey McEwana. Gold Bulletin 43 (2010): 298-306.

[87] Kolli, N.E., Delannoy, L., and Louis, C. Bimetallic Au–Pd catalysts for selective hydrogenation of butadiene: Influence of the preparation method on catalytic properties. Journal of Catalysis 297 (2013): 79-92.

[88] Crespo-Quesada, M., Dykeman, R.R., Laurenczy, G., Dyson, P.J., and Kiwi-Minsker, L. Supported nitrogen-modified Pd nanoparticles for the selective hydrogenation of 1-hexyne. Journal of Catalysis 279 (2011): 66-74.

[89] Semagina, N., Renken, A., and Kiwi-Minsker, L. Monodispersed Pd-nanoparticles on carbon fiber fabrics as structured catalyst for selective hydrogenation. Chemical Engineering Science 62 (2007): 5344-5348.

[90] Liprandi, D.A., Cagnola, E.A., Quiroga, M.E., and L'Argentière, P.C. Influence of the Reaction Temperature on the 3-Hexyne Semi-Hydrogenation Catalyzed by a Palladium(II) Complex. Catalysis Letters 128 (2009): 423-433.

[91] Lederhos, C.R., L'Argentière, P.C., and Fígoli, N.S. 1-Heptyne selective hydrogenation over Pd supported catalysts. Industrial and Engineering Chemistry Research 44 (2005): 1752-1756.

[92] Papp, A., Molnár, Á., and Mastalir, Á. Catalytic investigation of Pd particles supported on MCM-41 for the selective hydrogenations of terminal and internal alkynes. Applied Catalysis A: General 289 (2005): 256-266.

[93] Panpranot, J., Phandinthong, K., Sirikajorn, T., Arai, M., and Praserthdam, P. Impact of palladium silicide formation on the catalytic properties of Pd/SiO_2 catalysts in liquid-phase semihydrogenation of phenylacetylene. Journal of Molecular Catalysis A: Chemical 261 (2007): 29-35.

[94] Marín-Astorga, N., Pecchi, G., Fierro, J.L.G., and Reyes, P. A comparative study of Pd supported on MCM-41 and SiO_2 in the liquid phase hydrogenation of phenyl alkyl acetylenes mixtures. Journal of Molecular Catalysis A: Chemical 231 (2005): 67-74.

[95] Al-Dawery, S.K., and Dakhil, H.M. Acetylene hydrogenation process, mathematical modeling and control. In, The Third International Conference on Modeling, Simulation and Applied Optimization, Sharjah, U.A.E., 2009.

[96] Al-Dawery, S., and Dakhil, H.M. Modeling and control of acetylene hydrogenation process. Emirates Journal for Engineering Research 17 (2012): 9-16.

[97] Kim, W.-J., and Moon, S.H. Modified Pd catalysts for the selective hydrogenation of acetylene. Catalysis Today 185 (2012): 2-16.

[98] Osswald, J. Active-site isolation for the selective hydrogenation of acetylene: the Pd-Ga and Pd-Sn intermetallic compounds. Doctoral dissertation, Technische Universität Berlin Berlin, 2005.

[99] Lee, S. Partial catalytic hydrogenation of acetylene in ethylene production. Retrieved from http://www.klmtechgroup.com/PDF/Articles/articles/acetylene_converter.pdf

[100] Bond, G.C. Catalysis by Metals. New York: Academic Press, 1962.

[101] Ertl, G., Knözinger, H., and Weitkamp, J. Handbook of Heterogeneous Catalysts. vol. 5. Weinheim, Germany VCH, 1997.

[102] Park, Y.H., and Price, G.L. Deuterium Tracer Study on the Effect of CO on the Selective Hydrogenation of Acetylene over Pd/Al_2O_3. Industrial & Engineering Chemistry Research 30 (1991): 1693-1699.

[103] Duca, D., Frusteri, F., Parmaliana, A., and Deganello, G. Selective hydrogenation of acetylene in ethylene feedstocks on Pd catalysts. Applied Catalysis A: General 146 (1996): 269-284.

[104] Margitfalvi, J., Guczi, L., and Weiss, A.H. Reactions of acetylene during hydrogenation on Pd black catalyst. Journal of Catalysis 72 (1981): 185-198.

[105] Johannessen, T., et al. Flame Synthesis of Nanoparticles: Applications in Catalysis and Product/Process Engineering. Chemical Engineering Research and Design 82 (2004): 1444-1452.

[106] Mueller, R., Mädler, L., and Pratsinis, S.E. Nanoparticle synthesis at high production rates by flame spray pyrolysis. Chemical Engineering Science 58 (2003): 1969-1976.

[107] Chang, H., Kim, S.J., Jang, H.D., and Choi, J.W. Synthetic routes for titania nanoparticles in the flame spray pyrolysis. Colloids and Surfaces A: Physicochemical and Engineering Aspects 313–314 (2008): 282-287.

[108] Tok, A.I.Y., Boey, F.Y.C., and Zhao, X.L. Novel synthesis of Al_2O_3 nano-particles by flame spray pyrolysis. Journal of Materials Processing Technology 178 (2006): 270-273.

[109] Tani, T., Mädler, L., and Pratsinis, S.E. Homogeneous ZnO Nanoparticles by Flame Spray Pyrolysis. Journal of Nanoparticle Research 4 (2002): 337-343.

[110] Qin, X., Ju, Y., Bernhard, S., and Yao, N. Flame Synthesis of Y_2O_3:Eu Nanophosphors Using Ethanol as Precursor Solvents. Journal of Materials Research 20 (2005): 2960-2968.

[111] Hoxha, F., et al. Hydrogenation of acetophenone derivatives: Tuning the enantioselectivity via the metal–support interaction. Journal of Catalysis 278 (2011): 94-101.

[112] Strobel, R., Stark, W.J., Mädler, L., Pratsinis, S.E., and Baiker, A. Flame-made platinum/alumina: structural properties and catalytic behaviour in enantioselective hydrogenation. Journal of Catalysis 213 (2003): 296-304.

[113] Ogi, T., Nandiyanto, A.B.D., Purwanto, A., and Okuyama, K. Synthesis and Characterization of Pt/WO_3 Nanparticles Photocatalyst Prepared by Flame Spray Pyrolysis. In, eac2012, 2012.

[114] Pisduangdaw, S., et al. Characteristics and catalytic properties of $Pt–Sn/Al_2O_3$ nanoparticles synthesized by one-step flame spray pyrolysis in the dehydrogenation of propane. Applied Catalysis A: General 370 (2009): 1-6.

[115] Chaisuk, C., Boonpitak, P., Panpranot, J., and Mekasuwandumrong, O. Effects of Co dopants and flame conditions on the formation of Co/ZrO_2 nanoparticles by flame spray pyrolysis and their catalytic properties in CO hydrogenation. Catalysis Communications 12 (2011): 917-922.

[116] Schimmoeller, B., et al. Structure of flame-made vanadia/titania and catalytic behavior in the partial oxidation of *o*-xylene. Journal of Catalysis 256 (2008): 74-83.

[117] Hannemann, S., Grunwaldt, J.-D., Krumeich, F., Kappen, P., and Baiker, A. Electron microscopy and EXAFS studies on oxide-supported gold–silver nanoparticles prepared by flame spray pyrolysis. Applied Surface Science 252 (2006): 7862-7873.

[118] Chiarello, G.L., Selli, E., and Forni, L. Photocatalytic hydrogen production over flame spray pyrolysis-synthesised TiO_2 and Au/TiO_2. Applied Catalysis B: Environmental 84 (2008): 332-339.

[119] Chiarello, G.L., Forni, L., and Selli, E. Photocatalytic hydrogen production by liquid- and gas-phase reforming of CH_3OH over flame-made TiO_2 and Au/TiO_2. Catalysis Today 144 (2009): 69-74.

[120] Pawinrat, P., Mekasuwandumrong, O., and Panpranot, J. Synthesis of Au–ZnO and Pt–ZnO nanocomposites by one-step flame spray pyrolysis and its application for photocatalytic degradation of dyes. Catalysis Communications 10 (2009): 1380-1385.

[121] Chomkitichai, W., et al. H_2 Sensor Based on Au/TiO_2 Nanoparticles Synthesized by Flame Spray Pyrolysis. ENGINEERING JOURNAL 16 (2012): 135-142.

[122] Strobel, R., Krumeich, F., Stark, W.J., Pratsinis, S.E., and Baiker, A. Flame spray synthesis of Pd/Al_2O_3 catalysts and their behavior in enantioselective hydrogenation. Journal of Catalysis 222 (2004): 307-314.

[123] Strobel, R., Grunwaldt, J.-D., Camenzind, A., Pratsinis, S.E., and Baiker, A. Flame-made Alumina Supported Pd–Pt Nanoparticles: Structural Properties and Catalytic Behavior in Methane Combustion. Catalysis Letters 104 (2005): 9-16.

[124] Hannemann, S., et al. Combination of flame synthesis and high-throughput experimentation: The preparation of alumina-supported noble metal particles and their application in the partial oxidation of methane. Applied Catalysis A: General 316 (2007): 226-239.

[125] Chiarello, G.L., Ferri, D., Grunwaldt, J.-D., Forni, L., and Baiker, A. Flame-synthesized $LaCoO_3$-supported Pd: 2. Catalytic behavior in the reduction of NO by H_2 under lean conditions. Journal of Catalysis 252 (2007): 137-147.

[126] Siriwong, C., Liewhiran, C., Wetchakun, N., and Phanichphant, S. Characterization and photocatalytic activity of Pd-doped ZnO nanoparticles synthesized by flame spray pyrolysis. In, Nanoelectronics Conference, 2008. INEC 2008. 2nd IEEE International, pp. 869-874. 2008.

[127] Liewhiran, C., and Phanichphant, S. Doctor-bladed thick films of flame-made Pd/ZnO nanoparticles for ethanol sensing. Current Applied Physics 8 (2008): 336-339.

[128] van Vegten, N., Maciejewski, M., Krumeich, F., and Baiker, A. Structural properties, redox behaviour and methane combustion activity of differently supported flame-made Pd catalysts. Applied Catalysis B: Environmental 93 (2009): 38-49.

[129] Huang, J., Jiang, Y., van Vegten, N., Hunger, M., and Baiker, A. Tuning the support acidity of flame-made Pd/SiO_2–Al_2O_3 catalysts for chemoselective hydrogenation. Journal of Catalysis 281 (2011): 352-360.

[130] Liewhiran, C., Tamaekong, N., Wisitsoraat, A., Tuantranont, A., and Phanichphant, S. Ultra-sensitive H_2 sensors based on flame-spray-made Pd-loaded SnO_2 sensing films. Sensors and Actuators B: Chemical 176 (2013): 893-905.

[131] Enache, D.I., et al. Solvent-free oxidation of benzyl alcohol using titania-supported gold–palladium catalysts: Effect of Au–Pd ratio on catalytic performance. Catalysis Today 122 (2007): 407-411.

[132] Edwards, J.K., et al. Comparison of supports for the direct synthesis of hydrogen peroxide from H_2 and O_2 using Au–Pd catalysts. Catalysis Today 122 (2007): 397-402.

[133] Edwards, J.K., et al. Direct Synthesis of H_2O_2 from H_2 and O_2 over Gold, Palladium, and Gold–Palladium Catalysts Supported on Acid-Pretreated TiO_2. Angewandte Chemie International Edition 48 (2009): 8512-8515.

[134] Lopez-Sanchez, J.A., et al. Au-Pd supported nanocrystals prepared by a sol immobilisation technique as catalysts for selective chemical synthesis. Physical Chemistry Chemical Physics 10 (2008): 1921-1930.

[135] Gu, Z., Luo, L., and Teng, M. Effect of supports on HDS activity of Au-Pd catalysts. INDIAN JOURNAL OF CHEMISTRY SECTION A 46 (2007): 742.

[136] Lopez-Sanchez, J.A., et al. Reactivity studies of Au–Pd supported nanoparticles for catalytic applications. Applied Catalysis A: General 391 (2011): 400-406.

[137] Kesavan, L., et al. Solvent-Free Oxidation of Primary Carbon-Hydrogen Bonds in Toluene Using Au-Pd Alloy Nanoparticles. Science 331 (2011): 195-199.

[138] Dimitratos, N., et al. Solvent-free oxidation of benzyl alcohol using Au-Pd catalysts prepared by sol immobilisation. Physical Chemistry Chemical Physics 11 (2009): 5142-5153.

[139] Pritchard, J., et al. Direct Synthesis of Hydrogen Peroxide and Benzyl Alcohol Oxidation Using Au–Pd Catalysts Prepared by Sol Immobilization. Langmuir 26 (2010): 16568-16577.

[140] Cao, E., et al. Reaction and Raman spectroscopic studies of alcohol oxidation on gold–palladium catalysts in microstructured reactors. Chemical Engineering Journal 167 (2011): 734-743.

[141] Beck, A., et al. Sol derived gold–palladium bimetallic nanoparticles on TiO_2: structure and catalytic activity in CO oxidation. Topics in Catalysis 44 (2007): 115-121.

[142] Kucherov, A.V., et al. Nanogold-Containing Catalysts for Low-Temperature Removal of S-VOC from Air. Topics in Catalysis 52 (2009): 351-358.

[143] Bawaked, S., et al. Selective oxidation of alkenes using graphite-supported gold-palladium catalysts. Catalysis Science & Technology 1 (2011): 747-759.

[144] Kittisakmontree, P., et al. The liquid-phase hydrogenation of 1-heptyne over Pd–Au/TiO_2 catalysts prepared by the combination of incipient wetness impregnation and deposition–precipitation. Journal of Catalysis 297 (2013): 155-164.

[145] Brown, J.M., Caga, I.T., Welsh, C.K., Wilson, S.J., and Winterbottom, J.M. Some studies of silica-supported Pd-Au catalysts and their behaviour in the hydrogenation of 1-octyne in the liquid phase. Journal of Chemical Technology and Biotechnology 32 (1982): 848-856.

[146] Ma, J., Huang, X., Liao, X., and Shi, B. Preparation of highly active heterogeneous Au@Pd bimetallic catalyst using plant tannin grafted collagen fiber as the matrix. Journal of Molecular Catalysis A: Chemical 366 (2013): 8-16.

[147] Pârvulescu, V.I., et al. Characterization and Catalytic-Hydrogenation Behavior of SiO_2-Embedded Nanoscopic Pd, Au, and Pd–Au Alloy Colloids. Chemistry – A European Journal 12 (2006): 2343-2357.

[148] Dash, P., Dehm, N.A., and Scott, R.W.J. Bimetallic PdAu nanoparticles as hydrogenation catalysts in imidazolium ionic liquids. Journal of Molecular Catalysis A: Chemical 286 (2008): 114-119.

[149] Lederhos, C.R., et al. Hept-1-yne partial hydrogenation reaction over supported Pd and W catalysts. Applied Catalysis A: General 396 (2011): 170-176.

[150] Lederhos, C.R., Badano, J.M., Quiroga, M.E., L'Argentière, P.C., and Coloma-Pascual, F. Influence of ni addition to a low-loaded palladium catalyst on the selective hydrogenation of 1-heptyne. Química Nova 33 (2010): 816-820.

[151] L'Argentière, P.C., Cagnola, E.A., Quiroga, M.E., and Liprandi, D.A. A palladium tetra-coordinated complex as catalyst in the selective hydrogenation of 1-heptyne. Applied Catalysis A: General 226 (2002): 253-263.

[152] Kittisakmontree, P., et al. The liquid-phase hydrogenation of 1-heptyne over Pd-Au/TiO_2 catalysts prepared by the combination of incipient wetness impregnation and deposition-precipitation. Journal of Catalysis 297 (2013): 155-164.

[153] Somboonthanakij, S., et al. Characteristics and Catalytic Properties of Pd/SiO_2 Synthesized by One-step Flame Spray Pyrolysis in Liquid-phase Hydrogenation of 1-Heptyne. Catalysis Letters 119 (2007): 346-352.

[154] Maccarrone, M., et al. Kinetic study of the partial hydrogenation of 1-heptyne on tungsten oxide supported on alumina. Journal of Chemical Technology & Biotechnology 87 (2012): 1521-1528.

[155] Lederhos, C.R., et al. Metal and Precursor Effect during 1-Heptyne Selective Hydrogenation Using an Activated Carbon as Support. The Scientific World Journal 2013 (2013): 9.

[156] Haruta, M., Kobayashi, T., Sano, H., and Yamada, N. Novel Gold Catalysts for the Oxidation of Carbon Monoxide at a Temperature far Below 0 °C. Chemistry Letters 16 (1987): 405-408.

[157] Hutchings, G. New directions in gold catalysis. Gold Bulletin 37 (2004): 3-11.

[158] Haruta, M. Novel catalysis of gold deposited on metal oxides. Catalysis Surveys from Asia 1 (1997): 61-73.

[159] Hvolbæk, B., et al. Catalytic activity of Au nanoparticles. Nano Today 2 (2007): 14-18.

[160] Azizi, Y., Petit, C., and Pitchon, V. Formation of polymer-grade ethylene by selective hydrogenation of acetylene over Au/CeO_2 catalyst. Journal of Catalysis 256 (2008): 338-344.

[161] Sárkány, A. Acetylene hydrogenation on SiO_2 supported gold nanoparticles. Reaction Kinetics and Catalysis Letters 96 (2009): 43-54.

[162] Pei, G.X., et al. Promotional effect of Pd single atoms on Au nanoparticles supported on silica for the selective hydrogenation of acetylene in excess ethylene. New Journal of Chemistry 38 (2014): 2043-2051.

[163] Sárkány, A., Geszti, O., and Sáfrán, G. Preparation of Pd_{shell}–Au_{core}/SiO_2 catalyst and catalytic activity for acetylene hydrogenation. Applied Catalysis A: General 350 (2008): 157-163.

[164] Mager-Maury, C., Chizallet, C., Sautet, P., and Raybaud, P. Platinum Nanoclusters Stabilized on γ-Alumina by Chlorine Used As a Capping Surface Ligand: A Density Functional Theory Study. ACS Catalysis 2 (2012): 1346-1357.

[165] Mei, D., Neurock, M., and Smith, C.M. Hydrogenation of acetylene–ethylene mixtures over Pd and Pd–Ag alloys: First-principles-based kinetic Monte Carlo simulations. Journal of Catalysis 268 (2009): 181-195.

[166] Kang, J.H., Shin, E.W., Kim, W.J., Park, J.D., and Moon, S.H. Selective Hydrogenation of Acetylene on TiO_2-Added Pd Catalysts. Journal of Catalysis 208 (2002): 310-320.

[167] Panpranot, J., Kontapakdee, K., and Praserthdam, P. Effect of TiO_2 Crystalline Phase Composition on the Physicochemical and Catalytic Properties of Pd/TiO_2 in Selective Acetylene Hydrogenation. The Journal of Physical Chemistry B 110 (2006): 8019-8024.

[168] Ota, A., et al. Intermetallic Compound Pd_2Ga as a Selective Catalyst for the Semi-Hydrogenation of Acetylene: From Model to High Performance Systems. The Journal of Physical Chemistry C 115 (2011): 1368-1374.

[169] Ahn, I.Y., Kim, W.J., and Moon, S.H. Performance of La_2O_3- or Nb_2O_5-added Pd/SiO_2 catalysts in acetylene hydrogenation. Applied Catalysis A: General 308 (2006): 75-81.

[170] Riyapan, S., et al. Improved catalytic performance of Pd/TiO_2 in the selective hydrogenation of acetylene by using H_2-treated sol–gel TiO_2. Journal of Molecular Catalysis A: Chemical 383–384 (2014): 182-187.

[171] Kim, S.K., et al. Performance of shape-controlled Pd nanoparticles in the selective hydrogenation of acetylene. Journal of Catalysis 306 (2013): 146-154.

[172] Ma, X.-Y., Chai, Y.-Y., Evans, D.G., Li, D.-Q., and Feng, J.-T. Preparation and Selective Acetylene Hydrogenation Catalytic Properties of Supported Pd Catalyst by the in Situ Precipitation–Reduction Method. The Journal of Physical Chemistry C 115 (2011): 8693-8701.

[173] Zhang, Y., Diao, W., Williams, C.T., and Monnier, J.R. Selective hydrogenation of acetylene in excess ethylene using Ag- and Au–Pd/SiO_2 bimetallic catalysts prepared by electroless deposition. Applied Catalysis A: General 469 (2014): 419-426.

[174] Liu, X., et al. Room temperature O_2 plasma treatment of SiO_2 supported Au catalysts for selective hydrogenation of acetylene in the presence of large excess of ethylene. Journal of Catalysis 285 (2012): 152-159.

[175] Kang, J.H., Shin, E.W., Kim, W.J., Park, J.D., and Moon, S.H. Selective hydrogenation of acetylene on Pd/SiO_2 catalysts promoted with Ti, Nb and Ce oxides. Catalysis Today 63 (2000): 183-188.

[176] Panpranot, J., Kontapakdee, K., and Praserthdam, P. Selective hydrogenation of acetylene in excess ethylene on micron-sized and nanocrystalline TiO_2 supported Pd catalysts. Applied Catalysis A: General 314 (2006): 128-133.

[177] Liu, X., et al. Selective hydrogenation of acetylene in excess ethylene over SiO_2 supported Au–Ag bimetallic catalyst. Applied Catalysis A: General 439–440 (2012): 8-14.

[178] Thamaphat, K., Limsuwan, P., and Ngotawornchai, B. Phase Characterization of TiO_2 Powder by XRD and TEM. Kasetsart Journal: Natural Science 42 (2008): 357-361.

[179] Hosseini, M., et al. Catalytic performance of core–shell and alloy Pd–Au nanoparticles for total oxidation of VOC: The effect of metal deposition. Applied Catalysis B: Environmental 111–112 (2012): 218-224.

[180] Tiwari, V., Jiang, J., Sethi, V., and Biswas, P. One-step synthesis of noble metal–titanium dioxide nanocomposites in a flame aerosol reactor. Applied Catalysis A: General 345 (2008): 241-246.

[181] Sánchez-Ramírez, J.F., and Pal, U. Optical absorption of colloidal dispersion of bimetallic nanoparticles Au/Pd. Superficies y Vacío 13 (2001): 114-116.

[182] Wolf, A., and Schüth, F. A systematic study of the synthesis conditions for the preparation of highly active gold catalysts. Applied Catalysis A: General 226 (2002): 1-13.

[183] Jin, M., et al. Low temperature CO oxidation over Pd catalysts supported on highly ordered mesoporous metal oxides. Catalysis Today 185 (2012): 183-190.

[184] Sohn, Y., Pradhan, D., and Leung, K.T. Electrochemical Pd Nanodeposits on a Au Nanoisland Template Supported on Si(100): Formation of Pd–Au Alloy and Interfacial Electronic Structures. ACS Nano 4 (2010): 5111-5120.

[185] Lee, Y.S., et al. Charge Redistribution and Electronic Behavior in Pd-Au Alloys. Journal of the Korean Physical Society 37 (2000): 451-455.

[186] Lamb, R.N., et al. Surface characterisation of Pd–Ag/Al_2O_3 catalysts for acetylene hydrogenation using an improved XPS procedure. Applied Catalysis A: General 268 (2004): 43-50.

[187] Mazumder, V., Chi, M., More, K.L., and Sun, S. Synthesis and Characterization of Multimetallic Pd/Au and Pd/Au/FePt Core/Shell Nanoparticles. Angewandte Chemie International Edition 49 (2010): 9368-9372.

[188] Liu, F., Wechsler, D., and Zhang, P. Alloy-structure-dependent electronic behavior and surface properties of Au–Pd nanoparticles. Chemical Physics Letters 461 (2008): 254-259.

[189] Regan, M.R., and Banerjee, I.A. Preparation of Au–Pd bimetallic nanoparticles in porous germania nanospheres: A study of their morphology and catalytic activity. Scripta Materialia 54 (2006): 909-914.

[190] Li, C., Cai, W., Kan, C., and Fu, G. Synthesis and optical characterization of Pd–Au bimetallic nanoparticles dispersed within monolithic mesoporous silica. Scripta Materialia 50 (2004): 1481-1486.

[191] Zanella, R., Louis, C., Giorgio, S., and Touroude, R. Crotonaldehyde hydrogenation by gold supported on TiO_2: structure sensitivity and mechanism. Journal of Catalysis 223 (2004): 328-339.

[192] Abbott, H.L., et al. CO Adsorption on Monometallic and Bimetallic Au–Pd Nanoparticles Supported on Oxide Thin Films. The Journal of Physical Chemistry C 114 (2010): 17099-17104.

[193] Tiengchad, N., Mekasuwandumrong, O., Na-Chiangmai, C., Weerachawanasak, P., and Panpranot, J. Geometrical confinement effect in the liquid-phase semihydrogenation of phenylacetylene over mesostructured silica supported Pd catalysts. Catalysis Communications 12 (2011): 910-916.

[194] Sárkány, A., Beck, A., Horváth, A., Révay, Z., and Guczi, L. Acetylene hydrogenation on sol-derived Pd/SiO_2. Applied Catalysis A: General 253 (2003): 283-292.

[195] Ulan, J.G., Maier, W.F., and Smith, D.A. Rational design of a heterogeneous palladium catalyst for the selective hydrogenation of alkynes. The Journal of Organic Chemistry 52 (1987): 3132-3142.

[196] Albers, P., Seibold, K., Prescher, G., and Müller, H. XPS and SIMS studies of carbon deposits on Pt/Al_2O_3 and Pd/SiO_2 catalysts applied in the synthesis of hydrogen cyanide and selective hydrogenation of acetylene. Applied Catalysis A: General 176 (1999): 135-146.

[197] Hermans, S., Deffernez, A., and Devillers, M. Au–Pd/C catalysts for glyoxal and glucose selective oxidations. Applied Catalysis A: General 395 (2011): 19-27.

[198] Wyrwalski, F., Giraudon, J.-M., and Lamonier, J.-F. Synergistic Coupling of the Redox Properties of Supports and Cobalt Oxide Co_3O_4 for the Complete Oxidation of Volatile Organic Compounds. Catalysis Letters 137 (2010): 141-149.

[199] Zhu, H., Qin, Z., Shan, W., Shen, W., and Wang, J. Pd/CeO_2–TiO_2 catalyst for CO oxidation at low temperature: a TPR study with H_2 and CO as reducing agents. Journal of Catalysis 225 (2004): 267-277.

[200] Lim, J.-S., et al. Formation of Au/Pd alloy nanoparticles on TMV. Journal of Nanomaterials 2010 (2010): 1-6.

[201] Etacheri, V., Seery, M.K., Hinder, S.J., and Pillai, S.C. Oxygen Rich Titania: A Dopant Free, High Temperature Stable, and Visible-Light Active Anatase Photocatalyst. Advanced Functional Materials 21 (2011): 3744-3752.

[202] Hanaor, D.H., and Sorrell, C. Review of the anatase to rutile phase transformation. Journal of Materials Science 46 (2011): 855-874.

[203] Ghosh, T.B., Dhabal, S., and Datta, A.K. On crystallite size dependence of phase stability of nanocrystalline TiO_2. Journal of Applied Physics 94 (2003): 4577-4582.

[204] Hirano, M., Nakahara, C., Ota, K., Tanaike, O., and Inagaki, M. Photoactivity and phase stability of ZrO_2-doped anatase-type TiO_2 directly formed as nanometer-sized

particles by hydrolysis under hydrothermal conditions. Journal of Solid State Chemistry 170 (2003): 39-47.

[205] Li, G., Li, L., Boerio-Goates, J., and Woodfield, B.F. High Purity Anatase TiO_2 Nanocrystals: Near Room-Temperature Synthesis, Grain Growth Kinetics, and Surface Hydration Chemistry. Journal of the American Chemical Society 127 (2005): 8659-8666.

[206] Carp, O., Huisman, C.L., and Reller, A. Photoinduced reactivity of titanium dioxide. Progress in Solid State Chemistry 32 (2004): 33-177.

[207] Kim, J., Song, K.C., Foncillas, S., and Pratsinis, S.E. Dopants for synthesis of stable bimodally porous titania. Journal of the European Ceramic Society 21 (2001): 2863-2872.

[208] Shannon, R.D., and Pask, J.A. Kinetics of the Anatase-Rutile Transformation. Journal of the American Ceramic Society 48 (1965): 391-398.

[209] Zhang, H., and Banfield, J.F. Phase transformation of nanocrystalline anatase-to-rutile via combined interface and surface nucleation. Journal of Materials Research 15 (2000): 437-448.

[210] Gouma, P.I., and Mills, M.J. Anatase-to-Rutile Transformation in Titania Powders. Journal of the American Ceramic Society 84 (2001): 619-622.

[211] Zhang, J., Xu, Q., Feng, Z., Li, M., and Li, C. Importance of the Relationship between Surface Phases and Photocatalytic Activity of TiO_2. Angewandte Chemie 120 (2008): 1790-1793.

[212] Hanaor, D.A.H., Triani, G., and Sorrell, C.C. Morphology and photocatalytic activity of highly oriented mixed phase titanium dioxide thin films. Surface and Coatings Technology 205 (2011): 3658-3664.

[213] Paulauskas, I.E., et al. Photocatalytic Activity of Doped and Undoped Titanium Dioxide Nanoparticles Synthesised by Flame Spray Pyrolysis. Platinum Metals Review 57 (2013): 32-43.

[214] Gribb, A.A., and Banfield, J.F. Particle size effects on transformation kinetics and phase stability in nanocrystalline TiO_2. American Mineralogist 82 (1997): 717-728.

[215] Amorim, C., Wang, X., and Keane, M.A. Application of Hydrodechlorination in Environmental Pollution Control: Comparison of the Performance of Supported and Unsupported Pd and Ni Catalysts. Chinese Journal of Catalysis 32 (2011): 746-755.

[216] Gucbilmez, Y., and Calis, I. Pd-SBA-15 Type Catalysts for One Pot Oxidative Synthesis of Ethyl Acetate. Retrieved from http://eurasia12.uoi.gr/Abstracts_pdf/Late%20Abstracts/LP3_Abstract_Gucbilmez_OP.pdf

[217] Panpranot, J., Tangjitwattakorn, O., Praserthdam, P., and Goodwin Jr, J.G. Effects of Pd precursors on the catalytic activity and deactivation of silica-supported Pd catalysts in liquid phase hydrogenation. Applied Catalysis A: General 292 (2005): 322-327.

[218] Lingaiah, N., Sai Prasad, P.S., Kanta Rao, P., Berry, F.J., and Smart, L.E. Structure and activity of microwave irradiated silica supported Pd–Fe bimetallic catalysts in the hydrodechlorination of chlorobenzene. Catalysis Communications 3 (2002): 391-397.

[219] Bonarowska, M., et al. Hydrodechlorination of CCl_2F_2 (CFC-12) over Pd-Au/C catalysts. Applied Catalysis B: Environmental 35 (2001): 13-20.

[220] Nag, N.K. A Study on the Formation of Palladium Hydride in a Carbon-Supported Palladium Catalyst. The Journal of Physical Chemistry B 105 (2001): 5945-5949.

[221] Gómez-Sainero, L.M., Seoane, X.L., Fierro, J.L.G., and Arcoya, A. Liquid-Phase Hydrodechlorination of CCl_4 to $CHCl_3$ on Pd/Carbon Catalysts: Nature and Role of Pd Active Species. Journal of Catalysis 209 (2002): 279-288.

[222] Wang, C.-B., Lin, H.-K., and Ho, C.-M. Effects of the addition of titania on the thermal characterization of alumina-supported palladium. Journal of Molecular Catalysis A: Chemical 180 (2002): 285-291.

[223] Tonetto, G.M., and Damiani, D.E. Performance of Pd-Mo/γ-Al_2O_3 catalysts for the selective reduction of NO by methane. Journal of Molecular Catalysis A: Chemical 202 (2003): 289-303.

[224] Krawczyk, N., Witonska, I., Krolak, A., Frajtak, M., and Karski, S. Catalytic hydrogenation of nitrates on Pd-In/TiO_2 catalysts. Revue Roumaine de Chimie 56 (2011): 595-600.

[225] McCue, A.J., and Anderson, J.A. Recent advances in selective acetylene hydrogenation using palladium containing catalysts. Frontiers of Chemical Science and Engineering 9 (2015): 142-153.

[226] Hazra, A., Hazra, S.K., Dutta, D., Sarkar, C.K., and Basu, S. Studies on Hydrogen Sensing by Anodized Nanoporous Titania Thin Film Using Soft Drink Electrolyte. Frontiers in Sensors 1 (2013): 17-26.

[227] Tew, M.W., Janousch, M., Huthwelker, T., and van Bokhoven, J.A. The roles of carbide and hydride in oxide-supported palladium nanoparticles for alkyne hydrogenation. Journal of Catalysis 283 (2011): 45-54.

[228] Chen, L., Wang, S., Chen, C., and Zhang, N. Catalytic partial oxidation of methanol over Au–Pd bimetallic catalysts: a comparative study of SBA-16, SBA-16-CeO_2, and CeO_2 as supports. Transition Metal Chemistry 36 (2011): 387-393.

[229] Chen, Q.-b., Luo, L.-t., and Yang, X. Partial oxidation of methanol on Au-Pd/ceria. Indian Journal of Chemistry 47A (2008): 1317-1322.

[230] Bowker, M. The surface structure of titania and the effect of reduction. Current Opinion in Solid State and Materials Science 10 (2006): 153-162.

[231] Zhang, C., He, H., and Tanaka, K.-i. Catalytic performance and mechanism of a Pt/TiO_2 catalyst for the oxidation of formaldehyde at room temperature. Applied Catalysis B: Environmental 65 (2006): 37-43.

[232] Hong, J., Chu, W., Chen, M., Wang, X., and Zhang, T. Preparation of novel titania supported palladium catalysts for selective hydrogenation of acetylene to ethylene. Catalysis Communications 8 (2007): 593-597.

[233] Zhu, Y., Liu, D., and Meng, M. H_2 spillover enhanced hydrogenation capability of TiO_2 used for photocatalytic splitting of water: a traditional phenomenon for new applications. Chemical Communications 50 (2014): 6049-6051.

[234] Paál, Z., and Menon, P.G. Hydrogen effects in catalysis : Fundamentals and practical applications. New York: M. Dekker, 1988.

[235] Nascente, P.A.P., de Castro, S.G.C., Landers, R., and Kleiman, G.G. X-ray photoemission and Auger energy shifts in some gold-palladium alloys. Physical Review B 43 (1991): 4659-4666.

[236] Rodriguez, J. Physical and chemical properties of bimetallic surfaces. Surface Science Reports 24 (1996): 223-287.

[237] Gao, F., and Goodman, D.W. Pd-Au bimetallic catalysts: understanding alloy effects from planar models and (supported) nanoparticles. Chemical Society Reviews 41 (2012): 8009-8020.

[238] Lee, Y.-S., et al. Charge redistribution and electronic behavior in Pd-Au alloys. Journal of the Korean Physical Society 37 (2000): 451-455.

[239] Zhang, Z., Wang, Y., Li, X., and Dai, W.-L. Synergistic effect on Au-Pd bimetallic catalyst during oxidation of benzyl alcohol to sodium benzoate. Chinese Journal of Catalysis 35 (2014): 1846-1853.

[240] Datye, A.K., et al. Catalyst microstructure and methane oxidation reactivity during the Pd↔PdO transformation on alumina supports. Applied Catalysis A: General 198 (2000): 179-196.

[241] Melendez, O., and Hoflund, G.B. Effect of Palladium Metal Particle Size and Particle Oxidation in the Oxidation of Methane. In, 18th North American Catalysis Society Meeting, Cancun, Mexico, 2009.

[242] Gai, P.L., and Boyes, E.D. Electron microscopy in heterogeneous catalysis. London: Institute of physics publishing, 2003.

[243] Augustine, R.L. Heterogeneous catalysis for the synthetic chemist. New york: M. Dekker, 1996.

[244] Herzing, A.A., Carley, A.F., Edwards, J.K., Hutchings, G.J., and Kiely, C.J. Microstructural Development and Catalytic Performance of Au–Pd Nanoparticles on Al_2O_3 Supports: The Effect of Heat Treatment Temperature and Atmosphere. Chemistry of Materials 20 (2008): 1492-1501.

[245] Edwards, J.K., et al. The effect of heat treatment on the performance and structure of carbon-supported Au–Pd catalysts for the direct synthesis of hydrogen peroxide. Journal of Catalysis 292 (2012): 227-238.

[246] Delannoy, L., et al. Surface Segregation of Pd from TiO_2-Supported AuPd Nanoalloys under CO Oxidation Conditions Observed In situ by ETEM and DRIFTS. ChemCatChem 5 (2013): 2707-2716.

[247] Yi, C.W., Luo, K., Wei, T., and Goodman, D.W. The Composition and Structure of Pd–Au Surfaces. The Journal of Physical Chemistry B 109 (2005): 18535-18540.

[248] Goguet, A., et al. Preparation of a Pt/SiO_2 Catalyst: I. Interaction between Platinum Tetrammine Hydroxide and the Silica Surface. Journal of Catalysis 209 (2002): 135-144.

[249] Pattamakomsan, K., et al. Selective hydrogenation of 1,3-butadiene over Pd and Pd–Sn catalysts supported on different phases of alumina. Catalysis Today 164 (2011): 28-33.

[250] Garcia Cervantes, G., Cadete Santos Aires, F.J., and Bertolini, J.C. Compared properties of Pd on thermo-conductor supports (SiC, Si_3N_4) and Pd on oxide supports (Al_2O_3, SiO_2) for the 1,3-butadiene hydrogenation reaction. Journal of Catalysis 214 (2003): 26-32.

[251] Kurzina, I., Cadete Santos Aires, F.J., Bergeret, G., and Bertolini, J.C. Total oxidation of methane over Pd catalysts supported on silicon nitride: Influence of support nature. Chemical Engineering Journal 107 (2005): 45-53.

[252] Aires, F.J.C.S., Kurzina, I., Cervantes, G.G., and Bertolini, J.C. Pd catalysts supported on silicon nitride for the combustion of methane: Influence of the crystalline and amorphous phases of the support and of the preparation method on the catalytic performances. Catalysis Today 117 (2006): 518-524.

[253] Santos Aires, F., et al. Size distribution of Bi clusters deposits on amorphous carbon substrates. Zeitschrift für Physik D Atoms, Molecules and Clusters 12 (1989): 149-152.

[254] Cadete Santos Aires, F.J., Sautet, P., Fuchs, G., Rousset, J.-L., and Mélinon, P. Model catalysts obtained by cluster deposition of Palladium onto HOPG. TEM and STM characterisation. Microscopy Microanalysis Microstructures 4 (1993): 441-452.

[255] Berthet, A., et al. Comparison of Pd/(Bulk SiC) Catalysts Prepared by Atomic Beam Deposition and Plasma Sputtering Deposition: Characterization and Catalytic Properties. Journal of Catalysis 190 (2000): 49-59.

[256] Mahfouz, R., Cadete Santos Aires, F.J., Brenier, A., Jacquier, B., and Bertolini, J.C. Synthesis and physico-chemical characteristics of nanosized particles produced

by laser ablation of a nickel target in water. Applied Surface Science 254 (2008): 5181-5190.

[257] Rousset, J.L., et al. Characterization and reactivity of Pd–Pt bimetallic supported catalysts obtained by laser vaporization of bulk alloy. Applied Surface Science 164 (2000): 163-168.

[258] Mahfouz, R., et al. Elaboration and characterization of bimetallic nanoparticles obtained by laser ablation of Ni75Pd25 and Au75Ag25 targets in water. Journal of Nanoparticle Research 12 (2010): 3123-3136.

[259] Pongthawornsakun, B., Fujita, S.-i., Arai, M., Mekasuwandumrong, O., and Panpranot, J. Mono- and bi-metallic Au–Pd/TiO_2 catalysts synthesized by one-step flame spray pyrolysis for liquid-phase hydrogenation of 1-heptyne. Applied Catalysis A: General 467 (2013): 132-141.

[260] Kittisakmontree, P., Yoshida, H., Fujita, S.-i., Arai, M., and Panpranot, J. The effect of TiO_2 particle size on the characteristics of Au–Pd/TiO_2 catalysts. Catalysis Communications 58 (2015): 70-75.

[261] Chen, Y., and Lee, D. Liquid Phase Hydrogenation of p-Chloronitrobenzene on Au-Pd/TiO_2 Catalysts: Effects of Reduction Methods. Modern Research in Catalysis 2 (2013): 25-34.

[262] Goodman, D.W. “Catalytically active Au on Titania:” yet another example of a strong metal support interaction (SMSI)? Catalysis Letters 99 (2005): 1-4.

[263] Schimpf, S., et al. Supported gold nanoparticles: in-depth catalyst characterization and application in hydrogenation and oxidation reactions. Catalysis Today 72 (2002): 63-78.

[264] Garetto, T.F., Borgna, A., and Apesteguía, C.R. Effect of alloying on the sulfur resistance of bimetallic Pt-based catalysts. In B. Delmon; G. F. Froment (eds.), Studies in Surface Science and Catalysis, vol. 88. pp. 369-376. Elsevier, 1994.

[265] Weerachawanasak, P., Praserthdam, P., and Panpranot, J. Liquid-Phase Hydrogenation of Phenylacetylene Over the Nano-Sized Pd/TiO_2 Catalysts. Journal of Nanoscience and Nanotechnology 14 (2014): 3170-3175.

[266] Lee, J.S., Khanna, A., Oh, M., Ranade, M.B., and Singh, R.K. Synthesis and Characterization of Zn_2SiO_4:Mn^{2+} Nanophosphors Prepared from Different Zn Source in Liquid Precursor by Flame Spray Pyrolysis. ECS Transactions 25 (2009): 107-112.

[267] Chiarello, G.L., Rossetti, I., and Forni, L. Flame-spray pyrolysis preparation of perovskites for methane catalytic combustion. Journal of Catalysis 236 (2005): 251-261.

[268] Tani, T., Mädler, L., and Pratsinis, S. Homogeneous ZnO Nanoparticles by Flame Spray Pyrolysis. Journal of Nanoparticle Research 4 (2002): 337-343.

[269] Mädler, L., and Pratsinis, S.E. Bismuth Oxide Nanoparticles by Flame Spray Pyrolysis. Journal of the American Ceramic Society 85 (2002): 1713-1718.

[270] Qin, X., Ju, Y., Bernhard, S., and Yao, N. Synthesis of Y_2O_3:Eu Phosphor Nanoparticles by Flame Spray Pyrolysis. In, NSTI-Nanotech 2005, pp. 9-12. 2005.

[271] Gröhn, A.J., Pratsinis, S.E., Sánchez-Ferrer, A., Mezzenga, R., and Wegner, K. Scale-up of Nanoparticle Synthesis by Flame Spray Pyrolysis: The High-Temperature Particle Residence Time. Industrial & Engineering Chemistry Research 53 (2014): 10734-10742.

[272] Teoh, W.Y., Li, D., Selomulya, C., Woodward, R., and Amal, R. Synthesis and characterisation of flame-sprayed superparamagnetic bare and silica-coated maghemite nanoparticles. In, NSTI-Nanotech 2007, pp. 187-190. 2007.

[273] Fujiwara, K., Deligiannakis, Y., Skoutelis, C.G., and Pratsinis, S.E. Visible-light active black TiO_2-Ag/TiO_x particles. Applied Catalysis B: Environmental 154–155 (2014): 9-15.

[274] Rainer, J., Roger, M., Sotiris, E.P., Mark, W., and Akhtar, M.K. Morphology and composition of spray-flame-made yttria-stabilized zirconia nanoparticles. Nanotechnology 16 (2005): S609.

[275] Bettini, L.G., et al. Mixed-phase nanocrystalline TiO_2 photocatalysts produced by flame spray pyrolysis. Applied Catalysis B: Environmental 178 (2015): 226-232.

[276] González, C.A., and Montes de Correa, C. Catalytic Hydrodechlorination of Tetrachloroethylene over Pd/TiO_2 Minimonoliths. Industrial & Engineering Chemistry Research 49 (2010): 490-497.

[277] Wengeler, R. Hydrodynamic stress induced dispersion of nanoscale agglomerates by a high pressure process. Cuvillier Verlag, 2007.

[278] Gordon, C.L., Lobban, L.L., and Mallinson, R.G. Selective hydrogenation of acetylene to ethylene during the conversion of methane in a catalytic dc plasma reactor. In J. J. S. E. Iglesia; T. H. Fleisch (eds.), Studies in Surface Science and Catalysis, vol. 136. pp. 271-276. Elsevier, 2001.

[279] Boitiaux, J.P., Cosyns, J., and Vasudevan, S. Hydrogenation of highly unsaturated hydrocarbons over highly dispersed palladium catalyst: Part I: behaviour of small metal particles. Applied Catalysis 6 (1983): 41-51.

[280] Kitamura, T., Sugeta, M., and Sakata, G. Liquid phase selective hydrogenation reaction of methylacetylene and propadiene in propylene over moderately dispersed palladium catalysts. In H. Hideshi; O. Kiyoshi (eds.), Studies in Surface Science and Catalysis, vol. 121. pp. 427-430. Elsevier, 1999.

[281] Bensalem, A., and Verduraz, F. Palladium-ceria catalysts: Metal-support interactions and reactivity of palladium in selective hydrogenation of but-1-yne. Reaction Kinetics and Catalysis Letters 60 (1997): 71-77.

[282] Gigola, C.E., Aduriz, H.R., and Bodnariuk, P. Particle size effect in the hydrogenation of acetylene under industrial conditions. Applied Catalysis 27 (1986): 133-144.

[283] Neri, G., Musolino, M.G., Milone, C., Pietropaolo, D., and Galvagno, S. Particle size effect in the catalytic hydrogenation of 2,4-dinitrotoluene over Pd/C catalysts. Applied Catalysis A: General 208 (2001): 307-316.

[284] Nikolaev, S.A., Leonid, N.Z., Smirnov, V.V., Vyacheslav, A.A., and Zanaveskin, K.L. Catalytic hydrogenation of alkyne and alkadiene impurities in alkenes. Practical and theoretical aspects. Russian Chemical Reviews 78 (2009): 231-247.

[285] Stakheev, A.Y., and Kustov, L.M. Effects of the support on the morphology and electronic properties of supported metal clusters: modern concepts and progress in 1990s. Applied Catalysis A: General 188 (1999): 3-35.

[286] KARPIŃSKI, Z. Catalysis by Supported, Unsupported, and Electron-Deficient Palladium. In, ADVANCES IN CATALYSIS, vol. 37. p 328. Academic Press, 1991.

[287] Yan, X., Wheeler, J., Jang, B., Lin, W.-Y., and Zhao, B. Stable Au catalysts for selective hydrogenation of acetylene in ethylene. Applied Catalysis A: General 487 (2014): 36-44.

[288] Teoh, W.Y., Amal, R., and Madler, L. Flame spray pyrolysis: An enabling technology for nanoparticles design and fabrication. Nanoscale 2 (2010): 1324-1347.

[289] Grossmann, H.K., et al. Experimental characterization of the Double Flame Spray Pyrolysis Process based on the deposition of Pt on a TiO_2 support. In, Aerosol Technology 2014, Karlsruhe Institute of Technology, 2014.

[290] Høj, M., et al. Two-Nozzle Flame Spray Pyrolysis (FSP) Synthesis of $CoMo/Al_2O_3$ Hydrotreating Catalysts. Catalysis Letters 143 (2013): 386-394.

[291] Wang, Z., et al. Palladium-doped silica–alumina catalysts obtained from double-flame FSP for chemoselective hydrogenation of the model aromatic ketone acetophenone. Journal of Catalysis 302 (2013): 10-19.

[292] Büchel, R., Strobel, R., Pratsinis, S.E., and Baiker, A. Two-nozzle flame synthesis of $Pt/Ba/Al_2O_3$ for NO_x storage. In, NSTI-Nanotech 2008, pp. 669-671. 2008.

[293] Strobel, R., et al. Two-Nozzle Flame Synthesis of $Pt/Ba/Al_2O_3$ for NO_x Storage. Chemistry of Materials 18 (2006): 2532-2537.

[294] Lee, Y.S., et al. Charge redistribution and electronic behavior in Pd-Au alloys. Journal of the Korean Physical Society 37 (2000): 451-455.

[295] Sohn, Y., Pradhan, D., and Leung, K.T. Electrochemical Pd nanodeposits on a Au nanoisland template supported on Si(100): Formation of Pd-Au alloy and interfacial electronic structures. ACS Nano 4 (2010): 5111-5120.

APPENDICES

APPENDIX A

CALCULATION FOR CATALYST PREPARATION

Preparation of 1 wt.% Au-1 wt.% Pd/TiO_2 catalysts by using the flame spray pyrolysis method

Preparation of 1 wt.% Au-1 wt.% Pd/TiO_2 catalysts by using flame spray pyrolysis synthesis is presented as follows:

Precursor

- Palladium (II) acetylacetonate ($Pd(C_5H_7O_2)_2$) , MW = 304.62
- Tetrachloroauric acid trihydrate ($HAuCl_4 \cdot 3H_2O$) , MW = 393.38
- Titanium (IV) butoxide or TBT ($Ti(OCH_2CH_2CH_2CH_3)_4$) , MW = 340.32

Calculation

For total concentration at 0.5 M

$$\frac{\text{wt Pd}}{\text{MW Pd}} + \frac{\text{wt Au}}{\text{MW Au}} + \frac{\text{wt } TiO_2}{\text{MW } TiO_2} = 0.5$$

Based on 100 g of catalyst

Palladium = 1 g

Gold = 1 g

TiO_2 = 100-1-1 = 98 g

Relationship of weight ratio for each metal

$$\frac{\text{wt Pd}}{\text{wt } TiO_2} = \frac{1}{98} = 0.010204 \rightarrow \text{wt Pd} = 0.010204 \times \text{wt } TiO_2$$

$$\frac{\text{wt Au}}{\text{wt } TiO_2} = \frac{1}{98} = 0.010204 \rightarrow \text{wt Au} = 0.010204 \times \text{wt } TiO_2$$

Substitution weight ratio and molecular weight of each component into the equation of total concentration

$$\frac{0.010204 \times \text{wt } TiO_2}{\text{MW Pd}} + \frac{0.010204 \times \text{wt } TiO_2}{\text{MW Au}} + \frac{\text{wt } TiO_2}{\text{MW } TiO_2} = 0.5$$

$$\frac{0.010204 \times \text{wt } TiO_2}{106.4} + \frac{0.010204 \times \text{wt } TiO_2}{196.97} + \frac{\text{wt } TiO_2}{79.9} = 0.5$$

$$\text{wt } TiO_2 = 39.48401 \text{ g}$$

$$\text{mole } TiO_2 = \frac{\text{wt } TiO_2}{\text{MW } TiO_2} = \frac{39.48401}{79.9} = 0.494168 \text{ mol}$$

Find weight and mole of Pd

$$\frac{\text{wt Pd}}{106.4} + \frac{0.010204 \times 39.48401}{196.97} + \frac{39.48401}{79.9} = 0.5$$

$$\text{wt Pd} = 0.402898 \text{ g}$$

$$\text{mole Pd} = \frac{\text{wt Pd}}{\text{MW Pd}} = \frac{0.402898}{106.4} = 0.003787 \text{ mol}$$

Find weight and mole of Au

$$\frac{0.402898}{106.4} + \frac{\text{wt Au}}{196.97} + \frac{39.48401}{79.9} = 0.5$$

$$\text{wt Au} = 0.402898 \text{ g}$$

$$\text{mole Au} = \frac{\text{wt Au}}{\text{MW Au}} = \frac{0.402898}{196.97} = 0.002045 \text{ mol}$$

For total concentration at 0.5 M

$$\text{TBT required} = \frac{\text{mol } TiO_2\text{required} \times \text{MW of TBT}}{\text{density of TBT} \times \text{purity}} \times \frac{1 \text{ mol Ti}}{1 \text{ mol } TiO_2} \times \frac{1 \text{ mol TBT}}{1 \text{ mol Ti}}$$

$$= \frac{0.0494168 \times 340.32}{1 \times 0.97} \times \frac{1 \text{ mol Ti}}{1 \text{ mol } TiO_2} \times \frac{1 \text{ mol TBT}}{1 \text{ mol Ti}}$$

$$= 173.3765 \text{ ml of TBT}$$

$$Pd(C_5H_7O_2)_2 \text{ required} = \frac{\text{mol Pd required} \times \text{MW of } Pd(C_5H_7O_2)_2}{\text{purity}} \times \frac{1 \text{ mol } Pd(C_5H_7O_2)_2}{1 \text{ mol Pd}}$$

$$= \frac{0.003787 \times 304.62}{0.99} \times \frac{1 \text{ mol } Pd(C_5H_7O_2)_2}{1 \text{ mol Pd}}$$

$$= 1.1652484 \text{ g of } Pd(C_5H_7O_2)_2$$

Due to 49% Au metal basis, 100 g of $HAuCl_4 \cdot 3H_2O$ contained Au about 49 g

So,

$$HAuCl_4 \cdot 3H_2O \text{ required} = \frac{\text{wt Au required}}{\text{purity}}$$

$$= \frac{0.402898}{0.49}$$

$$= 0.822241 \text{ g of } HAuCl_4 \cdot 3H_2O$$

Preparation of 1 wt.% Au-1 wt.% Pd/TiO_2 catalysts by using the incipient wetness impregnation method

Preparation of 1 wt.% Au-1 wt.% Pd/TiO_2 catalysts by using the incipient wetness impregnation method is presented as follows:

Precursor

- Palladium (II) nitrate ($Pd(NO_3)_2$) , MW = 230.43
- Tetrachloroauric acid trihydrate ($HAuCl_4 \cdot 3H_2O$) , MW = 393.83

Support

- Titania (TiO_2) synthesized by flame spray pyrolysis

Calculation

Based on 100 g of catalyst

Palladium = 1 g

Gold = 1 g

TiO_2 = 100-1-1 = 98 g

For 1 g of catalyst

Palladium required $= 1 \times \frac{1}{100} = 0.01$ g

Gold required $= 1 \times \frac{1}{100} = 0.01$ g

Titania required = 1-0.01-0.01 = 0.98 g

$$Pd(NO_3)_2 \text{ required} = \frac{\text{MW of } Pd(NO_3)_2 \times \text{Pd required}}{\text{MW of Pd}}$$

$$= \frac{230.43 \times 0.01}{106.4}$$

$$= 0.021657 \text{ g}$$

$$HAuCl_4 \cdot 3H_2O \text{ required} = \frac{\text{MW of } HAuCl_4 \cdot 3H_2O \times \text{Au required}}{\text{MW of Au}}$$

$$= \frac{393.83 \times 0.01}{196.97}$$

$$= 0.019994 \text{ g}$$

Due to 49% Au metal basis, 100 g of $HAuCl_4 \cdot 3H_2O$ contained Au about 49 g

So,

$$HAuCl_4 \cdot 3H_2O \text{ required} = 0.01 \times \frac{100}{49}$$

$$= 0.020408 \text{ g}$$

According to requirement of incipient wetness impregnation, the volume of de-ionized water which is used to dissolve Palladium nitrate and tetrachloroauric acid trihydrate precursors must equal to the pore volume of titania support. From N_2 physisorption result, the pore volume of the titania support synthesized by FSP is 0.44 cm^3/g. Consequently, the total volume of mixed precursor solution which is used for impregnation is 0.43 cm^3 for 0.98 g of titania support.

Preparation of 1 wt.% Au-1 wt.% Pd/TiO_2 catalysts by using the deposition-precipitation method

Preparation of 1 wt.% Au-1 wt.% Pd/TiO_2 catalysts by using the deposition-precipitation method is presented as follows:

Precursor

- Palladium (II) nitrate ($Pd(NO_3)_2$) , MW = 230.43
- Tetrachloroauric acid trihydrate ($HAuCl_4 \cdot 3H_2O$) , MW = 393.83

Support

- Titania (TiO_2) synthesized by flame spray pyrolysis

Calculation

Based on 100 g of catalyst

Palladium = 1 g

Gold = 1 g

TiO_2 = 100-1-1 = 98 g

For 1 g of catalyst

Palladium required $= 1 \times \frac{1}{100} = 0.01$ g

Gold required $= 1 \times \frac{1}{100} = 0.01$ g

Titania required = 1-0.01-0.01 = 0.98 g

$$\text{Pd(NO}_3\text{)}_2 \text{ required} = \frac{\text{MW of Pd(NO}_3\text{)}_2 \times \text{Pd required}}{\text{MW of Pd}}$$

$$= \frac{230.43 \times 0.01}{106.4}$$

$$= 0.021657 \text{ g}$$

$$\text{HAuCl}_4 \cdot 3\text{H}_2\text{O required} = \frac{\text{MW of HAuCl}_4 \cdot 3\text{H}_2\text{O} \times \text{Au required}}{\text{MW of Au}}$$

$$= \frac{393.83 \times 0.01}{196.97}$$

$$= 0.019994 \text{ g}$$

Due to 49% Au metal basis, 100 g of $\text{HAuCl}_4 \cdot 3\text{H}_2\text{O}$ contained Au about 49 g

So,

$$\text{HAuCl}_4 \cdot 3\text{H}_2\text{O required} = 0.01 \times \frac{100}{49}$$

$$= 0.020408 \text{ g}$$

APPENDIX B

CALCULATION OF CRYSTALLITE SIZE

Calculation of the crystallite size by using the Debye-Scherrer equation

The crystallite size was calculated from the width at half of height (or full-width-half-max) of diffraction peak of the XRD pattern by using the Debye-Scherrer equation.

$$D = \frac{K\lambda}{\beta \cos\theta}$$

where D = Crystallite size, A°

K = Cyrstallite-shape factor or Scherrer constant depending on shape of crystal (= 0.9 for FWHM of spherical crystals with cubic symmetry)

λ = X-ray wavelength, (=1.5418 A° for CuK_{α})

θ = Observed peak angle, degree

β = X-ray diffraction broadening, radian

The X-ray diffraction broadening (β) is the pure full-width-half-max of powder diffraction peak free from all broadening because of the experimental equipment or diffractometer. For a standard sample, α-Alumina is used as a standard sample to observe the instrumental broadening due to its crystallite size larger than 2000 A°. The X-ray diffraction broadening (β) can be determined by using the Warren's formula.

According to Warren's formula:

$$\beta = \sqrt{B_M^2 - B_S^2}$$

Where B_M = Measured peak width at half of peak height, radian

B_S = Corresponding full-width-half-max of the standard material (i.e., α-Alumina), radian

Example: Calculation of the crystallite size of anatase TiO_2

The major peak of anatase TiO_2 was observed at 25.48° 2θ.

Full-width-half-max of diffraction peak at 25.48° = 0.526°

$$= \frac{(2\pi \times 0.526°)}{360}$$

= 0.00918 radian

Corresponding full-width-half-max of α-alumina of diffraction peak at 25.48° = 0.00383 radian

$$\beta = \sqrt{B_M^2 - B_S^2}$$

$$= \sqrt{(0.00918)^2 - (0.00383)^2}$$

= 0.00834 radian

Thus,

β = 0.00834 radian

2θ = 25.48° ➔ θ = 12.74°

λ = 1.5418 A° for CuK_α

Crystallite size, $D = \frac{K\lambda}{\beta \cos\theta}$

$$= \frac{0.9 \times 1.5418}{0.00834 \times \cos 12.74°}$$

= 168.52 A°

= 16.852 nm

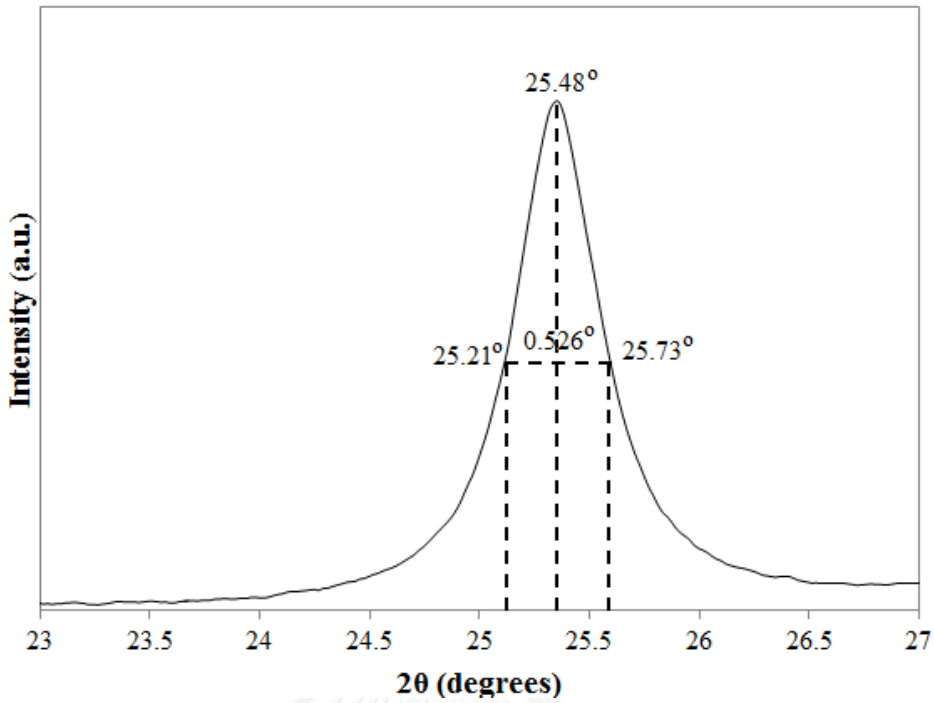

Figure B.1 The measured XRD peak of anatase TiO_2 for calculation of crystallite size of anatase TiO_2

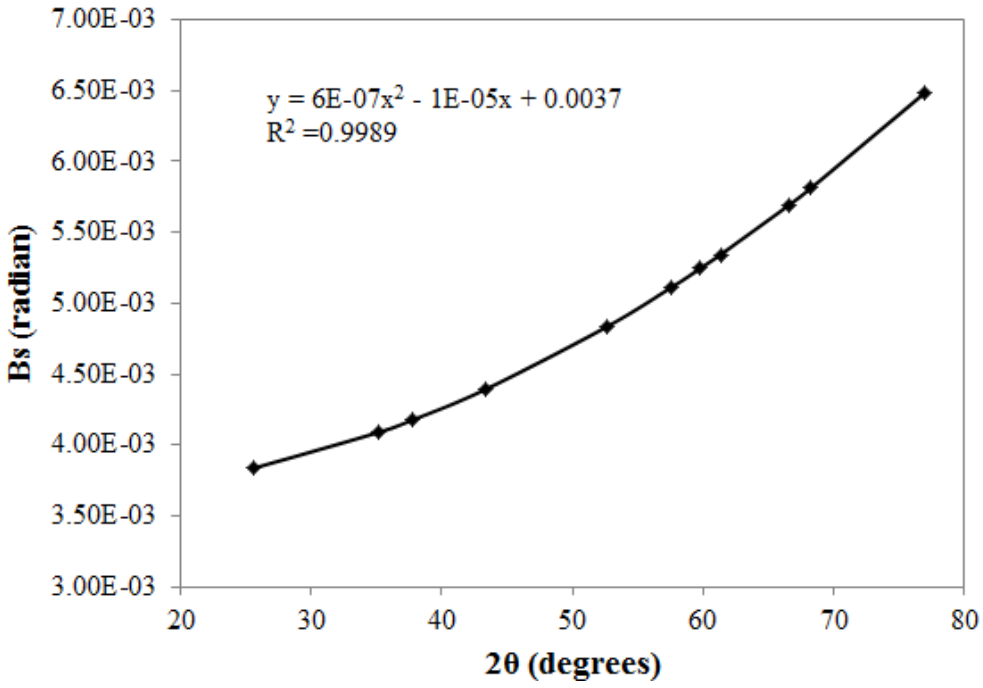

Figure B.2 The plot indicating the value of line broadening because of the equipment (data were obtained by using **α**-alumina as standard material)

APPENDIX C

CALCULATION OF PHASE COMPOSITION

The fraction of crystal phase of TiO_2 was determined from X-ray diffraction. The phase composition of TiO_2 was calculated by using the following equation [214]:

$$W_R = \left(\frac{1}{0.884 \left(\frac{A}{R} \right) + 1} \right) \times 100$$

where W_R = the percentage of rutile

A = the peak area of anatase TiO_2 at (101)

R = the peak area of anatase TiO_2 at (101)

The number of 0.884 is the coefficient of scattering.

APPENDIX D

CALCULATION FOR METAL ACTIVE SITE AND DISPERSION

The determination of the metal active sites and metal dispersion of the catalyst samples by using CO-chemisorption technique is shown as follows:

Calculation of metal active sites

$$\text{Volume of CO adsorbed on catalyst, } V_{ads} = \frac{V_{inj}}{g_{cat}} \times \left[1-\left(\frac{A_i}{A_f}\right)\right] \quad \text{L of CO/g}_{cat}$$

where V_{inj} = volume of CO injected per loop = 80 µl = 0.00008 L

g_{cat} = weight of catalyst used, g

A_i = integral area of CO peak after adsorption, unit

A_f = integral area of 80 µl of standard CO peak, unit

$$\text{Mole of CO adsorbed on catalyst} = \frac{P \times V_{ads}}{R \times T} \quad \text{mol of CO/g}_{cat}$$

where P = pressure at CO adsorbed = 1 atm

R = gas constant = 0.08206 L·atm/(mol·K)

T = temperature at CO adsorbed = 35 °C

$$\text{Molecules of CO adsorbed on catalyst} = \frac{P \times V_{ads}}{R \times T} \times 6.02\times10^{23} \quad \text{molecules of CO/g}_{cat}$$

$$\text{Metal active sites} = \frac{P \times V_{ads}}{R \times T} \times 6.02\times10^{23} \quad \text{molecules of CO/g}_{cat}$$

Calculation of metal dispersion

Definition of % metal dispersion

$$\text{Metal dispersion (\%)} = 100 \times \frac{\text{amount of Pd at surface in which CO adsorbed}}{\text{amount of Pd loading}}$$

According to CO chemisorption, the volume of CO adsorbed on catalyst is obtained as shown in earlier. Thus, the % metal dispersion can be estimated as follows:

$$\text{Dispersion, \%D} = S_f \times \frac{V_{ads}}{V_g} \times \frac{MW}{\%M} \times 100 \times 100$$

where %D = % metal dispersion

S_f = stoichiometry factor of CO adsorbed on Pd

V_{ads} = volume of CO adsorbed on catalyst per mass catalyst, L/g_{cat}

V_g = molar volume of CO gas at STP = 22,414 cm^3/mol = 22.414 L/mol

MW = molecular weight of metal, a.m.u.

%M = % metal loading (based on ICP)

APPENDIX E
ADDITIONAL WORK

The bimetallic AuPd supported on TiO_2 catalysts in this study was prepared with 1 wt.% and 1 wt.% for Au and Pd loadings, respectively. However, the effect of amount of Au loading on monometallic Pd catalyst should also been investigated. The catalytic performance of Pd/TiO_2 catalyst for acetylene hydrogenation is difficult to obvious the effect of Au loading on the selective hydrogenation of acetylene in excess of ethylene, so the effect of amount of Au loading on monometallic Pd was investigated over other supports i.e., SiO_2 support in the additional work. The bimetallic $xAu1Pd/SiO_2$ catalysts was studied and compared to the monometallic Pd/SiO_2 catalyst. The amount of Au addition (x) was varied between 0.1, 0.25, 0.5, and 1 wt.%, while the Pd amount was constantly loaded at 1 wt.%.

Catalytic characteristics of catalysts

The characteristics of catalysts were investigated by various techniques such as X-ray diffraction (XRD), N_2 physisorption, and CO chemisorption. The XRD patterns measured between 35 to 45° of $xAu1Pd/SiO_2$ and Pd/SiO_2 catalysts are shown in **Figure E.1**. The XRD peak of bimetallic AuPd alloy particles at 39.23 ° was clearly seen only for $1Au1Pd/SiO_2$ catalyst.

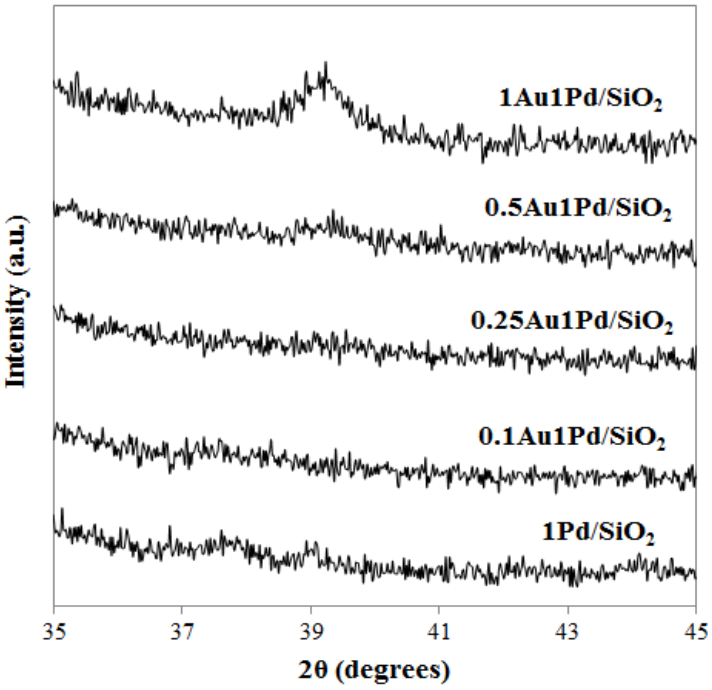

Figure E.1 XRD patterns of the monometallic 1 wt.% Pd/SiO_2 and bimetallic x wt.% Au-1 wt.% Pd/SiO_2 catalysts (Au loading (x) was varied between 0.1, 0.25, 0.5, and 1 wt.%)

The BET surface area of $xAu1Pd/SiO_2$ and Pd/SiO_2 catalysts are shown in **Table E.1**. The monometallic 1 wt.% Pd/SiO_2 catalyst exhibited highest BET surface area (297 m^2/g), while the monometallic 1 wt.% Au/SiO_2 catalyst exhibited lowest BET surface area (210 m^2/g). It was found that the BET surface area of the catalysts with Au addition was lower compared to monometallic 1 wt.% Pd/SiO_2 catalyst. The BET surface area of bimetallic $xAu1Pd/SiO_2$ catalysts (Au loading between 0.1-1 wt.%) was found to be in the range of 255-263 m^2/g.

The amounts of active surface Pd sites on the catalysts were measured by using CO chemisorption analysis as shown in **Table E.1**. No CO chemisorbed on the monometallic Au/SiO_2 was observed similar to the monometallic Au/TiO_2. The amount of CO adsorbed on the monometallic Pd/SiO_2 catalyst (11.46 μmol CO/g cat) was larger than those on the bimetallic $xAu1Pd/SiO_2$ catalysts. With increasing the Au addition from 0.1 to 0.5 wt.%, the amounts of CO adsorbed on the catalysts were

decreased from 9.4 to 3.31 μmol CO/g cat. Nevertheless, when the Au loading increased up to 1 wt.%, the amount of CO adsorbed on the catalyst was increased to 6.63 μmol CO/g cat. The Pd dispersions based on CO chemisorption are also reported in Table. According to CO chemisorption results, the highest Pd dispersion was found on the monometallic Pd/SiO_2 catalysts indicating to well-dispersed of small Pd particles. When the amount of Au less than 0.5 wt.% is added to form the bimetallic AuPd catalysts, the incorporate between Pd and Au might form to the larger particles, thus decreasing the Pd dispersion. However, with increasing Au loading up to 1 wt.% the Au and Pd incorporated to homogeneous bimetallic AuPd alloy particles (as shown in XRD result and the Part I) leading to increasing Pd dispersion.

Table E.1 BET surface areas and CO chemisorption results of the monometallic 1 wt.% Pd/SiO_2 and bimetallic x wt.% Au-1 wt.% Pd/SiO_2 catalysts (Au loading (x) was varied between 0.1, 0.25, 0.5, and 1 wt.%)

Catalysts	BET surface area (m^2/g)	CO uptake (μmol CO/g cat)	Pd dispersion (%)
1 wt.% Au/SiO_2	210.09	-	-
1 wt.% Pd/SiO_2	296.9	11.46	20.96
0.1 wt.% Au-1 wt.% Pd/SiO_2	254.97	9.4	17.2
0.25 wt.% Au-1 wt.% Pd/SiO_2	259.21	5.47	10.02
0.5 wt.% Au-1 wt. % Pd/SiO_2	261.84	3.31	6.05
1 wt.% Au-1 wt.% Pd/SiO_2	262.94	6.63	12.13

Catalytic study in the selective hydrogenation of acetylene in excess of ethylene

The effect of amount of Au addition on monometallic Pd catalyst was evaluated in the selective hydrogenation of acetylene in excess of ethylene. The Au loading (x) for bimetallic $AuPd/SiO_2$ catalysts was varied between 0.1, 0.25, 0.5, and 1

wt.%. The catalytic performance of monometallic Pd/SiO_2 and bimetallic $AuPd/SiO_2$ with 0.1-1wt.% Au loading for the selective hydrogenation of acetylene in excess of ethylene are presented in **Figure E.2**. With Au addition less than 0.5 wt.%, the C_2H_2 conversion was not improved (as seen at temperature of 60-80 °C); however, the C_2H_4 selectivity was slightly higher than that of monometallic Pd/SiO_2 catalyst. On the other hand, with Au addition more than 0.5 to 1 wt.%, the hydrogenation activity was increased compared to monometallic Pd/SiO_2 catalyst, especially at temperature of 60-80 °C. The acetylene (C_2H_2) could be fully hydrogenated at 80 °C. Nevertheless, the C_2H_4 selectivity at temperature of 100-120 °C was not much different compared to monometallic ones, except for the temperature at 80 °C. Thus, the C_2H_4 selectivity was mainly focused at the temperature of 80 °C because this point was the initial temperature to reach 100% C_2H_2 conversion.

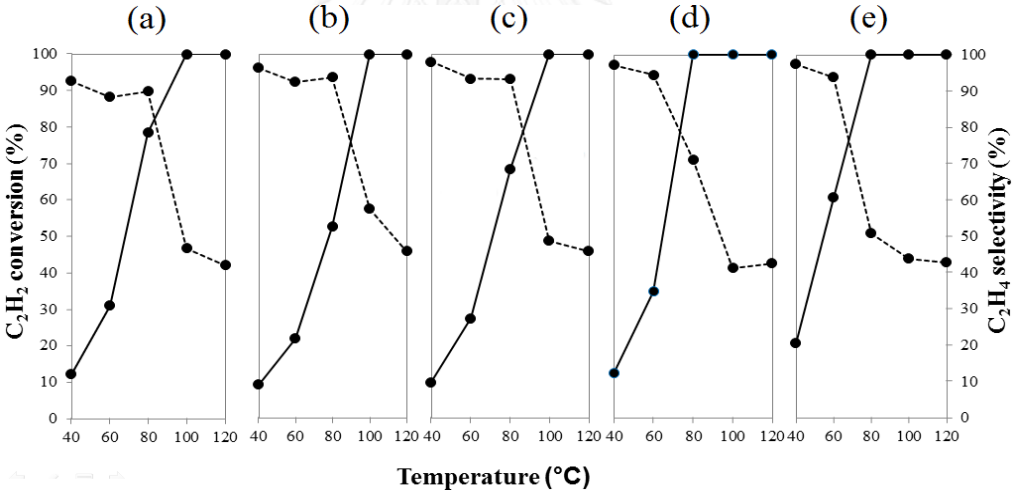

Figure E.2 Acetylene conversion (solid line) and ethylene selectivity (dash line) of monometallic Pd/SiO_2 and bimetallic $AuPd/SiO_2$ with Au loading between 0.1 (b), 0.25 (c), 0.5 (d), and 1 wt.% (e) for the selective hydrogenation of acetylene in excess of ethylene

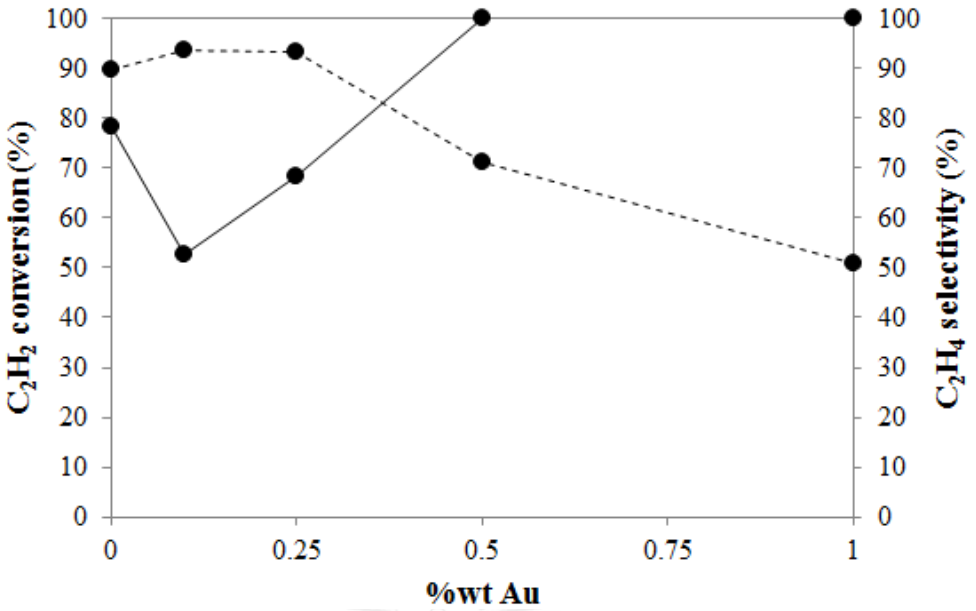

Figure E.3 Acetylene conversion (solid line) and ethylene selectivity (dash line) of monometallic Pd/SiO_2 and bimetallic $AuPd/SiO_2$ with Au loading from 0.1 -1 wt.% for the selective hydrogenation of acetylene in excess of ethylene at 80 °C

The C_2H_2 conversion and C_2H_4 selectivity for the selective hydrogenation of acetylene in excess of ethylene at the temperature of 80 °C are demonstrated in **Figure E.3**. It is obvious the effect of amount of Au addition on performance of bimetallic $AuPd/SiO_2$ catalysts in term of the ability to eliminate C_2H_2 by converting C_2H_2 to C_2H_4. Considering to the purposes of selective hydrogenation of acetylene, the high C_2H_2 conversion is firstly required in order to get rid off C_2H_2 in the ethylene feed. The Au addition to form the bimetallic $AuPd/SiO_2$ should be more than 0.5 wt.%. Then, the C_2H_4 selectivity is also regarded for selective hydrogenation of acetylene. Consequently, the 0.5 wt.% Au-1 wt.% Pd/SiO_2 catalyst could be the suitable catalyst for the selective hydrogenation of acetylene in excess of ethylene due to fully C_2H_2 elimination and high C_2H_4 selectivity. The C_2H_4 yield for the selective hydrogenation of acetylene in excess of ethylene at the temperature of 80 °C is shown in **Figure E.4**. The C_2H_4 yield for 0.5 wt.% Au-1 wt.% Pd/SiO_2 catalyst was similar to monometallic ones. However, in term of the ability of C_2H_2 elimination, the 0.5 wt.% Au-1 wt.% Pd/SiO_2 catalyst exhibited 100% C_2H_2 conversion, while the overall C_2H_2 could not be eliminated in the ethylene feed for the monometallic

Pd/SiO_2 catalyst. Interestingly, the amount of Au loading for the bimetallic AuPd catalysts affected the catalytic characteristics and behaviors for hydrogenation reaction and these results have been still required further investigation.

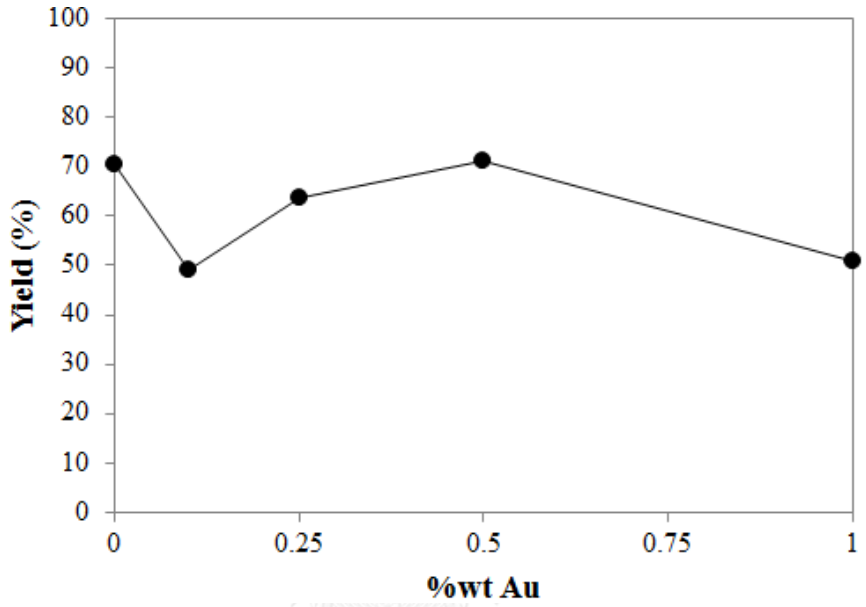

Figure E.4 Ethylene yield for the selective hydrogenation of acetylene in excess of ethylene at the temperature of 80 °C

LIST OF PUBLICATIONS

1. Boontida Pongthawornsakun, Shin-ichiro Fujita, Masahiko Arai, Okorn Mekasuwandumrong, and Joongjai Panpranot, “Mono- and bi-metallic Au-Pd/TiO_2 catalysts synthesized by one-step flame spray pyrolysis for liquid-phase hydrogenation of 1-heptyne”, Applied Catalysis A: General, (2013) 467, 132-141.
2. Boontida Pongthawornsakun, Okorn Mekasuwandumrong, Swamy Prakash, Eric Ehret, Francisco J. Cadete Santos Aires, and Joongjai Panpranot, “Effect of reduction temperature on the characteristics and catalytic properties of TiO_2 supported AuPd alloy particles prepared by one-step flame spray pyrolysis in the selective hydrogenation of 1-heptyne”, Applied Catalysis A: General (Accepted)
3. Boontida Pongthawornsakun, Okorn Mekasuwandumrong, Francisco J. Cadete Santos Aires, Robert Büchel, Sotiris E. Pratsinis, and Joongjai Panpranot, “Selective hydrogenation of acetylene in excess ethylene over AuPd/TiO_2 prepared by 2-nozzle flame spray pyrolysis” (manuscript in preparation)

VITA

Miss Boontida Pongthawornsakun was born in November 29th, 1988 in Bangkok, Thailand. She finished high school from Saipanya School Under the Royal Patronage of her Majesty the Queen, Bangkok in 2006. She received the Bachelor's Degree of Engineering in Chemical Engineering from King Mongkut's University of Technology Thonburi in April 2010. Afterward, she entered the Doctoral degree of Engineering program in Chemical engineering at Chulalongkorn University since June 2010. During her Doctoral degree, she received the Chulalongkorn University Dutsadi Phiphat Scholarship.

In 2012, she received the 1-month visiting research scholar from the National Research Council of Thailand-Japan Society for the Promotion of Science (NRCT-JSPS) Joint Research Program for short-term research at Hokkaido University, Sapporo, Japan. Later, she received the 3-month visiting research scholar from the Institut de Recherches sur la Catalyse et l'Environnement de Lyon (IRCELYON) to work with Doctor Francisco CADETE SANTOS AIRES on "Development of Supported Au-Pd Bimetallic Catalysts for Selective Hydrogenation Reactions" within the collaborative research program PHC SIAM N°29626VJ at France during September to November, 2013. In 2014, she visited the Swiss Federal Institute of Technology (ETH Zurich) for her short-term research at Switzerland during July to November. Then, she also visited the Institut de Recherches sur la Catalyse et l'Environnement de Lyon (IRCELYON) to work with Doctor Francisco CADETE SANTOS AIRES again at France in December, 2014.